UNIVERSITAT POLITÈCNICA DE VALÈNCIA

CSIC

Study of the differences in the fermentative metabolism of *S. cerevisiae*, *S. uvarum* and *S. kudriavzevii* species

Romain Minebois

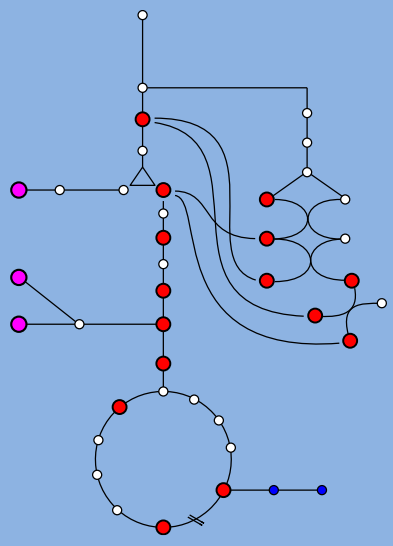

Supervised by

Dr. Amparo Querol

Dr. Roberto Pérez-Torrado

Valencia, September 2021

Instituto de Agroquímica y Tecnología de Alimentos (IATA-CSIC)

Grupo de Biología de Sistemas de Levaduras de Interés Biotecnológico

Study of the differences in the fermentative metabolism of *S. cerevisiae*, *S. uvarum* and *S. kudriavzevii* species

Tesis doctoral presentada por

Romain Minebois

para optar al grado de doctor en Ciencia, Tecnología y Gestión Alimentaria

Valencia, Septiembre 2021

Instituto de Agroquímica y Tecnología de Alimentos (IATA-CSIC)

Grupo de Biología de Sistemas de Levaduras de Interés Biotecnológico

La Dra. Amparo Querol Simón, Profesora de Investigación, y el Dr. Roberto Pérez-Torrado, Científico Titular, del Consejo Superior de Investigaciones Científicas (CSIC) en el Instituto de Agroquímica y Tecnología de Alimentos (IATA)

CERTIFICAN

Que la presente memoria titulada "Study of the differences in the fermentative metabolism of *S. cerevisiae*, *S. uvarum* and *S. kudriavzevii* species" constituye la tesis doctoral de Don Romain Minebois para optar al grado de doctor en Ciencia, Tecnología y Gestión Alimentaria por la Universidad Politécnica de Valencia. Asimismo, certifican haber dirigido y supervisado tanto los distintos aspectos del trabajo como su redacción.

Y para que conste a los efectos oportunos, firmamos el presente certificado en Valencia a de de

Fdo. Amparo Querol Simón Fdo. Roberto Pérez-Torrado

The present work has been carried out at the Department of Food Biotechnology of the IATA (CSIC). Romain Minebois was funded by a FPI grant (REF: BES-2016-078202) and supported by projects AGL2015-67504-C3-1R and RTI2018-093744-BC31 of the Ministerio de Ciencia e Inovación awarded to Amparo Querol.

Resumen

Saccharomyces cerevisiae, además de ser un importante organismo modelo en biología, es indiscutiblemente la especie de levadura más utilizada en procesos fermentativos industriales, incluyendo el sector enológico. Su capacidad de fermentar en concentraciones elevadas de azúcares, tolerar concentraciones altas de etanol y soportar la adición de sulfitos, son algunos de los factores que explican su éxito en fermentaciones vínicas. El metabolismo fermentativo de *S. cerevisiae* en condiciones enológicas se conoce bien gracias a una amplia bibliografía científica. En cambio, aún se sabe poco sobre el metabolismo de las especies de *Saccharomyces* criotolerantes, *S. uvarum* y *S. kudriavzevii*, quienes han suscitado recientemente el interés del sector vitivinícola por sus buenas propiedades fermentativas a bajas temperaturas, tales como la producción de vinos con mayor contenido en glicerol y alta complejidad aromática, llegando a veces a reducir su contenido en etanol. En este contexto, esta tesis pretende ampliar nuestros conocimientos sobre el metabolismo fermentativo de *S. uvarum* y *S. kudriavzevii* en condiciones enológicas, profundizando en el entendimiento de las diferencias existentes con el de *S. cerevisiae*, así como entre cepas de *S. cerevisiae* de distintos orígenes. Para ello, hemos utilizado varias técnicas ómicas para analizar la dinámica de los metabolomas (intra- y extracelulares) y/o transcriptomas de cepas representativas de *S. cerevisiae*, *S. uvarum* y *S. kudriavzevii* a alta (25 °C) y baja (12 °C) temperatura de fermentación. También, hemos desarrollado un modelo metabólico a escala de genoma que, junto a un análisis de balance de flujos, es capaz de cuantificar los flujos a través del metabolismo del carbono y del nitrógeno de levaduras en cultivo de tipo batch. Así, el conjunto de estos trabajos nos ha permitido identificar rasgos metabólicos y/o transcriptómicos relevantes para el sector enológico en estas especies. También se aporta nueva información sobre las especificidades de redistribución de flujos en la red metabólica de levaduras del género *Saccharomyces* acorde a la especie y las fluctuaciones ambientales que ocurren durante una fermentación vínica.

Abstract

Saccharomyces cerevisiae, besides being an important model organism in biology, is undoubtedly the most widely used yeast species in industrial fermentation processes, including the winemaking sector. Its ability to ferment at high levels of sugars, tolerate high ethanol concentrations and withstand the addition of sulfites are some of the factors explaining its success in wine fermentation. Accordingly, the fermentative metabolism of *S. cerevisiae* under oenological conditions is well described and benefits from a large scientific literature. In contrast, little is known about the metabolism of the cryotolerant *Saccharomyces* species, *S. uvarum* and *S. kudriavzevii*, which have recently attracted the interest of the wine industry for their good fermentative properties at low temperatures, such as the production of wines with higher glycerol content, high aromatic complexity and sometimes even reduced ethanol content. In this context, this thesis aims to expand our knowledge on the fermentative metabolism of *S. uvarum* and *S. kudriavzevii* under oenological conditions, deepening our understanding of the existing differences with that of *S. cerevisiae*, as well as between *S. cerevisiae* strains of different origins. For this purpose, we have used several omics techniques to analyze the dynamics of the (intra- and extracellular) metabolomes and/or transcriptomes of representative strains of *S. cerevisiae*, *S. uvarum* and *S. kudriavzevii* at high (25 °C) and low (12 °C) fermentation temperatures. Also, we have developed a genome-scale metabolic model that, together with a flux balance analysis, is able to quantify fluxes through carbon and nitrogen metabolism of yeast in batch culture. Taken together, this work has allowed us to identify metabolic and/or transcriptomic traits relevant to the oenological sector in these species. It also provides new information on the specificities of flux redistribution in the metabolic network of *Saccharomyces* yeasts according to the species and environmental fluctuations occurring during wine fermentation.

Resum

Saccharomyces cerevisiae, a més de ser un important organisme model en biologia, és indiscutiblement l'espècie de llevat més utilitzat en processos fermentatius industrials, incloent el sector enològic. La seua capacitat de fermentar grans concentracions de sucres, tolerar concentracions altes d'etanol i suportar l'addició de sulfits, són alguns dels factors que expliquen el seu èxit en fermentacions víniques. D'aquesta manera, el metabolisme fermentatiu de *S. cerevisiae* en condicions enològiques està ben descrit i es beneficia d'una àmplia bibliografia científica. En canvi, poc se sap encara sobre el metabolisme de les espècies de *Saccharomyces* criotolerants, *S. uvarum* i *S. kudriavzevii*, els qui han recentment suscitat l'interés del sector vitivinícola per les seues bones propietats fermentatives a baixes temperatures, com ara la producció de vins amb major contingut en glicerol, alta complexitat aromàtica i arribant a vegades a reduir el seu contingut en etanol. En aquest context, aquesta tesi pretén ampliar els nostres coneixements sobre el metabolisme fermentatiu de *S. uvarum* i *S. kudriavzevii* en condicions enològiques, aprofundint en l'enteniment de les diferències existents amb el de *S. cerevisiae*, així també com entre ceps de *S. cerevisiae* de diferents orígens. Per a això, hem utilitzat diverses tècniques omiques per a analitzar la dinàmica dels metabolomes (intra- i extracelul·lars) i/o transcriptomes de ceps representatius de *S. cerevisiae*, *S. uvarum* i *S. kudriavzevii* a alta (25 °C) i baixa (12 °C) temperatures de fermentació. També, hem desenvolupat un model metabòlic a escala del genoma que, al costat d'una anàlisi de balanç de fluxos, és capaç de quantificar els fluxos a través del metabolisme carbonat i nitrogenat de llevats en cultius de tipus batch. Així, el conjunt d'aquests treballs ens ha permés identificar trets metabòlics i/o transcriptómics rellevants per al sector enològic en aquestes espècies. També aporta nova informació sobre les especificitats de redistribució de fluxos en la xarxa metabòlica de llevats del gènere *Saccharomyces* concorde a l'espècie i les fluctuacions ambientals ocorrent durant una fermentació vínica.

Agradecimientos

Hace ahora ya más de cinco años que Ana Jiménez Belenguer, mi profesora de microbiología en la UPV, me recomendó que me pusiera en contacto con Amparo, "una investigadora muy simpática del IATA" según ella, cuando aún buscaba un instituto de investigación donde realizar mi TFM. A falta de este detalle y un pequeño e-mail a Amparo, el camino recorrido hasta hoy hubiese sido sin lugar a duda muy diferente y por eso se lo agradezco mucho. Porque, efectivamente, nunca hubiese pensado en ese momento que esto me iba a llevar a caer en un grupo de investigación tan bueno, a realizar una tesis doctoral, y menos aún que me llevaría a conocer a tanta gente de tantos sitios distintos con los que he podido compartir experiencias, dudas, trabajos, risas, viajes, y otros muchos buenos momentos que han contribuido a que estos años pasaran volando.

En primer lugar, quiero agradecer a mis directores de tesis por el apoyo demostrado durante estos ya cuatro años y medio. Amparo, muchas gracias por haberme acogido tan amablemente en tu grupo de investigación, por tu cercanía desde el mismísimo día que me entrevistaste y por haber confiado en mí desde el inicio de este trabajo. Cuando te contacté, venía con la idea de aprender un poco más sobre metabolismo, y la verdad es que de metabolismo he aprendido jeje. Gracias por tu apoyo, por todas las conversaciones y las experiencias compartidas dentro y fuera del IATA (nunca podré olvidar este congreso en Bariloche) y por todos estos consejos de viajes y rutas por España :) Roberto, gracias también por tu cercanía, por todo lo enseñado a lo largo de este periodo y por todos los consejos, las correcciones y discusiones habiendo permitido sacar adelante este trabajo.

En esta línea quiero agradecer la colaboración, las discusiones y el interés mostrado por mi tesis doctoral del resto de los investigadores del grupo SBYBI, Eladio Barrio, José Manuel Guillamón y Sergi Puig.

Quisiera agradecer fuertemente a Eva y David del Grupo de Ingeniería de (bio)procesos de Vigo por el gran trabajo obtenido fruto de la colaboración entre nuestros grupos. Eva, gracias por tu amabilidad, eres una crack y un ejemplo a seguir en la investigación científica. David, ha sido un placer poder trabajar contigo, no sabes lo mucho que he aprendido a raíz de estrujarme el cerebro discutiendo contigo de todas estas rutas y flujos metabólicos. Espero poder seguir colaborando con vosotros dos en el futuro.

Quiero agradecer también a tod@s mis compañer@s de bancada del grupo SBYBI. Empezando por mis inicios en el lab 307, gracias David Lázaro por haberme iniciado al trabajo de laboratorio, por tu paciencia, y por haberme enseñado todos tus trucos al principio cuando aún era estudiante de máster y que luego me sirvieron a lo largo de toda mi tesis doctoral. De la misma forma, quiero agradecer a Gabriel Castiglioni por haberme enseñado sobre el uso de los biorreactores y por compartir conmigo algo de su ingenio en el poco tiempo que coincidimos. Laupetra, gracias por tu generosidad, por todos tus consejos de laboratorio y por tu asistencia en los dolores de cabeza de la cromatografía. Ana Cris, gracias por tu ayuda, por tu disponibilidad y por asegurar el buen funcionamiento y abastecimiento del lab 307.

Por supuesto un gracias enorme a tod@s mi companer@s de la tercera planta o "secta" que siguen en el IATA o con los que he tenido la oportunidad de coincidir durante estos años. Mi compañero de labo y futbol Javi, mis primeras vecinas del "antiguo 309" Adri, Anto y Lucía, mi compi francofono Miguel, las bioinformáticas Laura y María, mis adversarios de AOE Peris y Ric, la incansable gimnasta Sara, Ying, Alba Y., Tania, Raquel, Andrés, David, etc.: mil gracias por el buen ambiente, por el ayuda, el compañerismo y por todos estos planes tan diversos compartidos. Así mismo, a las últimas dos reclutas Albita y Sonia, gracias por siempre tener esta sonrisa y transmitir esta vitalidad, energía y este buen rollo en cualquier circunstancia.

Gracias a Walter y Ángela, compañeros de trabajo, pero ante todo de buceo, patinaje y ahora incluso de voleiplaya jeje. Gracias igualmente a mi compi uruguaya, Flor, por hacerme descubrir el yoga y enseñarme a tomarme la vida de forma distinta.

No me quiero olvidar de la gente que pasó por el lab para diversas colaboraciones. Especialmente agradecer a Daniela y a Thelma por las risas y los buenos momentos pasados durante vuestras estancias en el IATA ("yo creo"), y a Ceci por tu simpatía, el acogedor trato en Bariloche, y todo lo compartido en Valencia (¡incluido el piso!).

Llegado a este punto, quiero agradecer particularmente a mis dos cómplices de batalla argentino y chileno con los que casi inicié esta aventura. Dolo/Dola, este párrafo es para vos. Gracias por todos estos momentos de apoyo mutuo en el lab, en particular para escribir papeeeeers, y fuera del IATA. Gracias por soportar mis comentarios

hirientes de delicadito francés que habla bajito (lo siento, pero tu letra… jaja ^^), por tu generosidad, por ser la niñera perfecta de mis gatos durante mis vacaciones, y por todos estos asados+pileta compartidos y que quedan por compartir (un abrazo a Moni). Seba, gracias por ser como eres (un wn, cachai?). Gracias por tu ayuda, por enseñarme toda tu sabiduría de biología molecular y sobre todo tu sabiduría del weveo. Gracias por darme a conocer a Ricardo Milos y por todas las experiencias bakan compartidas juntos en el lab así que fuera, como esas innumerables charlas acompañadas de una buena chela en el Tony's, los viajes, las rutas en bici o el buceo.

También he tenido la suerte de poder conocer y contar con el apoyo de varias personas de la segunda planta. Gracias Rafael Gavara por aceptar ser mi tutor de estancias y ofrecerme dar clases contigo en la UPV. Gracias Raquel por tu ayuda, por los buenos momentos compartidos fuera del IATA y por compartir (¿Japón 22?) y por recordarme siempre las deadlines de todos los trámites administrativos de esta tesis jeje ^^ Gracias Aida por tu amistad y buen rollo (¿para cuándo otro viaje a Canarias?). Gracias Laura Higueras por tu inmensa generosidad y tu ayuda. Gracias igualmente a Gracia por tu simpatía y por aceptarme como uno más cada vez que irrumpía en el lab 202 (¡que no han sido pocas veces!). Un agradecimiento especial también a Vicen por su cariño, su dedicación al cuidado de los gatos de la colonia del IATA, y por haberme dado dos hijos felinos :)

Quisiera agradecer fuertemente a Vicky y a Fernando (recepción) por su afecto y por todas esas charlas que te alegran el día. Así mismo, quisiera agradecer al resto de la gente de la tercera planta (Andrew, Marga, Antonio Ruiz, Pilar, etc.) con los que he tenido más oportunidad de tratar y cruzarme por el pasillo, y al resto del personal del IATA, que hacen que este instituto funcione correctamente.

Je tiens grandement à remercier Carole Camarasa pour m'avoir accueillie au sein de son équipe à Montpellier. Merci pour ton aide pour les manips, pour répondre à mes questions et pour la confiance accordée envers moi dès le premier jour. Merci à Audrey Bloem pour son soutien technique et les tips pour la réalisation des manips. Au cours de mes deux séjours à l'UMR j'ai également eu la chance de pouvoir travailler avec des camarades de choque au laboratoire. En primer lugar quiero agradecer al equipo español (aunque allí había un poco de todo ^^) del UMR-SPO : gracias a Rafa 1 (bajito), Rafa 2 (la pimienta, siempre reciéeen molida weeyyy), a

Juanma, a Pascale et à mister Bergler pour les inombrables moments de déconnes dans le labo 124, pendant les pauses cloppes et cafés, mais aussi en dehors du labo. Un grand merci également à Cécile pour avoir été ma colloque de bureau pendant mon premier séjour à Montpellier et pour tous les bons moments partagés. Finalement je tiens également à remercier le reste du personnel (Jean Roch, Teddy, Valérie, Thérèse, Christian, Marc, Eric, etc.) et étudiants/doctorants (Rémy, Carmen, Saül, Viwe, etc.) de l'UMR-SPO avec lesquels j'ai coïncidé et sans lesquels mon passage à Montpellier n'aurait été aussi productif et agréable :)

Je souhaiterais remercier l'ensemble de ma famille en France et en Espagne. Premièrement, du côté français, un grand merci à toi Papa. Je pense que ce travail est en grande mesure le reflet de l'effort et la réussite avec lesquels tu nous as éduqués moi, Théo et Hélène, en particulier après le départ de Maman, qui, je suis sûr serait super fière de toi et de ses trois enfants aujourd'hui. Merci de nous avoir soutenu dans nos études, de nous avoir transmis cet amour pour les choses bien faites, de nous avoir inculqué le goût pour les sciences, à travailler de façon rigoureuse, propre et ordonnée, ou encore de nous avoir enseigné à être débrouillards et autonomes. Merci à vous deux les frangins, Hélène et Théo, et à toi Josiane pour votre soutien et tous ces bons moments et voyages passés tous ensemble à Nubécourt, à Montpellier, à Valencia, à Jávea, en Martinique ou encore au Portugal, et qui m'ont permis de m'évader de la routine du travail au cours de ces quatre-cinq dernières années.

Del lado ibérico, quisiera agradecer calurosamente a los Settier Ramírez. Rosa, Tono, Vero y Hugo: me siento muy feliz y orgulloso de formar parte de vuestra familia. Estoy muy agradecido por todo lo que habéis hecho por mí, representáis un verdadero apoyo a diario para mí en Valencia y sé que puedo contar con vosotros ante cualquier problema.

Por fin, te quiero agradecer a ti Laura, por todas estas cosas que compartimos, por tu apoyo incondicional y por estar a mi lado en el día a día de esta vida. Ya sabes lo mucho que vales para mí y lo mucho que te quiero (i.e. MQTYLS).

À vous deux, Papa et Maman

Index

Introduction

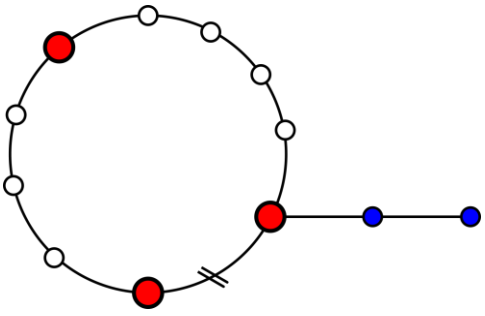

Introduction

I. The contribution of yeast within the winemaking process

a. From a complete stranger to a model organism

The production of wine is an activity that already existed several centuries ago as proven by evidence of winemaking found on an Egyptian jar dating back to 3000 years BC (Cavalieri *et al.*, 2003). However, from antiquity until the beginning of the 19th century, yeast, the main microorganism responsible for this transformation of a sweet drink into an alcoholic beverage – via alcoholic fermentation – was completely unknown to humankind. That said, this did not prevent man from exploiting the psychotropic, analgesic, disinfectant, and conservative properties of ethanol from that time, making it popular as a drug and medicine. In that sense, the contribution of yeasts, through winemaking and more generally through alcoholic fermentation, has therefore played an important role in the evolution of the human species and its societies. It was not until 1813 that Louis Pasteur discovered that yeasts were the main microscopic actors responsible for the transformation of grape must into alcoholic beverages through alcoholic fermentation (Barnett, 2000). Later in 1965, the first two commercially active dry yeast strains were produced for a large Californian winery (Pretorius, 2000). And starting in the 1970s, the inoculation of musts with pure cultures of selected

yeasts became a commonly established practice to better control the fermentation process, to the detriment of the more traditional spontaneous fermentations carried out by indigenous microbial species present on grape berries when harvested or introduced from the equipment and cellar during the vinification process. This is particularly the case for large-scale wine producers, for whom fast and reliable fermentations are essential to obtain a wine of consistent and predictable quality in successive years. Today, there are a multitude of starter cultures available on the market, most of them being yeast strains of the species *Saccharomyces cerevisiae* mostly because of their abundance and dominance in wine fermentations. Over the last fifty years, the popularity of *S. cerevisiae* has been and continues to be stimulated by an extensive knowledge acquired on yeast physiology, especially in the last years by the fast development and application of omics technologies and computational science. Beyond the wine market, *S. cerevisiae* has become a model organism in biology and medicine (Fields and Johnston, 2005), ecology and population genomics (Almeida *et al.*, 2015; Peter *et al.*, 2018), and an important multi-purpose cell factory (Hong and Nielsen, 2012).

b. The new challenges facing the wine industry today

“You can't make a great wine without good grapes” is a well-known statement by winemakers. In other words, 90% of the quality of the product comes from the starting grapes. Obtaining high quality grapes

is the result of a combination of good agronomic practices, a thorough knowledge of the phenology of the vine, and the pedo-climatic variables of the vineyard. Altogether, these factors contribute to reaching the optimum enological maturity of grapevines that relies on the delicate equilibrium between a good sugar/acidity balance (industrial maturity), an appropriate content of polyphenolic compounds (phenolic ripeness), and an adequate level of grape varietal aromas (aromatic ripeness) (**Figure 1**). Identifying this ephemeral point of optimal maturity is becoming more and more difficult because disturbances in maturity due to climate change make it impossible to set a harvesting date at which the industrial, phenolic, and aromatic maturities have reached an optimum synchronously. Broadly, higher temperatures tend to slow down or stop phenolic ripening while they accelerate the conversion of acids into sugar (Spayd *et al.*, 2002; Mira de Orduña, 2010). As a result, wines with excessive alcohol concentrations, low acidity, and undesirable palate hotness are increasingly frequent since more and more producers require harvesting grapes at higher levels of fermentable sugar to achieve typical varietal and phenolic characters (Pickering and Vanhanen, 1998; Goldner *et al.*, 2009). If we add to the climate change issue the concerns related to cardiovascular diseases caused by alcohol, taxation on alcoholic beverages, and consumer demand for full-flavored wines that are lower in ethanol, it is quite clear why the

wine sector has been looking for solutions to obtain less alcoholic and more aromatic wines over the past decades.

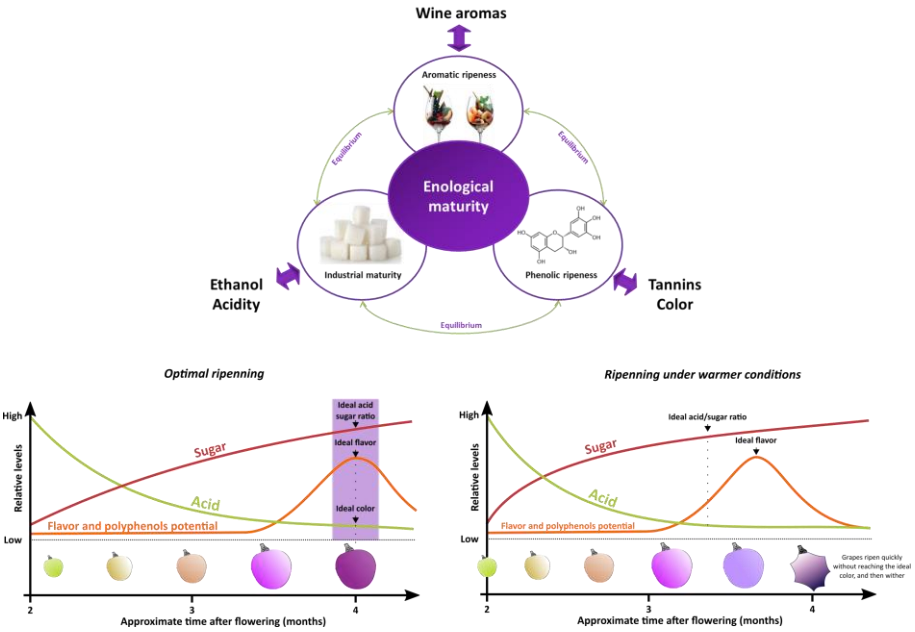

Figure 1. Diagram of the link between enological maturity, industrial maturity, aromatic ripeness, and phenolic ripeness and their sensorial component in wine. Adapted from Nicholas, (2015) and Querol *et al.* (2018).

c. Exploiting yeast diversity to meet the new expectations of wine consumers

Different approaches, targeting all steps of winemaking, have been proposed to reduce the alcohol content of wines: enzyme addition, reverse osmosis, agronomical practices, to name a few (Kontoudakis *et al.*, 2011; Schmidtke *et al.*, 2012). However, several of

these techniques have little impact on ethanol content, or the changes in the organoleptic characteristics of wine, their cost, or the difficulty of their implementation is often too important to consider them as simple and satisfactory solutions. On the contrary, the selection of yeast strains with reduced ethanol production during fermentation appeared to be a convenient, cheaper, and feasible (i.e., non-GMO approach) solution in the current wine market (Kutyna *et al.*, 2010; Contreras *et al.*, 2014; Quirós *et al.*, 2014). In this aspect, several research lines have screened yeasts for natural variants that are compromised in ethanol production. This has promoted the increasing interest of the so-called "non-conventional" strains other than *S. cerevisiae* that could respond to the current challenges of the wine industry, within but also outside the *Saccharomyces* genus (e.g., *Kluyveromyces thermotolerans*, *Metschnikowia pulcherrima*, *Pichia kluyveri*, and *Torulaspora delbrueckii*). However, the lack of competitiveness under oenological conditions of most non-*Saccharomyces* species – mainly because they do not ferment so vigorously and display lower stress resistance than *Saccharomyces* species– restricts their use mostly to mixed starter cultures or sequential fermentations with *S. cerevisiae* (Contreras *et al.*, 2015). In this way, pure starter strains of *Saccharomyces* other than *S. cerevisiae*, such as *S. uvarum* and *S. kudriavzevii*, or their interspecific hybrids with *S. cerevisiae*, have shown great enological potential in

monoculture fermentation, ultimately representing an easier and reliable alternative.

d. *S. cerevisiae* and alternative species of winemaking interest, *S. uvarum,* and *S. kudriavzevii*

The genus *Saccharomyces* belongs to the kingdom Fungi, the phylum *Ascomycota* (as the sexual reproduction is based on the formation of ascospores), the subphylum *Saccharomycotina*, the class *Saccharomycetes*, the order *Saccharomycetales,* and the family *Saccharomycetaceae*. Currently, the taxonomy of the genus *Saccharomyces* includes eight species (*S. cerevisiae*, *S. uvarum*, *S. kudriavzevii*, *S. jurei*, *S. paradoxus*, *S. eubayanus*, *S. mikatae,* and *S. arboricolus*), being *S. cerevisiae* the most widely studied member of the clade **(Figure 2).** While the eight species present relatively high genetic similarity (Borneman and Pretorius, 2014), they also manifest very different phenotypes (Salvadó *et al.*, 2011), which represent a huge potential for today's needs of winemakers. Here, we will focus on *S. cerevisiae* and the alternative species of interest for winemaking, *S. uvarum,* and *S. kudriavzevii*.

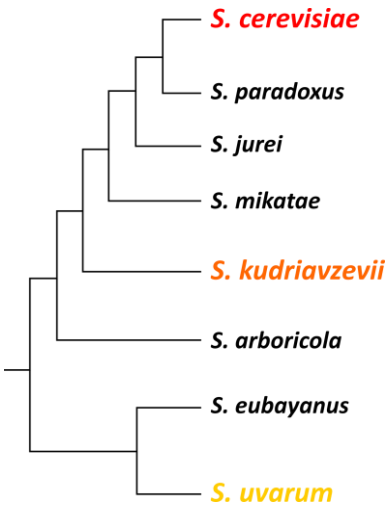

Figure 2. Schematic illustration of the *Saccharomyces* genus phylogeny.

i. *S. cerevisiae*

As mentioned earlier, *S. cerevisiae* is undoubtedly one of the most important eukaryote microorganisms in human history and scientific research. Aside from being the driving force behind the traditional elaboration of alcoholic beverages and fermented foodstuffs (e.g., wine, beer, sake, cider, and bread), it has proven to be a suitable industrial platform for the production of a large portfolio of value-added chemical building blocks, bioethanol, vaccines, and therapeutic proteins (Otero *et al.*, 2007, 2013). Moreover, several features including short cell cycle, easy and quick gene manipulations opportunity, small and compact genome, and haploid, diploid, or polyploid strains availability, to name just a few, make it a highly versatile model organism for scientific research (Petranovic and

Nielsen, 2008). For instance, many physiological processes occurring in plant and animal cells are highly similar in yeast cell. Thus, the knowledge gained in the studies of *S. cerevisiae* can further be applied to other higher eukaryotic organisms.

Besides being a widely distributed species in human-associated processes, such as winemaking, *S. cerevisiae* is also a widespread species in the wild (Wang *et al.*, 2012). In this context, the continuous isolation of new strains of *S. cerevisiae* from different origins, coupled with the development of genomic technology has enabled to perform a comprehensive survey of its population (Liti *et al.*, 2009; Almeida *et al.*, 2015; Gallone *et al.*, 2016; Legras *et al.*, 2018; Peter *et al.*, 2018). The aforementioned studies reported a complex pattern of genetic differentiation within the *S. cerevisiae* population, with different wild lineages found in Malaysia, North America, Asia, West Africa, Europe, New Zealand, Israel, and China, along with domesticated lineages as wine, beer, cheese, etc. and mosaic strains resulting from crosses between lineages. These lineages constitute genetically separated groups of *S. cerevisiae* strains which mostly differentiate according to their sources of isolation and lifestyle strategies rather than to their geographic origins (Deed and Pilkington, 2020). Actually, the wide variety of the environments from which *S. cerevisiae* isolates have been found represent a range of conditions and stressors that likely contributed to the emergence and divergence of different phenotypes (Will *et al.*, 2010; Camarasa *et al.*, 2011).

ii. *S. uvarum* and *S. kudriavzevii*

S. kudriavzevii and *S. uvarum* and their interspecific hybrids with *S. cerevisiae* – *S. cerevisiae* x *S. uvarum* and *S. cerevisiae* x *S. uvarum* – have recently been in the spotlight of the wine research because of their attractive enological properties (Peris *et al.*, 2016; Varela *et al.*, 2016; Pérez-Torrado *et al.*, 2018; Querol *et al.*, 2018). A key characteristic of these so-called cryotolerant species is their ability to grow and ferment well at low temperatures (Salvadó *et al.*, 2011), which is a suitable practice in winemaking for retention and enhancement of the flavor volatile content of wines (Molina *et al.*, 2007). Actually, fermenting at low temperatures is a procedure that has been used for white wines and "rosé" elaboration for a long time, but which use has recently regained interest because it could help to address the aforementioned demand of consumers for more aromatic beverages. However, low temperatures are also responsible for slower and sluggish fermentations when they are performed with *S. cerevisiae* (Blateyron and Sablayrolles, 2001), and that is why *S. uvarum* and *S. kudriavzevii* have appeared to be better candidates for this purpose. The cryotolerance of these species is likely to be the result of a long adaptation process to their original environments at different cellular level (Blein-Nicolas *et al.*, 2013; Paget *et al.*, 2014), as most part of the isolated strains up to date were found in cold climate areas, or in low temperature processes.

For instance, although several pure strains of *S. uvarum* have been sporadically isolated from insects, tree fluxes, or mushroom (Naumov *et al.*, 2003), this species has been mainly found in industrial environments, such as cider and wine fermentations processes (Gennadi I. Naumov *et al.*, 2000; Naumov *et al.*, 2001; Demuyter *et al.*, 2004) or even from a traditional Patagonian drink elaborated at low temperatures (Rodríguez *et al.*, 2014). On the other hand, none pure *S. kudriavzevii* isolates have been discovered yet in industrial fermentation conditions, but they have been found in natural environments, including decaying leaves in Japan (G. I. Naumov *et al.*, 2000) and European oak barks (Sampaio and Gonçalves, 2008; Lopes *et al.*, 2010). Until today, only interspecific hybrids between *S. kudriavzevii* and *S. cerevisiae* or *S. uvarum* species were encountered in industrial productions of wine, ale beer, cider, and also dietary supplements (Gonzalez *et al.*, 2007; Erny *et al.*, 2012; Peris *et al.*, 2018).

Besides their cryotolerance, these two species stand out from *S. cerevisiae* for their ability to synthesize a higher amount of valuable fermentation by-products under winemaking conditions. Glycerol, for example, is known to contribute to wine quality by providing slight sweetness, smoothness, and fullness to the wine (Goold *et al.*, 2017), and both *S. kudriavzevii* (Peris *et al.*, 2016) and *S. uvarum* (Masneuf-Pomarède *et al.*, 2010) have shown to be particularly good producers of this metabolite when compared with *S. cerevisiae*. In *S. kudriavzevii*,

this higher production of glycerol was associated with a differentiated import/efflux capacity under hyperosmotic conditions (Pérez-Torrado *et al.*, 2016). Additionally, *S. kudriavzevii* and *S. uvarum* have been characterized by their higher capability to release valuable flavor components in winemaking conditions. Several studies have highlighted that *S. uvarum* was able to release higher levels of 2-phenylethanol and 2-phenylethyl acetate, while yielding less acetic acid and less ethanol than *S. cerevisiae* without leaving residual sugars (Masneuf-Pomarède *et al.*, 2010; Gamero *et al.*, 2013; Varela *et al.*, 2016, 2017). Similarly, the positive contribution to higher alcohols and esters content of several pure strains of *S. kudriavzevii* (Peris *et al.*, 2016), as well as the beneficial impact of *S. kudriavzevii* x *S. cerevisiae* hybrids on thiols levels have been demonstrated in natural must fermentations (Swiegers *et al.*, 2009).

e. Yeast behavior during grape must fermentation

Grape must is an acidic medium whose pH can vary between 2.9 and 3.8. Its sugar content generally varies between 150 and 260 g/L in the form of an equimolar mixture of glucose and fructose. This medium also contains various sources of nitrogen in the form of amino acids and ammonium in addition to lipids, vitamins, and minerals, which are essential for yeast growth. Focusing on nitrogen sources, as in the case of sugars, their concentration in grape berries depends on vine phenology. Broadly, the concentration of amino acids increases

while that of ammonium decreases with maturity (Gutiérrez-Gamboa *et al.*, 2020). At the date of harvest, although some differences may exist due to grape varieties, vintage and agronomical practices, the amount of yeast-available nitrogen (or YAN) present in grape berries typically consists of 40% ammonium and 60% free amino acids, of which arginine, proline, and glutamine are the most abundant (Bell and Henschke, 2005).

Wine fermentation is a process traditionally conducted in batch mode, during which yeast cells are subjected to various and sequential stresses leading to a constant evolution of their metabolism. The monitoring of the fermentation activity of yeasts, in the form of the rate of CO_2 release, YAN and sugars consumption, and living cells make it possible to distinguish four successive phases during a classic fermentation: the lag phase, the exponential growth phase, the stationary phase, and the death phase (**Figure 3**).

During the lag phase, the yeasts smoothly adapt to the stress conditions (acid and osmotic stress among others) of the new grape juice with which they just came into contact after inoculation (Pérez-Torrado *et al.*, 2002). This phase can last from a few hours to several days depending on temperature conditions, oxygen availability, the quantity of inoculated yeasts, or the presence of sulfur dioxide (SO_2) used to inhibit the development of the indigenous flora in the grape must (Ribéreau-Gayon *et al.*, 2006). During this phase, the

fermentative activity is low, yeast cells consume very few nutrients, and principally synthesize the ribosomes and enzymes required in the next step (García-Ríos and Guillamón, 2019). Once cells initiate an active metabolism, DNA replication begins, and the cells divide soon after, thereby entering the second phase of the process named the exponential growth phase.

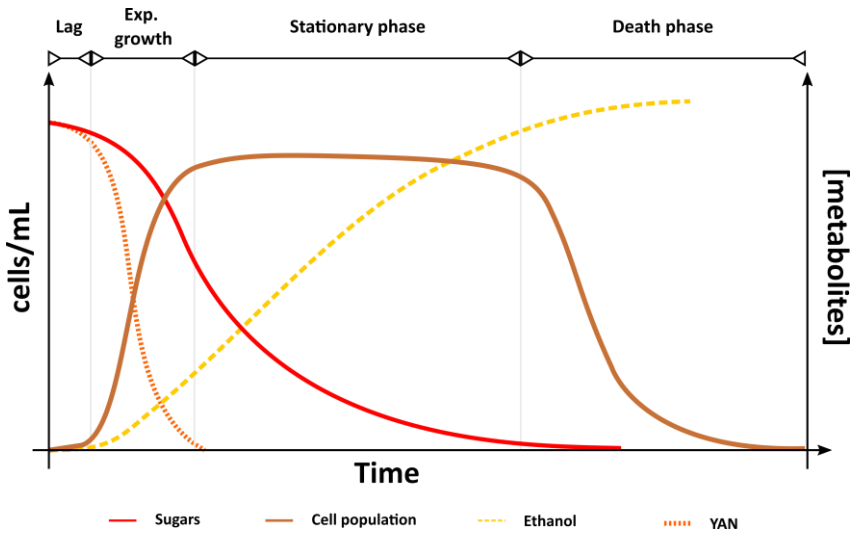

Figure 3. Schematic illustration of a typical growth in batch fermentation under winemaking conditions. Adapted from (Orozco *et al.*, 2012a).

During the growth phase, yeast cells multiply exponentially until they reach the maximum population (5 – 25x10^6 cells/mL), which highly depends on the nutrient composition of the grape must. This is the period during which cells duplicate at a maximum specific growth rate (μ_{max}). In general, growth arrest and the entry into the next so-called

stationary phase is caused by nitrogen depletion (Tesnière *et al.*, 2015), but lipid or vitamin deficiencies may also occur resulting in early growth arrest. Typically, at the end of the growth phase, about 1/3 of the total sugar has been consumed and the fermentation rate has reached its maximum.

Most of the sugar fermentation takes place during the stationary phase and the death phase, the latter being up to three times longer than the exponential growth phase. Thus, the viability and vitality of yeasts during these last two stages of fermentation are key factors for successful winemaking (Aranda *et al.*, 2019). The survival capacity of yeast cells in the stationary phase also referred to as chronological life span, is highly variable in natural isolates and commercial wine yeast strains (Orozco *et al.*, 2012a). Several metabolites, environmental factors, and nutrient-sensing/signaling pathways influence the life span during winemaking (Aranda *et al.*, 2019). During the stationary phase, nitrogen starvation stimulates autophagic processes, which in turn contribute to cell survival by recycling cell constituents, ensuring amino acids homeostasis, and maintaining energy levels (Alvers *et al.*, 2009; Huang *et al.*, 2015). Other molecular mechanisms, including glycerol synthesis, reactive oxygen species (ROS) detoxification, control of proteostasis, or the degradation of damaged proteins promote the longevity of cells (Orozco *et al.*, 2012a). On the contrary, the rising concentration of ethanol, acetate, acetaldehyde, and ROS to name just a few examples, shorten the wine yeast life span by

triggering a faster transition of the yeasts to the death phase (Orozco *et al.*, 2012b) (**Figure 3**).

II. Central carbon and nitrogen metabolisms under winemaking condition

a. What is metabolism?

As small as they are (between 5 and 10 µm), yeasts are eukaryotic unicellular organisms that do not evade the general laws of thermodynamics: they are open systems that exchange energy and matter with their environment and evolve far from equilibrium. The complex set of chemical reactions, most of which are catalyzed by specific enzymes, that contribute to maintaining the biological order of cells is known as metabolism (Nielsen, 2017). Some of these reactions are called exergonic because they are spontaneous and provide a form of chemical energy when they occur. Their Gibbs free enthalpy variation, noted ΔG, is negative. On the other hand, some of these reactions require a supply of energy to occur and are called endergonic (ΔG>0). Depending on the energy cost of the reaction (i.e., exergonic, or endergonic reaction), metabolism can be divided into catabolism and anabolism.

Catabolism refers to the set of cellular exergonic reactions in which nutrients are broken down into smaller precursor metabolites with the release of chemical energy. The chemical energy can be released in the form of adenosine triphosphate (ATP) or reduced co-factors, such as

nicotinamide adenine dinucleotide phosphate (NADPH) and reduced nicotinamide adenine dinucleotide (NADH). Remarkably, among most living organisms, only twelve precursor metabolites serve for the edification of more than 50 so-called “building blocks”, which include amino acids, fatty acids, and nucleotides (Noor *et al.*, 2010; Nielsen, 2017) (**Figure 4**).

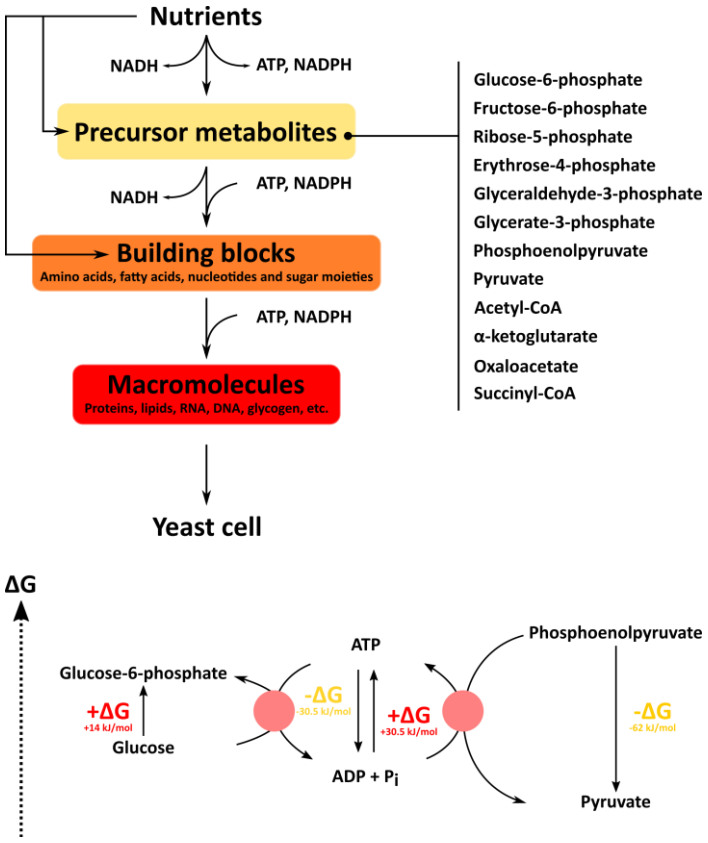

Figure 4. Above, schematic illustration of the division of metabolism with the list of the twelve precursor metabolites. Below, the principle of energetic coupling using ATP.

The chemical energy produced during the catabolism reactions is in turn used to power the endergonic reactions of anabolism. In these energy-consuming reactions, precursors metabolites are assembled into building blocks, that are further polymerized into macromolecules (e.g., proteins, lipids, and nucleic acids). When available in the extracellular pool of nutrients, the building blocks (e.g., an amino acid) can also be taken up and directly incorporated into assembling reactions (e.g., protein synthesis) of anabolism **(Figure 4).** ATP and redox co-factors play a crucial role in the metabolism network because they are at the interface between anabolism and catabolism, ultimately coupling together reactions which are in most cases parts of different pathways, and sometimes even taking place in different organelles (Bakker *et al.*, 2001). The use of an exergonic process to carry out an endergonic process is called energy coupling. For this reason, ATP and redox co-factors are often referred to as the "molecular units of currency" of intracellular energy transfer **(Figure 4)**.

The complete metabolic network involves a very wide range of compounds and chemical reactions, which may vary depending on the environmental conditions in which the system under study is found. Therefore, from now on, we will discuss the metabolism of yeast under winemaking conditions, focusing on the reactions leading to the formation of fermentative by-products such as ethanol, glycerol, or aromatic compounds. For this purpose, we will first introduce the

conversion of sugars into precursor metabolites under fermentative conditions, in which glycolysis, the Krebs cycle, and the pentose phosphate pathway are key biosynthetic pathways. In a second step, we will present nitrogen metabolism in winemaking conditions, which plays an important role as an interface between anabolism and cellular catabolism.

b. Fermentative metabolism

Yeasts of the genus *Saccharomyces* are facultative anaerobic microorganisms. In other words, they can grow by implementing a fermentative metabolism, which results in the reduction of sugars to ethanol, or a respiratory metabolism, which uses oxygen as the final electron acceptor in the respiratory chain of mitochondria (**Figure 5**). However, *S. cerevisiae* and other *Saccharomyces* species are also unique among yeasts in being able to restrict energy-efficient respiration in favor of fermentation, with lower energy efficiency, when glucose levels exceed 0.1% (w/v), and even in the presence of oxygen (De Deken, 1966). Owing to the sugar levels present in grape juice, this so-called “Crabtree” phenomenon leads the metabolism of *Saccharomyces* yeasts to be fermentative in winemaking conditions. In this aspect, one interesting hypothesis explains this energetically inefficient mechanism as a tool of *Saccharomyces* to out-compete other microorganisms in natural habitats through the antiseptic effect of ethanol (Piškur *et al.*, 2006). Under fermentative conditions, three

metabolic pathways, constituting the main central carbon metabolism, participate in the supply of the twelve precursor metabolites to the cell: the glycolytic pathway (also called Embden-Meyerhof-Parnas or EMP pathway), the Krebs cycle (also named tricarboxylic acid cycle or TCA), and the pentose phosphate pathway (or PPP) (**Figure 6**).

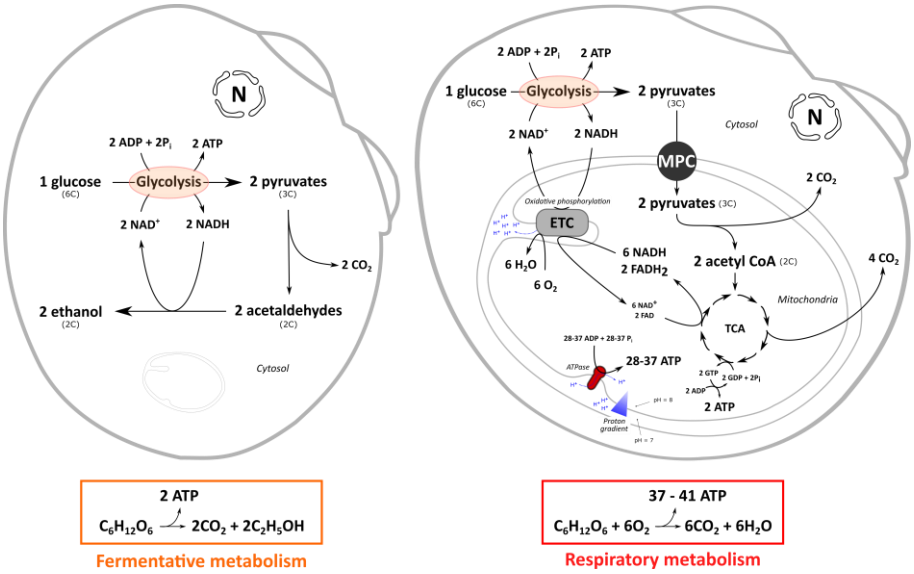

Figure 5. Comparison between fermentative and respiratory metabolisms.

In fermentative conditions, once inside the cell, the catabolism of sugars through central carbon metabolism initiates via the EMP pathway. One molecule of glucose catabolized through the EMP pathway in the cytosol results in the net formation of two molecules of pyruvate, two molecules of ATP, and two NADH (**Figure 5**). Contrary

to respiratory metabolism, the pyruvate formed through the EMP pathway is not shuttled through mitochondria but is decarboxylated inside the cytosol by pyruvate decarboxylase encoded by *PDC1* (major isoform), *PDC5,* and *PDC6* (minor isoforms) (Hohmann, 1991) (**Figure 5**). It results in the net formation of one carbon dioxide and one acetaldehyde per pyruvate molecule. Finally, acetaldehyde is reduced to ethanol by NADH-dependent alcohol dehydrogenase (*ADH1*, *ADH2*, *ADH3*, *ADH4,* and *ADH5*) yielding one molecule of ethanol and one oxidized co-factor NAD^+ per acetaldehyde. The NAD^+ formed in the latter reaction enables to newly supply glycolysis with this oxidized co-factor, which is why fermentation is said to be redox neutral. In summary, in anaerobic conditions or when sugar levels exceed 0.1% (w/v) alcoholic fermentation equation is:

$$\mathbf{C_6H_{12}O_6 \rightarrow 2CO_2 + 2C_2H_5OH\ (2\ ATP)}$$

The energy yielded by fermentation is much lower than by respiratory metabolism (**Figure 5**). Indeed, during fermentative metabolism, the energy necessary for cell growth and maintenance (ATP and reduced cofactors) is produced exclusively via the EMP pathway, because several mitochondrial enzymes of the electron transport chain and the TCA pathway are not active or are repressed by glucose (Kwast *et al.*, 1998; Camarasa *et al.*, 2003). According to the above equation, the theoretical conversion yield is therefore 0.51 grams of ethanol per gram of sugar consumed. However, in practice, about 8 to 10% of the

sugar is directed toward the synthesis of anabolic precursors required for biomass production and maintenance of the redox homeostasis within the cell (Albers *et al.*, 1998), which is why this conversion is closer to 0.47 grams of ethanol per gram of sugar. Some of these by-products are excreted outside the cell, the most abundant being glycerol, succinate, acetate, and pyruvate (**Figure 6**).

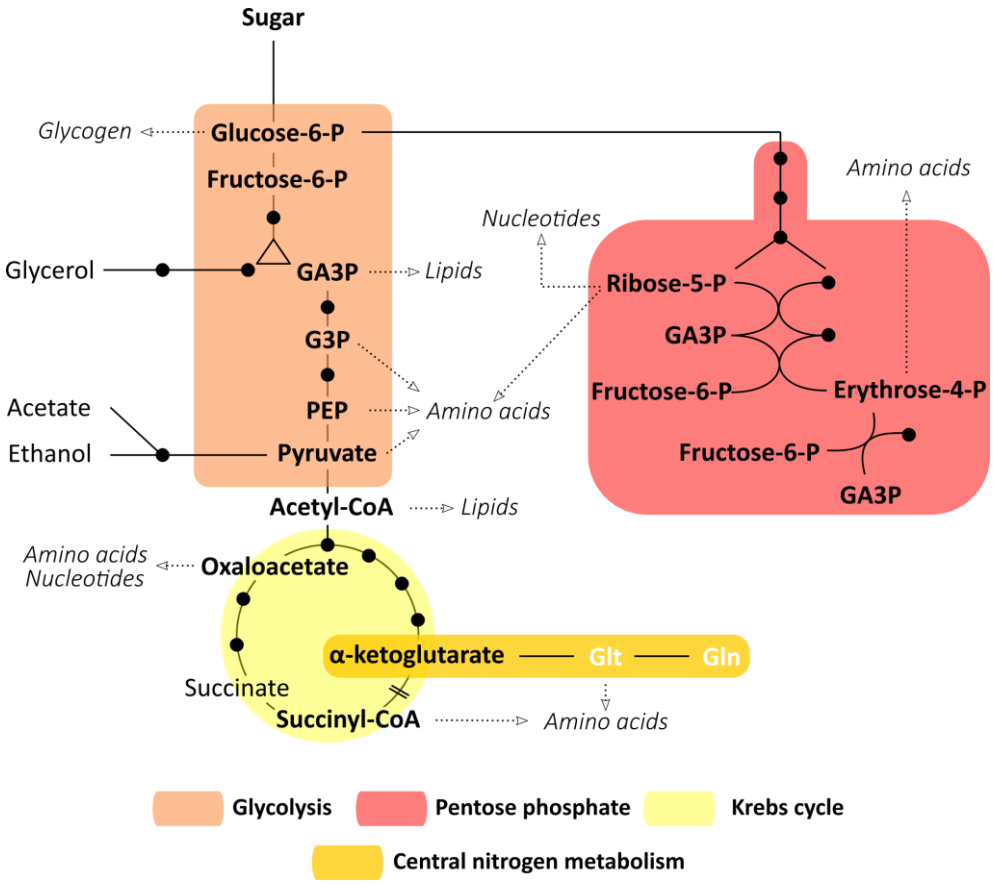

Figure 6. Diagram of central carbon metabolism in fermentative conditions, and its connection with central nitrogen metabolism at the level of α-

ketoglutarate. The twelve precursors metabolites are written in bold while the building blocks and macromolecules proceeding from these precursors are indicated in italics. Relevant fermentative by-products, including ethanol, acetate, glycerol, and succinate, are also presented. Abbreviations: GA3P (glyceraldehyde-3-phosphate), G3P (glycerate-3-phosphate), PEP (phosphoenolpyruvate).

If we include acetyl CoA, the catabolism of hexoses via glycolysis provides seven of the twelve precursor metabolites described above. The other precursors are produced by the two other key metabolic pathways of central carbon metabolism. On the one hand, the Krebs cycle which takes place in the mitochondria provides the cell, from the degradation of pyruvate and/or acetyl CoA, with α-ketoglutarate, oxaloacetate, and succinyl-CoA, required for the synthesis of amino acids and the prosthetic group heme (Noor *et al.*, 2010) (**Figure 6**). In winemaking conditions, the Krebs cycle is interrupted at the level of the succinate dehydrogenase complex due to glucose repression and does not operate as a cycle, but in a branched manner. One branch is oxidative, leading to α-ketoglutarate formation, whereas the other is reductive, leading to succinate formation via fumarate reductase (Gombert and Moreira, 2001; Camarasa *et al.*, 2003; Camarasa, 2007). On the other hand, part of the glycolysis flux can be diverted to the pentose phosphate pathway, which supplies the cell with erythrose-4-phosphate and ribose-5-phosphate, precursors of aromatic amino acids and nucleotides, respectively. Besides, the oxidative branch of

the PPP generates most of the reducing power in the form of NADPH necessary for anabolism reactions (Cadière *et al.*, 2011). It also plays an important role in the defense of yeast cells from oxidative stress, as NADPH is an essential cofactor for glutathione- and thioredoxin-dependent enzymes that protect cells from oxidative damage (Grant, 2001).

c. Nitrogen metabolism in winemaking

i. Amino acid catabolism

As explained above, amino acids are important building blocks that participate in macromolecules edification, like proteins. Thus, once internalized, one fate of exogenous amino acids can be their direct incorporation into proteins. Otherwise, according to their concentrations and the anabolic needs of the cell, amino acids can be catabolized or transiently stored inside the yeast vacuoles (Crépin *et al.*, 2017) (**Figure 7**).

The catabolism of amino acids consists in their cleavage to release their amino group according to one of the two following reactions. The most common reaction is the transfer of the amino group onto α-ketoglutarate to form glutamate, and which is catalyzed by aminotransferases or transaminases (1). On the other hand, some amino acids, such as serine and threonine which possess a hydroxyl group on their β carbon, can be directly deaminated by dehydration.

In this case, a dehydratase catalyzes this reaction, producing the corresponding keto acid and ammonium (2).

(1) amino acid + α-ketoglutarate → keto acid + glutamate

(2) amino acid + H_2O + oxidized cofactor → keto acid + NH_4^+ + reduced cofactor

The glutamate and ammonium produced in the above reactions join the central nitrogen metabolism. Regarding the released keto acid in reactions (1) and (2), two subcategories can be identified depending on the metabolic fate of the deaminated carbon skeleton. For some amino acids, such as alanine, aspartate, or GABA to name a few one, their corresponding keto acids can be fed into central carbon metabolism as pyruvate, oxaloacetate, and succinate. Arginine represents a special case within amino acids. Arginine metabolism initiates by a cleavage reaction, catalyzed by arginase, yielding the non-proteinogenic amino acid ornithine and urea. Further catabolism of ornithine is possible via proline, which is transformed into glutamate in two reactions steps occurring in the mitochondria. These reactions are catalyzed by proline oxidase and delta 1-pyrroline-5-carboxylate dehydrogenase, which are encoded by genes *PUT1* and *PUT2*. However, because *PUT1* is strongly downregulated under anaerobic conditions, proline cannot be used as a nitrogen source in winemaking conditions (Wang and Brandriss, 1987). Finally, for branched chain amino acids (valine, leucine, and isoleucine), aromatic

amino acids (phenylalanine, tyrosine, and tryptophan), sulfur-containing amino acid methionine, and threonine, the remaining carbon skeleton can continue to be catabolized in the Ehrlich pathway (**see details below**).

ii. Central nitrogen metabolism and anabolism of amino acids

In *S. cerevisiae*, the conversion of all nitrogen sources involves α-ketoglutarate, ammonium, glutamate and/or glutamine, which constitute the central nitrogen metabolism (Magasanik, 2003). These metabolites represent a key node at the interface between anabolism and catabolism of nitrogen, and a strong link with central carbon metabolism since α-ketoglutarate is generated at the level of the Krebs cycle (**Figure 7**). The central nitrogen metabolism can be summarized by four catalyzed reactions, involving five enzymes. The conversion of α-ketoglutarate to glutamate is reversible and is achieved by the three glutamate iso-enzymes, namely Gdh1p, Gdh2p, and Gdh3p (Miller and Magasanik, 1990; Avendano *et al.*, 1997). Gdh1p and Gdh3p are NADPH-dependent and are responsible for glutamate production while Gdh2p, which is NAD-dependent, catalyzes the reverse reaction. Glutamate can also associate with ammonium to form glutamine in a reaction catalyzed by Gln1p-dependent ATP glutamine synthetase (Magasanik, 2003). Finally, glutamate synthetase (GOGAT, encoded by *GLT1*) allows the formation of two glutamate molecules from

glutamine and α-ketoglutarate (Magasanik and Kaiser, 2002) (**Figure 7**).

These four reactions regulate intracellular levels of glutamate and glutamine, which play the role of amino group donor in the further transamination reactions of amino acid anabolism. Broadly, around 85% of total cellular nitrogen is provided via glutamate and the remaining 15% is derived from glutamine (Ljungdahl and Daignan-Fornier, 2012). In this way, *S. cerevisiae* can synthesize all amino acids from an amino group donor and different carbon precursors. When amino acids are *de novo* synthesized, the carbon precursor is provided by sugar catabolism. Otherwise, the carbon skeleton can come from exogenous amino acid catabolism. Depending on the carbon precursor from which they are derived, amino acids can be grouped into different families (Ljungdahl and Daignan-Fornier, 2012):

- α-ketoglutarate: glutamate, glutamine, arginine, proline, and lysine
- pyruvate: alanine, leucine, isoleucine, and valine
- oxaloacetate: aspartate, asparagine, threonine, cysteine, and methionine
- phosphoenolpyruvate: phenylalanine, tyrosine, and tryptophane
- glycerate-3-phosphate: serine, glycine, cysteine, and methionine
- ribose-5-phosphate: histidine

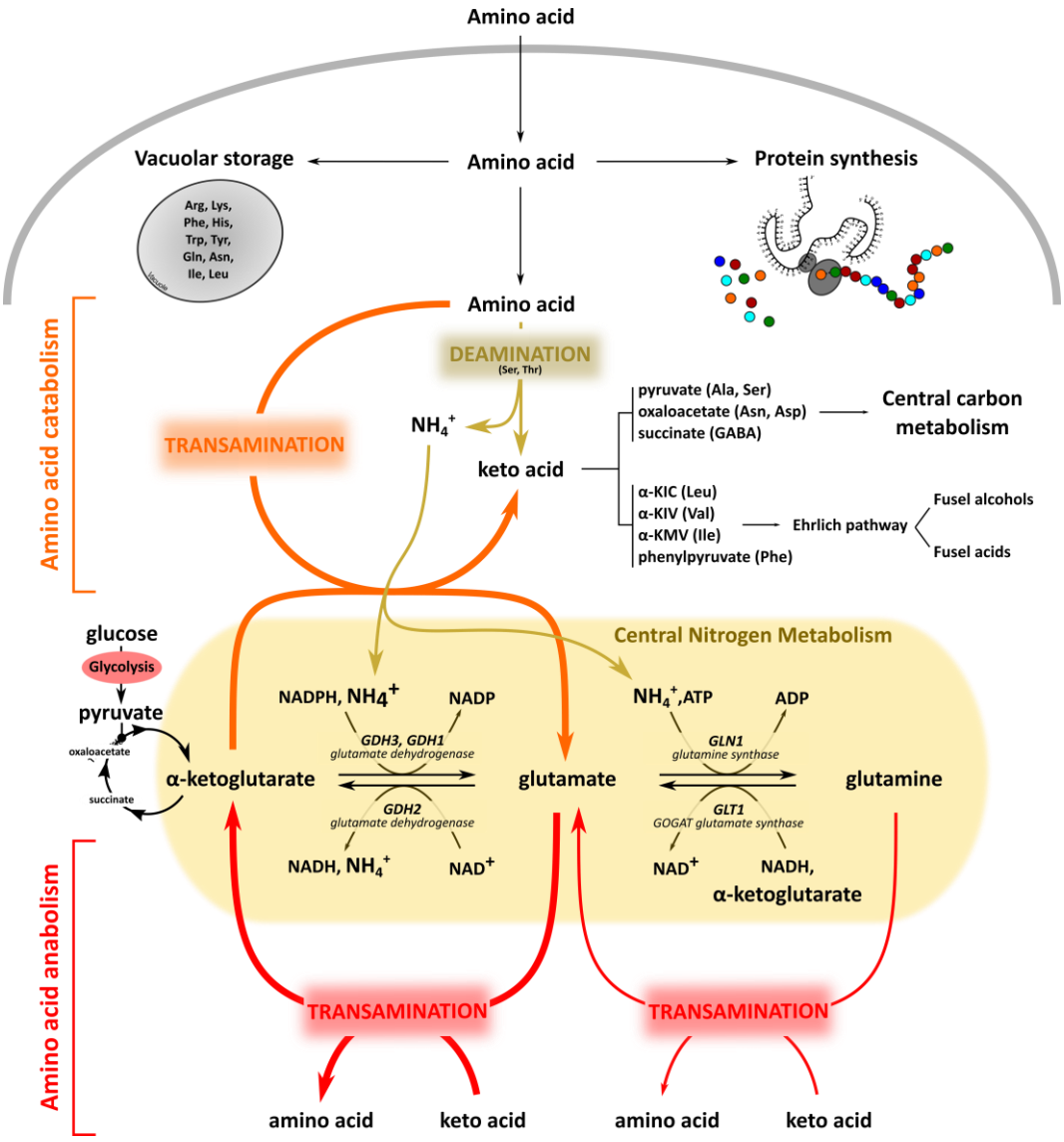

Figure 7. Schematic representation of the fate of exogenous amino acids once incorporated by yeast. Exogenous amino acid can be directly incorporated into proteins, stored inside the vacuoles, or catabolized and directed toward central nitrogen metabolism. Abbreviations: α-KIC (α-ketoisocaproate), α-KIV (α-ketoisovalerate), α-KMV (α-ketomethylvalerate).

d. Metabolism of wine aromas

During alcoholic fermentation, yeasts produce a broad range of aroma-active substances which derive from the metabolism of carbon, nitrogen, or both at the same time. Among them, we will present in this section the metabolic reactions leading to the formation of fusel alcohols, fusel acids, acetate esters, and ethyl esters which play a determinant role in the aroma complexity of wine (Saerens *et al.*, 2010; Belda *et al.*, 2017).

The metabolic pathway involved in the formation of fusel alcohols and fusel acids is known as the Ehrlich pathway (Hazelwood *et al.*, 2008). It involves three enzyme-catalyzed reactions: transamination, decarboxylation, and reduction (fusel alcohol) or oxidation (fusel acid) (**Figure 8**). The starting substrate of this metabolic pathway can be an amino acid or its respective keto acid. Therefore, a fraction of the fusel alcohols and acids formed by the Ehrlich pathway can come from the catabolism of exogenous amino acids, and another fraction from *de novo* keto acids synthesized by the central carbon metabolism. In fact, in *S. cerevisiae* the central carbon metabolism provides most of the carbon skeletons for the biosynthesis of these volatile compounds through the Ehrlich pathway, while the contribution of keto acids derived from the catabolism of exogenous amino acids remains low (Crépin *et al.*, 2017). It should also be noted that the final step of the Ehrlich pathway, i.e. the aldehyde conversion to fusel alcohol

(oxidation) or fusel acid (reduction) involves the redox cofactors $NADH/NAD^+$ (**Figure 8**). Therefore, which of these two reactions occurs is thought to depend on the redox status of the cells and reflects the sensitivity of the Ehrlich pathway towards perturbations in cellular redox homeostasis (Styger *et al.*, 2011).

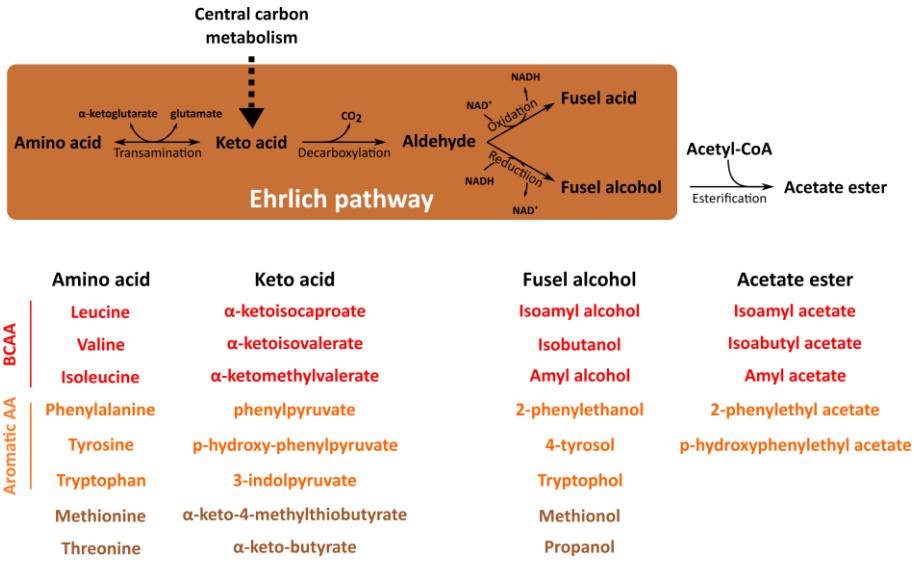

Figure 8. Diagram of the reactions contributing to the formation of fusel acids and fusel alcohols in the Ehrlich pathway. The esterification leading to acetate ester formation from fusel alcohol is also indicated. Below, the amino acids and keto acid precursors of the most relevant fusel alcohols and acetate esters in wine are indicated.

Both, fusel acids and fusel alcohols have direct impacts on the aroma of wine, the latter also often being precursors to the formation of another important family of wine aromas: acetate esters. Indeed,

acetyl-CoA can react with a fusel alcohol to yield the respective acetate ester in an esterification reaction mediated by alcohol acetyltransferases (Saerens *et al.*, 2010) (**Figure 8**).

Besides acetate esters, ethyl esters are other aroma-active esters produced by *S. cerevisiae* during the fermentation with relevant sensory properties for wine. They are the results of the enzyme-catalyzed esterification between ethanol and acyl-CoA compounds. In *S. cerevisiae*, the ethyl ester formation has been attributed to two acyl-CoA: ethanol O-acyltransferases encoded by the *EEB1* and *EHT1* genes (Saerens *et al.*, 2010). The major ethyl esters are ethyl hexanoate, ethyl octanoate, and ethyl decanoate (**Table 1**).

Table 1: List of the most significant higher alcohols, acetate esters, and ethyl esters produced by yeast during fermentation (adapted from (Lambrechts and Pretorius, 2000)).

Class	Compound	Descriptor
Fusel alcohols	Isoamyl alcohol	Marzipan
	Isobutanol	Alcoholic
	Amyl alcohol	Marzipan
	Propanol	Stupefying
	2-phenylethanol	Rose, floral
	4-tyrosol	Honey, bees wax
	Tryptophol	
	Methionol	
Acetate esters	Isoamyl acetate	Banana
	Isobutyl acetate	Fruity
	Amyl acetate	Banana
	2-phenylethyl acetate	Rose, fruity, flowery
	p-hydroxyphenylethyl acetate	Floral
Ethyl esters	Ethyl butanoate	Floral, fruity
	Ethyl hexanoate	Violets, apple
	Ethyl octanoate	Pear, pineapple
	Ethyl decanoate	Floral
	Ethyl acetate	Nail polish, fruity

III. Omics technologies and genome-scale modeling for the study of yeast metabolism

In the previous sections, we have seen that the reactions that make up the central carbon and nitrogen metabolisms in yeast are numerous and highly connected. Even if CCM and CNM only entail a small part of the vast and complex yeast metabolic network, they are key to understand yeast phenotypes in a complex biological process, like wine fermentation. However, one intuitively realized that to deeply understand physiological and metabolic variations between yeast species in winemaking conditions, like the one existing between *S. cerevisiae*, *S. uvarum,* and *S. kudriavzevii*, it is necessary to use several levels of analysis.

a. Omics technologies

High-throughput techniques also referred as “omics”, are suitable for observing and quantifying complex cellular behaviors. In the last decades, their advent has made it possible to integrate them into the daily methodology of scientific investigation, particularly in the field of biomedicine (Hasin *et al.*, 2017), but also in applied sciences as wine research even though their use is still emerging (Sirén *et al.*, 2019). Remarkably, among the firsts omics disciplines to be introduced, genomics, which focuses on the study of entire genomes, led to a dramatic transformation in yeast research because the first complete sequence of a eukaryotic genome to be obtained was that

of *S. cerevisiae* (Goffeau *et al.*, 1996). Nowadays, large amounts of sequences and annotated genomes of *Saccharomyces* isolates are available, mostly of *S. cerevisiae* (Peter *et al.*, 2018), but also of *S. uvarum* and *S. kudriavzevii* strains (Hittinger *et al.*, 2010; Scannell *et al.*, 2011), which are notably the basis for genome-wide modeling of metabolism (**see next section**). Besides genomics, other omics technologies like metabolomics, transcriptomics, proteomics, and flux analysis, among others, are relevant. These technologies can be used separately or, because their complementary nature, they can be combined into a multi-omics perspective to get a more detailed understanding of complex processes and networks, like yeast metabolism in winemaking conditions.

In this aspect, several single and multi-omics studies have successfully been applied to *S. cerevisiae*, and more specifically to *S. cerevisiae* wine strains. Transcriptome profiles have been obtained at different steps of wine fermentation (Rossignol *et al.*, 2003; Varela *et al.*, 2005; Marks *et al.*, 2008; Rossouw and Bauer, 2009), and under very different environmental conditions, including high sugar concentration (Erasmus *et al.*, 2003), nitrogen content (Backhus *et al.*, 2001; Marks *et al.*, 2003; Mendes-Ferreira *et al.*, 2007), oxygen concentration (Aceituno *et al.*, 2012; Orellana *et al.*, 2014) and fermentation temperature (Beltran *et al.*, 2006; Pizarro *et al.*, 2008).

Table 2: Glossary of the most common omics technologies used in the wine research

Omics name	Objectives	Target	Analytical technique(s)
Genomics	Comprehensive study of the interactions and functional dynamics of whole sets of genes and their products	DNA	Next Generation Sequencing (NGS)
Transcriptomics	Measurement of total mRNA expression levels in one or a population of biological cells for a given set of environmental conditions	Total RNA and mRNA	NGS/RNAseq
Proteomics	Identification and/or quantification of proteins expressed in a target matrix	Proteins	Liquid chromatography coupled with mass spectrometry
Metabolomics	Identification and/or quantification of metabolites using targeted and non-targeted analysis of chemical compounds in a target matrix	Metabolites	Liquid and gas chromatography, often coupled with mass spectrometry
Fluxomics	Study of the set of fluxes that are measured or calculated in a given metabolic reaction network	Flux	^{13}C-Fluxomics, Flux Balance Analysis (FBA)

Similarly, several studies have focused on deciphering proteome variations across alcoholic fermentation (Salvadó *et al.*, 2008; Rossignol *et al.*, 2009; Blein-Nicolas *et al.*, 2013), at low fermentation temperature or, more recently, the proteome of extracellular vesicles (Mencher *et al.*, 2020). Among the metabolomic studies, the realization of fermentation on isotopically labeled substrates has allowed unveiling some specificities of the metabolism in *S. cerevisiae*. Besides a better characterization of sequential nitrogen source assimilation during yeast fermentation, this technique has enabled the quantification of nitrogenous sources redistribution within the central carbon and nitrogen metabolism networks in *S. cerevisiae*, and in particular the contribution of individual nitrogen sources to protein and volatile compounds synthesis under different nutrient conditions (Crépin *et al.*, 2017; Rollero *et al.*, 2017).

Although these studies using a single omics technique have provided interesting information on some of the intricate behaviors of *S. cerevisiae*, it appears that the combination of omics data has generally provided a better understanding of yeast physiology and metabolic network in winemaking. For instance, the potential role of the sulfur assimilation pathway in adaptation at low temperature of *S. cerevisiae* was unveiled by comparing transcriptomic, proteomic, and genomic changes in two commercial wine strains (García-Ríos *et al.*, 2014), while dual metabolomics and transcriptomics data analysis enabled the characterization of genes involved in wine aromas metabolism

(Mendes *et al.*, 2017). The combination of isotopic filiation experiments with RNA sequencing has also proven to be suitable to correlate the transcription profile of nitrogen associated genes with flux redistribution of amino acids in the metabolic network of *Kluyveromyces marxianus* and *S. cerevisiae* (Rollero *et al.*, 2019). Finally, other good examples of the potential of the combined omics approach are those performed to study the physiological changes occurring in a modified yeast strain to produce low ethanol levels during alcoholic fermentation (Varela *et al.*, 2018), and to unveil regulation mechanisms involved in the control of NADPH homeostasis in *S. cerevisiae* (Celton *et al.*, 2012).

On the contrary, despite their potential in oenology, there are still few studies of this kind that have been applied to *S. uvarum* and *S. kudriavzevii* species. Only some aspects of *S. kudriavzevii* and *S. uvarum* have been highlighted to their cold resistance and winemaking characteristics using genomic (Macías *et al.*, 2019), transcriptomic (Beltran *et al.*, 2006; Gamero *et al.*, 2014; Tronchoni *et al.*, 2014), or metabolomic approaches (López-Malo *et al.*, 2013).

b. Genome-scale modeling approach

Omics data can also be interpreted in the context of systems biology which consists of the transformation of typically large-scale data sets (e.g. metabolomic data), into *in silico* models that provide

both interpretation and prediction of the behavior of a system (Nielsen, 2017).

A typical first step in the modeling approach is to reconstruct the metabolic network of the system under study based on a thorough literature examination, including biochemistry textbooks, online databases, and the annotated genome sequences. In the early 2000s, and largely due to the advancement of genomics, large-scale metabolic networks, also called genome-scale metabolic models (GEMs), of multiple model organisms were reconstructed, including *S. cerevisiae* (Förster *et al.*, 2003). The metabolic network is represented mathematically in the form of a matrix (S) in which appear the various stoichiometric coefficients of all the reactions that build it (**Figure 9**). Once the metabolic network is reconstructed, mathematical and computational analysis can be applied to simulate cellular behavior under different genetic and physiological conditions.

Among these computational methods, Flux Balance Analysis (FBA), a constraint-based approach, is one of the most widely used in the design of bio-processes (Park *et al.*, 2009; Orth *et al.*, 2010). FBA is a modeling concept that was first used in the mid-1970s for the analysis of citric production using a reduced metabolic network (Aiba and Matsuoka, 1979). More recently, several research groups extended this concept further to GEMs, i.e. genome-wide metabolic networks, in *Escherichia coli* (Feist *et al.*, 2007), *Staphylococcus aureus*

(Heinemann *et al.*, 2005), Human (Duarte *et al.*, 2007), and *S. cerevisiae* (Duarte *et al.*, 2004), to give some examples.

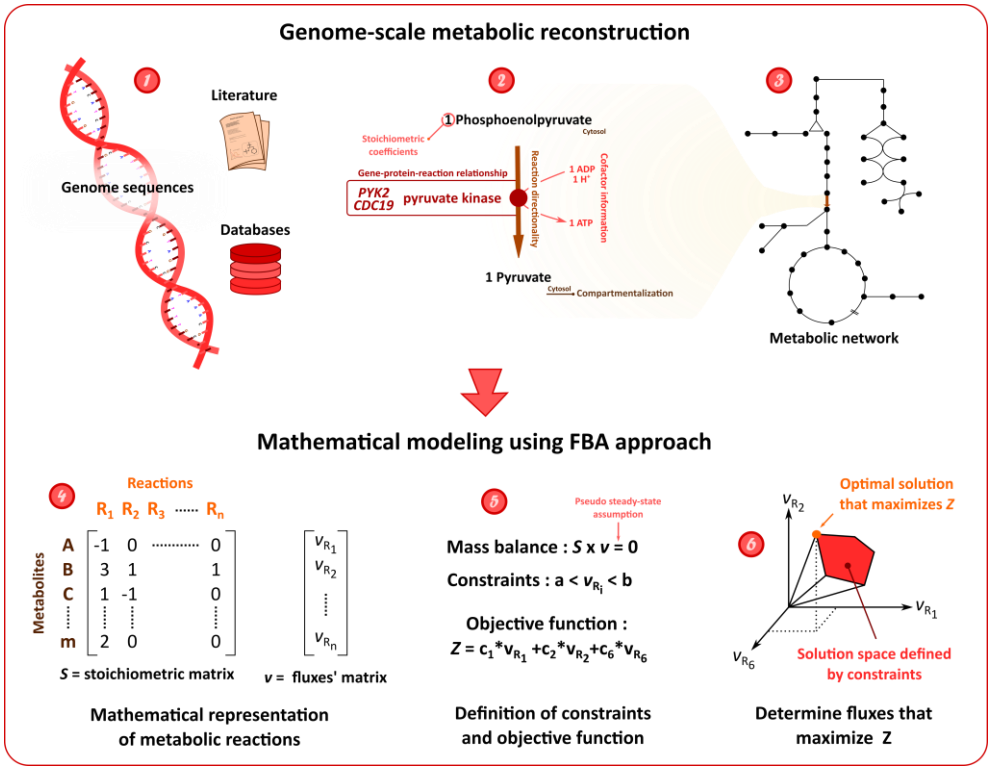

Figure 9. Diagram of the steps of genome-scale metabolic network reconstruction (steps 1, 2, and 3) and mathematical modeling using the flux balance analysis approach (steps 4, 5, and 6).

FBA is based on the balancing of metabolic fluxes around each of the metabolites in a considered network, which results in a set of constraints on metabolic fluxes (Orth *et al.*, 2010). The corresponding set of equations can be solved using a linear optimization procedure

that assumes a cellular objective, typically the growth rate maximization, and enables the calculation of metabolic fluxes from reactions' stoichiometry and intracellular metabolites' mass balances (Orth *et al.*, 2010). This modeling approach has been widely used for the analysis of metabolism and the metabolic engineering of *S. cerevisiae* strains in continuous fermentations (Österlund *et al.*, 2012), during which the cells are in a metabolic steady state, i.e. the concentrations of all metabolites, substrates and culture variables (pH, temperature and oxygen availability) are constant in time. On the contrary, their use to predict batch fermentation where yeast metabolism undergoes a series of adaptive changes in response to the continuous environmental variations is still scarce.

The first application of FBA to represent anaerobic batch fermentation with *S. cerevisiae*, comprising a reduced stoichiometric network, dates back to 2003 (Sainz *et al.*, 2003). Thereafter, several improvements were introduced to the latter procedure, including sugar kinetics consideration (Pizarro *et al.*, 2007), expansion to genome-scale (Vargas *et al.*, 2011), optimization of model parameters prediction, and reduction of computational complexity (Sánchez *et al.*, 2014). However, the development of an integrative modeling approach that describes the different phases of batch processes (i.e. lag, exponential growth, stationary, and decay phases), considers carbon and nitrogen metabolism throughout time and explains secondary metabolites' production is still required. For instance, important fusel alcohols,

ethyl esters, and acetate esters are lacking in the last consensus genome-scale reconstruction available of *S. cerevisiae* (Lu *et al.*, 2019).

Besides *S. cerevisiae*, genome-scale models have successfully been applied to other species of biotechnological interest, such as the methylotrophic *Pichia pastoris* (Irani *et al.*, 2016; Saitua *et al.*, 2017), or co-cultures of *Scheffersomyces stipitis* and *S. cerevisiae* (Hanly and Henson, 2013). On the contrary, little is known about the flux dynamics of *S. uvarum* and *S. kudriavzevii* under oenological conditions. Thus, the development and application of genome-scale FBA models to *S. uvarum* and *S. kudriavzevii*, including a detailed secondary metabolites' framework, could bring novel insights into how these species achieve wine fermentation and why they differ from *S. cerevisiae* in wine aroma production.

Aceituno, F.F., Orellana, M., Torres, J., Mendoza, S., Slater, A.W., Melo, F., and Agosin, E. (2012) Oxygen response of the wine yeast *Saccharomyces cerevisiae* EC1118 grown under Carbon-Sufficient, nitrogen-limited enological conditions. *Appl Environ Microbiol* **78**: 8340–8352.

Aiba, S. and Matsuoka, M. (1979) Identification of metabolic model: Citrate production from glucose by *Candida lipolytica. Biotechnol Bioeng* **21**: 1373–1386.

Albers, E., Liden, G., Larsson, C., and Gustafsson, L. (1998) Anaerobic redox balance and nitrogen metabolism in *Saccharomyces cerevisiae*. *Recent Res Dev Microbiol* **2**: 253–279.

Almeida, P., Barbosa, R., Zalar, P., Imanishi, Y., Shimizu, K., Turchetti, B., et al. (2015) A population genomics insight into the Mediterranean origins of wine yeast domestication. *Mol Ecol* **24**: 5412–5427.

Alvers, A.L., Fishwick, L.K., Wood, M.S., Hu, D., Chung, H.S., Dunn, W.A., and Aris, J.P. (2009) Autophagy and amino acid homeostasis are required for chronological longevity in *Saccharomyces cerevisiae*. *Aging Cell* **8**: 353–369.

Aranda, A., Orozco, H., Picazo, C., and Matallana, E. (2019) Yeast life span and its impact on food fermentations. *Fermentation* **5**: 37.

Avendano, A., Deluna, A., Olivera, H., Valenzuela, L., and Gonzalez, A. (1997) GDH3 encodes a glutamate dehydrogenase isozyme, a previously unrecognized route for glutamate biosynthesis in *Saccharomyces cerevisiae*. *J Bacteriol* **179**: 5594–5597.

Backhus, L.E., DeRisi, J., Brown, P.O., and Bisson, L.F. (2001) Functional genomic analysis of a commercial wine strain of *Saccharomyces cerevisiae* under differing nitrogen conditions. *FEMS Yeast Res* **1**: 111–125.

Bakker, B.M., Overkamp, K.M., Van Maris, A.J.A., Kötter, P., Luttik, M.A.H., Van Dijken, J.P., and Pronk, J.T. (2001) Stoichiometry

and compartmentation of NADH metabolism in *Saccharomyces cerevisiae*. *FEMS Microbiol Rev* **25**: 15–37.

Barnett, J.A. (2000) A history of research on yeasts 2: Louis Pasteur and his contemporaries, 1850-1880. *Yeast* **16**: 755–771.

Belda, I., Ruiz, J., Esteban-Fernández, A., Navascués, E., Marquina, D., Santos, A., and Moreno-Arribas, M.V. (2017) Microbial contribution to Wine aroma and its intended use for Wine quality improvement. *Molecules* **22**: 1–29.

Bell, S.J. and Henschke, P.A. (2005) Implications of nitrogen nutrition for grapes, fermentation and wine. *Aust J Grape Wine Res* **11**: 242–295.

Beltran, G., Novo, M., Leberre, V., Sokol, S., Labourdette, D., Guillamon, J.M., et al. (2006) Integration of transcriptomic and metabolic analyses for understanding the global responses of low-temperature winemaking fermentations. *FEMS Yeast Res* **6**: 1167–1183.

Blateyron, L. and Sablayrolles, J.M. (2001) Stuck and slow fermentations in enology: Statistical study of causes and effectiveness of combined additions of oxygen and diammonium phosphate. *J Biosci Bioeng* **91**: 184–189.

Blein-Nicolas, M., Albertin, W., Valot, B., Marullo, P., Sicard, D., Giraud, C., et al. (2013) Yeast proteome variations reveal different adaptive responses to grape must fermentation. *Mol Biol Evol* **30**: 1368–1383.

Borneman, A.R. and Pretorius, I.S. (2014) Genomic insights into the *Saccharomyces* sensu stricto complex. *Genetics* **199**: 281–291.

Cadière, A., Ortiz-Julien, A., Camarasa, C., and Dequin, S. (2011) Evolutionary engineered *Saccharomyces cerevisiae* wine yeast strains with increased in vivo flux through the pentose phosphate pathway. *Metab Eng* **13**: 263–271.

Camarasa, C. (2007) Role in anaerobiosis of the isoenzymes for *Saccharomyces cerevisiae* fumarate reductase encoded by OSM1 and FRDS1. *Yeast* **26**: 545–551.

Camarasa, C., Grivet, J.P., and Dequin, S. (2003) Investigation by 13C-NMR and tricarboxylic acid (TCA) deletion mutant analysis of pathways of succinate formation in *Saccharomyces cerevisiae* during anaerobic fermentation. *Microbiology* **149**: 2669–2678.

Camarasa, C., Sanchez, I., Brial, P., Bigey, F., and Dequin, S. (2011) Phenotypic landscape of *Saccharomyces cerevisiae* during wine fermentation: Evidence for origin-dependent metabolic traits. *PLoS One* **6**: e25147.

Cavalieri, D., McGovern, P.E., Hartl, D.L., Mortimer, R., and Polsinelli, M. (2003) Evidence for *S. cerevisiae* Fermentation in Ancient Wine. In, *Journal of Molecular Evolution*.

Celton, M., Sanchez, I., Goelzer, A., Fromion, V., Camarasa, C., and Dequin, S. (2012) A comparative transcriptomic, fluxomic and metabolomic analysis of the response of *Saccharomyces cerevisiae* to increases in NADPH oxidation. *BMC Genomics* **13**: 317.

Contreras, A., Hidalgo, C., Henschke, P.A., Chambers, P.J., Curtin, C., and Varela, C. (2014) Evaluation of Non-*Saccharomyces* Yeasts for the Reduction of Alcohol Content in Wine. *Appl Environ Microbiol* **80**: 1670–1678.

Contreras, A., Hidalgo, C., Schmidt, S., Henschke, P.A., Curtin, C., and Varela, C. (2015) The application of non-*Saccharomyces* yeast in fermentations with limited aeration as a strategy for the production of wine with reduced alcohol content. *Int J Food Microbiol* **205**: 7–15.

Crépin, L., Truong, N.M., Bloem, A., Sanchez, I., Dequin, S., and Camarasa, C. (2017) Management of multiple nitrogen sources during wine fermentation by *Saccharomyces cerevisiae*. *Appl*

Environ Microbiol **83**:.

Deed, R.C. and Pilkington, L.I. (2020) Lifestyle, lineage, and geographical origin influence temperature-dependent phenotypic variation across yeast strains during wine fermentation. *Microorganisms* **8**: 1–22.

De Deken, R.H. (1966) The Crabtree effect: a regulatory system in yeast. *J Gen Microbiol* **44**: 149–156.

Demuyter, C., Lollier, M., Legras, J.L., and Le Jeune, C. (2004) Predominance of *Saccharomyces uvarum* during spontaneous alcoholic fermentation, for three consecutive years, in an Alsatian winery. *J Appl Microbiol* **97**: 1140–1148.

Duarte, N.C., Becker, S.A., Jamshidi, N., Thiele, I., Mo, M.L., Vo, T.D., et al. (2007) Global reconstruction of the human metabolic network based on genomic and bibliomic data. *Proc Natl Acad Sci U S A* **104**: 1777–1782.

Duarte, N.C., Herrgård, M.J., and Palsson, B. (2004) Reconstruction and validation of *Saccharomyces cerevisiae* iND750, a fully compartmentalized genome-scale metabolic model. *Genome Res* **14**: 1298–1309.

Erasmus, D.J., Van Der Merwe, G.K., and Van Vuuren, H.J.J. (2003) Genome-wide expression analyses: Metabolic adaptation of *Saccharomyces cerevisiae* to high sugar stress. *FEMS Yeast Res* **3**: 375–399.

Erny, C., Raoult, P., Alais, A., Butterlin, G., Delobel, P., Matei-Radoi, F., et al. (2012) Ecological Success of a Group of *Saccharomyces cerevisiae*/*Saccharomyces kudriavzevii* hybrids in the Northern European wine-making environment. *Appl Environ Microbiol* **78**: 3256–3265.

Feist, A.M., Henry, C.S., Reed, J.L., Krummenacker, M., Joyce, A.R., Karp, P.D., et al. (2007) A genome-scale metabolic reconstruction for *Escherichia coli* K-12 MG1655 that accounts

for 1260 ORFs and thermodynamic information. *Mol Syst Biol* **3**: 121.

Fields, S. and Johnston, M. (2005) Whither model organism research? *Science (80-)* **307**: 1885–1886.

Förster, J., Famili, I., Fu, P., Palsson, B., and Nielsen, J. (2003) Genome-scale reconstruction of the *Saccharomyces cerevisiae* metabolic network. *Genome Res* **13**: 244–253.

Gallone, B., Steensels, J., Prahl, T., Soriaga, L., Saels, V., Herrera-Malaver, B., et al. (2016) Domestication and Divergence of *Saccharomyces cerevisiae* Beer Yeasts. *Cell* **166**: 1397-1410.e16.

Gamero, A., Belloch, C., Ibáñez, C., and Querol, A. (2014) Molecular analysis of the genes involved in aroma synthesis in the species *S. cerevisiae, S. kudriavzevii* and *S. bayanus* var. *uvarum* in winemaking conditions. *PLoS One* **9**: 1–10.

Gamero, A., Tronchoni, J., Querol, A., and Belloch, C. (2013) Production of aroma compounds by cryotolerant *Saccharomyces* species and hybrids at low and moderate fermentation temperatures. *J Appl Microbiol* **114**: 1405–1414.

García-Ríos, E. and Guillamón, J.M. (2019) Mechanisms of Yeast Adaptation to Wine Fermentations. *Prog Mol Subcell Biol* **58**: 37–59.

García-Ríos, E., López-Malo, M., and Guillamón, M.M. (2014) Global phenotypic and genomic comparison of two *Saccharomyces cerevisiae* wine strains reveals a novel role of the sulfur assimilation pathway in adaptation at low temperature fermentations. *BMC Genomics* **15**: 1059.

Goffeau, A., Barrell, G., Bussey, H., Davis, R.W., Dujon, B., Feldmann, H., et al. (1996) Life with 6000 genes. *Science (80-)* **274**: 546–567.

Goldner, M.C., Zamora, M.C., Lira, P.D.L., Gianninoto, H., and

Bandoni, A. (2009) Effect of ethanol level in the perception of aroma attributes and the detection of volatile compounds in red wine. *J Sens Stud* **24**: 243–257.

Gombert, A.K. and Moreira, M. (2001) Network Identification and Flux Quantification in the Central Metabolism of *Saccharomyces cerevisiae* under Different Conditions of Glucose Repression *J Bacteriol* **183**: 1441–1451.

Gonzalez, S.S., Gallo, L., Climent, M. a, Barrio, E., and Querol, A. (2007) Ecological characterization of natural hybrids from *Saccharomyces cerevisiae* and *S. kudriavzevii*. *Int J Food Microbiol* **116**: 11–18.

Goold, H.D., Kroukamp, H., Williams, T.C., Paulsen, I.T., Varela, C., and Pretorius, I.S. (2017) Yeast's balancing act between ethanol and glycerol production in low-alcohol wines. *Microb Biotechnol* **10**: 264–278.

Grant, C.M. (2001) Role of the glutathione/glutaredoxin and thioredoxin systems in yeast growth and response to stress conditions. *Mol Microbiol* **39**: 533–541.

Gutiérrez-Gamboa, G., Alañón-Sánchez, N., Mateluna-Cuadra, R., and Verdugo-Vásquez, N. (2020) An overview about the impacts of agricultural practices on grape nitrogen composition: Current research approaches. *Food Res Int* **136**: 109477.

Hanly, T.J. and Henson, M.A. (2013) Dynamic metabolic modeling of a microaerobic yeast co-culture: Predicting and optimizing ethanol production from glucose/xylose mixtures. *Biotechnol Biofuels* **6**: 44.

Hasin, Y., Seldin, M., and Lusis, A. (2017) Multi-omics approaches to disease. *Genome Biol* **18**: 1–15.

Hazelwood, L.A., Daran, J.M., Van Maris, A.J.A., Pronk, J.T., and Dickinson, J.R. (2008) The Ehrlich pathway for fusel alcohol production: A century of research on *Saccharomyces cerevisiae*

metabolism (Applied and Environmental Microbiology (2008) 74, 8, (2259-2266)). *Appl Environ Microbiol* **74**: 3920.

Heinemann, M., Kümmel, A., Ruinatscha, R., and Panke, S. (2005) In silico genome-scale reconstruction and validation of the *Staphylococcus aureus* metabolic network. *Biotechnol Bioeng* **92**: 850–864.

Hittinger, C.T., Gonçalves, P., Sampaio, J.P., Dover, J., Johnston, M., and Rokas, A. (2010) Remarkably ancient balanced polymorphisms in a multi-locus gene network. *Nature* **464**: 54–58.

Hohmann, S. (1991) Characterization of PDC6, a third structural gene for pyruvate decarboxylase in *Saccharomyces cerevisiae*. *J Bacteriol* **173**: 7963–7969.

Hong, K.K. and Nielsen, J. (2012) Metabolic engineering of *Saccharomyces cerevisiae*: A key cell factory platform for future biorefineries. *Cell Mol Life Sci* **69**: 2671–2690.

Huang, H., Kawamata, T., Horie, T., Tsugawa, H., Nakayama, Y., Ohsumi, Y., and Fukusaki, E. (2015) Bulk RNA degradation by nitrogen starvation-induced autophagy in yeast . *EMBO J* **34**: 154–168.

Irani, Z.A., Kerkhoven, E.J., Shojaosadati, S.A., and Nielsen, J. (2016) Genome-scale metabolic model of *Pichia pastoris* with native and humanized glycosylation of recombinant proteins. *Biotechnol Bioeng* **113**: 961–969.

Kontoudakis, N., Esteruelas, M., Fort, F., Canals, J.M., and Zamora, F. (2011) Use of unripe grapes harvested during cluster thinning as a method for reducing alcohol content and pH of wine. *Aust J Grape Wine Res* **17**: 230–238.

Kutyna, D.R., Varela, C., Henschke, P.A., Chambers, P.J., and Stanley, G.A. (2010) Microbiological approaches to lowering ethanol concentration in wine. *Trends Food Sci Technol* **21**: 293–302.

Introduction references

Kwast, K.E., Burke, P. V, and Poyton, R.O. (1998) Oxygen sensing and the transcriptional regulation of oxygen responsive genes in yeast. *J Exp Biol* **201**: 1177–1195.

Lambrechts, M.G. and Pretorius, I.S. (2000) Yeast and its Importance to Wine Aroma - A Review. *South African J Enol Vitic* **21**: 97–129.

Legras, J.L., Galeote, V., Bigey, F., Camarasa, C., Marsit, S., Nidelet, T., et al. (2018) Adaptation of *S. cerevisiae* to fermented food environments reveals remarkable genome plasticity and the footprints of domestication. *Mol Biol Evol* **35**: 1712–1727.

Liti, G., Carter, D.M., Moses, A.M., Warringer, J., Parts, L., James, S.A., et al. (2009) Population genomics of domestic and wild yeasts. *Nature* **458**: 337–341.

Ljungdahl, P.O. and Daignan-Fornier, B. (2012) Regulation of amino acid, nucleotide, and phosphate metabolism in *Saccharomyces cerevisiae*. *Genetics* **190**: 885–929.

Lopes, C.A., Barrio, E., and Querol, A. (2010) Natural hybrids of *S. cerevisiae* × *S. kudriavzevii* share alleles with European wild populations of Saccharomyces kudriavzevii. *FEMS Yeast Res* **10**: 412–421.

López-Malo, M., Querol, A., and Guillamon, J.M. (2013) Metabolomic Comparison of *Saccharomyces cerevisiae* and the cryotolerant species *S. bayanus* var. *uvarum* and *S. kudriavzevii* during wine fermentation at low temperature. *PLoS One* **8**:.

Lu, H., Li, F., Sánchez, B.J., Zhu, Z., Li, G., Domenzain, I., et al. (2019) A consensus *S. cerevisiae* metabolic model Yeast8 and its ecosystem for comprehensively probing cellular metabolism. *Nat Commun* **10**:.

Macías, L.G., Morard, M., Toft, C., and Barrio, E. (2019) Comparative genomics between *Saccharomyces kudriavzevii* and *S. cerevisiae* applied to identify mechanisms involved in adaptation. *Front Genet* **10**: 187.

Magasanik, B. (2003) Ammonia Assimilation by *Saccharomyces cerevisiae*. *Eukaryot Cell* **2**: 827–829.

Magasanik, B. and Kaiser, C.A. (2002) Nitrogen regulation in *Saccharomyces cerevisiae*. *Gene* **290**: 1–18.

Marks, V.D., Ho Sui, S.J., Erasmus, D., Van Der Merwe, G.K., Brumm, J., Wasserman, W.W., et al. (2008) Dynamics of the yeast transcriptome during wine fermentation reveals a novel fermentation stress response. *FEMS Yeast Res* **8**: 35–52.

Marks, V.D., Van Der Merwe, G.K., and Van Vuuren, H.J.J. (2003) Transcriptional profiling of wine yeast in fermenting grape juice: Regulatory effect of diammonium phosphate. *FEMS Yeast Res* **3**: 269–287.

Masneuf-Pomarède, I., Bely, M., Marullo, P., Lonvaud-Funel, A., and Dubourdieu, D. (2010) Reassessment of phenotypic traits for *Saccharomyces bayanus* var. *uvarum* wine yeast strains. *Int J Food Microbiol* **139**: 79–86.

Mencher, A., Morales, P., Valero, E., Tronchoni, J., Patil, K.R., and Gonzalez, R. (2020) Proteomic characterization of extracellular vesicles produced by several wine yeast species. *Microb Biotechnol* 1751-7915.13614.

Mendes-Ferreira, A., Del Olmo, M., García-Martínez, J., Jiménez-Martí, E., Mendes-Faia, A., Pérez-Ortín, J.E., and Leão, C. (2007) Transcriptional response of *Saccharomyces cerevisiae* to different nitrogen concentrations during alcoholic fermentation. *Appl Environ Microbiol* **73**: 3049–3060.

Mendes, I., Sanchez, I., Franco-Duarte, R., Camarasa, C., Schuller, D., Dequin, S., and Sousa, M.J. (2017) Integrating transcriptomics and metabolomics for the analysis of the aroma profiles of *Saccharomyces cerevisiae* strains from diverse origins. *BMC Genomics* **18**: 455.

Miller, S.M. and Magasanik, B. (1990) Role of NAD-linked glutamate

dehydrogenase in nitrogen metabolism in *Saccharomyces cerevisiae*. *J Bacteriol* **172**: 4927–4935.

Mira de Orduña, R. (2010) Climate change associated effects on grape and wine quality and production. *Food Res Int* **43**: 1844–1855.

Molina, A.M., Swiegers, J.H., Varela, C., Pretorius, I.S., and Agosin, E. (2007) Influence of wine fermentation temperature on the synthesis of yeast-derived volatile aroma compounds. *Appl Microbiol Biotechnol* **77**: 675–687.

Naumov, G.I., Gazdiev, D.O., and Naumova, E.S. (2003) The finding of the yeast species *Saccharomyces bayanus* in Far East Asia. *Microbiology* **72**: 738–743.

Naumov, G. I., James, S.A., Naumova, E.S., Louis, E.J., and Roberts, I.N. (2000) Three new species in the *Saccharomyces* sensu stricto complex: *Saccharomyces cariocanus*, *Saccharomyces kudriavzevii* and *Saccharomyces mikatae*. *Int J Syst Evol Microbiol* **50**: 1931–1942.

Naumov, Gennadi I., Masneuf, I., Naumova, E.S., Aigle, M., and Dubourdieu, D. (2000) Association of *Saccharomyces bayanus* var. *uvarum* with some French wines: Genetic analysis of yeast populations. *Res Microbiol* **151**: 683–691.

Naumov, G.I., Nguyen, H. V., Naumova, E.S., Michel, A., Aigle, M., and Gaillardin, C. (2001) Genetic identification of *Saccharomyces bayanus* var. *uvarum*, a cider-fermenting yeast. *Int J Food Microbiol* **65**: 163–171.

Nicholas, K.A. (2015) Will we still enjoy pinot noir? *Sci Am* **312**: 60–67.

Nielsen, J. (2017) Systems Biology of Metabolism: A Driver for Developing Personalized and Precision Medicine. *Cell Metab* **25**: 572–579.

Noor, E., Eden, E., Milo, R., and Alon, U. (2010) Central Carbon Metabolism as a Minimal Biochemical Walk between Precursors for Biomass and Energy. *Mol Cell* **39**: 809–820.

Orellana, M., Aceituno, F.F., Slater, A.W., Almonacid, L.I., Melo, F., and Agosin, E. (2014) Metabolic and transcriptomic response of the wine yeast *Saccharomyces cerevisiae* strain EC1118 after an oxygen impulse under carbon-sufficient, nitrogen-limited fermentative conditions. *FEMS Yeast Res* **14**: 412–424.

Orozco, H., Matallana, E., and Aranda, A. (2012a) Oxidative stress tolerance, adenylate cyclase, and autophagy are key players in the chronological life span of *Saccharomyces cerevisiae* during winemaking. *Appl Environ Microbiol* **78**: 2748–2757.

Orozco, H., Matallana, E., and Aranda, A. (2012b) Two-carbon metabolites, polyphenols and vitamins influence yeast chronological life span in winemaking conditions. *Microb Cell Fact* **11**: 104.

Orth, J.D., Thiele, I., and Palsson, B.O. (2010) What is flux balance analysis? *Nat Biotechnol* **28**: 245–248.

Österlund, T., Nookaew, I., and Nielsen, J. (2012) Fifteen years of large scale metabolic modeling of yeast: Developments and impacts. *Biotechnol Adv* **30**: 979–988.

Otero, J.M., Cimini, D., Patil, K.R., Poulsen, S.G., Olsson, L., and Nielsen, J. (2013) Industrial Systems Biology of *Saccharomyces cerevisiae* Enables Novel Succinic Acid Cell Factory. *PLoS One* **8**: e54144.

Otero, J.M., Panagiotou, G., and Olsson, L. (2007) Fueling industrial biotechnology growth with bioethanol. *Adv Biochem Eng Biotechnol* **108**: 1–40.

Paget, C.M., Schwartz, J.M., and Delneri, D. (2014) Environmental systems biology of cold-tolerant phenotype in *Saccharomyces* species adapted to grow at different temperatures. *Mol Ecol* **23**:

5241–5257.

Park, J.M., Kim, T.Y., and Lee, S.Y. (2009) Constraints-based genome-scale metabolic simulation for systems metabolic engineering. *Biotechnol Adv* **27**: 979–988.

Pérez-Torrado, R., Barrio, E., and Querol, A. (2018) Alternative yeasts for winemaking: *Saccharomyces* non-*cerevisiae* and its hybrids. *Crit Rev Food Sci Nutr* **58**: 1780–1790.

Pérez-Torrado, R., Carrasco, P., Aranda, A., Gimeno-Alcañiz, J., Pérez-Ortín, J.E., Matallana, E., and Del Olmo, M. (2002) Study of the first hours of microvinification by the use of osmotic stress-response genes as probes. *Syst Appl Microbiol* **25**: 153–161.

Pérez-Torrado, R., Oliveira, B.M., Zemancíková, J., Sychrová, H., and Querol, A. (2016) Alternative glycerol balance strategies among *Saccharomyces* species in response to winemaking stress. *Front Microbiol* **7**: 435.

Peris, D., Pérez-Torrado, R., Hittinger, C.T., Barrio, E., and Querol, A. (2018) On the origins and industrial applications of *Saccharomyces cerevisiae* × *Saccharomyces kudriavzevii* hybrids. *Yeast* **35**: 51–69.

Peris, D., Pérez-Través, L., Belloch, C., and Querol, A. (2016) Enological characterization of Spanish *Saccharomyces kudriavzevii* strains, one of the closest relatives to parental strains of winemaking and brewing *Saccharomyces cerevisiae* × *S. kudriavzevii* hybrids. *Food Microbiol* **53**: 31–40.

Peter, J., De Chiara, M., Friedrich, A., Yue, J.X., Pflieger, D., Bergström, A., et al. (2018) Genome evolution across 1,011 *Saccharomyces cerevisiae* isolates. *Nature* **556**: 339–344.

Petranovic, D. and Nielsen, J. (2008) Can yeast systems biology contribute to the understanding of human disease? *Trends Biotechnol* **26**: 584–590.

Pickering, G.J. and Vanhanen, L. (1998) The effect of ethanol concentration on the temporal perception of viscosity and density in white wine. *Am J Enol Vitic* **49**: 306–318.

Piškur, J., Rozpedowska, E., Polakova, S., Merico, A., and Compagno, C. (2006) How did *Saccharomyces* evolve to become a good brewer? *Trends Genet* **22**: 183–186.

Pizarro, F., Vargas, F.A., and Agosin, E. (2007) A systems biology perspective of wine fermentations. *Yeast* **24**: 977–991.

Pizarro, F.J., Jewett, M.C., Nielsen, J., and Agosin, E. (2008) Growth temperature exerts differential physiological and transcriptional responses in laboratory and wine strains of *Saccharomyces cerevisiae*. *Appl Environ Microbiol* **74**: 6358–6368.

Pretorius, I.S. (2000) Tailoring wine yeast for the new millennium: Novel approaches to the ancient art of winemaking. *Yeast* **16**: 675–729.

Querol, A., Pérez-Torrado, R., Alonso-del-Real, J., Minebois, R., Stribny, J., Oliveira, B.M., and Barrio, E. (2018) New Trends in the Uses of Yeasts in Oenology. In, *Advances in Food and Nutrition Research*., pp. 177–210.

Quirós, M., Rojas, V., Gonzalez, R., and Morales, P. (2014) Selection of non-*Saccharomyces* yeast strains for reducing alcohol levels in wine by sugar respiration. *Int J Food Microbiol* **181**: 85–91.

Ribéreau-Gayon, P., Dubourdieu, D., Donèche, B., and Lonvaud, A. (2006) Handbook of Enology: Volume 1, The Microbiology of Wine and Vinifications. *Handb Enol* **1**: 1–441.

Rodríguez, M.E., Pérez-Través, L., Sangorrín, M.P., Barrio, E., and Lopes, C.A. (2014) *Saccharomyces eubayanus* and *Saccharomyces uvarum* associated with the fermentation of Araucaria araucana seeds in Patagonia. *FEMS Yeast Res* **14**: 948–965.

Rollero, S., Bloem, A., Ortiz-Julien, A., Bauer, F.F., Camarasa, C., and Divol, B. (2019) A comparison of the nitrogen metabolic networks of *Kluyveromyces marxianus* and *Saccharomyces cerevisiae*. *Environ Microbiol* **21**: 4076–4091.

Rollero, S., Mouret, J.R., Bloem, A., Sanchez, I., Ortiz-Julien, A., Sablayrolles, J.M., et al. (2017) Quantitative 13C-isotope labelling-based analysis to elucidate the influence of environmental parameters on the production of fermentative aromas during wine fermentation. *Microb Biotechnol* **10**: 1649–1662.

Rossignol, T., Dulau, L., Julien, A., and Blondin, B. (2003) Genome-wide monitoring of wine yeast gene expression during alcoholic fermentation. *Yeast* **20**: 1369–1385.

Rossignol, T., Kobi, D., Jacquet-Gutfreund, L., and Blondin, B. (2009) The proteome of a wine yeast strain during fermentation, correlation with the transcriptome. *J Appl Microbiol* **107**: 47–55.

Rossouw, D. and Bauer, F.F. (2009) Comparing the transcriptomes of wine yeast strains: Toward understanding the interaction between environment and transcriptome during fermentation. *Appl Microbiol Biotechnol* **84**: 937–954.

Saerens, S.M.G., Delvaux, F.R., Verstrepen, K.J., and Thevelein, J.M. (2010) Production and biological function of volatile esters in *Saccharomyces cerevisiae*. *Microb Biotechnol* **3**: 165–177.

Sainz, J., Pizarro, F., Pérez-Correa, J.R., and Agosin, E. (2003) Modeling of yeast metabolism and process dynamics in batch fermentation. *Biotechnol Bioeng* **81**: 818–828.

Saitua, F., Torres, P., Pérez-Correa, J.R., and Agosin, E. (2017) Dynamic genome-scale metabolic modeling of the yeast *Pichia pastoris*. *BMC Syst Biol* **11**:.

Salvadó, Z., Arroyo-López, F.N., Guillamón, J.M., Salazar, G., Querol, A., and Barrio, E. (2011) Temperature adaptation Markedly

Determines evolution within the genus *Saccharomyces*. *Appl Environ Microbiol* **77**: 2292–2302.

Salvadó, Z., Chiva, R., Rodríguez-Vargas, S., Rández-Gil, F., Mas, A., and Guillamón, J.M. (2008) Proteomic evolution of a wine yeast during the first hours of fermentation. *FEMS Yeast Res* **8**: 1137–1146.

Sampaio, J.P. and Gonçalves, P. (2008) Natural populations of *Saccharomyces kudriavzevii* in Portugal are associated with Oak bark and are sympatric with *S. cerevisiae* and *S. paradoxus*. *Appl Environ Microbiol* **74**: 2144–2152.

Sánchez, B.J., Pérez-Correa, J.R., and Agosin, E. (2014) Construction of robust dynamic genome-scale metabolic model structures of *Saccharomyces cerevisiae* through iterative re-parameterization. *Metab Eng* **25**: 159–173.

Scannell, D.R., Zill, O.A., Rokas, A., Payen, C., Dunham, M.J., Eisen, M.B., et al. (2011) The awesome power of yeast evolutionary genetics: New genome sequences and strain resources for the *Saccharomyces* sensu stricto genus. *G3 Genes, Genomes, Genet* **1**: 11–25.

Schmidtke, L.M., Blackman, J.W., and Agboola, S.O. (2012) Production technologies for reduced alcoholic wines. *J Food Sci* **77**: R25–R41.

Sirén, K., Mak, S.S.T., Fischer, U., Hansen, L.H., and Gilbert, M.T.P. (2019) Multi-omics and potential applications in wine production. *Curr Opin Biotechnol* **56**: 172–178.

Spayd, S., Tarara, J., Mee, D., and Ferguson, J. (2002) Separation of sunlight and temperature effects on the composition of *Vitis vinifera* cv. *Am J Enol Vitic* **53**: 171–182.

Styger, G., Jacobson, D., and Bauer, F.F. (2011) Identifying genes that impact on aroma profiles produced by *Saccharomyces cerevisiae* and the production of higher alcohols. *Appl Microbiol Biotechnol*

91: 713–730.

Swiegers, J.H., Kievit, R.L., Siebert, T., Lattey, K.A., Bramley, B.R., Francis, I.L., et al. (2009) The influence of yeast on the aroma of Sauvignon Blanc wine. *Food Microbiol* **26**: 204–211.

Tesnière, C., Brice, C., and Blondin, B. (2015) Responses of *Saccharomyces cerevisiae* to nitrogen starvation in wine alcoholic fermentation. *Appl Microbiol Biotechnol* **99**: 7025–7034.

Tronchoni, J., Medina, V., Guillamón, J.M., Querol, A., and Pérez-Torrado, R. (2014) Transcriptomics of cryophilic *Saccharomyces kudriavzevii* reveals the key role of gene translation efficiency in cold stress adaptations. *BMC Genomics* **15**: 432.

Varela, C., Barker, A., Tran, T., Borneman, A., and Curtin, C. (2017) Sensory profile and volatile aroma composition of reduced alcohol Merlot wines fermented with *Metschnikowia pulcherrima* and *Saccharomyces uvarum*. *Int J Food Microbiol* **252**: 1–9.

Varela, C., Cárdenas, J., Melo, F., and Agosin, E. (2005) Quantitative analysis of wine yeast gene expression profiles under winemaking conditions. *Yeast* **22**: 369–383.

Varela, C., Schmidt, S.A., Borneman, A.R., Pang, C.N.I., Krömerx, J.O., Khan, A., et al. (2018) Systems-based approaches enable identification of gene targets which improve the flavour profile of low-ethanol wine yeast strains. *Metab Eng* **49**: 178–191.

Varela, C., Sengler, F., Solomon, M., and Curtin, C. (2016) Volatile flavour profile of reduced alcohol wines fermented with the non-conventional yeast species *Metschnikowia pulcherrima* and *Saccharomyces uvarum*. *Food Chem* **209**: 57–64.

Vargas, F.A., Pizarro, F., Pérez-Correa, J.R., and Agosin, E. (2011) Expanding a dynamic flux balance model of yeast fermentation to genome-scale. *BMC Syst Biol* **5**: 17–19.

Wang, Q.-M., Liu, W.-Q., Liti, G., Wang, S.-A., and Bai, F.-Y. (2012) Surprisingly diverged populations of *Saccharomyces cerevisiae* in natural environments remote from human activity. *Mol Ecol* **21**: 5404–17.

Wang, S.S. and Brandriss, M.C. (1987) Proline utilization in *Saccharomyces cerevisiae*: sequence, regulation, and mitochondrial localization of the PUT1 gene product. *Mol Cell Biol* **7**: 4431–4440.

Will, J.L., Kim, H.S., Clarke, J., Painter, J.C., Fay, J.C., and Gasch, A.P. (2010) Incipient balancing selection through adaptive loss of aquaporins in natural *Saccharomyces cerevisiae* populations. *PLoS Genet* **6**:.

Justification & objectives

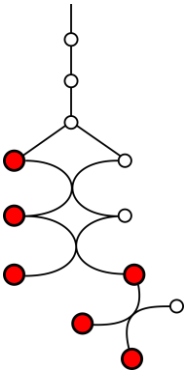

Justification & objectives

In recent decades the Spanish wine-producing sector has experienced tremendous growth, becoming the world export leader. However, to maintain competitiveness, the industrial sector needs to adapt to the new market demands as well as to face the challenges posed by climate change. On the one hand, consumers demand products with lower alcohol content and fruitier aromas. On the other hand, climate change influences the characteristics of the grape must (acidity, content in sugars or tannins, etc), impacting the quality of the final product.

Previous studies have shown that non-conventional *Saccharomyces* yeasts, including *S. kudriavzevii* and *S. uvarum* species, could be good candidates to overcome these issues. Some strains of these species exhibit good fermentative capabilities at low temperatures, producing wines with lower alcohol and higher glycerol amounts while resulting in good aromatic profiles. These fermentative by-products are the result of a complex set of anabolic and catabolic reactions using exogenous nutrients, principally carbohydrates, and amino acids, through the metabolic network of yeast. Given that most of the pathways involved in the metabolic framework are conserved among yeasts species, the phenotypes of oenological interest exhibited by *S. uvarum* and *S. kudriavzevii* are probably related to different nutrient

redistribution strategies within this network from those of *S. cerevisiae*. However, and despite their potential, these species are still underestimated and their metabolism is poorly studied compared to *S. cerevisiae*, which, as a model organism and a species widely implemented in industrial fermentations, has the benefit of an extensive scientific bibliography.

This doctoral thesis was part of the IMPROWINE project (AGL2015-67504-C3-1-R awarded to Amparo Querol) which the main goal is to equip the Spanish wine industry with new knowledge and tools to produce wines tailored to the consumer demands, ultimately developing new fermentation processes based on the use of *S. kudriavzevii* and *S. uvarum*. In this context, in the development of this thesis, distinct omics technologies, and a mathematical modeling approach were combined in an integrated manner to accomplish the following specific objectives:

Objective 1. Comparative study of the fermentative metabolism of *S. cerevisiae*, *S. uvarum,* and *S. kudriavzevii* at low and high fermentation temperatures, in winemaking conditions, using a metabolomic approach.

Justification & objectives

- Analyze the dynamic of intra- and extracellular metabolomes of selected strains of *S. cerevisiae*, *S. uvarum,* and *S. kudriavzevii* species in batch culture mimicking winemaking conditions
- Identify differential metabolic traits between *S. cerevisiae*, *S. uvarum,* and *S. kudriavzevii* species occurring across fermentation
- Discern temperature dependant metabolic traits

The results are presented in **CHAPTER 1** and **CHAPTER 2**.

Objective 2. *In silico* modeling of the fermentative behavior of *S. uvarum* and *S. cerevisiae* during wine fermentation using a genome-scale dynamic flux balance analysis.

- Develop a genome-scale metabolic model of *S. cerevisiae* and *S. uvarum* species able to fit and predict their fermentative behavior in batch culture
- Determine the intracellular flux of *S. cerevisiae* and *S. uvarum* cultures performed at 25 °C (chapter 1) using this model and a dynamic flux balance analysis approach

The results are presented in **CHAPTER 3**.

Objective 3. Unveiling metabolic differences between wild and wine strains of *Saccharomyces cerevisiae* during fermentation using a multi-omic analysis.

- Identify differential metabolic and transcriptomic traits between a wine strain and a natural strain of *S. cerevisiae*
- Compare their metabolome and transcriptomes at low and high fermentation temperature
- Identify temperature dependent responses among the two strains

The results are presented in **CHAPTER 4**.

CHAPTER 1

A time course metabolism comparison among *Saccharomyces cerevisiae*, *S. uvarum* and *S. kudriavzevii* species in wine fermentation.

Romain Minebois[a], Roberto Pérez-Torrado[a] and Amparo Querol[a]*

[a]Instituto de Agroquímica y Tecnología de los Alimentos, IATA-CSIC. E-46980 Paterna, Spain.

*Corresponding author: aquerol@iata.csic.es

Published in **Food Microbiology**

[DOI: 10.1016/j.fm.2020.103484]

Abstract

In this study, we presented the first metabolome time course analysis performed among a set of *S. uvarum*, *S. kudriavzevii* and *S. cerevisiae* strains under winemaking conditions. Extracellular and intracellular metabolites, as well as physiological parameters of yeast cells, were monitored along the process to find evidence of different metabolic strategies among species to perform alcoholic fermentation. A thorough inspection of time trends revealed several differences in utilization or accumulation of fermentation by-products. We confirmed the ability of *S. uvarum* and *S. kudriavzevii* strains to produce higher amounts of glycerol, succinate or some fusel alcohols and their corresponding esters. We also reported differences in the yields of less common fermentative by-products involved in redox homeostasis, namely 2,3 butanediol and erythritol. 2,3 butanediol yield was higher in must ferment with cryophilic strains and erythritol, a pentose phosphate pathway derivative, was particularly overproduced by *S. uvarum* strains. Contrary to *S. cerevisiae*, a singular production-consumption rate of acetate was also observed in *S. uvarum* and *S. kudriavzevii* fermentations. Since acetate is a precursor for acetyl-CoA production which is involved in the biosynthesis of membrane lipids, cryophilc strains might take advantage of extracellular acetate to remodel cell membrane as ethanol content increased during fermentation.

Chapter 1

1. Introduction

During wine fermentation, the majority of sugar content is metabolized by yeasts to produce ethanol and carbon dioxide. The remaining fraction of sugars is used for the synthesis of biomass and hundreds of additional metabolites, including organic acids (acetic acid, succinate), flavor-active secondary metabolites (esters, fusel alcohols, aldehydes, ketones, volatile sulfur compounds) or sugar alcohols such as glycerol, the most important by-product after carbon dioxide and ethanol. Therefore, there is a high diversity in the fermentative compounds originated from central carbon metabolism of yeasts, which determine the organoleptic properties (flavor and aroma) of wine. For this reason, the knowledge of their individual contribution to the global profile of the wine is a principal concern for oenologists who look for the most equilibrated beverages in terms of aromas, astringency, acidity and alcohol perception (Lambrechts and Pretorius, 2000). Today, with the increase of temperature during the growing season of grapes - as a result of climate change - the sugar level of grape musts tends to be higher at the cost of phenolic ripeness and acidity in most of the wine-producing regions (Cohen *et al.*, 2008; Mira de Orduña, 2010). This high sugar content – subsequently converted to ethanol by yeasts – lead wines to be more alcoholic, increasing the perception of heat, altering the perception of wine aromas complexity and decreasing the color intensity and stability (Pickering and Vanhanen, 1998; Goldner *et al.*, 2009). Thus,

the production of wines with reduced ethanol concentration and enhanced aroma content without weakening product value has been the focus of extensive research over the past decades.

Viticulture techniques and dealcoholization treatments are some of the techniques currently employed to reduce alcohol concentration (Pickering, 2000; Aguera *et al.*, 2010; Catarino and Mendes, 2011; Kontoudakis *et al.*, 2011; Schmidtke *et al.*, 2012). However, these approaches are difficult and expensive to implement. Alternative *Saccharomyces* species have attracted attention as a poor exploited resource of yeast biodiversity with interesting attributes not present in *S. cerevisiae*, the dominant species in alcoholic fermentation. Notably, the cryophilic species *S. uvarum* and *S. kudriavzevii* and their interspecific hybrids, have recently demonstrated interesting properties, especially at low fermentation temperatures. In particular, *S. uvarum* and *S. kudriavzevii* fermentation profiles differ from that of *S. cerevisiae* in terms of fermentative by-products yields and biomass production. Both cryophilic species generate higher levels of volatile fermentative compounds, particularly 2-phenylethanol and 2-phenylethyl acetate in *S. uvarum* (Masneuf-Pomarède *et al.*, 2010; Gamero *et al.*, 2013). These differences in aroma production have been correlated with differential gene regulations and enzymatic activities as compared to *S. cerevisiae* (Gamero *et al.*, 2014; Stribny *et al.*, 2015, 2016) . Moreover, besides it produces lower levels of ethanol and acetic acid, *S. uvarum* also

produces higher levels of glycerol and succinate (Castellari *et al.*, 1994; Kishimoto, 1994; Rainieri *et al.*, 1999). Focusing on *S. kudriavzevii*, it was observed that this species mainly directed carbon flux towards glycerol synthesis instead of ethanol at low pH, high sugar concentrations and low temperatures in comparison with *S. cerevisiae* (Arroyo-López *et al.*, 2010). It has also been reported in chemostat cultures performed at 12°C that *S. kudriavzevii* produces more biomass and glycerol than *S. cerevisiae* and that this increase in the glycerol yield was due to a higher expression and enhanced enzymatic parameters of the glycerol-3-phosphate dehydrogenase 1 (Gpd1) protein (Oliveira *et al.*, 2014). Finally, in a metabolomics comparison carried out in steady-state among the three species, it was also pointed out the existence of another regulation of the central carbon metabolism involved in cold resistance strategies in cryophilic species (López-Malo *et al.*, 2013). *S. uvarum* presented elevated shikimate pathway activity, while *S. kudriavzevii* displayed increased NAD^+ synthesis.

Since *S. cerevisiae* is the most employed yeast in the field of food and fermented beverages, it has been the subject of many studies, and strong fundamental knowledge of its physiology, metabolism, and genetics are now available. On the contrary, there is still little information available on the metabolic basis that explains the fermentative characteristics of the cryophilic species *S. uvarum* and *S. kudriavzevii*. The aim of this study was to explore the dynamic

alcoholic fermentation profile of a set of wine commercial (T73 and BMV58) and other isolates (CECT12600 and CR85) of the species *S. cerevisiae*, *S. uvarum* and *S. kudriavzevii* in mimicked wine elaboration. During the fermentation process and using a metabolomics approach, the main intracellular and extracellular fermentative by-products, gases yields and physiological parameters were registered to understand the metabolic differences among the three species that could explain their oenological performance in those conditions.

2. Material and methods

2.1 Yeast strains

A commercial *S. cerevisiae* wine strain (T73, Lallemand, Montreal), originally isolated from wine in Alicante, Spain (Querol *et al.*, 1992) as well as two *S. uvarum* strains, respectively a wine commercial (Velluto BMV58) and a non-commercial strain isolated from a non-fermentative environment (CECT12600) and a wild (no commercial strains are available) *S. kudriavzevii* strain (CR85), previously identified and differentiated in Lopes et al. (2010) were used in this work. The isolation source and geographical origin of the strains used herein are shown in **Table 1**.

Table 1. List of the *Saccharomyces* strains used in this study

Strain †	Species	Commercial name	Source	Isolation region
T73	*S. cerevisiae*	Lalvin T73 ‡	Wine	Alicante, Spain
BMV58	*S. uvarum*	Velluto BMV58 YSEO (Lallemand) ‡	Wine	Alicante, Spain
CECT12600	*S. uvarum*	---	Non fermented liquor (Mistela)	Alicante, Spain
CR85	*S. kudriavzevii*	---	*Quercus ilex* bark	Ciudad Real, Spain

† Reference yeast used in the present work.

‡Yeast strains currently commercialized as active dry yeasts.

Cryogenically preserved (-80ºC) strains were cultured and maintained on GPY plates (2% glucose, 2% agar, 0,5% peptone, 0,5% yeast extract) and stored at 4ºC. Bioreactors were inoculated at OD600 0.1 (approximately 1 x 10^6 cells/ml) from starter culture. Starter culture was prepared by growing strains overnight in an Erlenmeyer flask containing 25 ml of GPY liquid medium (2% glucose, 0.5% peptone, 0.5% yeast extract) at 25°C in an agitated incubator (Selecta, Barcelona, Spain) under aerobic conditions.

2.2 Microvinification experiments

The must obtained from the Merseguera white grapes variety, collected in Titaguas (Spain) winery and stored in several small frozen volumes (4 L, -20°C) was used for the microvinification assays. Before use, must was clarified by sedimentation for 24 h at 4°C and dimethyl dicarbonate (DMDC) at 1 $ml.L^{-1}$ was added for sterilization. Before fermentation, the fermentable sugar level was corrected as performed in most European countries by adding chemically pure sucrose (AppliChem Panreac, Darmstadt, Germany) to reach a probable alcoholic grade of 12.5%. To avoid any stuck or sluggish fermentations, nitrogen content was adjusted by adding a nitrogen supplement, which consisted of 0.2 g/l of ammonium sulfate and 0.1 mg/l of thiamine hydrochloride (Sigma-Aldrich, Barcelona, Spain). Nitrogen composition of the grape juice is available in supplementary material (**Table S1**). All the fermentations were carried out in independent biological triplicates by using 470 ml of must in sterile 500 ml laboratory bioreactors (MiniBio, Applikon, the Netherlands). Data were integrated into the MyControl and BioExpert software (Applikon, The Netherlands). Dynamic evolution of the fermentation was controlled by using different probes and detectors measuring temperature, dissolved O_2 (AppliSens, Applikon, The Netherlands) and effluent gas content (Multi-Gas Monitors INNOVA 1316, LumaSense Technologies). Fermentations were monitored by

measuring the residual sugar content by HPLC until constant values were reached, considered to be the end of the fermentation.

2.3 Sampling

Bioreactors were sampled in selected time points of the fermentation. In order not to perturb the fermentation conditions, the total sampling volume was limited to 10% (47 ml) of the initial working volume. Metabolic profiling was performed for extra and intracellular metabolites. Extracellular metabolites were determined from sample supernatants and included sugars, organic acids, glycerol, ethanol, 2,3 butanediol, erythritol, ammonia, amino acids, and volatile compounds. Intracellular metabolites including, sugars, intermediates of central carbon metabolism and amino acids, were extracted from quenched cell pellets following an adapted procedure from Villas-Bôas et al. (2005). Extracellular metabolites were determined in 10 sampling points along the fermentation, and in 5 of these points, intracellular metabolites were also measured. For intracellular metabolites determination approximately 20-30 OD_{600} of cells were rapidly sampled from the bioreactor and quenched in a tube containing pure cold methanol (-40°C). The samples were carefully released into the center of the pure methanol solution to avoid freezing on the sides of the tubes. Cell separation was accomplished through 90 sec centrifugation of the sample tubes in an R5100 centrifuge (Eppendorf, Hamburg, Germany) at 4,000 rpm using a precooled rotor at minimum temperature (-9°C). The supernatant

was discarded, cell pellet flashes frozen with nitrogen and tubes stored at -80°C until intracellular metabolites extraction. During all the procedure, sample tubes were handled at temperature below -20°C by using dry ice to prevent any reaction to proceed until complete protein denaturation during the extraction step.

2.4 Intracellular metabolites extraction and quantification

Intracellular metabolites were extracted by adapting the pure cold methanol extraction procedure used in Villas-Bôas et al. (2005). A 250 µl volume of cold (-40ºC) absolute methanol was added to the cell pellet in 15 ml falcon tube. After rapid mixing, the tube was transferred into dry ice for 30 min. The sample was then thawed in an ice bath for 10 min and the cells were centrifuged in a pre-cooled Eppendorf centrifuge at maximum speed (4000 rpm) for 10 min at 0ºC. The first supernatant was then transferred to a screw cap Eppendorf tube and to the extracted pellet, another 250 µl volume of pure cold methanol was added to extract any metabolites left after the first extraction. The first and second extracts were combined and stored at -80ºC until quantification by GC-MS. Primary metabolite analysis was performed at the Instituto de Biología Molecular y Celular de Plantas (UPV-CSIC, Valencia, Spain) Metabolomics Platform by a method modified from that described by Roessner et al. (2000). An extract volume corresponding to 0.5 mg of yeast fresh weight (2-5 µl) was mixed with 3 µl of internal standard (0.2 mg/ml ribitol in water) and reduced to dryness in a speed-vac. For derivatization, dry

residues were redissolved in 40 µl of 20 mg/ml methoxyamine hydrochloride in pyridine and incubated for 90 min at 37ºC, followed by addition of 60 µl MSTFA (N-methyl-N-[trimethylsilyl]trifluoroacetamide) and 6 µl of a retention time standard mixture (3.7% [w/v] mix of fatty acid methyl esters ranging from 8 to 24ºC) and further incubation for 30 min at 37 ºC. Sample volumes of 2 µl were injected in the split and splitless mode to increase metabolite detection range in a 6890 N gas chromatograph (Agilent Technologies Inc. Santa Clara, CA) coupled to a Pegasus 4D TOF mass spectrometer (LECO, St. Joseph, MI). Gas chromatography was performed on a BPX35 (30 m × 0. 32 mm × 0.25 µm) column (SGE Analytical Science Pty Ltd., Australia) with helium as a carrier gas, constant flow 2 ml/min. The liner was set at 230°C. Oven program was 85°C for 2 min, 8°C/min ramp until 360°C. Mass spectra were collected at 6. 25 spectra s^{-1} in the m/z range 35–900 and ionization energy of 70 eV. Chromatograms and mass spectra were evaluated using the CHROMATOF program (LECO, St. Joseph, MI). Peak areas were normalized with the internal standard area (ribitol) and with the average weight of yeast cells used for cold-methanol extraction. Finally, for each strain, the relative amount of each compound was computed in relation to the first sampling time point, excepting trehalose and citramalate for which last sampling time point was used.

2.5 Extracellular metabolites quantification

Sugars (glucose, fructose), fermentative by-products (glycerol, ethanol, 2,3 butanediol, and erythritol) and organic acids (acetate, succinate, tartrate, citrate and malate) were respectively determined by HPLC (Thermo Fisher Scientific, Waltham, MA) using a refraction index detector and UV/VIS (210nm) detector equipped with a HyperREZTM XP Carbohydrate H+ 8 mm column (Thermo Fisher Scientific, Waltham, MA) and HyperREZTM XP Carbohydrate Guard (Thermo Fisher Scientific, Waltham, MA). The analysis conditions were: eluent, 1.5 mM of H2SO4; 0.6 ml.min-1 flux and oven temperature of 50°C. For sucrose determination, the same HPLC was equipped with a Hi-Plex Pb, 300 x 7.7 mm column (Agilent Technologies, CA, USA) and peaks quantified by the RI detector. The analysis conditions were: eluent, Milli-Q water; 0.6 ml.min-1 flux and oven temperature of 50°C. The retention times of the eluted peaks were compared to those of commercial analytical standards (Sigma-Aldrich, Madrid, Spain). Concentrations, in g/l, were quantified by the calibration graphs (R2 value > 0.99) of the standards that were previously obtained from a linear curve fit of the peak areas using ten standards mixtures.

Determination of yeast assimilable nitrogen in the form of amino-acids and ammonia was carried following the same protocol than Su et al. (2020). A volume of supernatant was derivatised and amino acids and ammonia separated by UPLC (Dionex Ultimate 3000,

Thermo Fisher Scientific, Waltham, MA) equipped with a Kinetex 2.6u C18 100A column (Phenomenex, Torrance, CA, USA) and Accucore C18 10 x 4.6 mm 2.6um Defender guards (Thermo Fisher Scientific, Waltham, MA). For derivatization, 400 µl of the sample were mixed with 430 µl borate buffer (1M, pH 10.2), 300 µl absolute methanol and 12 µl of diethyl ethoxymethylenemalonate (DEEMM), and ultra-sonicated for 30 min at 20ºC. After ultra-sonicating, the sample was warmed up at 80ºC for 2 hours to allow the complete degradation of excess DEEMM. Once the derivatization finished, the sample was filtered with 0.22 µm filter before inection. The target compounds in the sample were then identified and quantified according to the retention times, UV-vis spectral characteristics and calibration curves (R2 value > 0.99) of the derivatives of the corresponding standards. Amino acid astandard (ref AAS18), asparagine and glutamine purchased from Sigma-Aldrich were used for calibration.

2.6 Volatile compounds extraction and quantification

Volatile compounds extraction and gas chromatography were performed following the protocol of Stribny et al. (2015). 1.5 mL of the supernatant was transferred to 15-mL vials with 0.35 g of NaCl. 20 µl volume of 2-heptanone (0.005 %) was added as an internal standard. Higher alcohols and esters were analyzed by the headspace solid-phase microextraction (HS-SPME) technique with 100-µm polydimethylsiloxane (PDMS) fiber (Supelco, Sigma-Aldrich, Madrid, Spain). Solutions were maintained for 2 h at 20°C to establish the

headspace-liquid equilibrium. The fiber was inserted into the headspace through a vial septum and was held for 7 min. The fiber was then inserted into the gas chromatograph inlet port for 4 min at 220°C with helium flow (1 mL/min) to desorb analytes. A Thermo Science TRACE GC Ultra gas chromatograph with a flame ionization detector (FID) was used, equipped with an HP INNOWax 30 m × 0.25 m capillary column coated with a 0.25-m layer of cross-linked polyethylene glycol (Agilent Technologies, Valencia, Spain). The oven temperature program was: 5 min at 35°C, 2°C/min to 150°C, 20°C/ min to 250°C and 2 min at 250°C. The detector temperature was kept constant at 300°C. A chromatographic signal was recorded by the ChromQuest program. Volatile compounds were identified by the retention time for reference compounds. Quantification of the volatile compounds was determined using the calibration graphs of the corresponding standard volatile compounds.

2.7 Biomass and physiological parameters determination

Biomass and physiological parameters - OD600, dry weight (DW), colonies-forming unit (CFUs) and average cell diameter (ACD) - were determined in every sampling point providing that cell sample was sufficient to perform the corresponding measure. For DW determination, 2 ml of fresh sample placed in a pre-weighed Eppendorf tube were centrifuged at maximum speed (13.400 rpm) in a MiniSpin centrifuge (Eppendorf, Spain) for 5 minutes. The supernatant was carefully removed with a pipette, the pellet washed

with 70 % (v/v) ethanol and centrifuged in the same conditions. After washing, the aqueous supernatant was carefully removed and tube stored at 65ºC for 72h. DW was obtained by measuring the mass weight difference of tubes with a BP121S analytical balance (Sartorius, Goettingen, Germany). Due to the working volume limitation, DW determination was impossible at the beginning of the process. OD600 was measured at each sampling point using a diluted volume of sample and a Biophotometer spectrophotometer (Eppendorf, Hamburg, Germany). CFUs were determined using a 100-200 µl of a diluted volume of samples plated in GPY solid medium and incubated two days at 25ºC. After what, the resulting colonies were counted with a Comecta S.A Colony Counter. Plates with CFUs between 30 and 300 were used to calculate the CFUs of the original sample. For ACD determination, a volume of cell sample was diluted into phosphate-buffered saline solution and cell diameter measured using a Scepter Handled Automated Cell Counter equipped with a 40 µm sensor (Millipore, Billerica, USA).

2.8 Statistical analysis

The presented values are averages of biological triplicates with standard errors. Kinetics parameters were calculated by fitting OD_{600} values to reparametrized Gompertz equation using the Statsoft Statistica 10 Package. The extracellular concentration over time of the main by-products (ethanol, glycerol, succinate, and 2,3 butanediol) were represented and fitted by nonlinear regression to

allosteric sigmoidal, sigmoidal 4PL or asymmetric sigmoidal 5PL equations of the GraphPad Prism 6.0 Software package (La Jolla, CA, USA). Best-fit curves were selected following the recommandations of Motulsky and Christopoulos (2004). The first derivative of the fitted curve was subsequently calculated to determine the specific production rate (q) of each compound.

3. Results

3.1 Fermentative and kinetic parameters

To determine the metabolic differences among different species of *Saccharomyces* in wine fermentation, we performed fermentation in 0.5 L vessel bioreactors at 25 ºC using natural white must with *S. cerevisiae* T73 strain, BMV58 and CECT12600 *S. uvarum* strains and CR85 *S. kudriavzevii* strain. Monitoring and evaluation of sugar consumption, OD600, dissolved oxygen and carbon dioxide released were used as an indicator of yeast growth and fermentative activity while YAN (Yeast Assimilable Nitrogen) content was used as a limiting factor. These parameters are presented in **Figure 1**.

Kinetic parameters were determined by adjusting OD600 measures to the reparametrized Gompertz equations and are presented in **Table 2**.

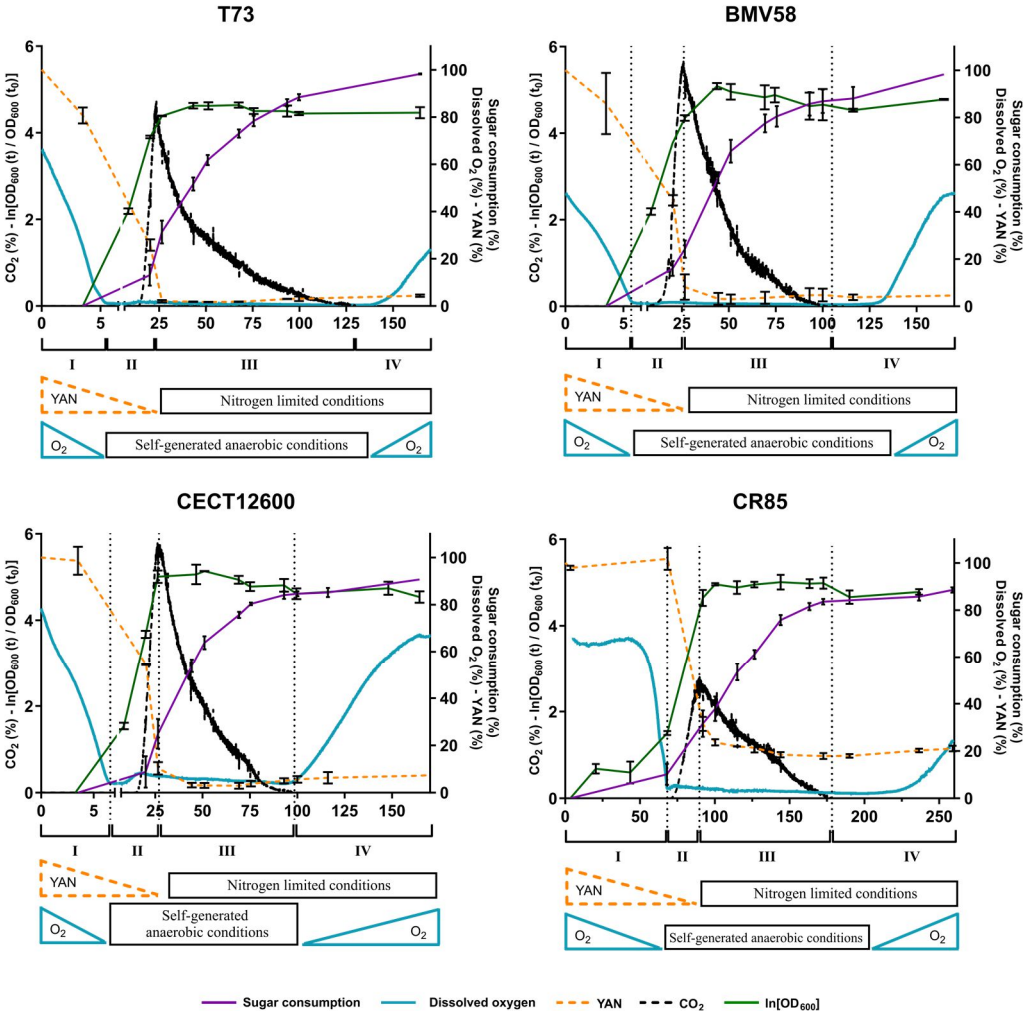

Figure 1. Progress of total sugar consumption expressed as percentage (purple solid line), YAN content expressed as percentage (orange dashed line), dissolved oxygen expressed as percentage (solid blue line), CO_2 exhaust concentration as percentage (black dashed line) and cell population expressed as ln[OD600 (t) / OD600 (t0)] (green solid line) with t0 the time of inoculation, during natural grape must fermentation in bioreactors at 25 ºC.

Metabolic phases (I, II, III and IV) are indicated below the x-axis of time expressed in hours. The values are displayed as mean and standard deviations from triplicate experiments.

Table 2. Growth curve parameters and biomass levels during natural grape must fermentations in bioreactors at 25ºC

Strain	Species	μmax	λ	A	Max DW
T73	*S. cerevisiae*	0,33 ± 0,01^{b,c}	2,14 ± 0,1^{a}	5,19 ± 0,05^{b}	5,63 ± 0,72^{b}
BMV58	*S. uvarum*	0,34 ± 0,03^{c}	5,49 ± 0,98^{a}	5,32 ± 0,18^{b}	4,40 ± 1,57^{a,b}
CECT12600	*S. uvarum*	0,28 ± 0,01^{b}	4,22 ± 0,75^{a}	5,08 ± 0,05^{b}	4,70 ± 0,30^{a,b}
CR85	*S. kudriavzevii*	0,23 ± 0,01^{a}	60,2 ± 2,99^{b}	4,8 ± 0,03^{a}	3,30 ± 0,20^{a}

μ_{max} is the maximum growth rate (h^{-1}), λ is the lag phase period (h), A is the maximum cell population value and Max DW is the maximum dry weight value. Superscript letters indicate the significant homogeneous groups obtained by one-way ANOVA analysis (Tukey test, n = 3, p-value <0.05).

The T73 wine strain was the quickest initiating fermentation with the lowest lag phase estimated at 2.14 hours according to Gompertz parametrization (**Table 2**). Both *S. uvarum* strains showed a slightly

higher lag phase –approximately 2 folds higher– compared to the commercial *S. cerevisiae* strain. However, BMV58 strain was the strain with the highest maximum growth rate among the four strains estimated at 0.34 h^{-1} consistent with previously described anaerobic growth values. There were no significant differences between the *S. cerevisiae* wine strain and both *S. uvarum* strains in terms of cell population reached during stationary phase. Non-surprisingly, at 25°C, the natural and cryophilic CR85 strain was the slowest in performing the alcoholic fermentation. CR85 strain showed a significantly larger lag phase, respectively 28-folds, 14-folds and 11-folds higher than T73, CECT12600 and BMV58 strains. Results obtained from the end of exponential growth phase showed that at 25ºC, the T73 wine strain produced more biomass than BMV58, CECT12600 and CR85 strains. Regarding the CR85 strain, it had the lowest DW values as well as the lowest cell population in stationary phase (**Table 2**; **Figure 2A**). Moreover, it did not consume the totality of the fermentable sugars presented in the must (**Figure 1**), which pointed out its regular fermentative ability at 25ºC.

To obtain additional physiological information, the average cell diameter (ACD) was measured along the fermentation process in T73, CECT12600 and BMV58, the three strains that showed good fermentative behavior. Along the entire fermentation process, ACD of the *S. cerevisiae* wine strain was higher than both *S. uvarum* strains (**Figure 2B**).

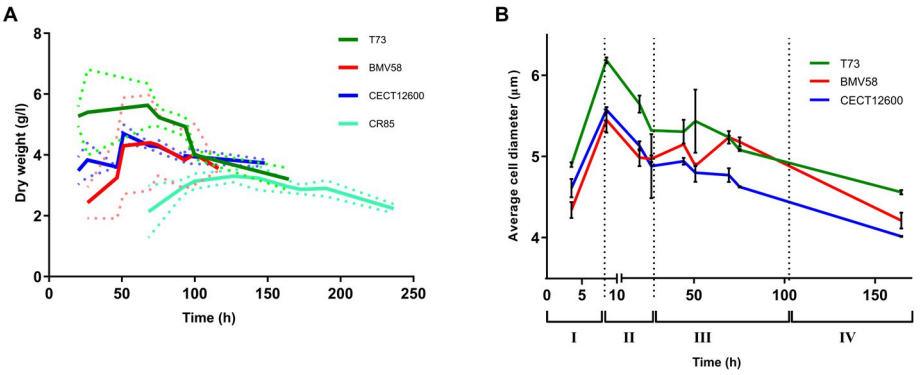

Figure 2. A) Dry weight amount (g/l) and B) average cell diameter (µm) along the fermentation process. For average cell diameter, the metabolic phases (I, II, III and IV) are indicated below the x-axis of time expressed in hours. The values are displayed as mean and standard deviations from triplicate experiments

Nearly after 8 hours of fermentation, maximum ACD values of 6.19 µm, 5.58 µm, and 5.45 µm were reached by T73, CECT12600 and BMV58 strains respectively. In addition, we observed that the three strains globally shared the same pattern of ACD. Very interestingly, the comparison of ACD with the rest of metabolic data led us to confirm that slope changes observed in **Figure 2B** were concomitant with metabolic transitions during cell growth due to modifications in the fermentation conditions.

Based on this observation and the timing of the fermentative activity parameters (CO_2 released, dissolved oxygen, sugar consumption, and

YAN content), the cultivation could be divided into four phases, namely a transitory aerobic phase (I), an exponential growth phase delimited by the nitrogen content (II), a stationary phase (III) and the end of fermentation (IV), as indicated on the bottom of **Figure 1**.

3.2 Phase I - a transitory aerobic phase

Gas probes registered a rapid depletion of the dissolved oxygen initially present inside the bioreactors. There was no more dissolved oxygen present in the medium nearly after 8 hours in T73, BMV58 and CECT12600 fermentations (**Figure 1**). In CR85, oxygen depletion occurred after 70 hours, which was in accordance with its longer lag phase (**Figure 1**; **Table 2**). Molecular oxygen exhaustion represented the end of phase I and the transition from aerobic to self-generated anaerobic conditions. Interestingly, molecular oxygen depletion concurred with the mentioned peak of ACD observed after 8 hours in *S. cerevisiae* and *S. uvarum* fermentations (**Figure 2B**). Moreover, the extracellular levels of acetate and proline, relative to their initial concentration at the time of inoculation, were calculated and are presented in **Figure 3**. We observed that the relative extracellular level of acetate decreased a the beginning of the fermentation in the four strains (**Figure 3A**). The same occurred with the proline level in BMV58, CECT12600 and CR85 strains, while in T73 fermentation no decrease was observed (**Figure 3B**).

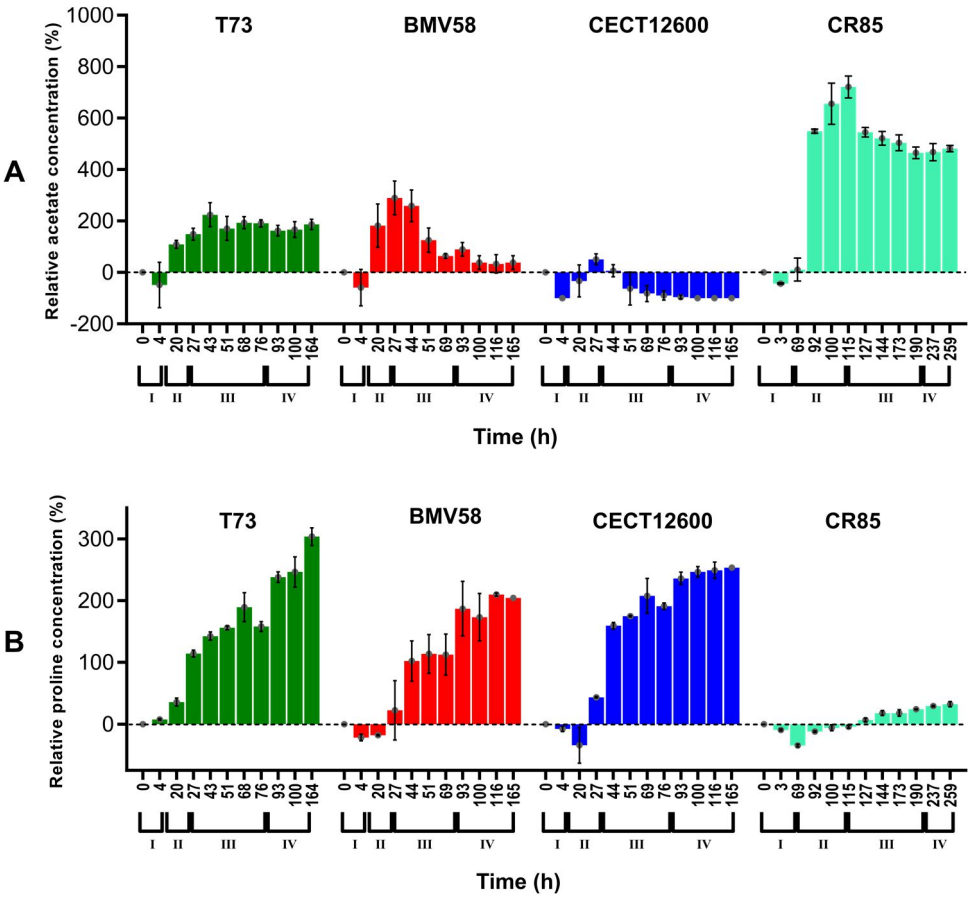

Figure 3. Relative extracellular acetate (A) and proline (B) concentrations (%) during natural grape must fermentation in bioreactors at 25 ºC. The relative concentrations were calculated as the difference between the extracellular concentration of the metabolite and its initial concentration in the must, and divided by the initial metabolite concentration. Metabolic phases (I, II, III and IV) are indicated below the x-axis of time expressed in hours. The values are displayed as mean and standard deviations from triplicate experiments.

3.3 Phase II - an exponential growth phase delimited by the nitrogen content

Nitrogen availability is a critical factor for yeasts during alcoholic fermentation because it affects both fermentation kinetics and the formation of metabolites. In the present work, extracellular ammonium and free amino acids concentrations in the medium were determined by UPLC (**Figure S1**) and served for the calculation of the yeast assimilable nitrogen (YAN) presented in **Figure 1**.Moreover, for each strain, the the extracellular concentration across time of each nitrogen source was presented in the form of a heatmap in **Figure 4**.

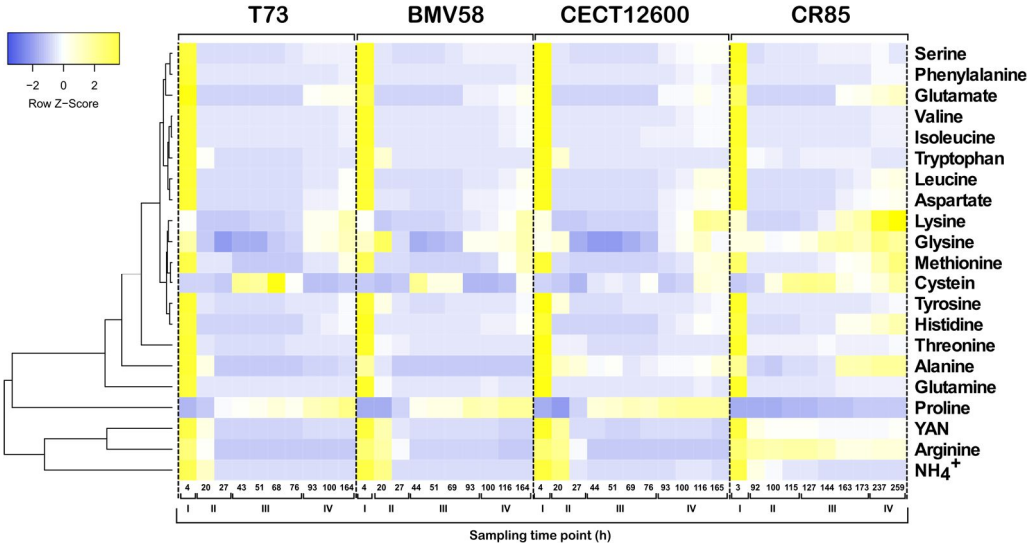

Figure 4. Heat map of the extracellular concentration across time of amino acids, ammonia and yeast assimilable nitrogen (YAN). Metabolic phases (I, II, III and IV) are indicated below the x-axis of time expressed in hours.

Hierarchical clustering (average linkage with Euclidean distance measurement) was used to group the compounds with the online tool Heatmapper.

The timing of nitrogen uptake and cell growth was coherent with growth arrest triggered by total (T73, BMV58, and CECT12600) or partial depletion (CR85) of YAN corresponding with the end of phase II (**Figure 1**; **Figure 4**). Monitoring of YAN showed that the assimilable nitrogen was completely consumed after the exponential growth phase finished in *S. cerevisiae* and *S. uvarum* fermentations. YAN decreased below 2% of its initial content after 27 and 44 hours in *S. cerevisiae* and *S. uvarum* fermentations respectively. Focussing on arginine, the predominant amino-acid in the natural white must (**Table S1**), 25% of its initial content was still available after 27 hours in BMV58 and CECT12600 fermentations while it was already depleted at this time in T73 fermentation (**Figure 4**; **Figure S1**). In CR85 strain, YAN content decreased until 22% after 115 hours of fermentation and coincided with the end of its exponential growth phase (**Figure 1**). Consistent with its lower biomass yield and its poor fermentability at 25ºC, we observed that CR85 strain consumed only a half of the arginine content initially present in the grape must (**Figure 4**; **Figure S1**).

A

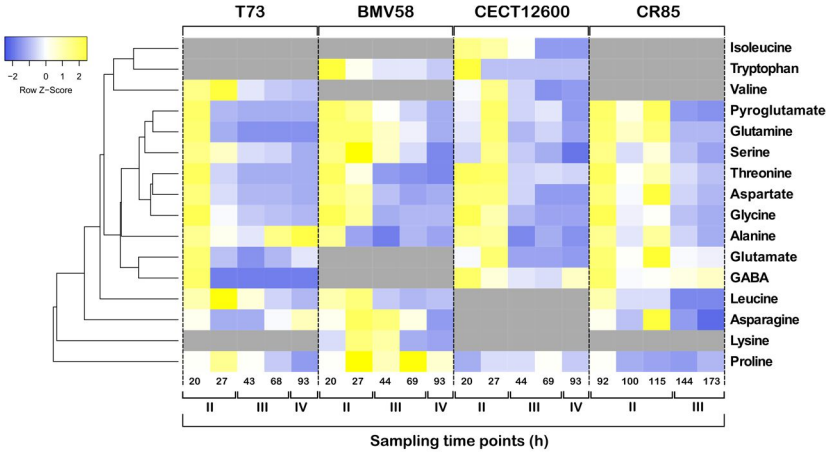
T73
BMV58
CECT12600
CR85
−2 0 1 2
Row Z−Score
Isoleucine
Tryptophan
Valine
Pyroglutamate
Glutamine
Serine
Threonine
Aspartate
Glycine
Alanine
Glutamate
GABA
Leucine
Asparagine
Lysine
Proline
20 27 43 68 93 20 27 44 69 93 20 27 44 69 93 92 100 115 144 173
II III IV II III IV II III IV II III
Sampling time points (h)

B

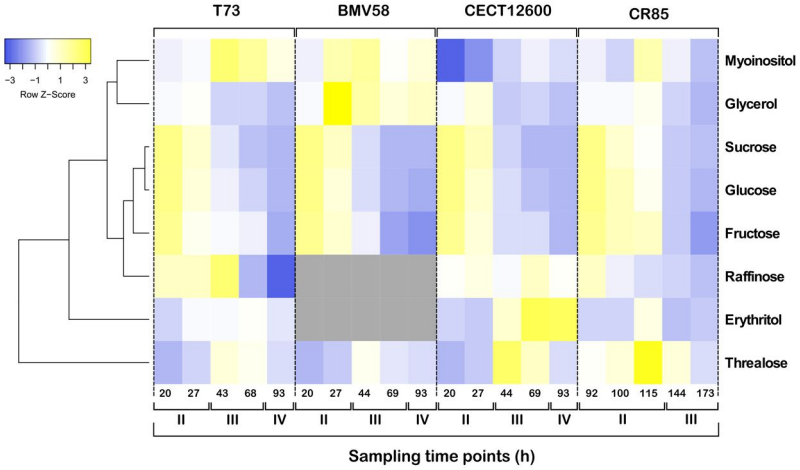
T73
BMV58
CECT12600
CR85
−3 −1 1 3
Row Z−Score
Myoinositol
Glycerol
Sucrose
Glucose
Fructose
Raffinose
Erythritol
Threalose
20 27 43 68 93 20 27 44 69 93 20 27 44 69 93 92 100 115 144 173
II III IV II III IV II III IV II III
Sampling time points (h)

C

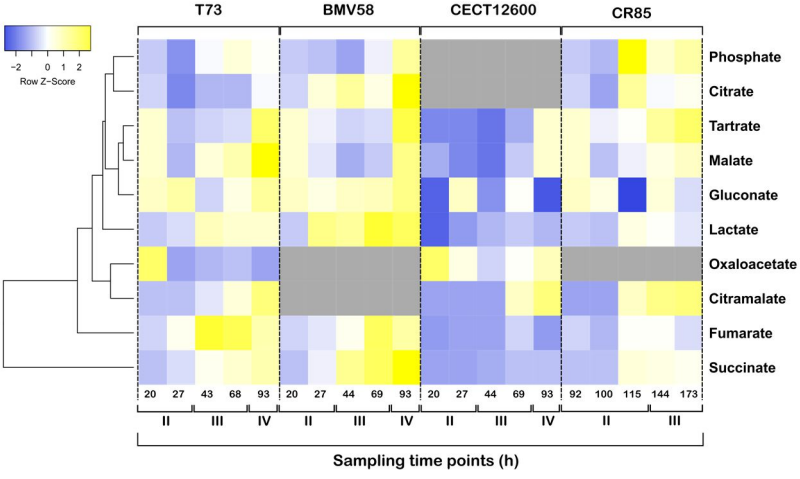
T73
BMV58
CECT12600
CR85
−2 0 1 2
Row Z−Score
Phosphate
Citrate
Tartrate
Malate
Gluconate
Lactate
Oxaloacetate
Citramalate
Fumarate
Succinate
20 27 43 68 93 20 27 44 69 93 20 27 44 69 93 92 100 115 144 173
II III IV II III IV II III IV II III
Sampling time points (h)

Figure 5. Heat maps of the relative intracellular content of amino acids (A), organic acids (B) and carbohydrates (C), determined in five sampling time points in our set of *Saccharomyces* strains. Metabolic phase (II, III and IV) are indicated below the horizontal axis of time expressed in hours. Hierarchical clustering (average linkage with Euclidean distance measurement) was used to group the compounds with the online tool Heatmapper. Missing values corresponding to compounds not detected by GC-MS are shown in light grey.

The level of intracellular amino-acids was determined by GC-MS for the four strains (**Figure 5A**; **Figure S2**) and in the five intracellular sampling points. Except for leucine, valine, and proline, the rest of amino-acids reached their minimum intracellular level after 27 hours (Glutamine, GABA) or 44 hours (others) in T73 strain fermentation, coinciding with the end of the exponential growth phase.

From then on, an increase in alanine, asparagine and glutamate content inside T73 cells was reported while levels of other amino-acids remained stable or null. In BMV58 strain, most of the amino-acids reached their minimal value after 44 hours of fermentation excepting asparagine, serine, glutamine, pyroglutamic acid and proline. In CECT12600 strain, tryptophan depletion was observed earlier (27 h) and isoleucine and aspartate seemed to be totally catabolized after 69 hours. On the other hand, minimum intracellular nitrogen values were mostly reported after 44 hours (**Figure 5A**; **Figure S2**). In CR85 strain, the maximum intracellular amino-acid

levels were observed after 115 hours of fermentation, corresponding to the end of phase II (**Figure 5A**; **Figure S2**). From that time on, most amino acid levels dropped to reach their minimum value after 144 hours. To sum up, despite some individual variations between the four strains, results showed that a general decrease in the intracellular amino-acids levels occurred with the entry into stationary phase at the end of phase II.

The extracellular concentration of the main by-products and sugars during the fermentations were determined by HPLC (**Figure S3**). For ethanol, glycerol, succinate and 2.3 butanediol, their extracellular concentration over time were fitted to distinct mathematical models and the derived function subsequently calculated to obtain the specific production rate (qEth, qGly, qSucc and qBut) of each compound (**Figure 6**). During the whole growth phase, qEth and qGly increased in parallel in the four fermentations (**Figure 6**), pointing out the importance of glycerol as redox valve during biomass synthesis. Moreover, qEth and qGly peaks were concomitant with both CO_2 exhaustion (**Figure 1**) and intracellular glycerol peaks at the end of phase II (**Figure 5B**; **Figure S4**). In concordance with their higher glycerol yields, *S. uvarum* strains BMV58 and CECT12600 and *S. kudriavzevii* CR85 strains showed the highest values for qGly (**Figure 6**).

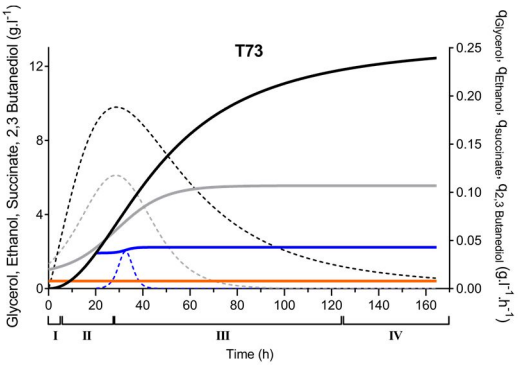

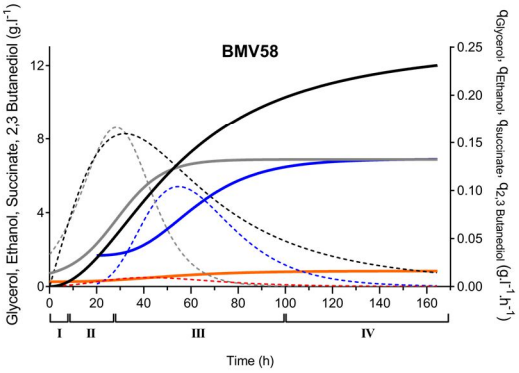

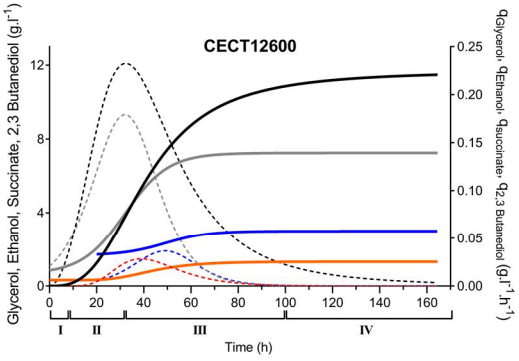

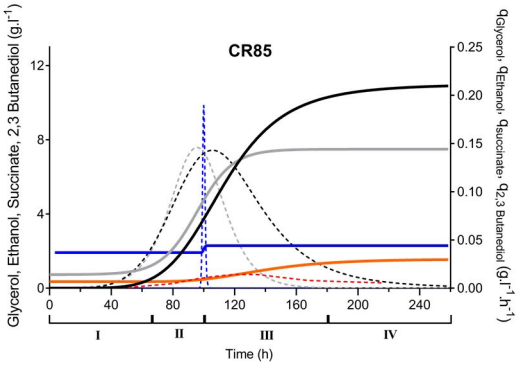

Legends

- Ethanol
- Glycerol
- $q_{Ethanol}$
- $q_{Glycerol}$
- 2,3 Butanediol
- Succinate
- $q_{2,3\ Butanediol}$
- $q_{Succinate}$

Figure 6. Fit curves of the main by-products responsible for NADH reoxidation during alcoholic fermentation according to Klerk (2010). Best-fit curves were determined as reported by Motulsky and Christopoulos (2004) and the first derivative of the fitted curves subsequently calculated to determine the correspondent specific production rates. Ethanol (black solid line), glycerol (grey solid line), 2,3 butanediol (orange solid line) and succinate (blue solid line) with their corresponding derivatives qEth (black dashed line), qGly (grey dashed line), qBut (red dashed line) and qSuc (blue dashed line). Metabolic phases (I, II, III and IV) are indicated below the x-axis of time expressed in hours.

Interestingly, the natural isolate CECT12600 was the strain with the highest qEth at the end of phase II but it was not able to ferment all the sugars (**Figure 1**), pointing out a certain sensitivity to ethanol. A clear production of acetate by the four strains was observed during the exponential growth phase, and CR85 strain had the highest acetate level at the end of phase II (**Figure 3**). During phase II, we also observed the decrease of ACD in T73, BMV58 and CECT12600 fermentations (**Figure 2B**), which most likely accounted for the accumulation of smaller daughter cells during exponential growth.

3.4 Phase III – distinct metabolic responses among species following the onset of nitrogen starvation

When yeast cells enter into nitrogen starvation, the production of the main carbon products of the fermentation, ethanol, and glycerol, decreased (**Figure 6**), and also the level of carbon dioxide reached 0 (**Figure 1**). Only 20-25% of total sugars were exhausted when the four strains entered into stationary phase (**Figure 1**). Interestingly we reported a variety of metabolic responses among the four strains to sustain fermentation following the onset of nitrogen starvation. Among others, significant differences were observed in the yields of organic molecules that participate in redox homeostasis, and in the evolution of the extracellular acetate content.

3.4.1 Succinate and 2,3 butanediol, redox sinks in cryophilic strains

Beside ethanol and glycerol, other organic molecules can serve as electron acceptors from reduced forms of redox cofactors. For instance, succinate and 2,3 butanediol can also contribute to NADH reoxidation during alcoholic fermentation. A summary of the organic molecules that balance ratios of nicotinamide and flavin adenine redox cofactors during alcoholic fermentation and their places in the central carbon metabolism is presented in **Figure 7**. For each compound, the yield (g of compound produced/ g of sugar consumed) at the end of the fermentation was calculated and

compared between the four strains. Our results suggested that *S. uvarum* and *S. kudriavzevii* strains had other balancing strategies in comparison to the *S. cerevisiae* wine strain. BMV58 (0,033 g/g), CECT12600 (0,034 g/g) and CR85 (0,038 g/g) strains had significantly higher glycerol yields than T73 (0,023 g/g) strain (**Figure 7**). Also CR85 strain had the highest 2,3 butanediol yield ($6{,}6.10^{-3}$ g/g), followed by CECT12600 ($5{,}6.10^{-3}$ g/g) and BMV58 ($3{,}1.10^{-3}$ g/g) strains. On the contrary, almost no 2,3 butanediol (4.10^{-4} g/g) was yielded by the *S. cerevisiae* wine strain (**Figure 7**). It was concordant with the horizontal linear fitting of 2.3 butanediol concentration across time obtained for T73 in **Figure 6**. Regarding succinate, the BMV58 (0.038 g/g) strain had the highest yield, far from CECT12600 ($6{,}4.10^{-3}$ g/g), CR85 ($3{,}6.10^{-3}$ g/g) and T73 ($2{,}3.10^{-3}$ g/g) strains. In the BMV58 fermentation, the increase in q2,3But rate concurred with the decreases of ethanol and glycerol yields at the end of phase II, while, interestingly, the increase in qSucc rate seemed to occurred only a few hours later during phase III (**Figure 6**). Moreover, qSucc and q2,3But peaked approximately at the same time in CECT12600 and BMV58 strains. Nevertheless, CECT12600 and CR85 strains had significantly higher 2.3 butanediol yields than BMV58 (**Figure 7**). This last observation suggested that CECT12600 and CR85 may preferably shuttled carbon flux from pyruvate to 2,3 butanediol synthesis to control NADH/NAD+ ratio. On the contrary, the BMV58 strain might preferably used the succinate sink. Finally, both *S. uvarum* strains had

significantly higher D-Lactate yields compared with the T73 and CR85 strains (**Figure 7**).

3.4.2 Differences in acetate metabolism

Following the onset of nitrogen starvation, we reported interesting fluctuations in the extracellular acetate content in BMV58, CECT12600 and CR85 fermentations. In T73 fermentation, the extracellular acetate concentration increased and remained constant from the entry into stationary phase (**Figure 3**). On the contrary, for BMV58, CECT12600 and CR85 strains, the extracellular acetate level decreased when they entered into stationary phase. This decrease was particularly pronounced in CECT12600 strain in which no acetate was detected when the fermentation concluded (**Figure 3**; **Figure 7**).

In addition, among the organic acids intracellularly detected by GC-MS (**Figure 5C**; **Figure S5**), citramalate (produced from acetate) showed a different accumulation pattern in T73, CECT12600 and CR85 strains (no data was available for BMV58 strain). Its accumulation occurred almost with the entry into nitrogen limited conditions in T73 and CR85 strains while it seemed to occur later in CECT12600 (**Figure 5C**, **Figure S5**).

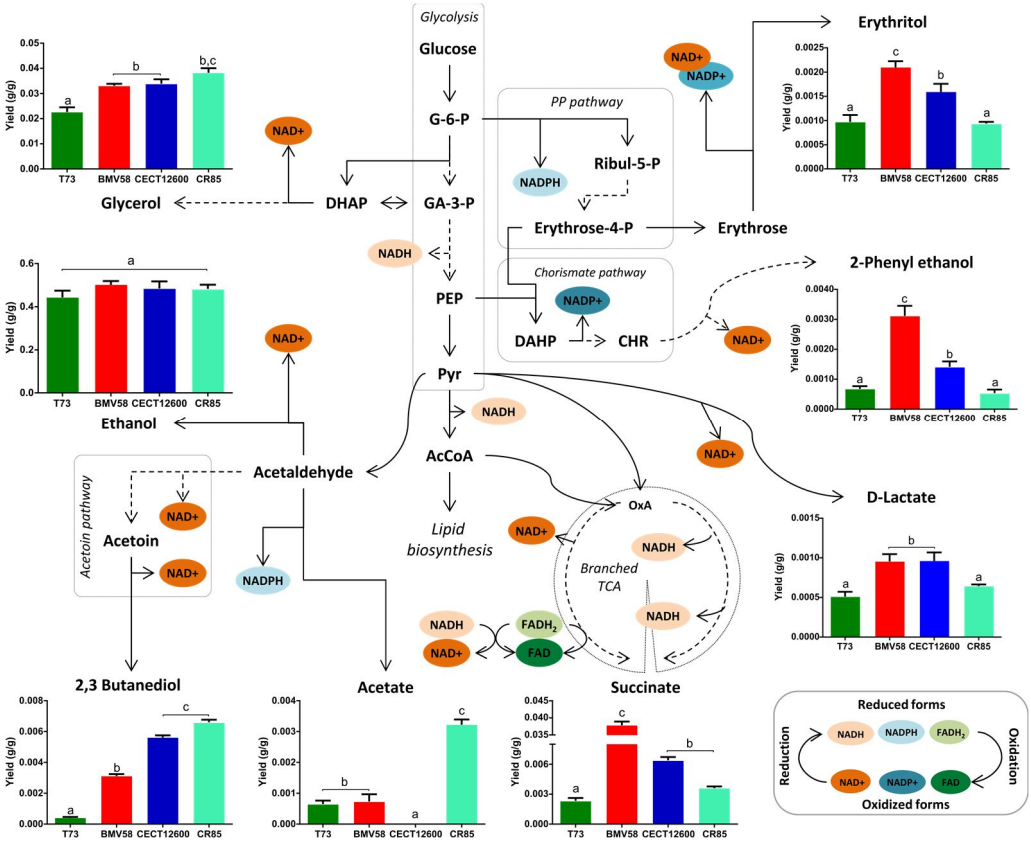

Figure 7. Role of nicotinamide adenine dinucleotide and flavin adenine dinucleotide cofactors in central carbon metabolism under anaerobic conditions in *S. cerevisiae*. Only the main representative redox balance reactions are represented. For each strain, the yields of the main fermentative by-products, computed as g of compound produced/g of sugar consumed, were represented. The values are displayed as mean and standard deviations from triplicate experiments. Superscript letters indicate the significant homogeneous groups obtained by one-way ANOVA analysis (Tukey test, n = 3, p-value <0.05). G-6-P: glucose-6-phosphate; F-6-P: fructose-6-phosphate; DHAP: dihydoxyacetone phosphate; GA-3-P:

glyceraldehyde-3-phosphate; PEP: phosphoenolpyruvate; Pyr: pyruvate; AcCoA: acetyl coenzyme A; OxA: oxaloacetate; Ribul-5-P: ribulose-5-phosphate; DAHP: 3-deoxy-D-arabino-heptulosonate-7-phosphate; CHR: chorismate.

3.4.3 Differences in erythritol synthesis

In this study, the quantification of yeast intracellular compounds by GC-MS led us to detect the production of erythritol by our set of *Saccharomyces* strains (**Figure 5B**). After what, the extracellular erythritol accumulation was also determined by HPLC. We observed that *S. uvarum* strains BMV58 ($2{,}1.10^{-3}$ g/g) and CECT12600 ($1{,}6.10^{-3}$ g/g) had the highest erythritol yields in our experimental conditions (**Figure 7**; **Table S2**). These results were notably in accordance with the higher intracellular accumulation of erythritol observed in CECT12600 strain (**Figure 5B**). In addition, the increase of extracellular and intracellular levels of erythritol seemed to concur with the entry into stationary phase in CECT12600 fermentation (**Figure 5B**; **Figure S4**). On the contrary, intracellular level of erythritol increased during exponential growth phase (phase II) in T73 and CR85 strains, and then decreased in phase III when cells entered into nitrogen starved conditions (**Figure 5B**; **Figure S4**).

3.4.4 Trehalose accumulation

Trehalose is an important reserve carbohydrate and a stress protectant in yeasts that was intracellularly measured by GC-MS

(Figure 5B; Figure S4). We observed that trehalose accumulation started simultaneously with the end of the exponential phase and respectively ended after in the four strains (Figure 5B; Figure S4). It started to be consumed after 44h of fermentation in T73, BMV58 and CECT12600 strains while after 115h in CR85 strain and concurred with the timing of YAN depletion. Interestingly, CECT12600 and CR85 strains seemed to accumulate higher intracellular amounts of trehalose if compared with the T73 and BMV58 wine strains (Figure 5B; Figure S4). This high trehalose accumulation suggest a higher stress response in CECT12600 and CR85 natural isolate strains in comparison with both wine strains, maybe to cope with nutrient starvation and to face to ethanol stress.

3.5 Phase IV – end of fermentation

The end of the fermentation process was marked by the end of carbon dioxide released in the four fermentations and the following increase in molecular oxygen concentration in the medium (Figure 3). In parallel, we reported an increase in the extracellular content of various amino acids like lysine, glysine or glutamate, above all in the CR85 strain (Figure 4). Moreover,for T73 and BMV58 strains which showed good fermentative behavior, we reported a decrease in cell viability from 90-100 hours of fermenations (Figure S6). Thus, some autolysis processes were likely to occur at the end of fermentation due to nutrient depletion and ethanol accumulation. Interestingly, the decrease in cell viability was steeper in BMV58

strain than in T73 (**Figure S6**), pointing out a higher ethanol resistance of cells of the *S. cerevisiae* wine strain.

In this study, we also evaluated the final concentration of a set of fusel alcohols, acetate esters and ethyl esters due to their relevance in oenological production processes as well as a mechanism to compensate the redox balance. The timing of aroma synthesis is presented in the form of a heat map including the four phases of the fermentation process and suggested that aromas compounds are principally being synthesized at the end of phase II (**Figure 8**; **Figure S7**). In addition, a PCA analysis was used to integrate the various aroma traits of the four strains. In the resulting PCA plot, the Factor 1 axis (42.83% of the variance) mostly corresponds to 2-phenylethanol, 2-phenylethyl acetate, and total fusels variables, on the left, 1-hexanol, benzyl alcohol and benzyl acetate on the right. The Factor 2 axis (30,52% of the variance) mostly corresponds to the total esters and ethyl acetate variables, on the top, and isobutanol, isoamyl alcohol and ethyl caprylate on the bottom; these two groups of variables being negatively correlated. Consistent with previous studies of our group (Gamero *et al.*, 2013), BMV58 and CECT12600 strains produced higher amounts of 2-phenylethanol and 2-phenylethyl acetate (**Figure 8**; **Table S2**). CECT12600 was also the strain with the highest total esters yield, mainly on account of its high ethyl acetate production. 2-phenylethanol represented approximately 56% and 48% of the total fusel alcohols yield in

BMV58 and CECT12600, while only 21% and 26% in T73 and CR85 strains respectively. Interestingly, benzyl alcohol and benzyl acetate were more produced by T73, CECT12600 and CR85 strains. Finally, isoamyl alcohol, its acetate ester, and several medium chain fatty acid ethyl esters (caproate, caprylate) were presents in a significantly higher amount in T73 fermentation.

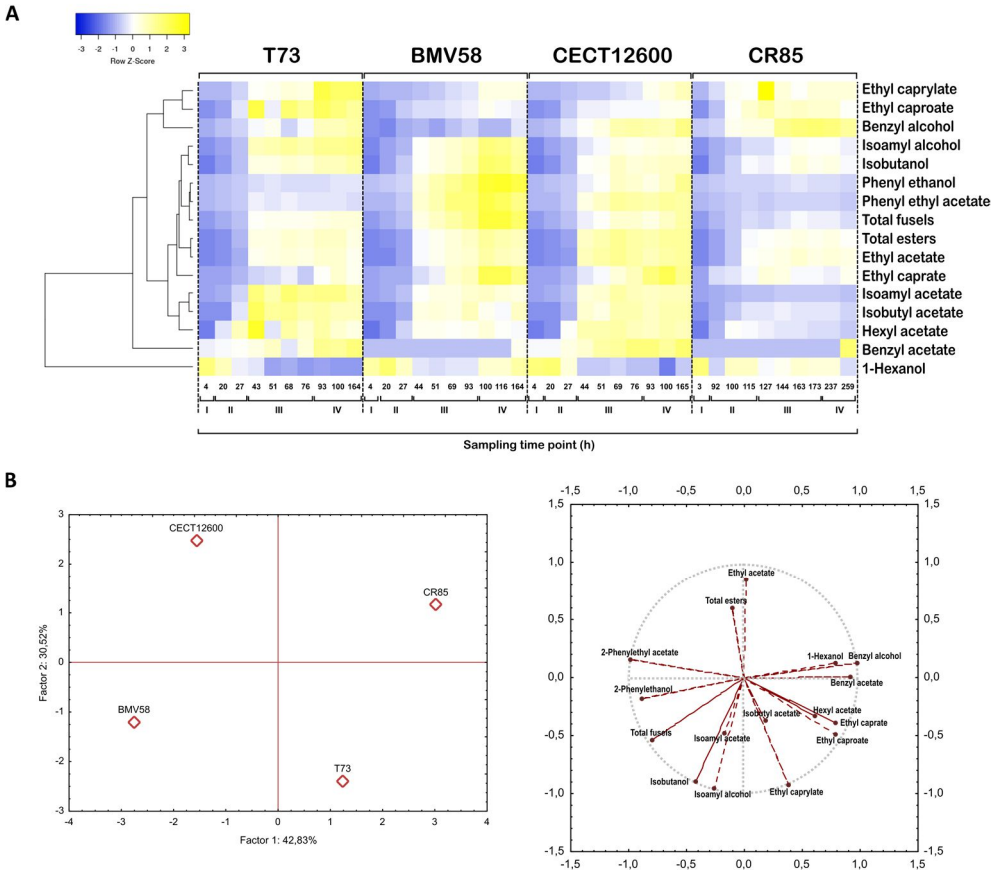

Figure 8. Heat map of the complete aroma dataset obtained in this work for each strain (A) and PCA plots of the aroma compounds quantified at the

end of the fermentations (B). We included five fusel alcohols, nine esters and their respective total content, namely: isobutanol, isoamyl alcohol, 1-hexanol, benzyl alcohol, 2-phenylethanol, ethyl acetate, isoamyl acetate, isobutyl acetate, ethyl caprylate, ethyl caproate, ethyl caprate, hexyl acetate, benzyl acetate, 2-phenylethyl acetate, total fusels and total esters levels. For heat map, hierarchical clustering (average linkage with Spearman's rank correlation for distance measurements) was used to group the compounds with the online tool Heatmapper.

4. Discussion

The results presented above illustrate that yeast strains of species *S. cerevisiae*, *S. uvarum* and *S. kudriavzevii* show distinct responses with respect to the occurrence of alcoholic fermentation under mimicked winemaking conditions. In this study, we used a dynamic approach to explore the time course metabolome of four strains isolated from distinct sources. The yeasts *S. cerevisiae* T73 and *S. uvarum* BMV58 are commercial wine strains currently used in the winemaking process, while *S. uvarum* CECT12600 and *S. kudriavzevii* CR85 strains are not used in industrial fermentations. The monitoring of fermentation was performed in conditions representative of white wine elaboration. To mimic winemaking conditions, we used a natural grape must rather than synthetic media. Indeed, frozen grape juices conserved their fermentation properties and can be kept for long periods (Da Silva *et al.*, 2015). Throughout the complex ripening

process of grapes, a wide range of compounds like sugars, organic acids, phenolic compounds, fatty acids, amino acids, vitamins or nucleic acids are synthesized and enter in must composition which is further fermented by yeasts. Consequently, because it is very difficult to reproduce such a complex matrix, synthetic media might be less pertinent than a natural must for assessing quantitative traits due to their incomplete composition (Marullo *et al.*, 2007; Ambroset *et al.*, 2011; Peltier *et al.*, 2018). Recently, most of the studies that focused on comparing phenotypic or metabolomics traits of *S. uvarum* and *S. kudriavzevii* species with *S. cerevisiae* were performed in model synthetic medium, using steady-state culture and in aerobic or strict anaerobic conditions (Masneuf-Pomarède *et al.*, 2010; López-Malo *et al.*, 2013). Thus they give us little information about how these species could metabolically respond to self-generated anaerobic conditions that are generated in wineries, notably during white wine elaboration. In our study, the consumption of the initial dissolved oxygen present in grape must and the subsequent release of carbon dioxide by yeasts lead to self-generated anaerobic conditions inside the fermenters.

In this work, starter cultures were prepared in GPY liquid medium at 25ºC and in aerobic conditions. According to Salmon et al. (1998), in such conditions yeast cells exhibited normal mitochondria, high cytochrome content as well as high oxygen uptake rate at the time of inoculation. On the other hand, *Saccharomyces* yeasts are Crabtree-

positive and ferment when sugar concentrations are high, even if oxygen is present for more efficient aerobic respiration (Piškur *et al.*, 2006). Here, following the inoculation, we observed that the four strains behaved quite similarly while dissolved oxygen was present at the beginning of the alcoholic fermentation. In accordance with the duration of their lag phase and their fermentative ability, the level of dissolved oxygen in the grape juice rapidly decreased for the four strains. Dissolved oxygen depletion occurred between 6 and 8 hours in T73, BMV58 and CECT12600 fermentations while it happened slower (70 hours) in CR85 fermentation. Thus, the previous observations together with the aerobic pre-culture preparation suggested that yeast cells could have been aerobically active at the beginning of the fermentation, and that existed a transitory respire-fermentative phase during step I, while dissolved oxygen was available. Consistent with this hypothetic transitory oxidative activity, we reported that extracellular acetate was consumed by the four strains in the early hours of phase I. After acetate uptake by yeasts, cytosolic acetate could be activated to acetyl CoA by the cytosolic acetyl CoA synthetase ACS1 before being shuttled through the mitochondria membrane by acetyl-carnitine shuttle and subsequently metabolized through the TCA cycle as a carbon energy source (Krivoruchko *et al.*, 2015).

In the early stages of the fermentation, we also observed differences in the metabolism of nitrogen sources between *S. cerevisiae* and

cryophilic species *S. uvarum* and *S. kudriavzevii*, notably proline and arginine. We noticed that BMV58, CECT12600 and CR85 strains picked up proline from the medium when dissolved oxygen was present while the wine strain T73 did not. Regarding arginine, its removal was carried out slower by BMV58 and CECT12600 strains, or even only partially by the CR85 strain while in T73 it was removed rapidly. These results suggested differences in the regulation of nitrogen metabolism. Proline catabolism is capable of a high-energy output and may provide amino nitrogen and reducing power to cells. Each molecule of proline, when oxidized, can yield 30 ATP equivalents (Hare and Cress, 1997). Nevertheless, despite its interesting energetic properties, its catabolism by yeasts under oenological conditions is extremely limited because the presence of oxygen is a requirement for proline oxidases PUT1 catalytic activity which is responsible for the first step in proline ring catabolism into the mitochondria (Duteurtre *et al.*, 1971). In addition, nitrogen sources are generally classified on the basis of the growth rate reached when present as the unique source, and on their impact on the transcriptional regulation of the pathways involved in the utilization of other nitrogen sources (Magasanik and Kaiser, 2002). According to both criteria, proline is widely considered a poor source of nitrogen among *Saccharomyces* and non-*Saccharomyces* yeasts while arginine as a good one. The difference observed in proline uptake may, therefore, account for a higher Crabtree effect

repression on the respiration pathway or for stronger nitrogen-catabolite repression of proline permeases in the *S. cerevisiae* wine strain (T73). On the contrary, in BMV58, CECT12600 and CR85 strains, the early proline uptake was concordant with an hypothetic transient oxidative activity during phase I. Nevertheless, further studies are needed to deeply explore that difference in proline assimilation between cryophilic species and *S. cerevisiae* under aerobic conditions at the beginning of fermentation.

We also noticed important differences in the metabolism of acetate among the three species. The CR85 strain showed important shortcomings in growth and produced the highest level of acetate. In T73 fermentation, the extracellular acetate level remained almost constant after the entry into stationary phase while we observed a singular production-consumption profile in CR58, BMV58 and CECT12600 strains. This consumption was particularly pronounced in CECT12600 strain in which no acetate was detected when the fermentation concluded. During growth on glucose, the assimilation of ammonium and the excretion of oxidized low-molecular metabolites by yeast cells result in a net production of reduced equivalent of NADH (Bakker *et al.*, 2001). Consequently, biomass formation has a determinant impact on redox metabolism. It is responsible for NADPH consumption and for the largest part of NADH produced during the growth phase. Regarding NADPH, the oxidative branch of the pentose phosphate pathway supplies most of the

NADPH requested together with various precursors for the biosynthesis of nucleic acids and amino acids. But besides the pentose phosphate pathway, the conversion of acetaldehyde into acetate by acetaldehyde dehydrogenase (ACDH) can also generate reducing equivalents in the form of NADPH (Saint-Prix *et al.*, 2004).

As an activated form of acetate, acetyl-CoA serves as a crucial intermediate metabolite in the metabolic network of yeasts and is involved in metabolism in multiple subcellular compartments like cytosol, mitochondrion, peroxisome and nucleus (Krivoruchko *et al.*, 2015). Among others, acetyl-CoA is required for the synthesis of fatty acids, sterols, glutathione, amino acids (e.g. leucine, arginine, cysteine, and methionine) and it is the substrate for protein acetylation, which plays a role in the regulation of enzyme function and DNA transcription (Galdieri *et al.*, 2014). Except in mitochondria where acetyl-CoA can be generated from pyruvate by the actions of the pyruvate dehydrogenase complex (PDH), acetate is the precursor used to meet acetyl-CoA requirements via the action of acetyl-CoA synthetase (ACS) in the rest of subcellular compartments. The singular profile of extracellular acetate concentration observed in BMV58, CECT12600 and CR85 fermentations following nitrogen starvation suggested higher requirements in acetyl-CoA in cryophilic strains at this stage of the process that could be related with lipid synthesis or transcription control mechanisms. Tronchoni et al. (2012) showed in synthetic media and aerobic conditions that *S.*

kudriavzevii strains, including the CR85 strain, had different lipid composition compared with the *S. cerevisiae* T73 strain, notably higher percentages of medium-chain fatty acids and squalene and shorter chain lengths regardless of the growth temperature. Moreover, we detected an earlier intracellular accumulation of citramalate by T73 and CR85 strains between the end of the growth phase (phase II) and the entry into stationary phase (phase III), in comparison with the *S. uvarum* CECT12600 strain. Yeasts condense acetic acid (in the form of acetyl-CoA) and pyruvate to produce citramalate (Ribéreau-Gayon *et al.*, 2006). The entry into the stationary phase is an important step of alcoholic fermentation that is associated with major changes in the physiological state of yeast. Cell size and cell membrane composition are influenced by the stage of the cell cycle and the environmental conditions, like ethanol stress or anaerobic conditions (Turner *et al.*, 2012). Here we notably showed that ACD could be used as an indicator of the stage of the fermentation process since the time trends of ACD coincided with major changes in the medium conditions. The management of cell size and the remodeling of the membrane between the beginning and the end of fermentation are key factors for the cell to balance metabolism expenditure or to acquire a higher ethanol tolerance. Thus, it is possible that the evolutionary adaptation of T73 cells to fermentation conditions enable their higher ethanol resistance and might not require such important membrane remodeling. On the

other hand, both strains of *S. uvarum* (BMV58 and CECT12600) and to a lesser extent, the *S. kudriavzevii* strain (CR85), might partially take advantage of the extracellular acetate they produced during the growth phase to fulfill their acetyl-CoA requirement for membrane remodeling. Interestingly, this acetate uptake seemed to be triggered by nitrogen depletion in BMV58, CECT12600 and CR85 strains. Also, the earlier citramalate production by T73 and CR85 strains might be aimed at balancing the intracellular levels of acetyl-CoA and pyruvate from the end of the exponential growth phase.

The dynamic approach used in our study also enables us to obtain the timing of esters and fusel alcohols production. In accordance with Mouret et al. (2014), we confirm that their synthesis mainly started with the beginning of the stationary phase. Notably, the higher production of 2-phenyl ethanol and 2-phenylethyl acetate produced by BMV58 and CECT12600 strains was accompanied by an erythritol overproduction concomitant with the entry into nitrogen-limited conditions. On the contrary, erythritol production was detected later and to a lesser extent in and CR85 strains. In accordance with the phenotypic traits – low acetate yield and high phenyl ethanol yield – described by Cadière et al. (2011) in the evolved strain ECA5, our results suggested a higher activity of the pentose phosphate pathway in BMV58 and CECT12600 strains when entering into stationary phase. Erythritol, phenylethanol and phenylethyl acetate share the same precursor, erythrose-4-phosphate, an intermediate of the non-

oxidative branch of the pentose phosphate pathway. In yeasts, erythritol could serve as an osmolyte and can be synthesized from erythrose-4-phosphate after dephosphorylation and a reduction reaction catalyzed by an erythrose reductase, an NAD(P)H-dependant aldose reductase, resulting in the net regeneration of NAD(P)+ from NAD(P)H (Moon *et al.*, 2010). Nevertheless, to the best of our knowledge, there is no bibliography that reported the synthesis of such metabolite during alcoholic fermentation within the *Saccharomyces* genus. Thus, only high carbon fluxes through both the pentose phosphate pathway and glycolysis generate sufficient reduction capacity to lead to the overflow of erythritol we observed in BMV58 and CECT12600 strains. Finally, concordant with the production consumption profile of acetate in *S. uvarum* and *S. kudriavzevii* strains and with the hypothesis of membrane remodelling, flux analysis obtained from ^{13}C label experiments with the ECA5 strain by Cadière et al. (2011) suggested that the lower level of acetate excretion by the ECA5 strain might result from an increase in carbon flux from acetate towards acetyl-CoA for lipid synthesis.

The cellular machinery also involves the rapid synthesis of protective and storage carbohydrate molecules to cope with stress conditions. Intracellular data revealed that both natural isolate strains, CECT12600 and CR85, accumulated higher amount of trehalose among the four strains used, the timing of trehalose accumulation

being concurrent with nitrogen depletion. Trehalose is present in yeast cells as a reserve carbohydrate and as a stress protectant but, according to recent studies, the functional role of trehalose seemed to be as a stress protectant rather than as an energy store (Wang *et al.*, 2014). Its accumulation is highly correlated with ethanol production and could be responsible for sustaining cell viability in nitrogen-poor musts independent of the initial assimilable nitrogen content (Varela *et al.*, 2004). Moreover, the trehalose pathway appears to be required to balance ATP consumption and production with phosphate homeostasis when the upper glycolytic flux suddenly increases (van Heerden *et al.*, 2014). Thus, on the one hand the higher trehalose synthesis by CECT12600 and CR85 natural strains seemed to be an evidence of their lower adaptability to fermentative conditions, notably to face to the increasing ethanol content. On the other hand, it might be a mechanism for regulating phosphate homeostasis when they entered into stationary phase

Finally, monitoring of fermentation also revealed that the four strains differed one from another in their redox balancing strategies. Following the onset of nitrogen starvation, we observed that strains of *S. uvarum* and *S. kudriavzevii* produced higher levels of a number of by-products responsible for the maintenance of redox homeostasis in comparison to the *S. cerevisiae* strain. We observed that the CR85 strain yielded the highest levels of glycerol and 2,3 butanediol. BMV58 and CECT12600 strains yielded highest amount of D-lactate

among the four strains, and also more 2,3 butanediol and succinate than the *S. cerevisiae* T73 strain. In addition, within the set of *S. uvarum* strains, the non-wine isolate CECT1600 produced higher levels of 2,3 butanediol and less succinate than the BMV58 wine strain. In yeasts, metabolic networks have evolved to have tight regulation to maintain redox homeostasis which is principally manifested by the relative levels of cofactors pairs $NADH/NAD^+$ and $NADPH/NADP^+$ which are involved as electron carriers in about 200 reactions in *Saccharomyces cerevisiae* (Nielsen, 2017). In anaerobic conditions, NADH cannot be reoxidized by NADH dehydrogenases and none of the wine-related yeasts that were investigated contained transhydrogenase activity able to transfer excess reducing equivalents in the form of NADH to $NADP^+$. Thus balancing the $NADH/NAD^+$ ratio can be achieved by the formation of organic molecules which serve as the final acceptors of reducing equivalents from NADH. After acetaldehyde, the glycolytic intermediate dihydroxyacetone phosphate is the second most important acceptor of reducing equivalents from NADH within fermenting yeasts. Nevertheless, besides ethanol and glycerol formation, the production of 2,3 butanediol, succinate or D-lactate, which are all originated from pyruvate, can act as useful redox valves during alcoholic fermentation (Camarasa *et al.*, 2003; Ribéreau-Gayon *et al.*, 2005; Camarasa, 2007; de Klerk, 2010). Both succinate and 2,3 butanediol are derivatives from pyruvate. However, even under anaerobic

conditions, most of the reactions leading to succinate formation via the reductive or oxidative branch of the truncated TCA occurred inside the mitochondrion, requiring then its incorporation by a mitochondrial pyruvate carrier. On the contrary, reactions related to 2,3 butanediol occurred in the cytosol. Prevalence in CECT12600 and CR85 fermentations (both non-wine strains), for 2,3 butanediol production might be linked to compartmentation reasons or might account for the different affinity of the enzymes acting around the pyruvate node.

5. Conclusion

This study advances our understanding of the metabolic response within strains of the species *S. cerevisiae*, *S. uvarum* and *S. kudriavzevii* to conditions representative of the winemaking industry at the metabolic level. The differences observed in the management of the nitrogen substrates, in the production of polyols and organic molecules responsible for the maintenance redox balance including glycerol, erythritol, 2.3 butanediol and succinate, in the acetate metabolism and in the production of fusel alcohols and esters, indicate that it is possible to segregate the metabolism of the *S. cerevisiae* wine strain (T73) from cryophilic strains of *S. uvarum* (BMV58, CECT12600) and *S. kudriavzevii* (CR85). The *S. kudriavzevii* CR85 strain had important shortcomings in growth at 25ºC but still produced higher glycerol level than T73 strain. On the other hand,

the good fermentative ability of the *S. uvarum* strains and their interesting oenological skills at 25°C, notably to reduce extracellular acetate level or to produce more glycerol or succinate point out their biotechnological interest. The selection of strains of the *S. uvarum* species could help to reduce volatile acidity of wines, as well as to enhance their acidity and their mouth-feel properties by the mean of higher succinate and glycerol content.

Acknowledgments

RM was supported by a FPI grant from the Ministerio de Economía y Competitividad (ref. BES-2016-078202). This work was supported by the Spanish government projects AGL2015-67504-C3-1-R and RTI2018-093744-B-C31 awarded to AQ

Supplementary files

Supplementary files can be downloaded from https://doi: 10.1016/j.fm.2020.103484 or found at **page 325** of this manuscript.

References

Aguera, E., Bes, M., Roy, A., Camarasa, C., and Sablayrolles, J.M. (2010) Partial removal of ethanol during fermentation to obtain reduced-alcohol wines. *Am J Enol Vitic* **61**: 53–60.

Ambroset, C., Petit, M., Brion, C., Sanchez, I., Delobel, P., Guérin, C., et al. (2011) Deciphering the Molecular Basis of Wine Yeast Fermentation Traits Using a Combined Genetic and Genomic Approach. *G3: Genes|Genomes|Genetics* **1**: 263–281.

Chapter 1

Arroyo-López, F.N., Pérez-Torrado, R., Querol, A., and Barrio, E. (2010) Modulation of the glycerol and ethanol syntheses in the yeast *Saccharomyces kudriavzevii* differs from that exhibited by Saccharomyces cerevisiae and their hybrid. *Food Microbiol* **27**: 628–637.

Bakker, B.M., Overkamp, K.M., Van Maris, A.J.A., Kötter, P., Luttik, M.A.H., Van Dijken, J.P., and Pronk, J.T. (2001) Stoichiometry and compartmentation of NADH metabolism in *Saccharomyces cerevisiae*. *FEMS Microbiol Rev* **25**: 15–37.

Cadière, A., Ortiz-Julien, A., Camarasa, C., and Dequin, S. (2011) Evolutionary engineered *Saccharomyces cerevisiae* wine yeast strains with increased in vivo flux through the pentose phosphate pathway. *Metab Eng* **13**: 263–271.

Camarasa, C. (2007) Role in anaerobiosis of the isoenzymes for *Saccharomyces cerevisiae* fumarate reductase encoded by OSM1 and FRDS1. *Yeast* **26**: 545–551.

Camarasa, C., Grivet, J.P., and Dequin, S. (2003) Investigation by 13C-NMR and tricarboxylic acid (TCA) deletion mutant analysis of pathways of succinate formation in *Saccharomyces cerevisiae* during anaerobic fermentation. *Microbiology* **149**: 2669–2678.

Castellari, L., Ferruzzi, M., Magrini, A., Giudici, P., Passarelli, P., and Zambonelli, C. (1994) Unbalanced wine fermentation by cryotolerant vs. non-cryotolerant *Saccharomyces* strains. *Vitis* **33**: 49–52.

Catarino, M. and Mendes, A. (2011) Dealcoholizing wine by membrane separation processes. *Innov Food Sci Emerg Technol* **12**: 330–337.

Cohen, S.D., Tarara, J.M., and Kennedy, J.A. (2008) Assessing the impact of temperature on grape phenolic metabolism. *Anal Chim Acta* **621**: 57–67.

Duteurtre, B., Bourgeois, C., and Chollot, B. (1971) Study of the assimilation of proline by brewing yeasts. *J Inst Brew* **77**: 28–35.

Galdieri, L., Zhang, T., Rogerson, D., Lleshi, R., and Vancura, A. (2014) Protein Acetylation and Acetyl Coenzyme A Metabolism in Budding Yeast. *Eukaryot Cell* **13**: 1472–1483.

Gamero, A., Belloch, C., Ibáñez, C., and Querol, A. (2014) Molecular analysis of the genes involved in aroma synthesis in the species *S. cerevisiae*, *S. kudriavzevii* and *S. bayanus* var. *uvarum* in winemaking conditions. *PLoS One* **9**: 1–10.

Gamero, A., Tronchoni, J., Querol, A., and Belloch, C. (2013) Production of aroma compounds by cryotolerant *Saccharomyces* species and hybrids at low and moderate fermentation temperatures. *J Appl Microbiol* **114**: 1405–1414.

Goldner, M.C., Zamora, M.C., Lira, P.D.L., Gianninoto, H., and Bandoni, A. (2009) Effect of ethanol level in the perception of aroma attributes and the detection of volatile compounds in red wine. *J Sens Stud* **24**: 243–257.

Hare, P.D. and Cress, W.A. (1997) Metabolic implications of stress-induced proline accumulation in plants. *Plant Growth Regul* **21**: 79–102.

van Heerden, J.H., Wortel, M.T., Bruggeman, F.J., Heijnen, J.J., Bollen, Y.J.M., Planque, R., et al. (2014) Lost in Transition: Start-Up of Glycolysis Yields Subpopulations of Nongrowing Cells. *Science (80-)* **343**: 1245114–1245114.

Kishimoto, M. (1994) Fermentation characteristics of hybrids between the cryophilic wine yeast *Saccharomyces bayanus* and the mesophilic wine yeast *Saccharomyces cerevisiae*. *J Ferment Bioeng* **77**: 432–435.

de Klerk, J.-L. (2010) Succinic acid production by wine yeasts. *Notes*.

Kontoudakis, N., Esteruelas, M., Fort, F., Canals, J.M., and Zamora, F. (2011) Use of unripe grapes harvested during cluster thinning as a method for reducing alcohol content and pH of wine. *Aust J Grape Wine Res* **17**: 230–238.

Krivoruchko, A., Zhang, Y., Siewers, V., Chen, Y., and Nielsen, J. (2015) Microbial acetyl-CoA metabolism and metabolic engineering. *Metab Eng* **28**: 28–42.

Lambrechts, M.G. and Pretorius, I.S. (2000) Yeast and its Importance to Wine Aroma - A Review. *South African J Enol Vitic* **21**: 97–129.

Lopes, C.A., Barrio, E., and Querol, A. (2010) Natural hybrids of *S. cerevisiae* × *S. kudriavzevii* share alleles with European wild populations of *Saccharomyces kudriavzevii*. *FEMS Yeast Res* **10**: 412–421.

López-Malo, M., Querol, A., and Guillamon, J.M. (2013) Metabolomic comparison of *Saccharomyces cerevisiae* and the cryotolerant species *S. bayanus* var. *uvarum* and *S. kudriavzevii* during wine fermentation at low temperature. *PLoS One* **8**:.

Magasanik, B. and Kaiser, C.A. (2002) Nitrogen regulation in *Saccharomyces cerevisiae*. *Gene* **290**: 1–18.

Marullo, P., Aigle, M., Bely, M., Masneuf-Pomarède, I., Durrens, P., Dubourdieu, D., and Yvert, G. (2007) Single QTL mapping and nucleotide-level resolution of a physiologic trait in wine *Saccharomyces cerevisiae* strains. *FEMS Yeast Res* **7**: 941–952.

Masneuf-Pomarède, I., Bely, M., Marullo, P., Lonvaud-Funel, A., and Dubourdieu, D. (2010) Reassessment of phenotypic traits for *Saccharomyces bayanus* var. *uvarum* wine yeast strains. *Int J Food Microbiol* **139**: 79–86.

Mira de Orduña, R. (2010) Climate change associated effects on grape and wine quality and production. *Food Res Int* **43**: 1844–1855.

Moon, H.J., Jeya, M., Kim, I.W., and Lee, J.K. (2010) Biotechnological production of erythritol and its applications. *Appl Microbiol Biotechnol* **86**: 1017–1025.

Motulsky, H. and Christopoulos, A. (2004) Fitting Models to Biological Data Using Linear and Nonlinear Regression. A practical guide to

curve fitting. In, *Fitting Models to Biological Data Using Linear and Nonlinear Regression*., pp. 160–165.

Mouret, J.R., Cadiere, A., Aguera, E., Rollero, S., Ortiz-Julien, A., Sablayrolles, J.M., and Dequin, S. (2014) Dynamics and quantitative analysis of the synthesis of fermentative aromas by an evolved wine strain of *Saccharomyces cerevisiae*. *Yeast* **32**: 257–269.

Nielsen, J. (2017) Systems Biology of Metabolism: A Driver for Developing Personalized and Precision Medicine. *Cell Metab* **25**: 572–579.

Oliveira, B.M., Barrio, E., Querol, A., and Pérez-Torrado, R. (2014) Enhanced enzymatic activity of glycerol-3-phosphate dehydrogenase from the cryophilic *Saccharomyces kudriavzevii*. *PLoS One* **9**:.

Peltier, E., Bernard, M., Trujillo, M., Prodhomme, D., Barbe, J.C., Gibon, Y., and Marullo, P. (2018) Wine yeast phenomics: A standardized fermentation method for assessing quantitative traits of *Saccharomyces cerevisiae* strains in enological conditions. *PLoS One* **13**: e0190094.

Pickering, G.J. (2000) Low- and reduced-alcohol wine: A review. *Int J Phytoremediation* **21**: 129–144.

Pickering, G.J. and Vanhanen, L. (1998) The effect of ethanol concentration on the temporal perception of viscosity and density in white wine. *Am J Enol Vitic* **49**: 306–318.

Piškur, J., Rozpedowska, E., Polakova, S., Merico, A., and Compagno, C. (2006) How did *Saccharomyces* evolve to become a good brewer? *Trends Genet* **22**: 183–186.

Querol, A., Huerta, T., Barrio, E., and Ramon, D. (1992) Dry Yeast Strain For Use in Fermentation of Alicante Wines: Selection and DNA Patterns. *J Food Sci* **57**: 183–185.

Rainieri, S., Zambonelli, C., Hallsworth, J.E., Pulvirenti, A., and Giudici,

P. (1999) *Saccharomyces uvarum* , a distinct group within *Saccharomyces sensu stricto*. *FEMS Microbiol Lett* **177**: 177–185.

Ribéreau-Gayon, P., Dubourdieu, D., Donèche, B., and Lonvaud, A. (2005) Biochemistry of Alcoholic Fermentation and Metabolic Pathways of Wine Yeasts. In, *Handbook of Enology*. Chichester, UK: John Wiley & Sons, Ltd, pp. 53–77.

Ribéreau-Gayon, P., Dubourdieu, D., Donèche, B., and Lonvaud, A. (2006) Handbook of Enology: Volume 1, The Microbiology of Wine and Vinifications. *Handb Enol* **1**: 1–441.

Roessner, U., Wagner, C., Kopka, J., Trethewey, R.N., and Willmitzer, L. (2000) Simultaneous analysis of metabolites in potato tuber by gas chromatography-mass spectrometry. *Plant J* **23**: 131–142.

Saint-Prix, F., Bönquist, L., and Dequin, S. (2004) Functional analysis of the ALD gene family of Saccharomyces cerevisiae during anaerobic growth on glucose: the NADP+-dependent Ald6p and Ald5p isoforms play a major role in acetate formation. *Microbiology* **150**: 2209–2220.

Salmon, J.M., Fornairon, C., and Barre, P. (1998) Determination of oxygen utilization pathways in an industrial strain of *Saccharomyces cerevisiae* during enological fermentation. *J Ferment Bioeng* **86**: 154–163.

Schmidtke, L.M., Blackman, J.W., and Agboola, S.O. (2012) Production technologies for reduced alcoholic wines. *J Food Sci* **77**: R25–R41.

Da Silva, T., Albertin, W., Dillmann, C., Bely, M., La Guerche, S., Giraud, C., et al. (2015) Hybridization within Saccharomyces genus results in homoeostasis and phenotypic novelty in winemaking conditions. *PLoS One* **10**: e0123834.

Stribny, J., Gamero, A., Pérez-Torrado, R., and Querol, A. (2015) *Saccharomyces kudriavzevii* and *Saccharomyces uvarum* differ from *Saccharomyces cerevisiae* during the production of aroma-active higher alcohols and acetate esters using their amino

acidic precursors. *Int J Food Microbiol* **205**: 41–46.

Stribny, J., Romagnoli, G., Pérez-Torrado, R., Daran, J.M., and Querol, A. (2016) Characterisation of the broad substrate specificity 2-keto acid decarboxylase Aro10p of *Saccharomyces kudriavzevii* and its implication in aroma development. *Microb Cell Fact* **15**: 1–12.

Su, Y., Seguinot, P., Sanchez, I., Ortiz-Julien, A., Heras, J.M., Querol, A., et al. (2020) Nitrogen sources preferences of non-*Saccharomyces* yeasts to sustain growth and fermentation under winemaking conditions. *Food Microbiol* **85**:.

Tronchoni, J., Rozès, N., Querol, A., and Guillamón, J.M. (2012) Lipid composition of wine strains of *Saccharomyces kudriavzevi*i and *Saccharomyces cerevisiae* grown at low temperature. *Int J Food Microbiol* **155**: 191–198.

Turner, J.J., Ewald, J.C., and Skotheim, J.M. (2012) Cell size control in yeast. *Curr Biol* **22**: R350-9.

Varela, C., Pizarro, F., and Agosin, E. (2004) Biomass content governs fermentation rate in nitrogen-deficient wine musts. *Appl Environ Microbiol* **70**: 3392–3400.

Villas-Bôas, S.G., Højer-Pedersen, J., Åkesson, M., Smedsgaard, J., and Nielsen, J. (2005) Global metabolite analysis of yeast: Evaluation of sample preparation methods. *Yeast* **22**: 1155–1169.

Wang, P.-M., Zheng, D.-Q., Chi, X.-Q., Li, O., Qian, C.-D., Liu, T.-Z., et al. (2014) Relationship of trehalose accumulation with ethanol fermentation in industrial *Saccharomyces cerevisiae* yeast strains. *Bioresour Technol* **152**: 371–376.

CHAPTER 2

Metabolome segregation of four strains of *Saccharomyces cerevisiae*, *S. uvarum* and *S. kudriavzevii* conducted under low temperature oenological conditions.

Romain Minebois[a], Roberto Pérez-Torrado[a] and Amparo Querol[a]*

[a]Instituto de Agroquímica y Tecnología de los Alimentos, IATA-CSIC. E-46980 Paterna, Spain.

*Corresponding author: aquerol@iata.csic.es

Published in **Environmental Microbiology**

[DOI: 10.1111/1462-2920.15135]

Abstract

The monitoring of fermentation at low temperatures (12-15ºC) is a current practice in the winery for retention and enhancement of the flavour volatile content of wines. Among *Saccharomyces* species, *S. uvarum* and *S. kudriavzevii* have revealed interesting industrial properties, including better adaptation at low temperatures. To gather deeper knowledge of the fermentative metabolism at a low temperature of these species together with *S. cerevisiae*, we performed a comparative metabolomic analysis using four representative strains. We used batch cultures to obtain an exhaustive and dynamic image of the metabolome of strains passing through the sequential stresses related to the winemaking environment. A great variety of intra- and extracellular metabolites (>500 compounds) were quantified across fermentation using distinct chromatographic methods. Besides a global decrease in the lipid composition of the four strains when they entered into the stationary phase, we reported some strain-specific high magnitude changes. Examples of these differences included divergent patterns of production of short-chain fatty acids and erythritol in the *S. uvarum* strain. Strains also differed in expression for aromatic amino acid biosynthesis and sulphur metabolism, including the glutathione pathway. These data will allow us to refine and obtain the most value of fermentations with this alternative *Saccharomyces* species.

Chapter 2

1. Introduction

In winemaking, fermentation temperature and yeast strains are two critical parameters that govern the final organoleptic qualities of wine. The use of low temperatures (12-15ºC) during fermentation is a current practice in the winery. It enables not only retention but also enhancement of the flavour volatile content of wines (Molina *et al.*, 2007). Nowadays *S. cerevisiae* is the most important yeast involved in wine fermentation. However, *S. cerevisiae* has an optimal growth temperature around 32ºC, which supposes some disadvantages for the winemakers when fermenting at low temperatures (12-15ºC). For instance, the lag phase of *S. cerevisiae* increases, and its growth rate decreases, which can lead to prolong the duration of the process with a greater risk of halted or sluggish fermentation (Blateyron and Sablayrolles, 2001).

Consequently, the finding of new *Saccharomyces* and non-*Saccharomyces* yeasts able to correctly ferment in low temperature environments has been in the spotlight of worldwide wine yeast research over the past few years (Pérez-Torrado *et al.*, 2018). Within the *Saccharomyces* genus, this is the case of the cryotolerant yeasts *S. uvarum* and *S. kudriavzevii*. *S. kudriavzevii* has been isolated only from natural environments (Sampaio and Gonçalves, 2008; Lopes *et al.*, 2010), most likely because of its poor ethanol resistance (Belloch *et al.*, 2008). On the contrary, *S. uvarum* has been mainly isolated

from fermentation at cold temperatures (Naumov *et al.*, 2000; Demuyter *et al.*, 2004; Tosi *et al.*, 2009; Masneuf-Pomarède *et al.*, 2010). Previous physiological and oenological characterisations of *S. uvarum* and *S. kudriavzevii* strains have demonstrated their potential for fermenting wine musts at low temperatures. For instance, Masneuf-Pomarède *et al.* (2010) demonstrated that several strains of *S. uvarum* were able to complete alcoholic fermentation at 13ºC faster than commercial *S. cerevisiae* strains. Regarding *S. kudriavzevii*, because even at low temperature, *S. cerevisiae* is the most fermentative competitive species, overall hybrids *S. cerevisiae x S. kudriavzevii* have revealed interesting technological applications (Peris *et al.*, 2016, 2018). Likewise, both *S. uvarum* and *S. kudriavzevii* species have additional advantages as compared to *S. cerevisiae* in terms of organoleptic properties, such as greater glycerol production, and lower ethanol synthesis (Arroyo-López *et al.*, 2010; Varela *et al.*, 2016). However, up-to day there are still very few studies that aimed to deeper understand the metabolism of *S. uvarum* and *S. kudriavzevii,* and particularly at low fermentation temperatures. From an industrial outlook, such knowledge is necessary to develop better hybridization and metabolic engineering strategies that look at the role of genes and pathways on cold adaptation.

High-throughput experimental techniques, also called omics techniques, represent valuable tools to investigate in-depth how an environmental parameter, like temperature, can impact the variety

of cellular processes and the phenotype characteristics in *Saccharomyces* species. Comparative transcriptomic studies at high (25-28ºC) and low temperatures (12-15ºC) have shown that the enhanced production of fermentative aromas in *S. cerevisiae*, *S. uvarum* and *S. kudriavzevii* at low temperatures may be due in part to differential expression of genes implicated in their synthesis, e.g., genes involved in the catabolism of amino acids by the Ehrlich pathway and in the degradation of branched chain amino acids (Beltran *et al.*, 2006; Gamero *et al.*, 2014). Another transcriptomic work also suggested that *S. kudriavzevii* strains had enhanced their translation efficiency as an adaptive mechanism to better grow at low temperatures (Tronchoni *et al*., 2014). Moreover, a recent proteomic study has shown that genes and proteins involved in lipid metabolism belong to one of the metabolic groups most affected by low temperatures in *S. cerevisiae*, *S. uvarum,* and *S. kudriavzevii* (García-Ríos *et al.*, 2016). Regarding metabolomics studies, López-Malo *et al.* (2013) offered a first detailed metabolic comparison between *S. cerevisiae*, *S. uvarum,* and *S. kudriavzevii* performed in chemostat culture at 12ºC. In the latter study, strains were grown at a dilution rate fitting the initial exponential phase of wine fermentation, and the authors found that the main differences among the four species were in carbohydrate metabolism, especially fructose metabolism. Likewise, they found that *S. uvarum* presented

elevated shikimate pathway flux, while *S. kudriavzevii* displayed increased NAD+ synthesis at 12ºC.

In most of the aforementioned studies, experiments were conducted in chemostat cultures. Chemostat cultures enable precise control of specific growth rate and, at steady-state, the concentrations of all metabolites, substrates, and culture variables (pH, temperature, and oxygen availability) are constant in time. Thus, chemostat steady-states cultures are convenient for the study of prolonged exposure to low temperature and the identification of gene expression, proteome profiles, or specific pathway activity. However, wine fermentations are traditionally conducted in batch mode, which can be regarded as unfavourable conditions for yeast growth since yeast cells are subjected to various and sequential stresses (Matallana and Aranda, 2017). During alcoholic fermentation, yeasts go through a lag phase, a growth phase, and a stationary phase during which more than half of the sugar is fermented. A complete study of yeast physiology under winemaking conditions must, therefore, include yeasts in a non-growing phase. This condition is impossible to achieve within a chemostat (Clement *et al.*, 2011). Besides, in batch fermentations, culture variables, extra- and intracellular metabolites and biomass evolve over time. This makes batch cultures more suitable to study the dynamics of adaptation to low temperature and the identification of changes in metabolic pathways across time. Accordingly, in an attempt to identify inter-specific metabolic differences between *S.*

cerevisiae, *S. uvarum,* and *S. kudriavzevii* at high fermentation temperature, we recently performed a metabolomic comparison using batch fermentations at 25ºC (Minebois *et al.*, 2020). We observed interesting variations among four strains of *S. cerevisiae*, *S. uvarum,* and *S. kudriavzevii* for the consumption of some nitrogenous compounds and in the levels of some metabolites involved in redox homeostasis such as succinate, glycerol, and 2,3 butanediol. The most important differences were found in *S. uvarum* strains. For instance, the two *S. uvarum* strains used were characterized by a "production-consumption" profile of extracellular acetate that we hypothetically associated with lipids synthesis and membrane remodelling. Also, we found some evidence that *S. uvarum* strains were metabolically more active than *S. cerevisiae* strains through the pentose phosphate pathway when entering into the stationary phase as demonstrated by a higher erythritol synthesis, a downstream metabolite of this pathway. On the contrary, because the *S. kudriavzevii* strain had a very important shortcoming in growth at 25ºC*,* the identification of clear metabolic strategies was limited.

On the first hand, the present work aimed to encounter inter-specific metabolic differences between *S. cerevisiae*, *S. uvarum,* and *S. kudriavzevii* at low fermentation temperature (12ºC). We selected four yeast strains, including one winemaking strain of *S. cerevisiae* (T73), one natural-isolate of *S. cerevisiae* (YPS128), one winemaking strain of *S. uvarum* (BMV58), and one natural-isolate of *S.*

kudriavzevii (CR85). On the other hand, because strains T73, BMV58, and CR85 were previously characterized at 25ºC using a similar methodology (Minebois *et al.*, 2020), we also tried to discern intra-specific metabolomic strategies between low (12ºC) and high temperature (25ºC). From the large intra- and extracellular metabolites data set we obtained (>500 compounds), we proceeded to a thorough inspection of the general pathways and time trends that could differentiate the strains. We looked for performance differences between the strains based on their utilization or production of various compounds over time, in the context of their biochemical pathway associations and the evolution of the environmental parameters.

2. Material and methods

2.1 Yeast strains

Four strains from three different *Saccharomyces* species were used in this study. The commercial strain, T73 (Lalvin T73 from Lallemand, Montreal) originally isolated from wine in Alicante, Spain (Querol *et al.*, 1992) was used as our winemaking *S. cerevisiae* representative. We also included YPS128, isolated from Pennsylvania woodlands (Sniegowski *et al.*, 2002) as a representative of a wild *S. cerevisiae* strain. The commercial strain, BMV58, selected in our laboratory and commercialized for winemaking (Velluto BMV58 from Lallemand, Montreal) was used as a representative of *S. uvarum*.

Finally, for *S. kudriavzevii*, we choose strain CR85, a wild isolate from oak tree bark identified by Lopes et al. (2010). Cryogenically preserved (-80ºC) strains were cultured and maintained on GPY plates (2% glucose, 2% agar, 0.5% peptone, 0.5% yeast extract) and stored at 4ºC.

2.2 Microvinification experiments

Bioreactors were inoculated at OD_{600} 0.1 (approximately 1 x 10^6 cells/ml) from starter cultures. Starter cultures were prepared by growing cells in an Erlenmeyer flask containing 25 ml of GPY liquid medium (2% glucose, 0.5% peptone, 0.5% yeast extract) at 12°C and during 48 hours in an agitated incubator (Selecta, Barcelona, Spain) under aerobic conditions. We used a natural white must of Merseguera grapes variety collected in Titaguas (Spain) for the microvinification assays. Before its use, must was clarified by sedimentation for 24 h at 4°C and dimethyl dicarbonate (DMDC) at 1 $ml.L^{-1}$ added for sterilization purposes as described elsewhere (Peris *et al.*, 2016). Before fermentation, the fermentable sugar level was corrected as performed in most European countries by adding 47 g/l of chemically pure sucrose (AppliChem Panreac, Darmstadt, Germany) to reach a probable alcoholic grade of 12.5%. To avoid any stuck or sluggish fermentations, nitrogen content was adjusted by adding a nitrogen supplement, which consisted of 0.2 g/l of ammonium sulphate and 0.1 mg/l of thiamine hydrochloride (Sigma-

Aldrich, Barcelona, Spain). All the fermentations were carried out in independent biological triplicates by using 470 ml of must in sterile 500 ml laboratory bioreactors (MiniBio, Applikon, the Netherlands). Data were integrated into the MyControl and BioExpert software (Applikon, The Netherlands). The evolution of the fermentation was followed by using different probes and detectors measuring temperature, pH, dissolved O_2 (AppliSens, Applikon, The Netherlands), and the proportion of carbon dioxide in the outgoing gas flow (Multi-Gas Monitors INNOVA 1316, LumaSense Technologies). Fermentations were monitored by measuring the residual sugar content by HPLC (see details below) until constant values were reached, considered to be the end of the fermentation.

2.3 Sampling

Bioreactors were sampled for extra- and intracellular metabolites profiling ensuring that total sampling volume remained below 10% of the total working volume. Approximately 3 ml of supernatant collected in ten time points distributed from the beginning to the end of the fermentation were used for extracellular metabolite quantification. For intracellular metabolites, a specific protocol was applied in four sampling points which were determined in function of growth curve value and time cultivation. The growth curve was calculated as $G(t) = \ln[OD_{600}\ (t)/OD_{600}(t_0)]$ and fitted to the Gompertz equation where A represents the maximum population

level (details of the Gompertz equation are presented below). Intracellular samples were taken so that $G(t_1) = 0.75A$ (growth phase or GP), $G(t_2) = A$ (end of growth phase or EGP), $G(t_3=t_2+50/90h) = A$ (early stationary phase or ESP) and $G(t_4=t_3+70h) = A$ (mid-stationary phase or MSP). When the set-point was reached, a sample volume corresponding to approximately 30 OD_{600} of cells was rapidly harvested from the bioreactor and transferred to a 15 ml polypropylene tube. The tube was gently centrifuged at 750 x g for 3 min to pellet cells. The supernatant was removed and discarded all but ~0.75 ml. Cell pellets were softly re-suspended, transferred to a 2.0 ml polypropylene tube, and centrifuged in the same conditions. Then, the supernatant was carefully removed using micropipette tips to ensure a dry pellet for freezing, the tube was then flash-frozen in liquid nitrogen, and stored at -80 ºC until shipment to the HD4 platform of Metabolon, Inc. (Durham, NC, USA) for extraction and analysis.

2.4 Intracellular metabolites extraction and quantification

Samples were prepared using the automated MicroLab STAR® system from Hamilton Company. Several recovery standards were added before the first step in the extraction process for QC purposes. Samples were extracted with methanol under vigorous shaking for 2 min to precipitate protein and dissociate small molecules bound to protein or trapped in the precipitated protein matrix, followed by

centrifugation to recover chemically diverse metabolites. The resulting extract was divided into five fractions: two for analysis by two separate reverse phase (RP)/UPLC-MS/MS methods using positive ion mode electrospray ionization (ESI), one for analysis by RP/UPLC-MS/MS using negative ion mode ESI, one for analysis by HILIC/UPLC-MS/MS using negative ion mode ESI, and one reserved for backup. Samples were placed briefly on a TurboVap® (Zymark) to remove the organic solvent. The sample extracts were stored overnight under nitrogen before preparation for analysis by Ultrahigh Performance Liquid Chromatography-Tandem Mass Spectroscopy (UPLC-MS/MS) as described in the supplementary material.

2.5 Extracellular metabolite quantification

Sugars (glucose, fructose), fermentative by-products (glycerol, ethanol, 2,3 butanediol, and erythritol) and organic acids were respectively determined by HPLC (Thermo Fisher Scientific, Waltham, MA) using a refraction index detector and UV/VIS (210 nm) detector equipped with a HyperREZ^{TM} XP Carbohydrate H+ 8 mm column (Thermo Fisher Scientific, Waltham, MA) and HyperREZ^{TM} XP Carbohydrate Guard (Thermo Fisher Scientific, Waltham, MA). The analysis conditions were: eluent, 1.5 mM of H_2SO_4; 0.6 ml.min^{-1} flux, and oven temperature of 50°C. For sucrose determination, the same HPLC was equipped with a Hi-Plex Pb, 300 x 7.7 mm column (Agilent Technologies, CA, USA), and peaks quantified by the RI detector. The

analysis conditions were: eluent, Milli-Q water; 0.6 ml.min-1 flux, and oven temperature of 50°C. The retention times of the eluted peaks were compared to those of commercial analytical standards (Sigma-Aldrich, Madrid, Spain). Concentration of the target compounds, in g/l, were quantified by the calibration graphs (R2 value > 0.99) of the standards that were previously obtained from a linear curve fit of the peak areas using standards mixtures.

Determination of yeast assimilable nitrogen (YAN) in the form of amino-acids and ammonia was carried out using the same protocol as Su *et al*. (2020). For derivatization, 400 µl of the sample was mixed with 430 µl borate buffer (1 M, pH 10.2), 300 µl absolute methanol and 12 µl of diethyl ethoxymethylenemalonate (DEEMM), and ultra-sonicated for 30 min at 20ºC. After ultra-sonicating, the sample was warmed up at 80ºC for 2 hours to allow the complete degradation of excess DEEMM, and once derivatization finished the sample was filtered with 0.22 µm filter. The chromatographic instrument consisted in a UPLC Dionex Ultimate 3000 (Thermo Fisher Scientific, Waltham, MA) equipped with a Kinetex 2.6u C18 100A column (Phenomenex, Torrance, CA, USA) and Accucore C18 10 x 4.6 mm 2.6 um Defender guards (Thermo Fisher Scientific, Waltham, MA). Amino-acids and ammonia in the samples were identified and quantified according to the retention times, UV-vis spectral characteristics and calibration curves (R2 value > 0.99) of the derivatives of the corresponding standards. Amino acid standard (ref

AAS18), asparagine and glutamine purchased from Sigma-Aldrich were used for calibration.

2.6 Volatile compounds extraction and quantification

Volatile compounds extraction and gas chromatography were performed following the protocol of Stribny et al. (2015). 1.5 mL of the supernatant was transferred to 15-mL vials with 0.35 g of NaCl. 20 µl volume of 2-heptanone (0.005 %) was added as an internal standard. Higher alcohols and esters were analyzed by the headspace solid-phase microextraction (HS-SPME) technique with 100-µm polydimethylsiloxane (PDMS) fiber (Supelco, Sigma-Aldrich, Madrid, Spain). Solutions were maintained for 2 h at 20°C to establish the headspace-liquid equilibrium. The fiber was inserted into the headspace through a vial septum and was held for 7 min. The fiber was then inserted into the gas chromatograph inlet port for 4 min at 220°C with helium flow (1 mL/min) to desorb analytes. A Thermo Science TRACE GC Ultra gas chromatograph with a flame ionization detector (FID) was used, equipped with an HP INNOWax 30 m × 0.25 m capillary column coated with a 0.25-m layer of cross-linked polyethylene glycol (Agilent Technologies, Valencia, Spain). The oven temperature program was: 5 min at 35°C, 2°C/min to 150°C, 20°C/ min to 250°C and 2 min at 250°C. The detector temperature was kept constant at 280°C. Volatile compounds were identified by the retention time for reference compounds. Quantification of the

volatile compounds was determined using the calibration graphs of the corresponding standard volatile compounds.

2.7 Biomass and physiological parameters determination

Biomass and physiological parameters - OD_{600}, dry weight (DW), and average cell diameter (ACD) - were determined in every sampling point providing that cell sample was sufficient to perform the corresponding measure. For DW determination, 2 ml of a fresh sample placed in a pre-weighed Eppendorf tube were centrifuged at maximum speed (13.400 rpm) in a MiniSpin centrifuge (Eppendorf, Spain) for 5 minutes. The supernatant was carefully removed with a pipette, the pellet washed twice with 70 % (v/v) ethanol and centrifuged in the same conditions. After washing, the aqueous supernatant was carefully removed and tube stored at 65ºC for 72h until dryness. DW was obtained by measuring the mass weight difference of tubes with a BP121S analytical balance (Sartorius, Gottingen, Germany). OD_{600} was measured at each sampling point using a diluted volume of sample and a Biophotometer spectrophotometer (Eppendorf, Hamburg, Germany). For ACD determination, a volume of cell sample was diluted into phosphate-buffered saline solution and cell diameter measured using a Scepter Handled Automated Cell Counter equipped with a 40 µm sensor (Millipore, Billerica, USA).

2.8 Statistical analysis

To describe the temporal production of the main fermentative by-products (ethanol, glycerol, 2,3 butanediol, succinate, acetate, and erythritol), the consumption of YAN and the cell population, biological data were fitted to mathematical equations using non-linear regression and the GraphPad Prism 6.0 Software package (La Jolla, CA, USA) to provide biological parameters. Best-fit parameters were determined minimizing the sum of squares of the difference between experimental data and the fitted model, and following the general recommendations of Motulsky and Christopoulos (2004). For each parameter, a 95% confidence interval was approximated by using the estimated predictions and standard errors. Conditions for which the confidence intervals do not intersect can be considered significantly different. The following mathematical equations were used:

- Gompertz decay function, previously described by Tronchoni et al. (2009). Function to fit: Y(t) = Ymin+(Ymax-Ymin)*exp(-exp(r*(t-T50))). Where Ymin and Ymax are the minimum and maximum values (Y units), r the maximum consumption rate (h^{-1}) and T50 the time to reach ½Ymax (h).
- Modified Boltzman sigmoidal function, previously described by Motulsky and Christopoulos (2004). Function to fit: Y(t) = Ymin+(Ymax-Ymin)/(1+exp(r*(T50-t))). Where Ymin and Ymax

are the minimum and maximum values (Y units), r the maximum production rate (h^{-1}), and T50 the time to reach ½Ymax (h).

- Modified Gompertz function, used for cell growth curve and previously described by Zwietering et al. (1990). Function to fit: $G(t) = A*\exp(-\exp((((\mu_{max}*e)/A)*(\lambda-t))+1))$. Where G(t) is the cell population at time t (in this study calculated as $\ln[OD_{600}(t)/OD_{600}(t_0)]$), A is the maximum population level (Y units), μ_{max} the maximum growth rate (h^{-1}) and λ the lag time (h) defined as the time axis intercept of the tangent through the inflection point.
- One phase exponential association, previously described by Motulsky and Christopoulos (2004). Function to fit: Y(t) = Ymin + (Ymax-Ymin)*(1-exp(-K*t)). Ymin and Ymax are the minimum and maximum values (Y units), and K the rate constant (h^{-1}).

For a general overview of growth, fermentative by-products production and nitrogen consumption trait data, a principal component analysis (PCA) was performed using the Statsoft Statistica 10 Package, with the following variables obtained from the above models: DW_{max} (maximum dry weight biomass), μ_{max} (maximum growth rate), λ (lag phase), r_{YAN} (maximum consumption rate of YAN), T_{50}YAN (estimated time at which 50% of the total YAN content was consumed), g_{DW}/g_{YAN} (maximum biomass yield), r_{EtOH} (maximum

production rate of ethanol), $EtOH_{max}$ (maximum ethanol concentration at the end of fermentation), r_{Gly} (maximum production rate of glycerol), Gly_{max} (maximum glycerol concentration at the end of fermentation), r_{But} (maximum production rate of 2,3 butanediol), But_{max} (maximum 2,3 butanediol concentration at the end of fermentation), r_{Ac} (maximum production rate of acetate), Ac_{max} (maximum acetate concentration at the end of fermentation), r_{Succ}(maximum production rate of succinate), $Succ_{max}$ (maximum succinate concentration at the end of fermentation), r_{Ery} (maximum production rate of erythritol) and Ery_{max} (maximum erythritol concentration at the end of fermentation). PCA plot of aroma compounds at the end of the fermentation was also obtained using the Statsoft Statistica 10 Package.

For intracellular samples, data were normalized for internal consistency by processing a constant amount of sample per volume of extraction solvent. Data were scaled to the median value for each compound, and missing values (if any) were imputed with the minimum detected value for that compound. Statistical calculations and figures were performed and obtained using natural log-transformed scaled imputed data. Thanks to Metabolon for technical support.

3. Results

In this work, we performed an in-depth study of the metabolic behaviour of four yeast strains at 12ºC under winemaking conditions. The wine strain T73 and the wild strain YPS128 belong to *S. cerevisiae* species, while strain BMV58 and strain CR858 belong to *S. uvarum* and *S. kudriavzevii* species respectively. An overview of the fermentation course with the kinetics of the main fermentative parameters (OD_{600}, dissolved oxygen, YAN, carbon dioxide release, sugar consumption, and ethanol production) is presented in **Figure 1A** for each strain. Also, the extracellular concentration of the principal compounds accounting for YAN, namely ammonia, arginine, and glutamine, as well as the extracellular proline content are presented below in **Figure 1B**. We compared the growth capacity and the kinetics of the main fermentative by-products (ethanol, glycerol, succinate, 2,3 butanediol, acetate, and erythritol) generated through the central carbon metabolism (CCM) of yeasts at 12ºC. To do so, the experimental data of OD_{600}, biomass, YAN, and the by-products cited above were fitted to distinct mathematical equations as described in the material and methods section. The fermentative parameters calculated from models are listed in **Table 1**.

Table 1: Growth and fermentative parameters of the four strains at 12ºC

	T73 *S. cerevisiae*		BMV58 *S. uvarum*		CR85 *S. kudriavzevii*		YPS128 *S. cerevisiae*	
	mean ± SE	**95% CI**	**mean ± SE**	**95% CI**	**mean ± SE**	**95% CI**	**mean ± SE**	**95% CI**
DW_{max} ($g.l^{-1}$)	3.9 ± 0.10	3.7 to 4.1 ^{b}	6.0 ± 0.2	5.6 to 6.4 ^{d}	2.9 ± 0.1	2.7 to 3.0 ^{a}	5.1 ± 0.2	4.7 to 5.5 ^{c}
μ_{max} (h^{-1})	0.082 ± 0.001	0.078 to 0.085 ^{c}	0.098 ± 0.002	0.092 to 0.10 ^{d}	0.053± 0.002	0.048 to 0.57 ^{a}	0.071 ± 0.002	0.067 to 0.074 ^{b}
λ (h)	12.6 ± 0.8	11 to 14 ^{a}	23.3 ± 0.8	22 to 26 ^{b}	24.3 ± 2.3	20 to 29 ^{b}	10.8 ± 1.2	8.5 to 13 ^{a}
r_{YAN} (h^{-1})	0.029 ± 0.006	0.015 to 0.043 ^{b}	0.034 ± 0.006	0.022 to 0.046 ^{b}	0.011± 0.002	0.0048 to 0.013 ^{a}	0.028 ± 0.005	0.020 to 0.042 ^{b}
T_{50} YAN (h)	62 ± 5.4	51 to 73 ^{a}	68.5 ± 3.0	62 to 75 ^{a}	121.4 ± 15	119 to 150 ^{c}	87.6 ± 3.7	82 to 95 ^{b}
g_{DW}/g_{YAN}	13.7 ± 0.4	12.9 to 14.4 ^{b}	18.8 ± 0.8	17.2 to 20.4 ^{c}	12.3 ± 0.2	11.9 to 12.8 ^{a}	19.3 ± 1.4	16.3 to 22.3 ^{c}
r_{Eth} (h^{-1})	0.52 ± 0.016	0.48 to 0.55 ^{d}	0.45 ± 0.012	0.43 to 0.47 ^{c}	0.39 ± 0.008	0.37 to 0.40 ^{b}	0.29 ± 0.017	0.25 to 0.32 ^{a}
Eth_{max} ($g.l^{-1}$)	97.9 ± 1.6	94 to 101 ^{a}	96.2 ± 0.98	94 to 98 ^{a}	103.9 ± 0.95	95 to 105 ^{a}	92.2 ± 3.4	85 to 99 ^{a}
r_{Gly} (h^{-1})	0.034 ± 0.0014	0.032 to 0.037 ^{a}	0.045 ± 0.0025	0.040 to 0.051 ^{b}	0.040 ± 0.0015	0.036 to 0.043 ^{a,b}	0.049 ± 0.003	0.042 to 0.055 ^{b}
Gly_{max} ($g.l^{-1}$)	4.38 ± 0.06	4.26 to 4.51 ^{a}	8.22 ± 0.24	7.73 to 8.71 ^{b}	7.79 ± 0.13	7.53 to 8.05 ^{b}	4.42 ± 0.10	4.21 to 4.63 ^{a}
r_{But} (h^{-1})	0.032 ± 0.006	0.020 to 0.044 ^{b}	0.078 ± 0.015	0.05 to 0.11 ^{c}	0.020 ± 0.001	0.018 to 0.022 ^{b}	0.011 ± 0.003	0.005 to 0.017 ^{a}
But_{max} ($g.l^{-1}$)	0.53 ± 0.01	0.51 to 0.54 ^{b}	0.88 ± 0.01	0.85 to 0.90 ^{c}	1.74 ± 0.02	1.7 to 1.8 ^{d}	0.34 ± 0.01	0.31 to 0.36 ^{a}
r_{Ac} (h^{-1})	0.030 ± 0.005	0.02 to 0.04 ^{a}	0.156 ± 0.163	0 to 0.53 ^{a}	0.158 ± 0.131	0 to 0.42 ^{a}	0.10 ± 0.02	0.06 to 0.13 ^{a}
Ac_{max} ($g.l^{-1}$)	0.43 ± 0.01	0.42 to 0.44 ^{d}	0.03 ± 0.004	0.02 to 0.03 ^{a}	0.34 ± 0.004	0.33 to 0.35 ^{c}	0.214 ± 0.004	0.20 to 0.22 ^{b}
r_{Succ} (h^{-1})	0.021 ± 0.006	0.009 to 0.033 ^{b,c}	0.0018 ± 0.0006	0.0005 to 0.003 ^{a}	0.0069 ± 0.0012	0.004 to 0.009 ^{b}	0.031 ± 0.007	0.016 to 0.046 ^{c}
$Succ_{max}$($g.l^{-1}$)	1.90 ± 0.02	1.85 to 1.93 ^{a}	5.63 ± 0.41	5.5 to 5.9 ^{c}	2.22 ± 0.04	2.1 to 2.3 ^{b}	2.00 ± 0.03	1.9 to 2.1 ^{a,b}
r_{Ery} (h^{-1})	0.045 ± 0.008	0.028 to 0.062 ^{b}	0.025 ± 0.004	0.016 to 0.034 ^{b}	0.0048 ± 0.001	0.0028 to 0.0068 ^{b}	0.014 ± 0.003	0.0076 to 0.021 ^{a}
Ery_{max} ($g.l^{-1}$)	0.14 ± 0.003	0.13 to 0.15 ^{a}	0.26 ± 0.01	0.23 to 0.29 ^{c}	0.24 ± 0.01	0.24 to 0.36 ^{c}	0.18 ± 0.01	0.16 to 0.20 ^{b}

Growth and fermentative parameters obtained by fitting models to biological data using non-linear regression. Best-fit parameters were determined minimizing the sum of squares of the difference between experimental data and the mathematical model using GraphPad Prism 6.0 Software. Parameters are presented as mean ± standard error (SE). For each parameter, a 95% confidence interval was approximated by using the estimated predictions and standard error. Parameters for which the confidence intervals do not intersect can be considered significantly different. Shared superscript letters (a, b, c) in the same row indicate no significant difference.

Abbreviations: DW_{max} (maximum dry weight biomass), μ_{max} (maximum growth rate), λ (lag phase), r_{YAN} (maximum consumption rate of YAN), T_{50} YAN (estimated time at which 50% of the total YAN content was consumed), g_{DW}/g_{YAN} (maximum biomass yield expressed as g of dry weight biomass produced/g of YAN consummed), r_{Eth} (maximum production rate of ethanol), Eth_{max} (maximum ethanol concentration at the end of fermentation), r_{Gly} (maximum production rate of glycerol), Gly_{max} (maximum glycerol concentration at the end of fermentation), r_{But} (maximum production rate of 2, 3 butanediol), But_{max} (maximum 2,3 butanediol concentration at the end of fermentation), r_{Ac} (maximum production rate of acetate), Ac_{max} (maximum acetate concentration at the end of fermentation), r_{Succ} (maximum production rate of succinate), $Succ_{max}$ (maximum succinate concentration at the end of fermentation), r_{Ery} (maximum production rate of erythritol), Ery_{max} (maximum erythritol concentration at the end of fermentation).

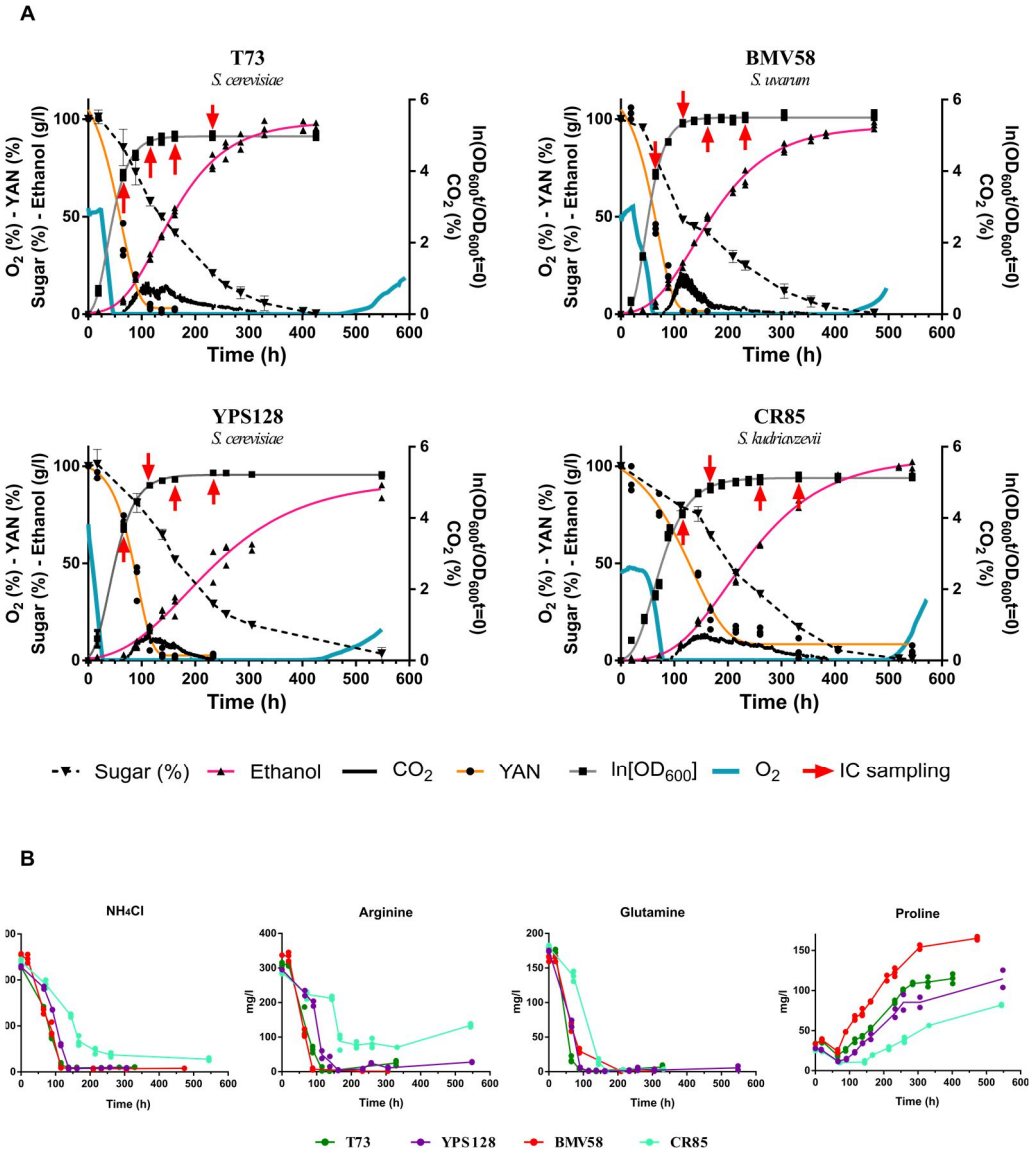

Figure 1. A) Overview of the fermentation kinetics of the four strains at 12ºC, with total sugar consumption expressed as percentage (black dashed line), yeast assimilable nitrogen (YAN) content expressed as percentage (orange solid line), dissolved oxygen expressed as percentage (blue solid

line), CO_2 exhaust concentration as percentage (black dashed line), cell population expressed as ln[OD600 (t) / OD600 (t0)] (grey solid line) with t0 the time of inoculation and time of intracellular samplings (red arrows). B) Detail of the evolution of the extracellular concentration of the three preferable nitrogen sources (ammonia, arginine, and glutamine) in yeasts and proline.

3.1 General fermentation performances

As shown in **Figure 1A**, fermentations were completed between 430 and 550 hours, being T73 and BMV58 the first strains in this order to reach a dry white wine composition (<4g/l of residual sugars). Even if the *S. cerevisiae* strain YPS128 was the quickest in initiating alcoholic fermentation as shown by its shorter lag phase (**Table 1**), it did not consume the totality of sugars (**Figure 1A**). Regarding biomass production, BMV58 and YPS128 strains had the highest dry weight biomass values followed by T73 and CR85 strains (**Table 1**). Intriguingly, CR85 did not consume the totality of ammonium and arginine (**Figure 1B**), which could partially explain its lower biomass production. This inability of strain CR85 to totally consume arginine was also observed at 25ºC (Minebois *et al.*, 2020), which suggests that temperature is not the main parameter that influences arginine catabolism in CR85.

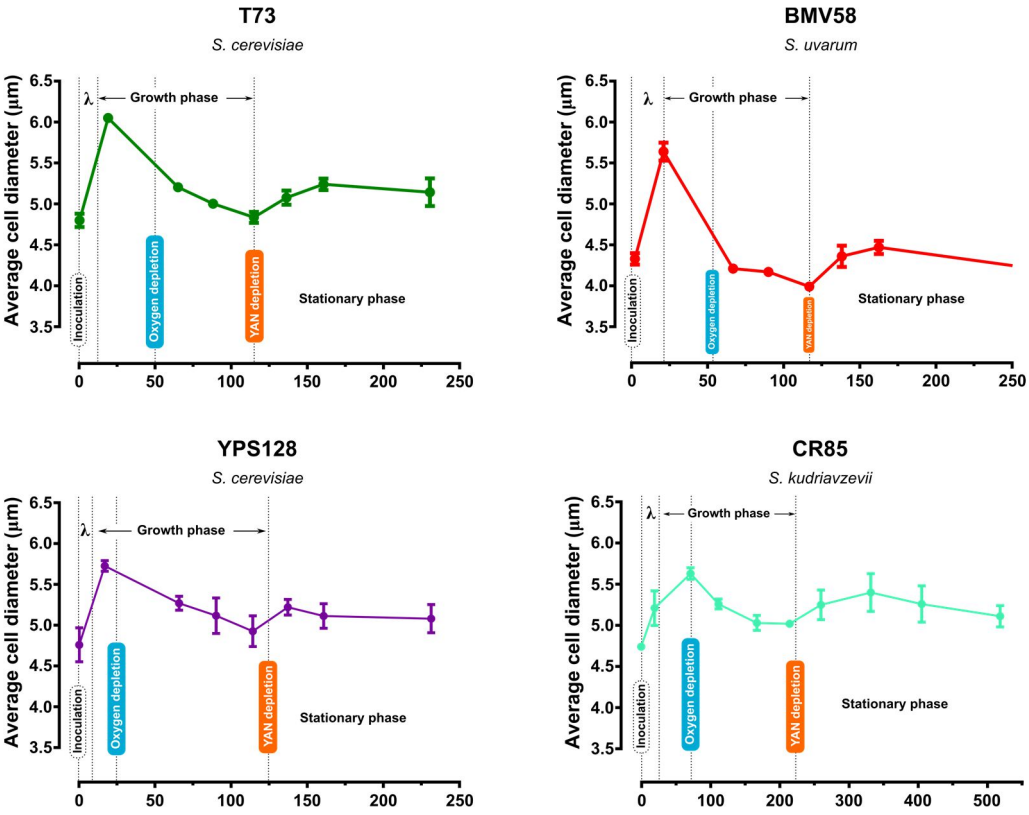

Figure 2. Average cell diameter (ACD) expressed in µm along the fermentation process. For each strain, the lag phase (λ), the growth phase and the stationary phase were indicated, as well as the timing of dissolved oxygen and YAN depletion. The values are displayed as mean and standard deviations from triplicate experiments.

The average diameter of cells (ACD) throughout the fermentation was determined and is presented in **Figure 2** . Cells of strain CR85 were overall as bigger as cells of strains T73 and YPS128. On the contrary, BMV58 cells were mostly smaller than the cells of the rest

of the strains. Moreover, the comparison of the timing of lag phase, dissolved oxygen depletion, and nitrogen starvation with ACD trends (**Figure 2**) suggested that ACD could be used as another indicator of the fermentation stage, as we previously observed (Minebois *et al.*, 2020).

Finally, a principal component analysis (**Figure 3**) was used to provide a general overview of the data set from **Table 1** which included the 6 growth and the 12 by-products variables. The four yeasts were mostly separated through the first axis which accounted for 36.73% of the total variation and was mainly defined by the correlated variables T_{50}YAN, Eth_{max} and $But_{max,}$ and the negatively correlated variable r_{Ery}. On the other hand, the final content of acetate and succinate, Ac_{max} and $Succ_{max}$, the maximum rate of butanediol, r_{But}, and the majority of the growth parameters (g_{DW}/g_{YAN}, DW_{max} and μ_{max}) were the variables that most contributed to the second principal component explaining 30.96% of the variance. In this defined space, strain T73 was separated from other strains, mainly because of its high acetate production and also due to its low biomass yield at 12ºC. Interestingly, the cryotolerant strains CR85 and BMV58 did not exactly cluster together, which was explained by differences in their by-products and biomass yields. The *S. kudriavzevii* strain was mainly associated with high butanediol and ethanol content (But_{max} and Eth_{max}), slow nitrogen consumption (T_{50}YAN), and low biomass production (DW_{max}). On the contrary

BMV58 strain segregated to the negative part of the y-axis by its high biomass yield, high succinate, and low acetate production. However, both CR85 and BMV58 strains clustered in the bottom right-hand corner respectively, which included the variables associated with low temperature and osmotic regulation strategies, for instance, high glycerol and high erythritol production (Gly_{max} and Ery_{max}). Finally, the natural isolate of *S. cerevisiae* had an intermediate position between T73 and BMV58 strains on this PCA projection. Indeed, YPS128 strain had a good biomass yield at 12ºC as well as lower acetate content in comparison to the *S. cerevisiae* wine strain.

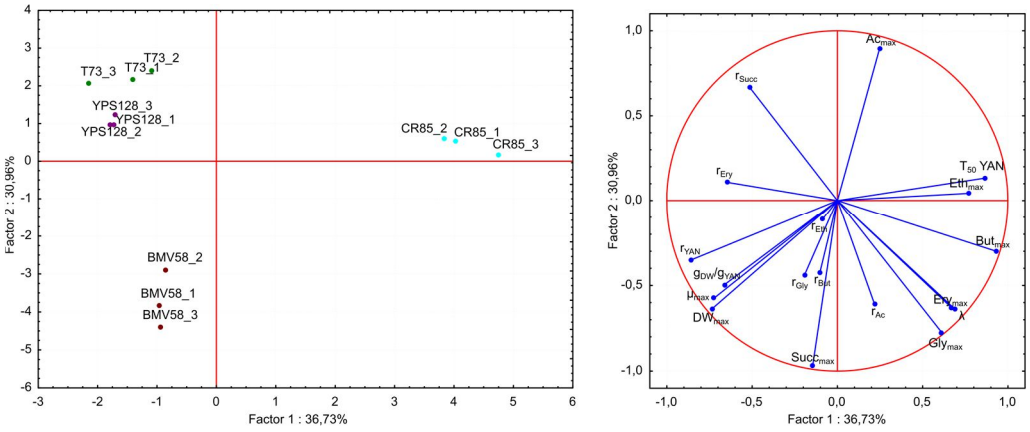

Figure 3. Principal component analysis plot of the growth and by-products variables obtained for each strain after fitting our biological data to mathematical models (Supporting information in material and methods section). A total of 18 variables (6 growth and 12 by-products variables) which values are available in Table 1, were used for the PCA analysis.

3.2 Extracellular and intracellular metabolomes comparison

The intra- and extracellular metabolomes were quantified along the fermentation process. Four sampling points which corresponded to growth phase (GP), end of growth phase (EGP), early stationary phase (ESP) and mid-stationary phase (MSP) were used to determine the intracellular metabolomes of each strain, while extracellular metabolomes were determined from tens points distributed from the beginning to the end of the fermentation (**Figure 1A**). Because the strains were grown under different time regimes it was not possible to compare them in a direct statistical manner. However, for both intra- and extracellular metabolomes, we attempted to discern the general pathways and time trends that differentiated the four strains. When possible, intra- and extracellular data were combined to detail specific pathway observations among the four strains.

3.3 Strain-specific intracellular metabolomes observations

The principal component analysis presented in **Figure 4A** was obtained from intracellular triplicates samples. As shown in **Figure 4A**, the triplicates tended to cluster closely and all samples segregated strongly by both strains (**Figure 4A left graph**) and time (**Figure 4A right graph**).

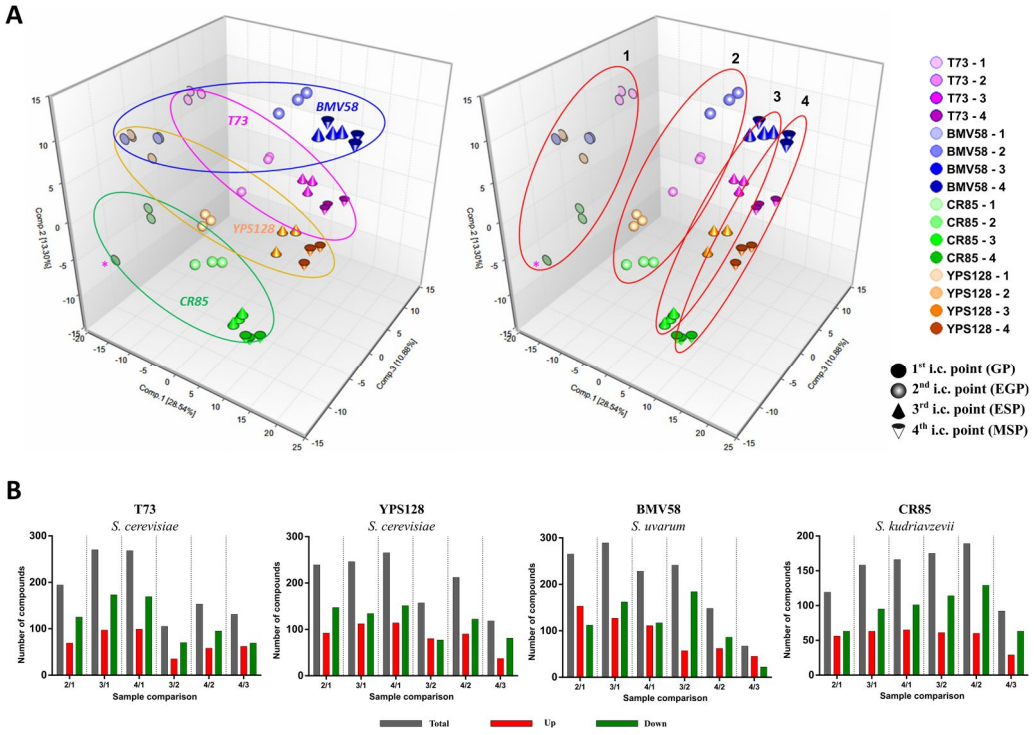

Figure 4. A) Principal component analysis plot of the intracellular samples. On the left PCA plot, color circles indicate the segregation of triplicates by strains. Blue circle for BMV58 strain, pink circle for T73 strain, yellow circle for YPS128 strain and green circle for CR85 strain. On the right PCA plot, red circles indicate segregation of the triplicates by sampling time point, namely first intracellular sampling point or GP (1), second intracellular sampling point or EGP (2), third intracellular sampling point or ESP (3) and fourth intracellular sampling point or MSP (4). B) Number of compounds which amount significantly changed ($p \leq 0.05$) in each pair-wise comparison of intracellular sampling points, and the direction of those changes. Grey bar indicate the total number of compounds that met the significant criteria, red bar the number of compounds that significantly increased and green bar the number of compounds that significantly decreased.

Separation by time accounted for the first component variance, while separation by strains was apparent in both the second and third components. Regarding the segregation by strains, only the earliest time points for BMV58 and YPS128 showed any overlap. Considering time segregation, we saw that the widest separation was between GP and EGP time points. For instance, we noticed a strong decrease in many lipids after the first time point in each strain (**Figure S1**). The third (ESP) and fourth (MSP) time points were more closely associated, although fully separated except for one sample in the BMV58 group. Another way to judge the magnitude of metabolic effects caused by specific variables was to summarize the number of compounds significantly changed ($p \leq 0.05$) in each pair-wise comparison of intracellular sampling points, and the direction of those changes (**Figure 4B**). Consistent with the PCA analysis above, the vast majority of changes were already apparent at the second time point of intracellular samples (relative to the first time point). Relatively few compounds, in terms of gross numbers, were added in the later samplings. Also, comparisons of the third and fourth sample times to each other yielded the smallest number of statistically significant differences in most cases.

As stated above, it was not feasible to compare data from the various strains directly. Consequently, we looked for ways to discern differences between the performance of the strains based on their utilization or production of various compounds over time, in the

context of their biochemical pathway associations. Due to the very large number of intracellular compounds quantified (>500 compounds), several approaches were attempted as presence vs. absence of a particular compound. As presented in **Figure 5A**, UDP-galactose was not detected in either of the *S. cerevisiae* strains but was present in all the samples of BMV58 and CR85, suggesting *S. uvarum* and *S. kudriavzevii* strains may have different cell wall sugar profiles. On the other hand, N-acetyltryptophan was only present in the *S. cerevisiae* strains. Octanoylcarnitine was found only in BMV58, while eicosanoylsphingosine was absent only in this strain, and ethanolamine was not detected in the *S. kudriavzevii* strain (**Figure 5A**).

Figure 5 (see on next page). On panel A), list of the present or absent compounds detected among the four strains. On panel B), compounds with high magnitude change observed during growth among the four strains. For each strain, superscript italic letters indicate the magnitude (M) of the change between the first (GP) and the fourth sampling point (MSP) computed as M=exp[log scaled intensity(MSP) – log scaled intensity (GP)]. When the intracellular amount increased (M >1), the black letter was used. When decreased (M<1), the inverse of the magnitude (1/M) between GP and MSP was calculated and indicated in italic red letter. Highest changed in magnitude are indicated in bold.

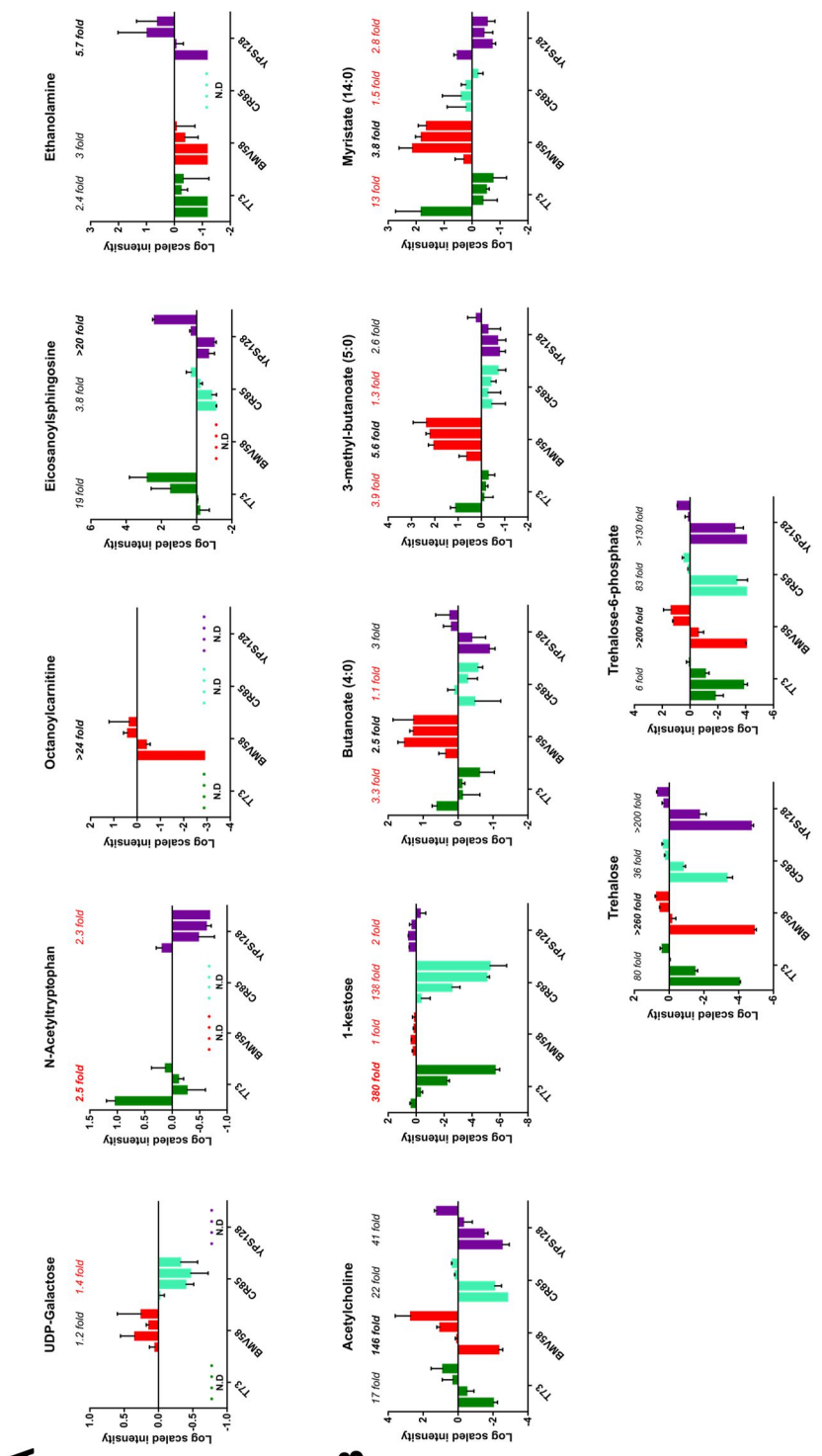
A
UDP-Galactose
1.2 fold
1.4 fold
N-Acetyltryptophan
2.5 fold
2.3 fold
Octanoylcarnitine
>24 fold
Eicosanoylsphingosine
19 fold
3.8 fold
>20 fold
Ethanolamine
2.4 fold
3 fold
5.7 fold
B
Acetylcholine
17 fold
146 fold
22 fold
41 fold
1-kestose
380 fold
1 fold
138 fold
2 fold
Butanoate (4:0)
3.3 fold
2.5 fold
1.1 fold
3 fold
3-methyl-butanoate (5:0)
3.9 fold
5.6 fold
1.3 fold
2.6 fold
Myristate (14:0)
13 fold
3.8 fold
1.5 fold
2.8 fold
Trehalose
80 fold
>260 fold
36 fold
>200 fold
Trehalose-6-phosphate
6 fold
>200 fold
83 fold
>130 fold
Log scaled intensity
N.D
T73
BMV58
CR85
YPS128

Another approach was to evaluate the magnitude of large changes observed during the fermentation and to determine if the strains differed significantly (**Figure 5B**). For instance, one compound with large accumulation was acetylcholine, which reached a 140-fold increase in *S. uvarum*, but was about two orders of magnitude lower than the other strains (**Figure 5B**). Also, we noted that the storage fructan oligosaccharide 1-kestose was apparently differentially utilized by the strains (**Figure 5B**). The compound was found at very similar levels in all strains at the first time point, but while *S. cerevisiae* T73 and *S. kudriavzevii* CR85 fully depleted this compound, *S. uvarum* BMV58 and *S. cerevisiae* YPS128 did not affect its levels significantly over time, suggesting that these two strains could not utilize this pool of carbon source for fermentation. Moreover, we observed differences in the intracellular level of some short and medium chain fatty acids (from C6 to C14) which might be relevant to wine production. Butanoate (C4) and 3-methyl-butanoate (C5) are considered odorants or flavour compounds in various foods, including wine. Both compounds declined in the *S. cerevisiae* T73 strain over time, but increase slightly in YPS128, and both were highest in the *S. uvarum* strain, increasing over the fermentation time. *S. kudriavzevii* CR85 had low levels that did not change significantly (**Figure 5B**). Also, BMV58 was the only strain that accumulated (almost 4 fold) the medium chain fatty acid myristate (C14). Regarding compounds that showed the greatest accumulation

over these fermentations, we found trehalose, followed closely by its immediate precursor trehalose-6-phosphate (T6P), as shown in **Figure 5B**. It accumulated to similarly high levels in all the strains, representing an increase of >260-fold in BMV58 strain. Finally, the tryptophan precursor anthranilate which increased >150-fold in *S. kudriavzevii* was one of the important differences observed among the four strains in the aromatic amino acid pathways (see below).

3.4 Differences in succinate and glycerol production pathways

The depletion of dissolved oxygen initially contained in the white must was completed between 30 and 80 hours of fermentation, strain YPS128 being the quickest in consuming oxygen (**Figure 1A**). During this period of time, a decrease in the extracellular amount of succinate was observed in the four fermentations (**Figure 6**). After oxygen depletion, the extracellular level of succinate remained constant during few hours (T73, BMV58, and CR85 strains) and newly started to increase when yeast cells entered into the stationary phase (**Figure 6**).

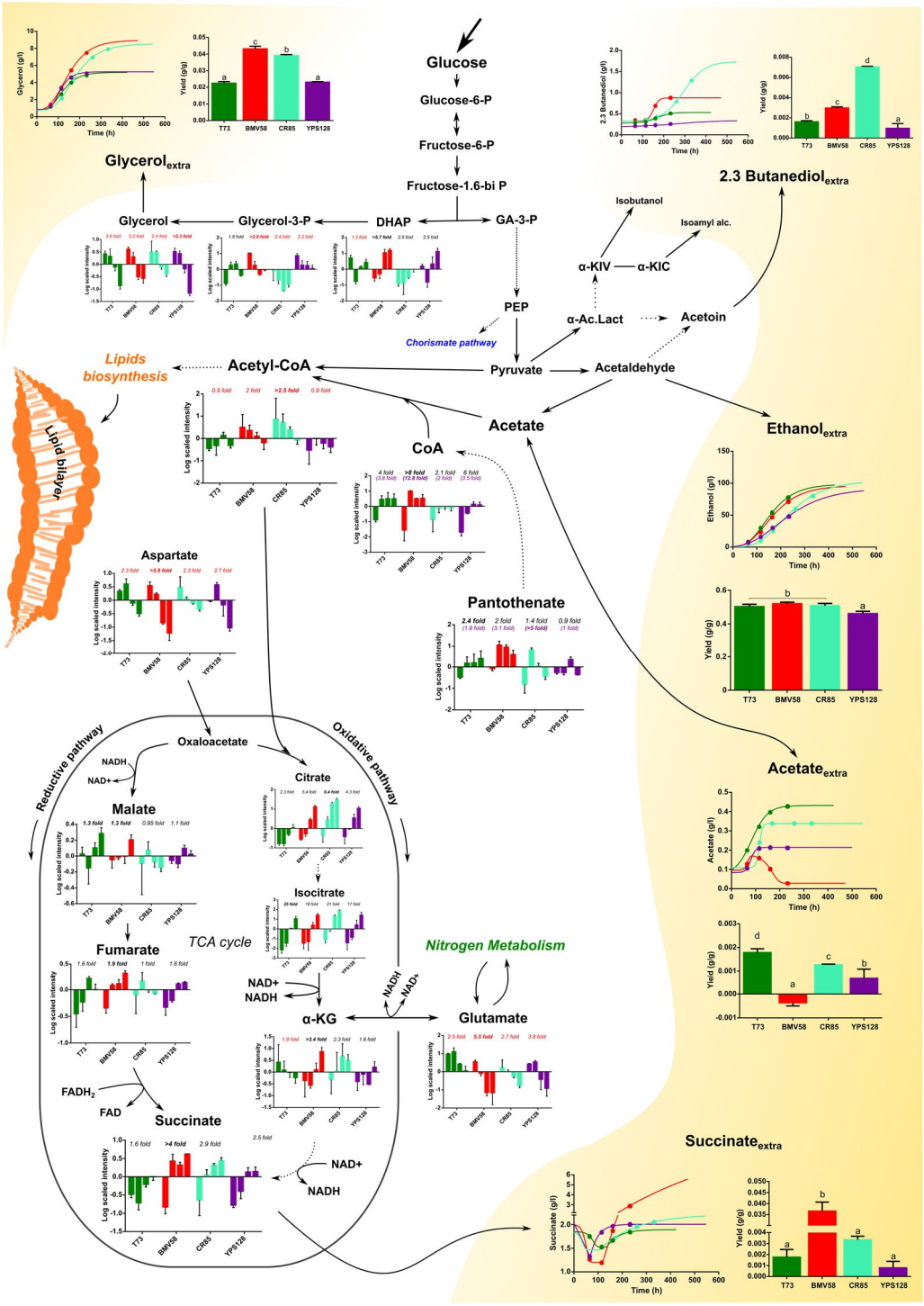
Glucose
Glucose-6-P
Fructose-6-P
Fructose-1.6-bi P
DHAP
GA-3-P
Glycerol
Glycerol-3-P
Glycerol$_{extra}$
PEP
Chorismate pathway
Pyruvate
Acetaldehyde
Acetoin
α-Ac.Lact
α-KIV
α-KIC
Isobutanol
Isoamyl alc.
2.3 Butanediol$_{extra}$
Acetyl-CoA
Lipids biosynthesis
Lipid bilayer
CoA
Acetate
Ethanol$_{extra}$
Aspartate
Pantothenate
Oxaloacetate
Reductive pathway
Oxidative pathway
Citrate
Malate
Isocitrate
Fumarate
TCA cycle
Nitrogen Metabolism
α-KG
Glutamate
Succinate
Succinate$_{extra}$
Acetate$_{extra}$
NADH
NAD+
FADH$_2$
FAD
Time (h)
T73
BMV58
CR85
YPS128

Figure 6. Overview of the reactions involved in the CCM of yeasts under enological fermentative conditions, including the glycolysis pathway and the tricarboxylic acid (TCA) cycle. Dashed arrows indicate the uncomplete pathways. The intracellular amount of relevant intermediates of the CCM is presented for each strain. On intracellular graph, for each strain, superscript italic letters indicate the magnitude (M) of the change between the first (GP) and the fourth sampling point (MSP) computed as M=exp[log scaled intensity(MSP) – log scaled intensity (GP)]. When the intracellular amount increased (M >1), the black letter was used. When decreased (M<1), the inverse of the magnitude (1/M) between GP and MSP was calculated and indicated in italic red letter. For CoA and Pantothenate compounds, the magnitude between the second and fourth intracellular point is also presented in purple. Highest changed in magnitude are indicated in bold. Fitted extracellular concentration (supporting information in material and methods) and yield (g product/g sugar consumed) of the related CCM by products, including glycerol, 2,3 butanediol, ethanol and acetate are also included. Superscript letters on yield graph indicate the significant homogeneous groups obtained by one-way ANOVA analysis (Tukey test, n = 3, p-value <0.05). Circles on the fitted curves represent the four intracellular sampling points. Abbreviations: DHAP (dihydroxyacetone phosphate), GA-3-P (Glyceraldehyde-3-phosphate), PEP (phosphoenolpyruvate), α-Ac.Lact (alpha-acetolactate), α-KIV (alpha-ketoisovalerate), α-KIC (alpha-ketoisocaproate), α-KG (apha-ketoglutarate).

This extracellular succinate uptake notably coincided with a proline uptake (**Figure 1B**). Besides, extracellular levels of succinate at the

end of the fermentation were proportional to the intracellular amounts of each strain. For instance, the highest intracellular accumulation of succinate between the first and the fourth intracellular sampling point was observed in BMV58 strain (>4 fold) and also produced the largest amount of succinate (5.63 $g \cdot l^{-1}$) (**Table 1, Figure 6**). In BMV58, the higher succinate synthesis might have contributed to acidification and to decrease the pH level of the final wine (**Figure S2**). In yeasts and in anaerobic conditions, succinate can be generated by the reductive or the oxidative pathway of the tricarboxylic acid cycle (TCA) (**Figure 6**). In accordance with this, the intracellular level of aspartate, a precursor of oxaloacetate, largely decreased between the mid-exponential phase and the advanced stage of the stationary phase in BMV58 (>5.8 fold). Moreover, except in CR85 fermentation, we observed an increase in the intracellular content of the two intermediates of the reductive branch of TCA, malate, and fumarate, between the first and fourth intracellular sampling point in T73, BMV58 and YPS218 strains (**Figure 6**). Regarding the oxidative branch of TCA, the intracellular levels of citrate and isocitrate, both precursors of alpha-ketoglutarate, increased largely during the fermentation in the four strains. Nevertheless, the intracellular amount of alpha-ketoglutarate, which is an important node between CCM and nitrogen metabolism, behaved very differently among the four strains (**Figure 6**). In CR85 and YPS128 fermentations, the content of this keto-acid showed a

small but significant increase, while in T73 fermentation it decreased along the whole fermentation. On the contrary, in BMV58 alpha-ketoglutarate content decreased between GP and EGP and increased between ESP and MSP. Moreover, BMV58 strains had the lowest intracellular glutamate level when entered into the early stationary phase (**Figure 6**). These results suggest that a higher amount of the alpha-ketoglutarate generated through the reductive branch of the TCA could contribute to the succinate production in BMV58 strain, notably during the early stationary phase.

The strains of the cryotolerant species *S. uvarum* and *S. kudriavzevii* produced the largest amount of glycerol (8.22 $g \cdot l^{-1}$ and 7.79 $g \cdot l^{-1}$ respectively) at the end of the fermentation (**Figure 6, Table 1**). On the other hand, T73 and YPS128 *S. cerevisiae* strains produced very similar quantities of glycerol (**Table 1**). Interestingly, if we compare the extracellular amount of glycerol at the time of each intracellular sampling point between the four strains, we can see that it was always equal or higher in BMV58 and CR85 fermentations than in both *S. cerevisiae* strains. In contrast, intracellular levels of glycerol as well as the pathway intermediates, namely DHAP and glycerol-3-phosphate, were higher only in the fourth time point in BMV58 (**Figure 6**). Besides, in strain CR85 the intracellular levels of glycerol-3-phosphate and DHAP were lower than the other strains which produced less glycerol. These observations suggest higher activity as well as increased catalytic properties of the CR85 enzymes involved

in the glycerol pathway, notably the activities involved in DHAP and Glycerol-3-phosphate catabolism as was previously suggested elsewhere (Oliveira et al., 2014).

3.5 Differences in acetate metabolism

In our winemaking simulations at 12ºC, the *S. cerevisiae* wine strain T73 produced the largest amount of extracellular acetate (0.43 $g \cdot l^{-1}$) (**Table 1**). On the contrary the natural isolate of *S. cerevisiae*, YPS128 strain produced 2 fold less acetate (0.21 $g \cdot l^{-1}$) than T73, and also less acetate than CR85 strain (0.34 $g \cdot l^{-1}$). Regarding the concentration of acetate in the *S. uvarum* fermentation, we observed a very similar pattern to the one obtained at 25ºC in previous work (Minebois *et al.*, 2020) with BMV58 and another *S. uvarum* strain (CECT12600). BMV58 strain released acetate until the entry into the stationary phase, after which the extracellular amount of acetate started to decrease to reach the lowest value of 0.03 $g \cdot l^{-1}$ (**Figure 6**; **Table 1**).

Acetate is a precursor for the synthesis of acetyl-CoA (**Figure 6**). Here we observed that the intracellular contents of acetyl-CoA in BMV58 and CR85 strains were greater than both *S. cerevisiae* strains (**Figure 6**). In agreement with the latter result, a higher increase in the synthesis of the precursors of acetyl-CoA, pantothenate and CoA compounds, occurred when we compare GP and EGP intracellular sampling points in BMV58 and CR85 strains. Also, we observed that

intracellular levels of CoA (BMV58 strain only) and pantothenate (BMV58 and CR85 strains) were higher from the second intracellular sampling point when compared to *S. cerevisiae* strains (**Figure 6**).

3.6 Higher activity of pentose phosphate and chorismate pathways in the *S. uvarum* strain

A clear difference between strains was found for the synthesis of the aromatic amino acids, accomplished through the pentose phosphate and shikimate pathways (**Figure 7**). Bar plots for the various aromatic precursors, including 3-dehydroquinate (>32 fold increase), 3-dehydro-shikimate (>58 fold increase), and shikimate (>3 fold increase), show clearly that the *S. uvarum* strain was much more anabolically active through the shikimate pathway. The proteinogenic aromatic amino acids themselves did not vary among strains (bar plots not shown), but catabolites of phenylalanine such as phenylacetate (>2.9 fold increase) and phenyl lactate (>5 fold increase) appeared to correlate to the precursor levels.

Moreover, these results were in accordance with both the timing of production and the higher extracellular levels of phenylpropanoids (2-phenylethanol and 2-phenylethyl acetate) that were quantified in the BMV58 fermentation (see below).

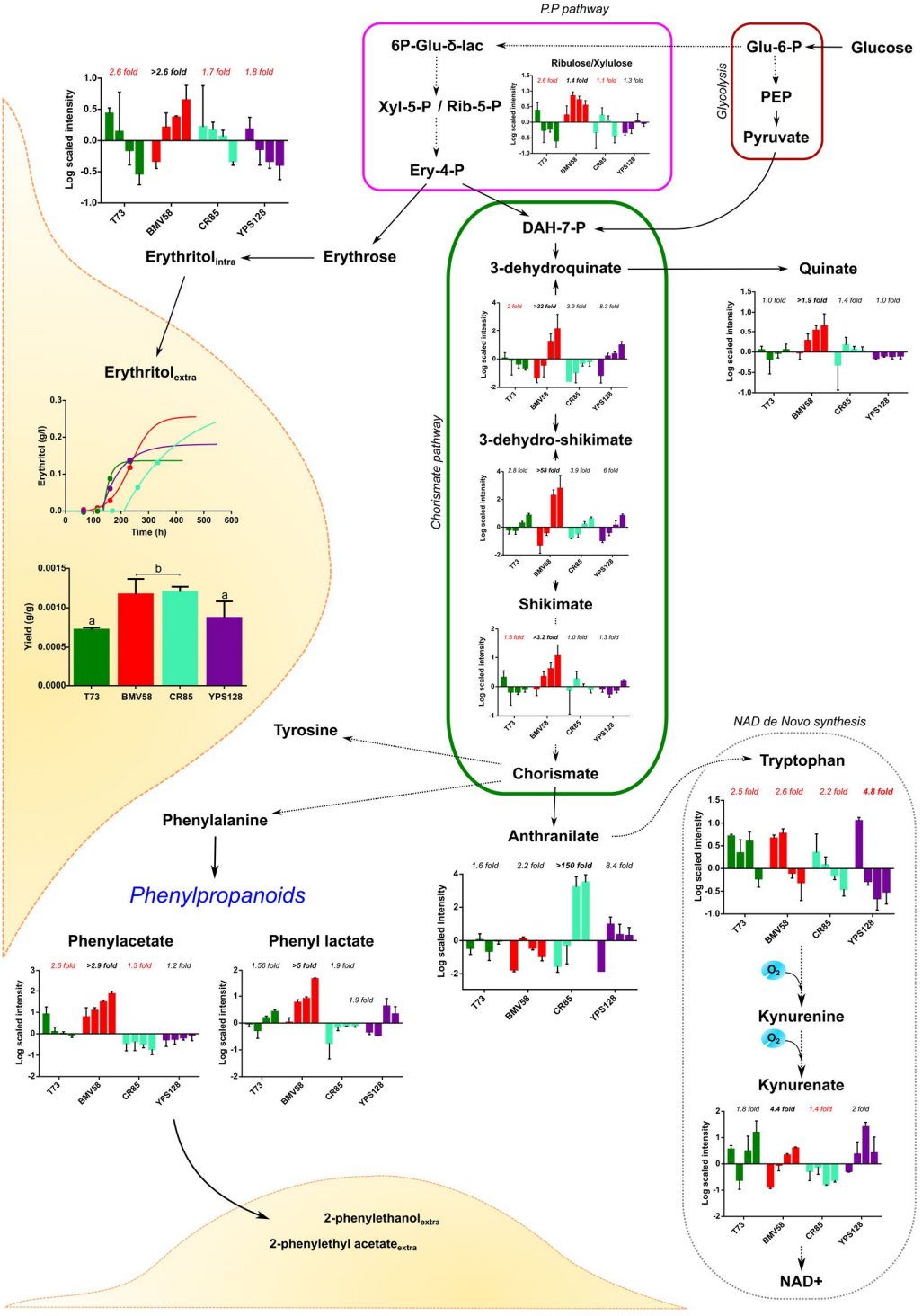
P.P pathway
6P-Glu-δ-lac
Ribulose/Xylulose
Xyl-5-P / Rib-5-P
Ery-4-P
Glu-6-P
Glucose
Glycolysis
PEP
Pyruvate
DAH-7-P
3-dehydroquinate
Quinate
3-dehydro-shikimate
Shikimate
Chorismate pathway
Erythrose
Erythritol$_{intra}$
Erythritol$_{extra}$
Tyrosine
Chorismate
Phenylalanine
Phenylpropanoids
Anthranilate
NAD de Novo synthesis
Tryptophan
Kynurenine
Kynurenate
NAD+
Phenylacetate
Phenyl lactate
2-phenylethanol$_{extra}$
2-phenylethyl acetate$_{extra}$
Log scaled intensity
Yield (g/g)
Time (h)
T73
BMV58
CR85
YPS128

Figure 7. Overview of the reactions involved in the pentose phosphate pathway (PPP) and the chorismate pathway. Dashed arrows indicate the uncomplete pathways. The intracellular amount of relevant intermediates of the PPP and the chorismate pathway is presented for each strain. On intracellular graph, for each strain, superscript italic letters indicate the magnitude (M) of the change between the first (GP) and the fourth sampling point (MSP) computed as M=exp[log scaled intensity(MSP) – log scaled intensity (GP)]. When the intracellular amount increased (M >1), black letter was used. When decreased (M<1), the inverse of the magnitude (1/M) between GP and MSP was calculated and indicated in italic red letter. Highest changed in magnitude are indicated in bold. Fitted extracellular concentration (supporting information in material and methods) and yield (g product/g sugar consumed) of one of the related PPP by product, namely erythritol is also included. Superscript letters on yield graph indicate the significant homogeneous groups obtained by one-way ANOVA analysis (Tukey test, n = 3, p-value <0.05). Circles on the fitted curves represent the four intracellular sampling points. Abbreviations: 6P-Glu-δ-lac (6-phospho D-glucono-1,5-lactone), Rib-5-P (Ribulose-5-phosphate), Xyl-5-P (Xylulose-5-Phosphate), Ery-4-P (D-erythrose-4-phosphate), PEP (phosphoenolpyruvate), DAH-7-P (3-deoxy-D-arabino-heptulosonate 7-phosphate), Glu-6-P (Glucose-6-phosphate).

Also, as stated above, anthranilate, which is the first committed precursor to the tryptophan pathway, was much higher in *S. kudriavzevii* CR85 (>150 fold), although this did not correlate to

tryptophan or its downstream catabolites kynurenine and kynurenate (**Figure 7**).

On the other hand, we previously mentioned that the cryotolerant strains BMV58 and CR85 produced higher levels of erythritol (**Table 1**). Erythritol is an endogenously made compound originated from erythrose-4-phosphate, a pentose phosphate pathway derivative that also serves as a precursor for the shikimate pathway (**Figure 7**). We observed that intracellular levels of erythritol decreased strongly overgrowth for all the strains except for *S. uvarum* strain, where it increased more than two-fold between GP and MSP (**Figure 7**). Moreover, the intracellular levels of xylulose and ribulose, precursors of xylulose-5-phosphate and ribulose-5-phosphate, were higher in BMV58 (**Figure 7**). The higher intracellular accumulation of erythritol in BMV58 was in agreement with the higher extracellular levels of erythritol found in BMV58. Also, the comparison between the evolution of the intra- and extracellular levels of erythritol in the four strains suggested two different modes of production of this metabolite. T73, YPS128 and CR85 strains accumulated this compound earlier during the fermentation process, probably during the growth phase, and started to release it into the extracellular medium when they entered into the stationary phase. On the contrary, the production of erythritol peaked after entry into the stationary phase in BMV58 (**Figure 1, Figure 7**).

3.7 Intracellular metabolism of sulphur

The metabolism of sulphur, through the production of cysteine and its used in the antioxidant glutathione pathway, also tended to differentiate the strains (**Figure 8**). The levels of sulphate in both T73 and BMV58 strains started relatively high and declined during early growth, but then they began to increase in the later time points. Both natural isolates strains, CR85 and YPS128, did not show this pattern, the former not changing, and the latter decreasing in sulphate over the whole time course. BMV58 strain started with the lowest levels of cysteine and glutathione, but it recovered similar levels to the other strains towards the end of the fermentation. The *S. cerevisiae* wine yeast T73 also was active in the synthesis of cysteine and glutathione. On the contrary, CR85 and YPS128 strains showed relatively flat levels of glutathione and their derivatives. Taurine biosynthesis, which is derived from cysteine, occurs only at very low levels in plants and fungi. In our conditions, its pattern was quite different between the strains. Regarding the two *S. cerevisiae* strains, T73 started with undetectable levels of taurine and then increased at the end, while YPS128 started with much higher levels and then declined. It is not clear if taurine occurs in high enough amounts to affect wine properties, but many sulphur containing compounds have flavour properties (usually negative).

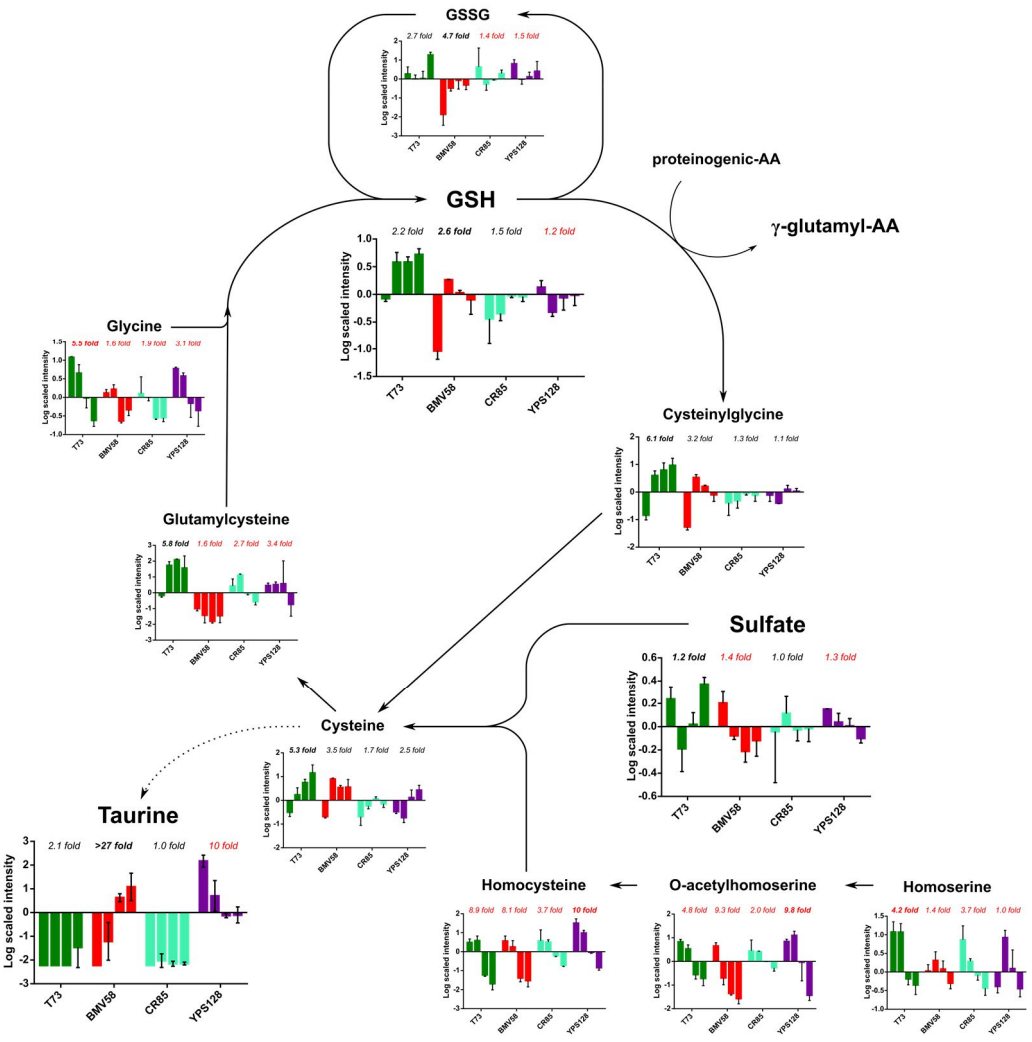

Figure 8. Overview of the glutathione biosynthesis pathway. Dashed arrows indicate the uncomplete pathways. On intracellular graph, for each strain, superscript italic letters indicate the magnitude (M) of the change between the first (GP) and the fourth sampling point (MSP) computed as M=exp[log scaled intensity(MSP) – log scaled intensity (GP)]. When the intracellular amount increased (M >1), black letter was used. When decreased (M<1),

the inverse of the magnitude (1/M) between GP and MSP was calculated and indicated in italic red letter. Highest changed in magnitude are indicated in bold. Abbreviations: GSH (L-γ-glutamyl-L-cysteinylglycine), GSSG (glutathione oxidized).

3.8 Differences in aroma production

Ten aroma compounds including fusel alcohols, acetate esters and ethyl esters were quantified along the fermentation process. The evolution of their extracellular concentrations across time was integrated into a heat map (**Figure 9, panel A**) and a principal component analysis was used to segregate the aroma profile of the final wines by strains (**Figure 9, panel B; Table S1**). Also, the reactions leading to aromas formation, including the intracellular amount of their precursor when detected, were depicted in **panel C** of **Figure 9**. At 12ºC, the natural *S. cerevisiae* YPS128 strain produced very few aroma compounds and segregated in the bottom right corner of the PCA plot (**Figure 9, panel B**). Cryotolerant strains produced more ethyl acetate than both *S. cerevisiae*, which was in accordance with the higher intracellular levels of acetyl-CoA found for CR85 and BMV58 (**Figure 4**, **Figure 7**). Strain BMV58 produced the largest amount of fusel alcohols and their acetate esters, notably 2-phenylethanol, isoamyl alcohol, isobutanol, 2-phenylethyl acetate, isoamyl acetate, and isobutyl acetate. On the contrary, T73 strain mainly produced ethyl esters (ethyl hexanoate, ethyl octanoate, and

ethyl decanoate). Finally, the CR85 strain had an intermediate position, producing higher levels of isobutanol, isobutyl acetate, and isoamyl alcohol than T73 and similar levels of ethyl decanoate. The previous results were in accordance with the higher intracellular levels of phenylpropanoids stated above in BMV58 (**Figure 7**) as well as with the higher intracellular amounts of alpha ketoisovalerate and alpha-keto isocaproate detected in BMV58 and CR85 strains (**Figure 9, panel C**). Also, in T73 strain which produced more ethyl esters, the intracellular levels of hexanoate and octanoate were higher if compared to BMV58 strain. Nevertheless, while in CR85 strain the intracellular amount of decanoate was in accordance with the extracellular levels of ethyldecanoate, surprisingly in T73 strain it was lower than in BMV58 strain.

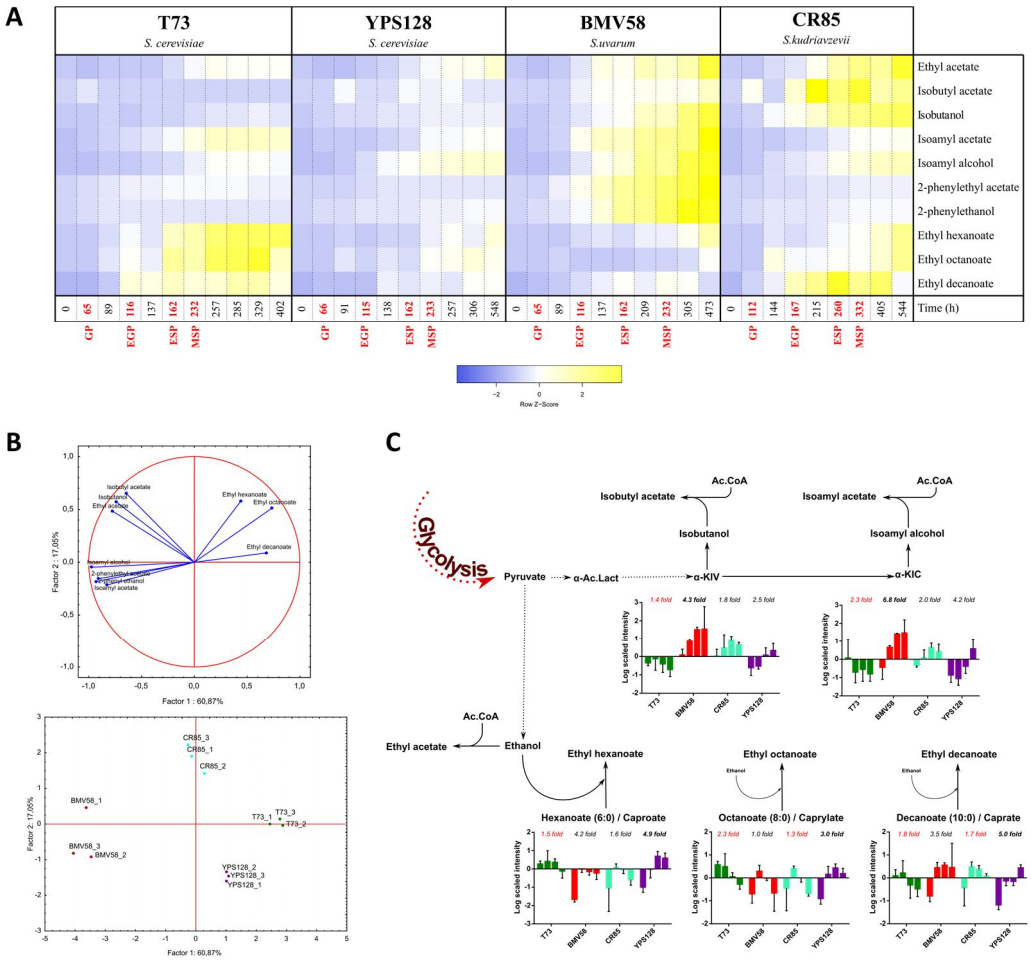

Figure 9. A) Heat map of the extracellular concentrations of the ten aroma compounds quantified in this study, including fusel alcohols (isobutanol, isoamyl alcohol and 2-phenylethanol), acetate esters (isobutyl acetate, isoamyl acetate and 2-phenylethyl acetate) and ethyl esters (ethyl hexanoate, ethyl octanoate and ethyl decanoate). On the time axis of the heat map, red letters indicate the intracellular sampling points (GP, EGP, ESP, and MSP). B) PCA plots performed with the concentrations of aroma

compounds at the end of the fermentation. C) Aroma compounds pathways with the intracellular amount of some precursors. On intracellular graph, for each strain, superscript italic letters indicate the magnitude (M) of the change between the first (GP) and the fourth sampling point (MSP) computed as M=exp[log scaled intensity(MSP) – log scaled intensity (GP)]. When the intracellular amount increased (M >1), black letter was used. When decreased (M<1), the inverse of the magnitude (1/M) between GP and MSP was calculated and indicated in italic red letter. Highest changed in magnitude are indicated in bold. For 2-phenyl-ethanol and 2-phenylethyl acetate pathway, report to Figure 7. Abbreviations: α-KIV (alpha-ketoisovalerate) and α-KIC (alpha-ketoisocaproate).

4. Discussion

4.1 Global fermentation performances comparison between 12ºC and 25ºC

We recently performed a metabolomic comparison in a similar way with strains T73, BMV58, and CR85 at 25ºC (Minebois *et al.*, 2020). At 12ºC and 25ºC, most of the physiological and metabolic changes among strains occurred during the transition between the growth phase and the stationary phase. When comparing the global fermentation performances at both temperatures, no significant differences were observed in the ethanol yields (g of ethanol produced/ g sugar consumed) for the three strains, but were observed for the yield of various fermentative by-products and the biomass production. The *S. cerevisiae* strain T73 was the most

negatively affected by low temperature. Its biomass production decreased and the yields of acetate and 2,3 butanediol increased. On the contrary, the CR85 strain performed much better at low temperature. We reported the absence of residual sugar (dry wine) at 12ºC in the CR85 fermentation, and we observed a significant decrease in the yields of acetate and lactate (data not shown) and a significant increase in erythritol yield. The last results pointed out the better adaptation of CR85 strain to low temperature. In BMV8 the yields of glycerol and lactate increased at 12ºC, while the yield of erythritol decreased. Interestingly, in CR85 strain, we observed that the intracellular levels of glycerol precursors, glycerol-3-phosphate and DHAP, were lower than those of BMV58 strain, as well as those of both *S. cerevisiae* strains which produced less glycerol. Consequently, only a higher catalytic property of the enzymes involved in the glycerol pathway of the CR85 strain could explain such intracellular amounts of the glycerol precursors. This meets with the described properties of the *S. kudriavzevii* Gpd1p enzyme encountered by Oliveira *et al.* (2014) but also with the adaptive evolution detected in the FBA1 gene of CR85, which is involved in the synthesis of dihydroxyacetone phosphate, the precursor of the glycerol synthesis (Macías *et al.*, 2019).

Regarding aroma production, at 12ºC BMV58 strain excelled in higher alcohol (2-phenyl ethanol, isoamyl alcohol, and isobutanol) and acetate esters (isoamyl acetate and 2-phenylethyl acetate)

production, whereas T73 and CR85 strains did so in ethyl esters synthesis (ethyl hexanoate and ethyl decanoate). Also, at 12ºC cryotolerant CR85 and BMV58 strains produced a higher amount of ethyl acetate compared to the same fermentation performed at 25ºC. At 25ºC, the production of higher alcohols and acetate esters by BMV58 strain was already remarkable, as was acetic acid synthesis carried out by CR85 (Minebois *et al.*, 2020). These results were in accordance with previous results (Gamero *et al.*, 2013). In particular, it has been shown that the aromatic amino acid decarboxylase *ARO10*, and the acetyltransferase *ATF2* were up-regulated in a *S. uvarum* strain when fermented at 12ºC (Gamero *et al.*, 2014), which supported the higher levels of fusel alcohols, notably 2-phenyl ethanol, and acetate esters produced by BMV58 at 12ºC. Gamero *et al.* (2014) also observed that alcohol dehydrogenases *ALD4* and *ALD5* (involved in acetaldehyde conversion into acetate) were up-regulated in the *S. uvarum* strain at 12ºC. One possible explanation for the low acetate levels detected in BMV58 is that part of this metabolite is used for ethyl acetate production since BMV58, together with CR85 strain, produced the largest ethyl acetate amount at 12ºC.

4.2 Anthranilate accumulation in *S. kudriavzevii*

In a metabolomic comparison performed at 12ºC, López-Malo et al. (2013) demonstrated that the CR85 strain was characterized by a high activity of the NAD^+ *de Novo* pathway. As evidence, most of

the intermediates of this pathway, including tryptophan, nicotinate, nicotinamide ribonucleotide, or nicotinate ribonucleoside were present in higher amounts in the CR85 strain in comparison with the *S. cerevisiae* wine strain (QA23) used as control. Intriguingly, we observed that anthranilate, an upstream compound of the NAD^+ *de Novo* pathway and a precursor of tryptophan was highly accumulated (>150 fold) by the CR85 strain. Nevertheless, this did not correlate to tryptophan either its downstream catabolite kynurenate. The reason for such anthranilate accumulation might be found in the characteristics of the enzymes involved in this pathway. Indeed, while the conversion of anthranilate to L-tryptophan can occur anaerobically, three reactions involved in the *de Novo* pathway from L-tryptophan to NAD^+ require oxygen. Notably, the 2,3 dioxygenase (Bna2p), the kynurenine 3-mono oxygenase (Bna4p), and the 3-hydroxyanthranilic acid dioxygenase (Bna1p) involved in the first, third and fifth steps from L-tryptophan respectively are oxygen-dependent (Panozzo *et al.*, 2002). In our study, anaerobic conditions were self-generated inside the bioreactors, but dissolved oxygen was already depleted at the time of the first intracellular sampling point (GP). On the contrary, López-Malo *et al.* (2013) used chemostat steady-state cultures, and it is not mentioned if fermenters were fed with a deoxygenized medium. Because it is not clear if anaerobic conditions were imposed in the work of López-Malo et al. (2013), it is likely that the higher activity of the *de Novo* NAD^+ pathway identified

in the CR85 strain was allowed by the presence of dissolved oxygen in the medium. A very similar phenomenon exists in yeasts with squalene. The initial steps of sterol synthesis do not require oxygen and are responsible for the accumulation of squalene under anaerobic conditions (Daum *et al.*, 1998; Rosenfeld and Beauvoit, 2003). In our study, we could then expect that CR85 strain accumulated anthranilate as an attempt to fulfill its NAD^+ requirements. The couple NAD^+/NADH is a conserved moiety that can serve as a marker of the cellular redox status (Bakker *et al.*, 2001). Since alcoholic fermentation is redox neutral, under anaerobic conditions, other organic molecules such as glycerol have to act as proton acceptors. This correlates with the observation that, with the *S. uvarum* strain, CR85 strain is characterized by high glycerol yield. Regrettably, we had no information of the *de Novo* NAD^+ pathway in CR85 at 25ºC due to the lower number of metabolites that could be quantified with the GC/MS procedure we used for intracellular samples (Minebois *et al.*, 2020). Thus further investigation is required to answer whether the CR85 strain also struggles to meet NAD+ levels via *de Novo* NAD^+ pathway at high temperature.

4.3 Higher pentose phosphate and chorismate pathways activity in BMV58 strain

In a previous study at 25ºC, we already reported the concomitant synthesis of erythritol, 2-phenyl ethanol, and 2-

phenylethyl acetate following the onset of nitrogen starvation and the significantly higher yields for these metabolites in two *S. uvarum* strains, namely BMV58 and CECT12600 (Minebois *et al.*, 2020). These results led us to suggest that both strains were metabolically more active than T73 strain through the pentose phosphate and the chorismate pathways when passing from growth phase to the stationary phase. Indeed, both pathways have in common erythrose-4-phosphate. On the one hand, erythrose-4-phosphate is the precursor for erythritol synthesis (Moon *et al.*, 2010). Moreover, it is also an upstream precursor of the chorismate pathway whose downstream metabolites can be converted through the Ehrlich pathway into 2-phenylethanol and 2-phenylethyl acetate among others (Braus, 1991; Hazelwood *et al.*, 2008). In this study, the higher intracellular levels found for sugar precursors of the pentose phosphate pathway (xylulose and ribulose), erythritol, and the various aromatic precursors (3-dehydroquinate, 3-dehydro-shikimate, and shikimate) were clear evidence that this higher activity was maintained at low temperature in BMV58 strain. Also, these results were in accordance with a similar observation made by López-Malo *et al.* (2013) in chemostat culture. However, because the intracellular levels of the aforementioned metabolites were not quantified absolutely at 12ºC either at 25ºC, we could not ascertain how much this activity is affected by low temperature in the *S. uvarum* strain.

4.4 Acetate and lipid metabolism in BMV58 strain

At 12°C, CR85 and BMV58 strains had lower acetate yields than the T73 strain. Also, the *S. cerevisiae* wine strain T73 produced more acetate at 12ºC when compared to the same fermentation performed at 25°C (Minebois *et al.*, 2020). The above results pointed out the better fermentative quality of both strains of *S. uvarum* and *S. kudriavzevii* at low fermentation temperature. Moreover, the dynamic approach used in our studies enabled us again to suggest a possible metabolism of "production-consumption" of acetate in the *S. uvarum* BMV58 strain at 12ºC. At 25ºC, this metabolomic trait was already observed in two *S. uvarum* strains, including BMV58, and occurs when cells are starved of nitrogen and in the absence of oxygen (Minebois *et al.*, 2020). Thus, these results suggest that this metabolic trait of BMV58 does not depend on temperature. But whether this mechanism requires strict anaerobic conditions or can occur under aerobic or limited aerobic conditions in the BMV58 strains has to be investigated. From an industrial point of view, it is relevant since it could help winemakers to reduce the volatile acidity of wines fermented at low or high temperature. Recently, the selection of yeast strains with the ability to consume acetate has already been explored for the deacidification of acidic wines (Vilela-Moura *et al.*, 2008, 2010, 2011). However, in the latter studies deacidification by both *S. cerevisiae* strains, namely S29 and S26, relies on their ability to consume acetate in the presence of glucose

and under limited-aerobic or aerobic conditions, i.e. on their ability to respire acetate even under glucose repression.

To explain this specific acetate metabolism in the *S. uvarum* BMV58 strain, we already suggested that acetate could be assimilated in the lipid-producing pathways at 25ºC (Minebois *et al.*, 2020). Although the assimilation mechanisms are not clear, other authors have suggested that acetate could be assimilated for such purpose (Ribéreau-Gayon *et al.*, 2006). Cadière *et al.* (2011) notably shown that the evolved strain ECA5 with higher pentose phosphate pathway activity tended to reduce acetate levels, hypothesizing greater lipid synthesis. At 12ºC, our intracellular data set revealed that the majority of high magnitude metabolic changes occurred for the four strains between the first (GP) and the second (EGP) intracellular sampling point were related to lipid metabolites. We reported that the CR85 and BMV58 strains had higher intracellular levels of acetyl-CoA. Also, the precursors of acetyl-CoA, pantothenate and CoA, were found in higher amount between GP and EGP in BMV58. In accordance with a higher acetyl-CoA requirement for lipids biosynthesis, the short chain fatty acids butanoate (4:0) and 3-methyl-butanoate (6:0), as well as the medium chain fatty acid myristate (14:0) were highly accumulated between GP and EGP in BMV58 and their intracellular levels remained higher until MSP. Moreover, octanoylcarnitine, a medium chain saturated fatty acyl-L-carnitine compound was only detected in BMV58. The presence of

octanoylcarnitine only in the BMV58 strain remained unclear. However, in accordance with the results obtained by Redón *et al.* (2011) and the levels of butanoate and 3-methyl-butanoate observed in BMV58, we suggest that the BMV58 strain may have favoured the synthesis of short and medium chain fatty acid as an adaptation mechanism to low fermentation temperature. Concordant with this, ethyl hexanoate, ethyl octanoate, and ethyl hexanoate aromas were barely detected in the *S. uvarum* fermentation when compared with T73 and CR85. Also, it is possible, that this medium chain fatty acid could enter into the specific mitochondrial membrane composition of the BMV58 strain.

In summary, this global metabolic profiling study gave us some new insights into the low fermentation temperature metabolism of strains of *S. cerevisiae*, *S. uvarum,* and *S. kudriavzevii*. The high resolution of the Metabolon HD4 platform (Durham, NC, USA) enabled us to accurately snapshot the intracellular levels of a large number of metabolites at four stages of the fermentation. Combining data of the intra- and extracellular metabolomes, we could reconstruct some relevant yeast pathways with their upstream and downstream metabolites. We already performed a similar metabolic profiling of strains T73, CR85, and BMV58 at 25ºC, but not with as much intracellular metabolome details. This made impossible a complete comparison between the 12ºC and the 25ºC metabolic data. Consequently, we could not ascertain whether the changes

presented above in the metabolism of these strains were due to low temperature. However, up to a point we succeeded in shading between inherent strain difference and temperature-dependent strain difference. For instance, the higher pentose phosphate and chorismate pathways activity, as well as the "production-consumption" profile of acetate observed in BMV58 at 12ºC and 25ºC, suggested it is inherent to this strain. This work can have practical implications, taking advantage of the specific metabolic properties and pathways identified in our set of *S. cerevisiae*, *S. kudriavzevii* and *S. uvarum* strains. From an industrial outlook, such knowledge is relevant to develop better metabolic engineering or hybridization strategies using cryotolerant strains of *S. uvarum* and *S. kudriavzevii*.

Acknowledgments

RM was supported by a FPI grant from the Ministerio de Economía y Competitividad (ref. BES-2016-078202). This work was supported by the Spanish government projects RTI2018-093744-B-C31 awarded to AQ.

Supplementary files

Supplementary files can be downloaded from https://doi:10.1111/1462-2920.15135 or found at **page 344** of this manuscript.

References

Arroyo-López, F.N., Pérez-Torrado, R., Querol, A., and Barrio, E. (2010) Modulation of the glycerol and ethanol syntheses in the yeast *Saccharomyces kudriavzevii* differs from that exhibited by *Saccharomyces cerevisiae* and their hybrid. *Food Microbiol* **27**: 628–637.

Bakker, B.M., Overkamp, K.M., Van Maris, A.J.A., Kötter, P., Luttik, M.A.H., Van Dijken, J.P., and Pronk, J.T. (2001) Stoichiometry and compartmentation of NADH metabolism in *Saccharomyces cerevisiae*. *FEMS Microbiol Rev* **25**: 15–37.

Belloch, C., Orlic, S., Barrio, E., and Querol, A. (2008) Fermentative stress adaptation of hybrids within the *Saccharomyces* sensu stricto complex. *Int J Food Microbiol* **122**: 188–195.

Beltran, G., Novo, M., Leberre, V., Sokol, S., Labourdette, D., Guillamon, J.M., et al. (2006) Integration of transcriptomic and metabolic analyses for understanding the global responses of low-temperature winemaking fermentations. *FEMS Yeast Res* **6**: 1167–1183.

Blateyron, L. and Sablayrolles, J.M. (2001) Stuck and slow fermentations in enology: Statistical study of causes and effectiveness of combined additions of oxygen and diammonium phosphate. *J Biosci Bioeng* **91**: 184–189.

Braus, G.H. (1991) Aromatic amino acid biosynthesis in the yeast *Saccharomyces cerevisiae*: A model system for the regulation of a eukaryotic biosynthetic pathway. *Microbiol Rev* **55**: 349–370.

Cadière, A., Ortiz-Julien, A., Camarasa, C., and Dequin, S. (2011) Evolutionary engineered *Saccharomyces cerevisiae* wine yeast strains with increased in vivo flux through the pentose phosphate pathway. *Metab Eng* **13**: 263–271.

Clement, T., Perez, M., Mouret, J.R., Sablayrolles, J.M., and Camarasa,

C. (2011) Use of a continuous multistage bioreactor to mimic winemaking fermentation. *Int J Food Microbiol* **150**: 42–49.

Daum, G., Lees, N.D., Bard, M., and Dickson, R. (1998) Biochemistry, cell biology and molecular biology of lipids of *Saccharomyces cerevisiae*. *Yeast* **14**: 1471–1510.

Demuyter, C., Lollier, M., Legras, J.L., and Le Jeune, C. (2004) Predominance of *Saccharomyces uvarum* during spontaneous alcoholic fermentation, for three consecutive years, in an Alsatian winery. *J Appl Microbiol* **97**: 1140–1148.

Gamero, A., Belloch, C., Ibáñez, C., and Querol, A. (2014) Molecular analysis of the genes involved in aroma synthesis in the species *S. cerevisiae*, *S. kudriavzevii* and *S. bayanus* var. *uvarum* in winemaking conditions. *PLoS One* **9**: 1–10.

Gamero, A., Tronchoni, J., Querol, A., and Belloch, C. (2013) Production of aroma compounds by cryotolerant *Saccharomyces* species and hybrids at low and moderate fermentation temperatures. *J Appl Microbiol* **114**: 1405–1414.

García-Ríos, E., Querol, A., and Guillamón, J.M. (2016) iTRAQ-based proteome profiling of *Saccharomyces cerevisiae* and cryotolerant species *Saccharomyces uvarum* and *Saccharomyces kudriavzevii* during low-temperature wine fermentation. *J Proteomics* **146**: 70–79.

Hazelwood, L.A., Daran, J.-M., van Maris, A.J.A., Pronk, J.T., and Dickinson, J.R. (2008) The Ehrlich pathway for fusel alcohol production: a century of research on *Saccharomyces cerevisiae* metabolism. *Appl Environ Microbiol* **74**: 2259–66.

Lopes, C.A., Barrio, E., and Querol, A. (2010) Natural hybrids of *S. cerevisiae* × *S. kudriavzevii* share alleles with European wild populations of *Saccharomyces kudriavzevii*. *FEMS Yeast Res* **10**: 412–421.

López-Malo, M., Querol, A., and Guillamon, J.M. (2013) Metabolomic

Comparison of *Saccharomyces cerevisiae* and the Cryotolerant species *S. bayanus* var. *uvarum* and *S. kudriavzevii* during Wine Fermentation at Low Temperature. *PLoS One* **8**:.

Macías, L.G., Morard, M., Toft, C., and Barrio, E. (2019) Comparative genomics between *Saccharomyces kudriavzevii* and *S. cerevisiae* applied to identify mechanisms involved in adaptation. *Front Genet* **10**: 187.

Masneuf-Pomarède, I., Bely, M., Marullo, P., Lonvaud-Funel, A., and Dubourdieu, D. (2010) Reassessment of phenotypic traits for *Saccharomyces bayanus* var. *uvarum* wine yeast strains. *Int J Food Microbiol* **139**: 79–86.

Matallana, E. and Aranda, A. (2017) Biotechnological impact of stress response on wine yeast. *Lett Appl Microbiol* **64**: 103–110.

Minebois, R., Pérez-Torrado, R., and Querol, A. (2020) A time course metabolism comparison among *Saccharomyces cerevisiae*, *S. uvarum* and *S. kudriavzevii* species in wine fermentation. *Food Microbiol* **90**: 103484.

Molina, A.M., Swiegers, J.H., Varela, C., Pretorius, I.S., and Agosin, E. (2007) Influence of wine fermentation temperature on the synthesis of yeast-derived volatile aroma compounds. *Appl Microbiol Biotechnol* **77**: 675–687.

Moon, H.J., Jeya, M., Kim, I.W., and Lee, J.K. (2010) Biotechnological production of erythritol and its applications. *Appl Microbiol Biotechnol* **86**: 1017–1025.

Motulsky, H. and Christopoulos, A. (2004) Fitting Models to Biological Data Using Linear and Nonlinear Regression. A practical guide to curve fitting. In, *Fitting Models to Biological Data Using Linear and Nonlinear Regression*., pp. 160–165.

Naumov, G.I., Masneuf, I., Naumova, E.S., Aigle, M., and Dubourdieu, D. (2000) Association of *Saccharomyces bayanus* var. *uvarum* with some French wines: Genetic analysis of yeast populations.

Res Microbiol **151**: 683–691.

Oliveira, B.M., Barrio, E., Querol, A., and Pérez-Torrado, R. (2014) Enhanced enzymatic activity of glycerol-3-phosphate dehydrogenase from the cryophilic *Saccharomyces kudriavzevii*. *PLoS One* **9**:.

Panozzo, C., Nawara, M., Suski, C., Kucharczyka, R., Skoneczny, M., Bécam, A.M., et al. (2002) Aerobic and anaerobic NAD+ metabolism in *Saccharomyces cerevisiae*. *FEBS Lett* **517**: 97–102.

Pérez-Torrado, R., Barrio, E., and Querol, A. (2018) Alternative yeasts for winemaking: *Saccharomyces* non-*cerevisiae* and its hybrids. *Crit Rev Food Sci Nutr* **58**: 1780–1790.

Peris, D., Pérez-Torrado, R., Hittinger, C.T., Barrio, E., and Querol, A. (2018) On the origins and industrial applications of *Saccharomyces cerevisiae* × *Saccharomyces kudriavzevii* hybrids. *Yeast* **35**: 51–69.

Peris, D., Pérez-Través, L., Belloch, C., and Querol, A. (2016) Enological characterization of Spanish *Saccharomyces kudriavzevii* strains, one of the closest relatives to parental strains of winemaking and brewing *Saccharomyces cerevisiae* × *S. kudriavzevii* hybrids. *Food Microbiol* **53**: 31–40.

Querol, A., Huerta, T., Barrio, E., and Ramon, D. (1992) Dry Yeast Strain For Use in Fermentation of Alicante Wines: Selection and DNA Patterns. *J Food Sci* **57**: 183–185.

Redón, M., Guillamón, J.M., Mas, A., and Rozès, N. (2011) Effect of growth temperature on yeast lipid composition and alcoholic fermentation at low temperature. *Eur Food Res Technol* **232**: 517–527.

Ribéreau-Gayon, P., Dubourdieu, D., Donèche, B., and Lonvaud, A. (2006) Handbook of Enology: Volume 1, The Microbiology of Wine and Vinifications. *Handb Enol* **1**: 1–441.

Rosenfeld, E. and Beauvoit, B. (2003) Role of the non-respiratory pathways in the utilization of molecular oxygen by *Saccharomyces cerevisiae*. *Yeast* **20**: 1115–1144.

Sampaio, J.P. and Gonçalves, P. (2008) Natural populations of *Saccharomyces kudriavzevii* in Portugal are associated with Oak bark and are sympatric with *S. cerevisiae* and *S. paradoxus*. *Appl Environ Microbiol* **74**: 2144–2152.

Sniegowski, P.D., Dombrowski, P.G., and Fingerman, E. (2002) *Saccharomyces cerevisiae* and *Saccharomyces paradoxus* coexist in a natural woodland site in North America and display different levels of reproductive isolation from European conspecifics. *FEMS Yeast Res* **1**: 299–306.

Stribny, J., Gamero, A., Pérez-Torrado, R., and Querol, A. (2015) *Saccharomyces kudriavzevii* and *Saccharomyces uvarum* differ from *Saccharomyces cerevisiae* during the production of aroma-active higher alcohols and acetate esters using their amino acidic precursors. *Int J Food Microbiol* **205**: 41–46.

Su, Y., Seguinot, P., Sanchez, I., Ortiz-Julien, A., Heras, J.M., Querol, A., et al. (2020) Nitrogen sources preferences of non-*Saccharomyces* yeasts to sustain growth and fermentation under winemaking conditions. *Food Microbiol* **85**:.

Tosi, E., Azzolini, M., Guzzo, F., and Zapparoli, G. (2009) Evidence of different fermentation behaviours of two indigenous strains of *Saccharomyces cerevisiae* and *Saccharomyces uvarum* isolated from Amarone wine. *J Appl Microbiol* **107**: 210–218.

Tronchoni, J., Gamero, A., Arroyo-López, F.N., Barrio, E., and Querol, A. (2009) Differences in the glucose and fructose consumption profiles in diverse *Saccharomyces* wine species and their hybrids during grape juice fermentation. *Int J Food Microbiol* **134**: 237–243.

Tronchoni, J., Medina, V., Guillamón, J.M., Querol, A., Pérez-Torrado,

R. (2014). Transcriptomics of cryophilic *Saccharomyces kudriavzevii* reveals the key role of gene translation efficiency in cold stress adaptations. BMC Genomics. 15:432.

Varela, C., Sengler, F., Solomon, M., and Curtin, C. (2016) Volatile flavour profile of reduced alcohol wines fermented with the non-conventional yeast species *Metschnikowia pulcherrima* and *Saccharomyces uvarum*. *Food Chem* **209**: 57–64.

Vilela-Moura, A., Schuller, D., Mendes-Faia, A., and Côrte-Real, M. (2010) Effects of acetic acid, ethanol, and SO2 on the removal of volatile acidity from acidic wines by two *Saccharomyces cerevisiae* commercial strains. *Appl Microbiol Biotechnol* **87**: 1317–1326.

Vilela-Moura, A., Schuller, D., Mendes-Faia, A., and Côrte-Real, M. (2008) Reduction of volatile acidity of wines by selected yeast strains. *Appl Microbiol Biotechnol* **80**: 881–890.

Vilela-Moura, A., Schuller, D., Mendes-Faia, A., Silva, R.D., Chaves, S.R., Sousa, M.J., and Côrte-Real, M. (2011) The impact of acetate metabolism on yeast fermentative performance and wine quality: Reduction of volatile acidity of grape musts and wines. *Appl Microbiol Biotechnol* **89**: 271–280.

Zwietering, M.H., Jongenburger, I., Rombouts, F.M., and Van't Riet, K. (1990) Modeling of the bacterial growth curve. *Appl Environ Microbiol* **56**: 1875–1881.

CHAPTER 3

A multi-phase multi-objective dynamic genome-scale model shows different redox balancing among yeast species of *Saccharomyces* genus in fermentation

David Henriques[a,*], Romain Minebois[b], Sebastian Mendoza[c], Laura G.Macías[b,d], Roberto Pérez-Torrado[b], Eladio Barrio[b,d], Bas Teusink[c], Amparo Querol[b], Eva Balsa-Canto[a,*]

[a] (Bio)process engineering group, IIM-CSIC, Vigo, Spain

[b] Instituto de Agroquímica y Tecnología de los Alimentos, Paterna, Spain

[c] Systems Bioinformatics, VU Amsterdam, The Netherlands

[d] Department of Genetics, University of Valencia, Burjassot, Spain

*Corresponding authors: davidh@iim.csic.es and ebalsa@iim.csic.es

Accepted in **mSystems**

Abstract

Yeasts constitute over 1500 species with great potential for biotechnology. Still, the yeast *Saccharomyces cerevisiae* dominates industrial applications, and many alternative physiological capabilities of lesser-known yeasts are not being fully exploited. While comparative genomics receives substantial attention, little is known about yeasts' metabolic specificity in batch cultures. Here we propose a multi-phase multi-objective dynamic genome-scale model of yeast batch cultures that describes the uptake of carbon and nitrogen sources and the production of primary and secondary metabolites. The model integrates a specific metabolic reconstruction, based on the consensus Yeast8, and a kinetic model describing the time-varying culture environment. Besides, we proposed a multi-phase multi-objective flux balance analysis to compute the dynamics of intracellular fluxes. We then compared the metabolism of *S. cerevisiae* and *S. uvarum* strains in a rich medium fermentation. The model successfully explained the experimental data and brought novel insights into how cryotolerant strains achieve redox balance. The proposed model (along with the corresponding code) provides a comprehensive picture of the main steps occurring inside the cell during batch cultures and offers a systematic approach to prospect or metabolically engineering novel yeast cell factories.

Chapter 3

1. Introduction

Yeasts have been used to produce fermented foods and beverages for millennia and are among the most frequently used microorganisms in biotechnology. *Saccharomyces cerevisiae* dominates the scene and many research efforts focus on engineering this species for particular applications (e.g., (Nielsen and Keasling, 2016; Q. Liu *et al.*, 2019; Guo *et al.*, 2020) or (Perli *et al.*, 2021)). Nowadays it is used to produce glycerol (Klein *et al.*, 2017), bio-pharmaceutical proteins (Wang *et al.*, 2017), or secondary metabolites, such as aroma or bio-flavours (van Wyk *et al.*, 2018; Liu *et al.*, 2020).

However, yeasts constitute a large group of 1500 (so far) described species and much less attention has been paid to non-conventional yeasts. These species remain a mostly untapped resource of alternative metabolic routes for substrate use and product formation as well as tolerances to specific stressors (Steensels and Verstrepen, 2014; Hittinger *et al.*, 2015). To exploit these alternatives efficiently, it is essential to understand the metabolic pathways of these species. Given the complexity of the endeavor, a modeling approach becomes indispensable.

Genome-scale models (GEMs) can contextualize high-throughput data and predict genotype-environment–phenotype relationships (Oberhardt *et al.*, 2009; Sánchez *et al.*, 2017). While GEMs have been

widely used for the study and metabolic engineering of *S. cerevisiae* strains in continuous (steady-state) fermentations (Lopes and Rocha, 2017), their use to predict batch (dynamic) fermentation is still scarce. Nevertheless, many yeast-based processes operate in batch mode.

In batch operation, cell culture follows a growth curve with the following phases: lag-phase, exponential growth, growth under nutrient limitation, stationary phase, and cellular decay. Available dynamic GEMs of yeast metabolism focus on the exponential phase and explain reasonably well the measured dynamics of biomass growth, carbon sources uptake, and the production of relevant primary metabolites (Hjersted *et al.*, 2007a; Vargas *et al.*, 2011; Sánchez *et al.*, 2014; Saitua *et al.*, 2017). The development of GEMs that describe the five phases of batch processes, considering carbon and nitrogen metabolism throughout time and explaining secondary metabolism, is still required.

In this work, we derived a multi-phase and multi-objective dynamic genome-scale model of batch fermentation, which accounts for carbon and nitrogen metabolism throughout time and explains secondary metabolism. The model required various refinements to succeed: i) a novel metabolic reconstruction, based on an extension of the current consensus genome-scale model of *S. cerevisiae* (Yeast8, (Lu *et al.*, 2019); ii) multi-phase multi-objective implementation of a parsimonious flux balance analysis (pFBA,

(Lewis *et al.*, 2010)) to compute the dynamics of the intracellular fluxes; iii) a model of protein turnover to explain nitrogen homeostasis and iv) a dynamic biomass equation to account for biomass composition variations throughout the process.

As relevant case study we considered the metabolism of *S. cerevisiae* and *S. uvarum* strains in rich medium fermentation. Recent studies revealed that *S. uvarum* strains show interesting physiological properties. *S. uvarum* is more cryotolerant than *S. cerevisiae*, produces more glycerol and less ethanol than *S. cerevisiae* wine strains, and different aroma profiles (Gamero *et al.*, 2013; Alonso-del-Real *et al.*, 2017; Goold *et al.*, 2017; Varela *et al.*, 2017). In addition, traits such as its increased 2-phenylethanol (Tosi *et al.*, 2009; Minebois *et al.*, 2020b) yield could make this species a good candidate for metabolic engineering studies (Wang *et al.*, 2019).

We applied the proposed model to investigate the origin of the phenotypic divergence between species. The model explained the experimental data successfully and revealed differences into how species achieve redox balance. Predicted intracellular fluxes led us to hypothesize that cryotolerant yeast strains can use the GABA shunt as an alternative NADPH source and store reductive power – necessary to subdue oxidative stress under cold conditions – in lipids or other polymers. Additionally, our results are compatible with recent experimental observations showing that most carbon

skeletons used to form higher alcohols (i.e., isoamyl alcohol, isobutanol, and 2-phenylethanol) are synthesized *de novo*.

2. Material and methods

2.1 Yeast strains

In this study, three yeast strains belonging to *S. cerevisiae* and *S. uvarum* species were used: the commercial strain, T73 (Lalvin T73 from Lallemand Montreal, Canada), originally isolated from wine in Alicante, Spain (Querol *et al.*, 1992) was selected as our wine *S. cerevisiae* (ScT73) representative; the commercial strain BMV58 (SuBMV58, Velluto BMV58 from Lallemand Montreal, Canada), originally isolated from wine in Utiel-Requena (Spain) and the non-commercial CECT12600 strain, isolated from a non-fermentative environment (SuCECT12600, Alicante, Spain) were selected as our *S. uvarum* representatives.

2.2 Fermentation experiments

Fermentation assays were performed with grape must obtained from the Merseguera white grapes, collected in the 2015 vintage in Titaguas (Spain) and stored in several small frozen volumes (4 l, -20 °C). Before its use, the must was clarified by sedimentation for 24 h at 4 °C and sterilized by adding dimethyl dicarbonate at 1 $ml.l^{-1}$. All fermentations were performed in three independent biological replicates in 500 ml controlled bioreactors (MiniBio,

Applikon, the Netherlands) filled with 470 ml of natural grape must. Each bioreactor was inoculated using an overnight starter culture cultivated in Erlenmeyer flasks containing 25 ml of YPD medium (2% glucose, 0.5% peptone, 0.5% yeast extract) at 25 °C, 120 rpm in an agitated incubator (Selecta, Barcelona, Spain). Strain inoculation was done at OD600 = 0.100. The dynamics of the fermentation was registered using different probes and detectors to control and measure temperature, pH, dissolved oxygen (Applikon, The Netherlands) and effluent carbon dioxide level (INNOVA 1316 Multi-Gas Monitors, LumaSense Technologies). Data were integrated into the BioExpert software tools (Applikon, The Netherlands). The fermentation was complete when a constant sugar content was reached as measured by HPLC.

2.3 Sampling and quantification of extracellular metabolites

Extracellular metabolites, including sugars, organic acids, main fermentative by-products, and yeast assimilable nitrogen (YAN) were determined at ten sampling times during the fermentation. Residual sugars (glucose, fructose), organic acids (acetate, succinate, citrate, malate and tartrate) and the main fermentative by-products (ethanol, glycerol and 2.3 butanediol) were quantified using HPLC (Thermo Fisher Scientific, Waltham, MA) coupled with refraction index and UV/VIS (210 nm) detectors. Metabolites were separated through a HyperREZ XP Carbohydrate H+ 8 µm column coupled with a HyperREZ XP Carbohydrate Guard (Thermo Fisher Scientific,

Waltham, MA). The analysis conditions were: eluent, 1.5 mM of H2SO4; 0.6 ml.min^{-1} flux and a 50 °C oven temperature. For sucrose determination, the same HPLC was equipped with a Hi-Plex Pb, 300 x 7.7 mm column (Agilent Technologies, CA, USA) and the following analysis conditions were used: eluent, Milli-Q water; 0.6 ml.min^{-1} flux and oven temperature of 50 °C. The retention times of the eluted peaks were compared to those of commercial analytical standards Sigma-Aldrich, Madrid, Spain). Metabolite concentrations were quantified by the calibration graphs (R2 value > 0.99) of the previously obtained standards from a linear curve fit of the peak areas using ten standard mixtures.

Determination of yeast assimilable nitrogen in the form of amino-acids and ammonia was carried out following the same protocol as Su *et al.*, (2020). A volume of supernatant was removed from the fermenter, and amino acids and ammonia separated by UPLC (Dionex Ultimate 3000, Thermo Fisher Scientific, Waltham, MA) equipped with an Accucore C18 150 x 4.6 mm 2.6 µm column (Thermo Fisher Scientific, Waltham, MA) and Accucore C18 10 x 4.6 mm 2.6 µm Defender guards (Thermo Fisher Scientific, Waltham, MA). For derivatization, 400 µl of the sample was mixed with 430 µl borate buffer (1M, pH 10.2), 300 µl absolute methanol and 12 µl of diethyl ethoxymethylenemalonate (DEEMM), and ultra-sonicated for 30 min at 20 °C. The ultra-sonicated sample was incubated up at 80 °C for 2 hours to allow the complete degradation of excess DEEMM. Once the

derivatization finished, the sample was filtered with 0.22 µm filter before injection. The target compounds in the sample were then identified and quantified according to the retention times, UV-vis spectral characteristics and calibration curves (R2 value > 0.99) of the derivatives of the corresponding standards. Amino acid standard (ref. AAS18), asparagine and glutamine purchased from Sigma-Aldrich were used for calibration.

2.4 Higher alcohols and esters

We also determined the concentrations of higher alcohols and esters for each sampling time. Volatile compound extraction and gas chromatography were performed following the protocol of Minebois *et al.*, (2020a). Extraction was performed using headspace solid phase-micro-extraction sampling (SPME) with polydimethylsiloxane (PDMS) fibers (Supelco, Sigma-Aldrich, Barcelona, Spain). Aroma compounds were separated by GC in a Thermo TRACE GC ULTRA chromatograph (Thermo Fisher Scientific, Waltham, MA) equipped with a flame ionization detector (FID), using a HP-INNOWAX 30 m x 0.25 mm capillary column coated with a 0.25 mm layer of cross-linked polyethylene glycol (Agilent Technologies, CA, USA). Helium was the carrier gas used (flow 1 $ml.min^{-1}$). The oven temperature program was: 5 min at 60 °C, 5 $°C.min^{-1}$ to 190 °C, 20 $°C.min^{-1}$ to 250 °C and 2 min at 250 °C. The detector temperature was 280 °C, and the injector temperature was 220 °C under splitless conditions. The internal standard was 2-heptanone (0.05% w/v). Volatile compounds

were identified by the retention time for reference compounds. The quantification of the volatile compounds was determined using the calibration graphs of the corresponding standard volatile compounds.

2.5 Physiological and biomass parameters

Physiological and biomass parameters, including OD600, dry weight (DW), colony forming units (CFUs) and average cell diameter (ACD), were determined at each sample time, providing that the cell sample was sufficient to perform the corresponding measure. DW determination was performed by centrifuging 2 ml of the fresh sample placed in a pre-weighed Eppendorf tube in a MiniSpin centrifuge (Eppendorf, Spain) at maximum speed (13.200 rpm) for 3 min. After centrifugation, the supernatant was carefully removed, the pellet washed with 70% (v/V) ethanol and centrifuged in the same conditions. After washing, the aqueous supernatant was removed carefully, and the tube placed in a 65 °C oven for 72h. DW was finally obtained by measuring the mass weight difference of the tube with a BP121S analytical balance (Sartorius, Goettingen, Germany). OD600 was measured at each sampling time using a diluted volume of sample and a Biophotometer spectrophotometer (Eppendorf, Germany). CFUs were determined using a 100-200 µl of a diluted volume of samples plated in YPD solid medium (2% glucose, 2% agar, 0.5% peptone, 0.5% yeast extract) and incubated two days at 25 °C. The resulting colonies were counted with a Comecta S.A Colony Counter. Only plates with CFUs between 30 and 300 were used to

calculate the CFUs of the original sample. For ACD determination, a volume of cell sample was diluted into a phosphate-buffered saline solution and cell diameter measured using a Scepter Handled Automated Cell Counter equipped with a 40 µm sensor (Millipore, Billerica, USA)

2.5 Orthology analysis and genome-scale metabolic reconstruction

Genomes of ScT73, SuBMV58 and SuCECT12600 were sequenced and assembled in previous works ((Morard *et al.*, 2019); Macías *et al.*, (unpublished)). Genome assemblies were annotated by homology and gene synteny using RATT (Otto *et al.*, 2011). This approach let us transfer the systematic gene names of *S. cerevisiae* S288c annotation (Goffeau *et al.*, 1996) to our assemblies and, therefore, to select only those syntenic orthologous genes in T73, CECT12600 and BMV58 genomes for subsequent analysis. We added to the consensus genome-scale reconstruction of *Saccharomyces cerevisiae* S288C (v.8.3.2) metabolites and reactions related to amino acid degradation and higher-alcohols and esters formation. This refined model was then used as a template for reconstructing strain-specific genome-scale models for SuBMV58, SuCECT12600 and ScT73. MetaDraft, AuReMe and the results from the orthology analysis were used to create the strain-specific models.

2.6 Flux balance analysis

Flux balance analysis (FBA) (Varma and Palsson, 1994; Orth *et*

al., 2010) is a modeling framework based on knowledge of reaction stoichiometry and mass/charge balances. The framework relies on the pseudo steady-state assumption (no intracellular accumulation of metabolites occurs). This is captured by the well-known expression:

$$S \cdot v = 0 \quad (15)$$

where S is stoichiometric matrix of (n metabolites by m reactions) and v is a vector of metabolic fluxes. The number of unknown fluxes is higher than the number of equations and thus the system is undetermined. Still it is possible to find a unique solution under the assumption that cell metabolism evolves to pursue a predetermined goal which is defined as the maximization (or minimization) of a certain objective function (J):

$$\max J \quad (16)$$

$$\text{s. t. :} \qquad (17)$$

$$S \cdot v = 0 \quad (18)$$

$$LB < v < UB \quad (19)$$

where LB and UB correspond to the lower and upper bounds on the estimated fluxes. Examples of objective functions J include growth rate, ATP, or the negative of nutrient consumption, etc.

Typically, multiple optimal solutions exist for a given FBA problem. In parsimonious FBA (pFBA), the result is the most parsimonious of optimal solutions, i.e., the solution that achieves the specific objective with the minimal use of gene products and the minimization of the total flux load (Machado and Herrgård, 2014).

2.7 Parameter estimation

The aim of parameter estimation is to compute the unknown parameters – growth related constants and kinetic parameters - that minimize some measure of the distance between the data and the model predictions. The maximum-likelihood principle yields an appropriate measure of such distance (Walter and Pronzato, 1997):

$$J_{mc}(\boldsymbol{\theta}) = \sum_{k=1}^{n_{exp}} \sum_{j=1}^{n_{obs}} \sum_{i=1}^{n_{st}} \left(\frac{y_{k,j,i}(\boldsymbol{\theta}) - y_{k,j,i}^{m}}{\sigma_{k,j,i}} \right)^{2} \qquad (20)$$

where n_{exp}, n_{obs} and n_{st} are, respectively, the number of experiments, observables (measured quantities), and sampling times while $\sigma_{k,j,i}$ represents the standard deviation of the measured data as obtained from the experimental replicates. y_j^m represents each of the measured quantities, X^m and C^m in our case, and $y_j(\boldsymbol{\theta})$ corresponds to model predicted values, X and C. Observation

functions were included for CFUs and OD600 in order to scale viable cell-mass (X_v) and active cell-mass (X_A), respectively.

Parameters are estimated by solving a nonlinear optimization problem where the aim is to find the unknown parameter values ($\boldsymbol{\theta}$) to minimize $J_{mc}(\boldsymbol{\theta})$, subject to the system dynamics - the model - and parameter bounds (Balsa-Canto *et al.*, 2010).

2.8 Uncertainty analysis

In practice, the value of the parameters $\boldsymbol{\theta}$ compatible with noisy experimental data is not unique, i.e., parameters are affected by some uncertainty (Balsa-Canto *et al.*, 2010). The consequence of significant parametric uncertainty is that it may impact the accuracy of model predictions.

To account for model uncertainty, we used an ensemble approach. To derive the ensemble, we apply the bootstrap smoothing technique, also known as bootstrap aggregation (the Bagging method) (Breiman, 1996; Bühlmann, 2012). The bagging method is a well-established and effective ensemble model/model averaging device that reduces the variability of unstable estimators or classifiers (Bühlmann, 2012). The underlying idea is to consider a family of models with different parameter values $\boldsymbol{\Theta} = [\boldsymbol{\theta}_1 \dots \boldsymbol{\theta}_n]^T$ compatible with the data y^m, when using the model to predict untested experimental setups. The matrix of parameter values $\boldsymbol{\Theta}$ consistent with the data is obtained using *N* realizations of the data

obtained by bootstrap (Efron and Tibshirani, 1993). Each data realization has the same size as the complete data-set, but it is constructed by sampling uniformly from all replicates (3 biological replicates per sampling time). Within each iteration, each replicate has an approximate chance of 37% of being left out, while others might appear several times. The family of solutions **Θ**, is then used to make *N* predictions (dynamic simulations) about a given experimental scenario. The median of the simulated trajectories regards the model prediction, while the distribution of the individual solutions at a given sampling time provides a measure of the uncertainty of the model.

2.9 Analysis of dynamic metabolic fluxes

We selected the most relevant metabolic pathways using a flux ratio, which provides a measure of the net flux over time during growth and stationary phases. In particular, we computed the integral of each flux multiplied by the biomass (mmol·h^{-1}) over time and normalized its value with the accumulated flux of consumed hexoses (glucose and fructose):

$$S_{i,G} = 100 \times \frac{\int_{t_L}^{t_S} v_i(t) \cdot DW(t)}{\int_{t_L}^{t_S} v_{Glx}(t) \cdot DW(t) + \int_{t_L}^{t_S} v_{Fr}(t) \cdot DW(t)} \quad (21)$$

$$S_{i,S} = 100 \times \frac{\int_{t_S}^{t_D} v_i(t) \cdot DW(t)}{\int_{t_S}^{t_D} v_{Glx}(t) \cdot DW(t) + \int_{t_S}^{t_D} v_{Fr}(t) \cdot DW(t)} \quad (22)$$

$$S_{i,O} = 100 \times \frac{\int_{t_0}^{t_F} v_i(t) \cdot DW(t)}{\int_{t_0}^{t_F} v_{Glx}(t) \cdot DW(t) + \int_{t_0}^{t_F} v_{Fr}(t) \cdot DW(t)} \quad (23)$$

where $S_{i,G}$ corresponds to the score of the flux i during growth, $S_{i,S}$ corresponds to the score during the stationary, and $S_{i,D}$ decay phases, $v_i(t)$ (mmol·h^{-1}·DW^{-1}) is the flux under scrutiny, $v_{Glx}(t)$ (mmol·h^{-1}·DW^{-1}) is the flux of glucose, $v_{Fr}(t)$ (mmol·h^{-1}·DW^{-1}) is the flux of fructose, and DW is the predicted dry-weight biomass (g). Results correspond to mmol of produced compound per mmol of consumed hexose x 100 (denoted as mmol/mmolH). Score values indicate the overall impact of each reaction in the net oxidation or reduction of electron carriers during the given phase of the fermentation.

2.10 Numerical tools

To automate the modeling pipeline we used the AMIGO2 toolbox (Balsa-Canto *et al.*, 2016). To solve the dFBA problem we used a variable-step, variable-order Adams-Bashforth-Moulton method to solve the system of ordinary differential equations that describe the dynamics of the extracellular metabolites. At each time step the pFBA problem was solved using the COBRA Toolbox (Schellenberger *et al.*, 2011). The global optimiser Enhanced Scatter Search (eSS, (Egea *et al.*, 2009)) was used to find the optimal parameter values in reasonable computational time.

The ensemble model generation procedure is computationally intensive. However, since each parameter estimation instance in the ensemble is an entirely independent task, we were able to solve this problem in less than a day using 60 CPU cores on a Linux cluster. These tasks were automated with the help of bash scripts and the Open Grid Scheduler. All the scripts necessary to reproduce the results are distributed (https://sites.google.com/site/amigo2toolbox/examples).

3. Results

3.1 The novel metabolic reconstruction

We updated the Yeast8 consensus genome-scale reconstruction of *S. cerevisiae* S288C (v.8.3.1) (Lu *et al.*, 2019) to include 38 metabolites and 50 reactions to explain secondary metabolism (**Table S1**). Furthermore, comprehensive metabolic annotations, such as BO terms and MetaNetX identifiers, were added to the new metabolites and reactions. Among the metabolites added, 13 aroma compounds were included. Noticeably, we found that prior genome-scale reconstructions lacked methionol and tyrosol impeding simulated growth on methionine and tyrosine as sole nitrogen sources, which is known to be possible for several *S. cerevisiae* strains, including S288C.

MetaDraft, AuReMe, and the results from the orthology analysis were used to create strain-specific models for two wine strains *S.*

cerevisiae T73 and *S. uvarum* BMV58 and a strain *S. uvarum* CECT12600 found in non-fermentation environments (further details can be found in **Text S1**). Strains will be denoted as ScT73, SuBMV58 and SuCECT12600 from now on. The three models had 2, 3 and 2 reactions that were not in Yeast8, respectively.

3.2 The multi-phase multi-objective flux balance analysis framework

Our results showed that batch fermentation modeling should be divided into five phases in which cellular objectives and flux constraints need to be modified: lag phase, exponential growth, growth under nitrogen limitation, stationary, and decay (**Figures 1.A-1.B** sketch the modeling approach). Their duration is imposed by the estimated parameters t_L, t_E, t_S and t_D, illustrated in **Figure 1.B**.

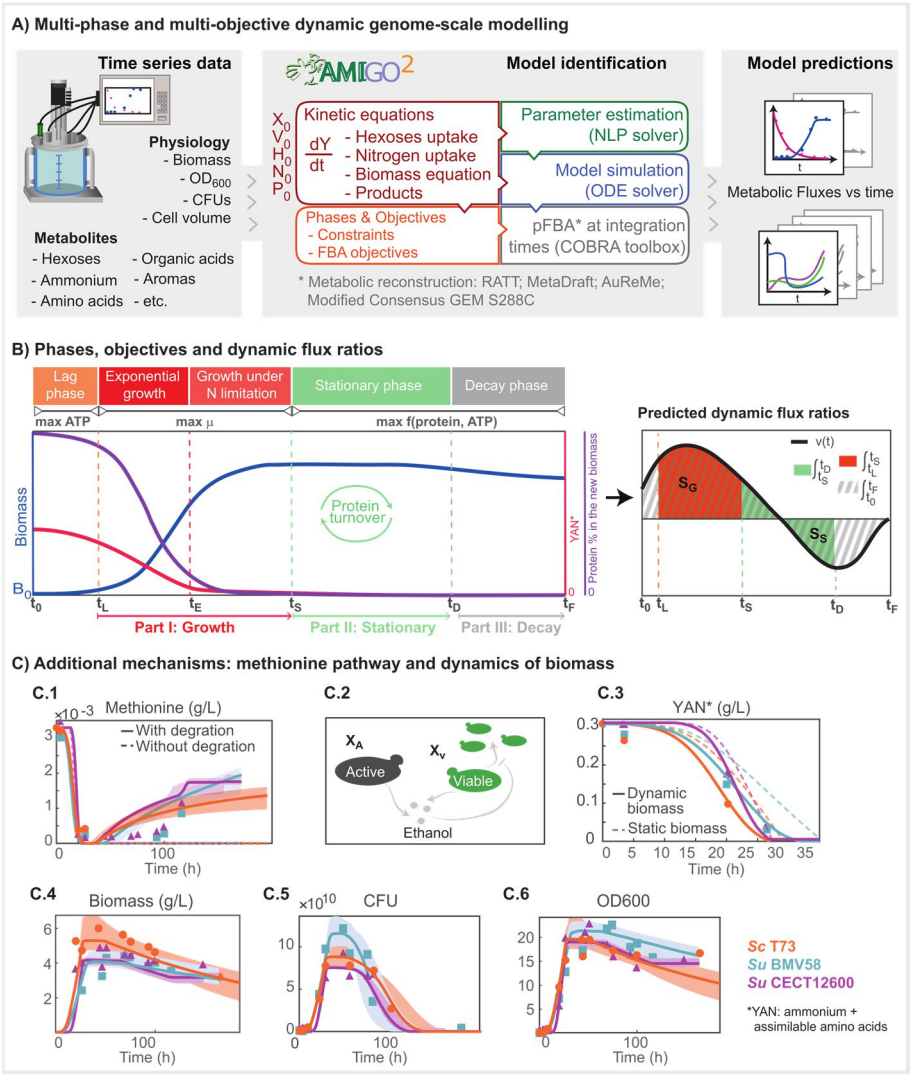

Figure 1. Details on the implementation of the multi-phase and multi-objective dynamic genome-scale model to simulate batch fermentation. A) Implementation, model formulation and solution approach; B) Multi-phase and multi-objective dynamic FBA and methodology to compute dynamic flux rates; the process starts at t0 = 0 and ends at tF, the timing of each phase tL , tE , tS and tD is computed through parameter estimation; C)

Model improvements through additional mechanisms: C1) model prediction vs the experimental dynamics of methionine with and without its degradation pathway, C2) schematic view of active vs viable biomass in the model, C3) YAN consumption prediction with static and dynamic biomass equations, C4-C6) model predictions vs biomass, CFU and OD600 measurements.

Once inoculated, cells encounter new nutrients and undergo a temporary period of non-replication, the lag-phase, during which we assumed that ATP production is maximized. The exponential growth phase covers only the first hours until nitrogen exhaustion. In this phase, cells maximize growth. During growth under nitrogen limitation cells, still maximizing growth, accumulate carbohydrates. Thenceforward, a substantial fraction of the sugar is consumed during the stationary and decay phases by quiescent cells, which adjust their metabolism to cope with environmental fluctuations. In the latter two phases, we assumed cells maximize both ATP and protein production. The general formulation of the FBA problem reads as follows:

$$\begin{aligned} &\textit{Maximize} && J_p \\ &v \\ &\textit{subject to} \\ & && S \cdot v = 0 \end{aligned}$$

$$v_{NH_4} \geq f_{NH_4}(NH_4)$$

$$v_{AA_i} \geq f_{AA}(AA_i);\ \forall\, i\ = 1, \dots, 20$$

$$v_{Glx}\ =\ f_{Glx}(Glx, E)$$

$$v_F = f_F\ (F, E)$$

$$v_{O_2} = f_O\ (O_2)$$

$$v_{P_j} = f_{P_j}\ (v_{Glx}, v_F);\ \forall\, j\ = 1, \dots, 20$$

where J_p is the function to be maximized in each phase p, S is the stoichiometric matrix, v is the vector of fluxes in mmol/(gDWh), v_{Glx} and v_F are the fluxes of glucose and fructose, v_{O_2} is the flux of O_2 present only at the beginning of the fermentation, v_{NH_4} is the flux of ammonium, v_{AA_i} is the exchange rate of the amino acid i (covering all 20 amino acids), v_{P_j} are the constraints associated with the $j = 1, \dots, 20$ fermentation products considered. Glx, F, NH_4, AA_i and P_j correspond to the concentrations of glucose, fructose, ammonium, amino acids, and products, all expressed in (mmol/L). The **Table S2** presents the specific formulation for each phase.

The uptake of glucose and fructose was modelled using Michaelis-Menten (MM) type kinetics with competitive ethanol inhibition (Hjersted *et al.*, 2007b):

$$v_{Glx} = -v_{max_G} \cdot \frac{Glx}{Glx+k_G} \cdot \frac{1}{1+E/K_{Ei}} \quad (1)$$

where v_{max_G} is the maximum uptake rate, k_G is the MM constant, K_{Ei} is the strength of ethanol inhibitory effect and E its concentration (mmol/L). A similar expression v_F exists for fructose (F). Additionally, in our case studies, the media was supplemented with sucrose; thus, we included a mass action type expression, characterized by the kinetic constant k_{hydro}, describing its hydrolysis.

Certain amount of dissolved oxygen is present in the media and consumed during the lag phase (see **Figure S3.B in supplemental Text S2**). Its uptake follows:

$$v_{O_2} = -k_{O_2} \cdot O_2 \quad (2)$$

where v_{O_2} and k_{O_2} are the oxygen uptake and transport rate constants and O_2 the concentration of oxygen in the media.

The uptake of ammonium was modeled by:

$$v_{NH_4} \geq -v_{max_{NH_4}} \cdot \frac{NH_4}{NH_4+k_{NH_4}} \quad (3)$$

where NH_4 is the extracellular concentration of ammonia (mmol/L), $v_{max_{NH_4}}$ is the maximum uptake rate achieved, k_{NH_4} is the MM constant. To avoid an excessive number of parameters, amino acid transport was modeled following mass action kinetics:

$$v_{AA_i} \geq -k_{AA_i} \cdot AA_i \quad (4)$$

where AA_i is the extracellular concentration of the amino acid (mmol/L) and k_{AA_i} is the associated kinetic parameter.

Production of alcohols and higher alcohols, carboxylic acids and esters follows mass action kinetics:

$$\dot{P}_i = X_A \cdot v_{P_i} \quad (5)$$

with X_A the active biomass, and the flux v_{P_i} proportional to the amount of transported hexoses:

$$v_{P_i} = -k_{P_i} \cdot (v_{Glx} + v_F) \quad (6)$$

where P_i refers to the excreted product $i = 1, \ldots, 20$ and k_{P_i} the production rates.

An exception to this was the formulation of the dynamics of acetate. This metabolite is produced during exponential growth and consumed during stationary phase following mass action kinetics.

3.3 The model of protein turnover

Since nitrogen sources are depleted before the stationary phase, we developed a new model of nitrogen homeostasis that considered turnover. The proposed model describes the combined use of the Ehrlich and *de novo* synthesis pathways during stationary and decay phases to guarantee optimal adaptation to perturbations in nitrogen homeostasis.

To introduce protein turnover, we simulated the degradation of the existing protein fraction inside biomass ($Prot$), into a pool of amino acids that subsequently produce new proteins. During stationary and decay phases, the lower bounds on the amino acid uptake are set as:

$$v_{AA_i} \geq -\lambda \cdot Prot \cdot \alpha_{AAi} \quad (7)$$

where λ is the turnover rate, $Prot$ is the concentration of protein and α_{AAi} is associated with the stoichiometric coefficient of the amino acid i in the protein pseudo reaction.

Mathematically, the dynamics of protein content reads:

$$\frac{dProt}{dt} = \mu \cdot X_v \cdot Prot_{content} - Prot \cdot k_{death} + X_A \cdot v_{Prot} - \lambda \cdot Prot \quad (8)$$

where μ is the growth rate, $Prot_{content}$ is the fraction of protein in the newly formed biomass, k_{death} (h^{-1}) is the rate of biomass degradation during decay phase, X_v is the viable biomass (g/L), X_A the simulated active biomass (g/L), v_{Prot} the protein production rate ($g \cdot gDW^{-1} \cdot h^{-1}$) and λ the protein turnover rate (h^{-1}).

The degraded proteins ($\lambda \cdot Prot$) are converted into extracellular amino acids whose concentrations are represented by the following equations:

$$\frac{dAA_i}{dt} = X \cdot v_{AA_i} + \lambda \cdot Prot \cdot \alpha_{AAi} \quad (9)$$

The rates v_{AA_i} are computed by maximizing protein production (v_{Prot}) and ATP (v_{ATP}) while solving the FBA problem:

$$\begin{array}{ll} \textit{Maximize} & v_{Prot}, \varphi \cdot v_{ATP} \\ v & \\ \textit{subject to} & \end{array}$$

$$S \cdot v = 0$$

$$v_{AA_i} < \lambda \cdot Prot \cdot \alpha_{AA}$$

$$v_{Prol} = (v_{Glx} + v_F) \cdot \alpha_{Prol}$$

...

where φ is estimated for each strain, S is the stoichiometric matrix, v is the vector of fluxes, v_{AA_i} is the exchange rate of amino acid AAi, v_{P_i} constraints associated with fermentation products and v_{Prol} (r_1904) is the amount of excreted proline. The later amino acid accumulates in the extracellular media throughout the fermentation (see **Figure S3 in supplemental Text S2**), likely as a consequence of stored arginine consumption in anaerobic conditions (Crépin *et al.*, 2014). The extracellular dynamics of proline is described as follows:

$$\frac{dProl}{dt} = X_A \cdot v_{Prol} \quad (10)$$

Depending on the kinetic constraints, amino acids can be directly incorporated into proteins or degraded to recover nitrogen for protein production. We observed that those amino acids which lacked pathways for their catabolism or elimination, accumulated in the extracellular compartment during stationary phase. As an example, **Figure 1.C1** shows how including a catabolic route for methionine, during stationary phase, successfully describes its

dynamics; possible indicating this route could be active during the stationary phase.

3.4 The dynamic biomass equation

A static biomass equation was not able to explain nitrogen assimilation (**Figure 1.C2**). Therefore we implemented the following dynamic biomass equation (Vargas *et al.*, 2011):

$$Prot_{content} = A \cdot (1 - e^{B \cdot YAN}) \quad (11)$$

where A and B are estimated parameters and YAN accounts for the ammonium and free amino acids present in the medium, excluding proline, which is not catabolized under anaerobic conditions.

Furthermore, we assumed that mRNA level was proportional to the protein content ($mRNA = prot\ /RNA\_to\_Protein\_Ratio$). In this framework, carbohydrates compensate for the variation in protein and mRNA content. Growth-associated ATP maintenance (GAM) was also updated to account for the polymerization costs of the different macromolecules (protein, RNA, DNA and carbohydrates):

$$GAM = GAM_{fitted} + GAM_{Prot} + GAM_{RNA} + GAM_{Carbs} + GAM_{DNA} \quad (12)$$

where GAM_{fitted} is a species or strain-dependent parameter estimated from data and the rest are polymerization costs of the different biomass precursors (adapted from Lu *et al.*, (2019)). Additionally, to represent the premature end of fermentations during the decay phase (observed in SuCECT12600), we estimated the non–growth-associated maintenance ($NGAM$).

In addition, we discriminated between active –able to ferment– and viable cells – able to divide and ferment – to capture the dynamics of CFUs and biomass (**Figure 1.C2**). The dynamics of active cell mass is represented by the equation:

$$\dot{X}_A = \mu \cdot X_v - X_A \cdot k_{decay} + X_A \cdot v_{Prot} - \lambda \cdot Prot \quad (13)$$

where X_A is the active cell mass (g/L), μ is the growth rate computed with pFBA, k_{decay} is the decay rate (only active during decay), v_{Prot} (r_4047) is the exchange flux for production and λ is the turnover rate (both, only active during stationary and decay phases).

The behavior of viable cell mass differed from that of active cell mass by a decline induced by ethanol (Cramer *et al.*, 2002):

$$\dot{X}_v = \dot{X}_A - X_v \cdot k_{Edeath} \cdot \frac{E^n}{E^n + k^n} \quad (14)$$

where X_v (g/L) is the growth rate obtained with the constraint-based model, E is the ethanol concentration (mmol/L) and k_{Edeath} , n and k are the parameters controlling susceptibility to ethanol.

The former mechanisms, coupled to parameter estimation, allowed us to predict nitrogen consumption, CFUs and biomass dynamics accurately (**Figures 1.C3-C6**).

3.5 Goodness-of-fit of the model in case studies

The final model consisted of 46 ordinary differential equations depending on 66 parameters which we estimated from time-series data for all measured external metabolites and biomass. The mean standard deviation on the parameters ranges from 2.5% for SuCECT12600 and a 12.6% for SuBMV58. The reasonably low distribution on the parameters resulted in a reasonably low uncertainty associated with the model simulations (as seen in **Figures 3-4**).

The model described the dynamics of our illustrative examples successfully. The best fit to the data plus the associated uncertainty, as computed by the bootstrap, are shown in **supplemental Text S2** and **Figures 3 and 4**. We determined the R-squared measure of goodness of fit (R^2) for each measured variable and each strain-based fermentation. The median of the R^2 values are above 0.94 for all strains.

Interested readers may find further details on the parameter estimation in **supplemental Text 2**. Optimal parameter values and R^2 values are reported in **Table S3**.

3.6 Species behavior differs significantly in the stationary phase

At the extracellular level, the most striking differences between strains occur in the production of compounds associated with the central carbon metabolism and nitrogen metabolism. In particular, in the dynamics of acetate and the yields of succinate, 2,3-butanediol and glycerol (**Figures 3.C-D,F-G**) and in the production of 2-phenylethanol and isoamyl alcohol (**Figures 4.B,4.D**). We used the model to decipher the metabolic strategies used by the different strains that lead to such differences. The supplemental Table S4 reports the dynamic flux ratios computed for the overall process and the different phases using expressions (21)-(23) for those reactions in which the maximum flux ratio value over the three species is above 0.01 mmol/mmolH. Uncertainties associated to the fluxes due to uncertainties on the parameters are also reported. **Supplemental Text S3** summarizes the differences observed in flux ratios between species and phases. Again the intracellular behavior differs significantly in the stationary phase. Thus subsequent sections elaborate on the metabolic study of the stationary phase. Remarkably this is also the phase in which higher alcohols and aromas are produced thus being relevant for industrial applications.

Synonyms (PubChem) :
DHAP: dihydroxyacetone phosphate; G3P: glycerol 3-phosphate; Isobutanal: isobutyraldehyde; PAL: phenylacetaldehyde;
PEA: 2-phenylethanol; PGLY: 3-phosphonato-D-glycerate(3-); RGP: L-gamma-glutamyl phosphate; DMV: (2R,3R)-2,3-dihydroxy-3-methylpentanoate
(R)-2,3-Dihydroxy-isovalerate: (R)-2,3-dihydroxy-3-methylbutanoate; HMG-CoA: 3-hydroxy-3-methylglutaryl-CoA; G6P: D-glucose 6-phosphate
4-P-L-aspartate:4-phospho-L-aspartate; Rbl5P: D-ribulose 5-phosphate; 6-Pgdl: 6-O-phosphono-D-glucono-1,5-lactone;

Figure 2. (See on left page) Comparative study of the fluxes through the reactions consuming and producing NADH and NADPH at the stationary phase. Figure illustrates how strains achieve redox balance. The most significant differences between strains are found at the level of the TCA cycle, the GABA shunt, the pentose phosphate pathway, the biosynthesis of aromatic amino acids which eventually lead to produce 2-phenylethanol (PEA) and the Ehrlich pathway toward producing isoamylol. It is also important to note that *S. uvarum* diverts flux to the production of mevalonate.

3.7 The GABA shunt as an NADPH source in cryotolerant species

Cells produced the most significant fraction of succinate during the stationary and decay phases, with a significantly higher dynamic flux ratio by SuBMV58 and SuCECT1600 (6.08 and 1.66) than ScT73 (0.42, r_2057). During the decay phase, most succinate was produced through the TCA cycle reductive branch in the two species. However, during the stationary phase, succinate production was distributed between the GABA shunt (ScT73: 0.42, SuBMV58: 2.00, SuCECT12600: 1.31; r_1023, **Figure 3.H**) and the reductive branch of TCA (ScT73: 0.00, SuBMV58: 4.10 and SuCECT12600: 0.35; r_1000, **Figure 3.H**). Remarkably, succinate production through the GABA shunt was between 3 and 4.6 times higher for *S. uvarum* species than for *S. cerevisiae* (**Figure 3.H**, r_0068, r_1023). This result suggested an important role of the GABA shunt in the maintenance of the cellular redox state. Incidentally, revisiting data from López-Malo *et*

al., (2013) we found a considerable accumulation of GABA (93.59 fold-change) by SuCECT12600 (**supplemental Table S4**).

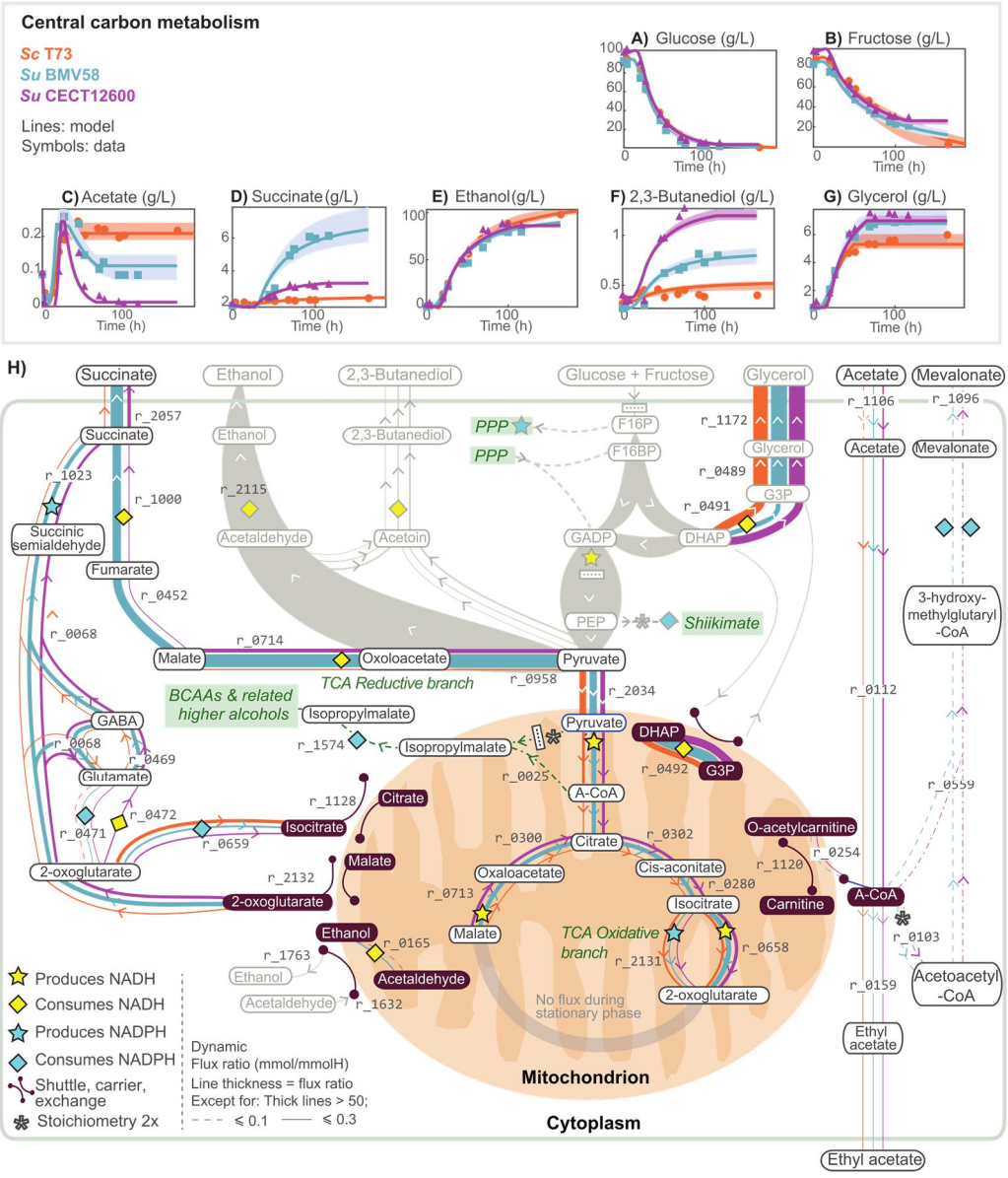

Figure 3. Redox balance in Central Carbon Metabolism. Figures A) to F) show model predictions vs the experimental data extracellular metabolite concentrations associated with glycolysis and central carbon metabolism for the three strains. Figure H) presents the predicted intracellular dynamic flux ratios during the stationary phase, showing how S. uvarum and S. cerevisiae strains use different redox balance strategies. These differences result in the differential production of relevant external metabolites such as acetate (C), succinate (D), ethanol (E), 2,3-butanediol (F) or glycerol (G). Explicit differences in the pathways in gray are presented in Text S3; otherwise, as indicated in the legend, width of the lines is proportional to the dynamic flux ratio.

3.8 Intracellular mevalonate as a reducing equivalent in cryotolerant yeast species

The three strains produced acetate during the growth phase (ScT73: 1.079, SuBMV58:1.145, SuCECT12600: 1.422; **Table S4**, r_1106) and until the entry into the stationary phase. Afterward, while extracellular acetate concentration remained constant in ScT73, a decrease was observed in both *S. uvarum* fermentations, indicating acetate consumption. As shown in **Figure 3.C**, our model successfully described these phenotypes. According to the modeling constraints, the most parsimonious explanation for this observation would have been an operative glyoxylate cycle. However, based on the repression by glucose of the key enzymes of the glyoxylate cycle (i.e. *ICL1* and *MLS1*) and previous intracellular data (López-Malo *et al.*, 2013), we decided to block this cycle and explore an alternative

hypothesis. As a result, the model suggested that *S. uvarum* strains incorporated the acetate derivative, acetyl-CoA, into mevalonate (SuBMV58: 0.19 and SuCECT12600: 0.10; r_0559, r_0103) also consuming NADPH. In addition, mevalonate is a reducing equivalent that can be further metabolized into, for example, ergosterol (r_0127 in our reconstruction) possibly acting as storage of NADPH in cryotolerant species.

S. uvarum strains also used the carnitine shuttle system to transport acetyl-CoA into the mitochondria (SuBMV58: 0.09 and SuCECT12600: 0.38; **Figure 3.H**, r_0254). Inside the mitochondria, acetyl-CoA was used to form isopropylmalate (**Figure 4.A**) – a precursor of leucine and isoamyl alcohol - or in the TCA oxidative branch towards the synthesis of 2-oxoglutarate (**Figure 3.H**).

Figure 4 (see on next page). Redox balance in higher alcohol production: Figure A) shows the predicted intracellular flux ratios (above 0.01 mmol/mmolH) related to higher alcohols 2- phenylethanol (PEA), isobutanol and isoamyl alcohol during the stationary phase and their corresponding impact on the redox co-factors balance NADPH/NADP+ and NADH/NAD+. Figures B-D correspond to the comparison between model predictions and raw measures of PEA, isobutanol and isoamyl alcohol, respectively. Other higher alcohols such as methionol and tyrosol, seemed to accumulate in minimal quantities (flux ratio x 100 $\simeq$ 0.001) in response to perturbations in the amino acid pool. Remarkably, the flux ratios corresponding to the degradation of amino acids are well below 0.01.

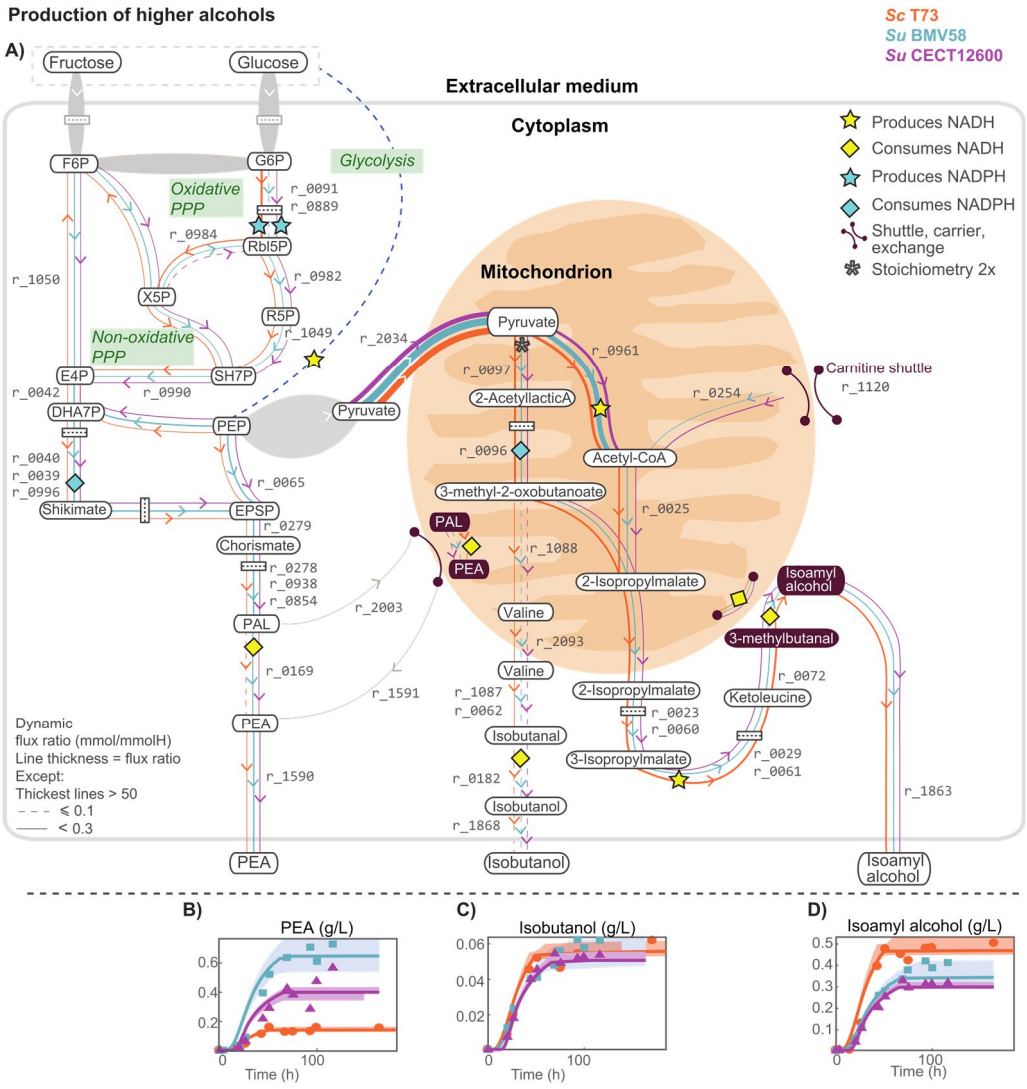

3.9 The production of higher alcohols contributed to the redox balance

Higher alcohol production was most prominent during the stationary phase for the three strains. Our model predicted that

carbon skeletons of isoamyl alcohol, 2-phenylethanol (PEA) and isobutanol were in great part synthesized de novo from glycolytic and pentose phosphate pathway intermediates, rather than coming from the catabolism of precursor amino acids (leucine, valine and phenylalanine respectively) (**Figure 4.A**). *S. uvarum* strains produced more PEA than ScT73 strain (ScT73: 0.158, SuBMV58: 0.659, SuCECT12600: 0.383; r_1590) while the opposite occurs for isoamyl alcohol (ScT73: 0.736, SuBMV58: 0.483, SuCECT12600: 0.394; r_1863). We found that the production of PEA and isoamyl alcohol contributed substantially to the redox metabolism related to glycerol accumulation. Approximately 43%, 36% and 27% of the glycerol produced by the ScT73, SuBMV58 and SuCECT12600 strains, was attributable to NADH derived from isoamyl alcohol and PEA.

The higher production of PEA observed in *S. uvarum* strains occurs through to the higher flux through the shikimate pathway (**Figure 4.A**, r_0996, r_0279). Interestingly, while ScT73 had a larger flux ratio through the oxidative pentose phosphate pathway (PPP, **Figure 4.A**, r_0091, r_0889) partly redirected toward glycolysis, *S. uvarum* simulations reflected the inverse pattern (Figure 4.A, r_0984), with glycolytic flux being shifted towards the non-oxidative PPP. Pyruvate in the mitochondrion showed two different fates: acetyl-CoA (r _0961) and 2-acetyllactic acid (r_0097). Noticeably, *S. uvarum* strains also contributed to acetyl-CoA using the carnitine shuttle (r_0254). 2-acetyllactic acid can further be converted to 3-methyl-2-

oxobutanoate, consuming one NADPH (r_0096), which also showed two different fates: the production of 2-isopropylmalate (leading to isoamyl alcohol; r_0025, r_0072, r_0179); or valine (leading to the synthesis of isobutanol via the Ehrlich pathway r_1087, r_0062, r_0182). Production of PEA and isoamyl alcohol also affected NADP+/NADPH metabolism. While the GABA shunt and oxidative PPP were the main producers of NADPH, consumption of NADPH was attributable mostly to isoamyl alcohol and PEA. In fact, the increased isocitrate dehydrogenase flux (r_0659) observed in ScT73 (1.646 against 0.917 and 0.727 in the *S. uvarum* strains) were associated with the need for shuttling NADPH into the mitochondria (r_2131), utilized in 3-methyl-2-oxobutanoate synthesis (precursor of the isoamyl alcohol; see **Figures 3.H** and **4.A**). On the other hand, production of PEA without the oxidative PPP (predicted in the *S. uvarum* strains), resulted in excess NADP+. In the case of *S. uvarum*, given the reduced influence of oxidative PPP, NADP+ recycling was achieved mostly through the GABA shunt.

4. Discussion

Genome scale models have the potential to decipher how non-conventional yeast species use metabolism to produce industrially relevant products and tolerate specific stressors, such as cold temperatures. This study aimed to develop a dynamic genome-scale model to investigate the dynamics of yeasts primary and secondary

metabolism in batch cultures. To generate biological hypotheses for modeling, we considered the description of the metabolism of *S. cerevisiae* and cryotolerant *S. uvarum* strains in a rich medium (grape must) fermentation.

The first question in this research was how to model all phases in the batch process: lag, exponential growth, limited nitrogen growth, stationary and decay. Prior studies focused on the exponential growth phase and were based on available reconstructions with many missing reactions, particularly those related to secondary metabolism (Hjersted *et al.*, 2007b; Vargas *et al.*, 2011; Vázquez-Lima *et al.*, 2014; Saitua *et al.*, 2017). Also, their static nature hinders the description of the sequential nature of amino acid consumption (Crépin *et al.*, 2012).

As a first step, we needed to extend a yeast genome-scale reconstruction to account for the production of higher alcohols, carboxylic acids or esters. We extended the Yeast8 consensus model incorporating missing reactions and metabolites. A similar curation process has been recently applied to the iMM904 reconstruction (Scott *et al.*, 2020). The authors fitted the model to data from the literature concluding that further curation and adaptations were necessary to successfully predict metabolism and biomass dynamics. We experienced such difficulties in our first iterations in the modeling process and introduced several new features to obtain more accurate simulations of carbon and nitrogen metabolism throughout time.

A critical aspect for an improved accuracy was the multi-phase multi-objective dynamic FBA scheme. Previous works focused on ATP consumption to explain the metabolism after depletion of the limiting nutrient (Raghunathan *et al.*, 2006; Pizarro *et al.*, 2007; Vargas *et al.*, 2011), we incorporated the production of protein as a cellular objective (together with protein degradation) with accurate results. Also, we modeled protein turnover to account for the uptake of amino acids and inorganic nitrogen in the stationary phase. To the best of our knowledge, this is the first dynamic genome-scale metabolic model describing nitrogen homeostasis during the stationary phase. Finally, we introduced a dynamic biomass equation which further improved the model accuracy. This result agrees with observations by previous studies (Schulze *et al.*, 1996; Varela *et al.*, 2004; Dikicioglu *et al.*, 2015) pointing out the relevance of detailing biomass composition in a context-specific manner.

The second question in this research was to decipher the differences in the metabolism of three strains of two different species, *S. cerevisiae* and *S. uvarum*, in rich medium (grape must) fermentation. Recently, Minebois *et al.* (2020a) hypothesized that *S. cerevisiae* and *S. uvarum* species might have different redox balance strategies. Notably, the model confirmed this hypothesis and brought novel insights into the specific routes used by the two species.

Our predictions suggest alternative pathways for cryotolerant species to produce succinate and consume acetate. In principle, yeasts might

form succinate via four main pathways, all based on the reactions of the TCA cycle (Coulter *et al.*, 2005). Selected pathway depends on the environmental conditions and strain. Our model predicted that ScT73 and SuBMW58 produced overall the most succinate via the TCA reductive branch, in agreement with Camarasa *et al.* (2003). However, our results also suggest an important role of the TCA oxidative branch until 2-oxoglutarate for the *S. uvarum* strains during the stationary phase. This result is consistent with the recent intracellular data obtained by Minebois *et al.* (2020b) who observed a noticeable intracellular accumulation of 2-oxoglutarate in SuBMV58.

One somewhat unexpected finding of the model was the extent to which the GABA shunt would contribute to succinate formation during the stationary phase, an effect particularly evident in the case of *S. uvarum* strains. The role of this pathway is not fully understood in yeast (Bach *et al.*, 2009; Cao *et al.*, 2013; Mara *et al.*, 2018). Bach *et al.* (2009) observed that glutamate decarboxylase (*GAD1*) was poorly expressed when succinate was produced in *S. cerevisiae* and that the GABA shunt played a minor role in redox metabolism. On the contrary,(Coleman *et al.* (2001) showed that *GAD1* expression is required for oxidative stress tolerance in *S. cerevisiae*. Similarly, (Cao *et al.*, 2013) showed that *GAD1* confers resistance to heat stress effect that might be related to NADPH production. Additionally, *GAD1* was up-regulated during the stationary phase under nitrogen starvation (Rossignol *et al.*, 2003; Bach *et al.*, 2009; Mara *et al.*,

2018); and (López-Malo *et al.*, 2013) observed high intracellular GABA levels in cryotolerant species *S. uvarum*.

Recently, H. Liu *et al.* (2019) found clear indication that the GABA shunt may be involved in supplying NADPH for lipid synthesis in the oleaginous yeast *Yarrowia lipolytica*. Also, Bach *et al.* (2009) showed that *S. cerevisiae* can degrade GABA into succinate or γ-Hydroxybutyric acid (GHB) and that GHB was used to form the polymer polyhydroxybutyrate (PHB). Also noteworthy is that PHBs are synthesized by numerous bacteria as carbon and energy storage compounds (Możejko-Ciesielska and Kiewisz, 2016). PHBs are also strongly associated with bacterial cold tolerance (Müller-Santos *et al.*, 2021) suggesting a similar function in yeast.

Another important finding is that *S. uvarum* strains consume acetate once nitrogen sources are depleted, coinciding with the extracellular accumulation of succinate. This finding was also reported by Kelly *et al.* (2020), who showed that a *S. uvarum* yeast isolate can metabolize acetate to significantly lower acetic acid, ethyl acetate, and acetaldehyde in wine. The model predicted that some of the acetate carbon was directed toward mevalonate, which is in line with recent experimental work by Minebois *et al.* (2020b). According to Bach *et al.* (2009), a route for acetyl-CoA incorporation into PHB polyester through 3-hydroxybutyrate-CoA seems plausible. However, this hypothesis is not taken into account by the genome-scale reconstructions. The fact that López-Malo *et al.*(2013) found high

intracellular GABA and GHB in cryotolerant strains grown in synthetic must (without GABA) at low-temperature, and the flux predicted in the present work, suggest that *S. uvarum* stores lipids or polyesters (i.e., PHBs) as reducing equivalents to withstand oxidative stress induced by low temperatures. The role of the GABA shunt and the production of reducing equivalents in the metabolism of cryotolerant species may be plausible routes worth exploring.

Our model also predicted that the carbon skeletons of higher alcohols (e.g., isobutanol and isoamyl alcohol) were mainly synthesized de novo rather than from the incorporation and catabolism of amino acids (e.g., leucine and valine). This result agrees with the findings of Crépin *et al.* (2017) who explored the fate of the carbon backbones of aroma-related exogenous amino acids using ^{13}C isotopic tracer experiments. Similarly, our results indicate that 2-phenylethanol was mostly synthesized *de novo*. We hypothesize that a positive contribution in glycerol content may also explain why the production of 2-phenylethanol and isoamyl alcohol is a conserved evolutionary trait in yeasts.

Noticeably, most of NADPH consumption was associated with higher alcohol synthesis. The increased flux through cytosolic isocitrate dehydrogenase associated with isoamyl alcohol, is compatible with reports associating high expression of *IDP2* with nitrogen deficiency (Mendes-Ferreira *et al.*, 2007) and stationary phase (Martinez *et al.*, 2004). Furthermore, the prediction that, during the stationary phase,

PEA produced through the chorismate synthesis path way (downstream of the non-oxidative PPP), thus regenerating some NADPH associated with the conversion of succinic semi-aldehyde into succinate, provides a counter-intuitive rationale for understanding the correlation between the observed differences in higher alcohol and succinate production between *S. cerevisiae* and *S. uvarum*.

Interestingly, the model predicts that most other higher alcohols (tyrosol, methionol, etc.) accumulate in small amounts due to perturbations in the amino acid pool. These results confirm the hypothesis raised by Shopska *et al.* (2019) who suggested that the two schemes to produce higher alcohols – Ehrlich and *de novo* synthesis – are not in contradiction but two extremes of a common mechanism. Incidentally, Yuan *et al.* (2017) showed that the assembled leucine biosynthetic pathway coupled with the Ehrlich degradation pathway results in high-level production of isoamyl alcohol.

5. Conclusion

Our bootstrap based identifiability analysis of the proposed model and the fact that model predictions are consistent with numerous previous findings lead us to conclude that the present model (along with the provided code) can simulate yeast metabolism in batch culture in a general chemically characterized medium; the only requirement would be to update the metabolic reconstruction if

required for the specific yeast species. The model can also be used to explore and engineering novel metabolic pathways towards specific bio-products.

Acknowledgments

This project has received funding from MCIU/AEI/FEDER, UE (grant references: RTI2018-093744-B-C31, RTI2018-093744-B-C32, RTI2018-093744-B-C33 and PID2019-104113RB-I00) and Xunta de Galicia (IN607B 2020/03). RM was supported by an FPI grant from the Ministerio de Economía y Competitividad, Spain (ref. BES-2016-078202). SNM acknowledges funding from CONICYT Becas Chile grant 72180373. SNM and BT acknowledge support from YogurtDesign, EraCoBioTech grant 053.80.733.

Supplementary files

Supplementary files can found at **page 359** of this manuscript.

References

Alonso-del-Real, J., Lairón-Peris, M., Barrio, E., and Querol, A. (2017) Effect of temperature on the prevalence of *Saccharomyces* non *cerevisiae* species against a *S. cerevisiae* wine strain in wine fermentation: competition, physiological fitness, and influence in final wine composition. *Front Microbiol* **8**:.

Bach, B., Sauvage, F.-X., Dequin, S., and Camarasa, C. (2009) Role of γ-Aminobutyric acid as a source of nitrogen and succinate in Wine. *Am J Enol Vitic* **60**: 508 LP – 516.

Balsa-Canto, E., Alonso, A.A., and Banga, J.R. (2010) An iterative identification procedure for dynamic modeling of biochemical networks. *BMC Syst Biol* **4**:.

Balsa-Canto, E., Henriques, D., Gábor, A., and Banga, J.R. (2016) AMIGO2, a toolbox for dynamic modeling, optimization and control in systems biology. *Bioinformatics* **32**: 3357–3359.

Breiman, L. (1996) Bagging predictors. *Mach Learn* **24**: 123–140.

Bühlmann, P. (2012) Bagging, Boosting and Ensemble Methods. In, *Handbook of Computational Statistics*. Springer Berlin Heidelberg, pp. 985–1022.

Camarasa, C., Grivet, J.P., and Dequin, S. (2003) Investigation by 13C-NMR and tricarboxylic acid (TCA) deletion mutant analysis of pathways of succinate formation in *Saccharomyces cerevisiae* during anaerobic fermentation. *Microbiology* **149**: 2669–2678.

Cao, J., Barbosa, J.M., Singh, N., and Locy, R.D. (2013) GABA transaminases from *Saccharomyces cerevisiae* and *Arabidopsis thaliana* complement function in cytosol and mitochondria. *Yeast* **30**: 279–289.

Coleman, S.T., Fang, T.K., Rovinsky, S.A., Turano, F.J., and Moye-Rowley, W.S. (2001) Expression of a glutamate decarboxylase homologue is required for normal oxidative stress tolerance in *Saccharomyces cerevisiae*. *J Biol Chem* **276**: 244–250.

Coulter, A.D., Godden, P.W., and Pretorius, I.S. (2005) Succinic acid - How it is formed, what is its effect on titratable acidity, and what factors influence its concentration in wine? *Aust New Zeal Wine Ind J* **19**: 16–25.

Cramer, A.C., Vlassides, S., and Block, D.E. (2002) Kinetic model for nitrogen-limited wine fermentations. *Biotechnol Bioeng* **77**: 49–60.

Crépin, L., Nidelet, T., Sanchez, I., Dequin, S., and Camarasa, C. (2012) Sequential use of nitrogen compounds by *Saccharomyces*

cerevisiae during wine fermentation: A model based on kinetic and regulation characteristics of nitrogen permeases. *Appl Environ Microbiol* **78**: 8102–8111.

Crépin, L., Sanchez, I., Nidelet, T., Dequin, S., and Camarasa, C. (2014) Efficient ammonium uptake and mobilization of vacuolar arginine by *Saccharomyces cerevisiae* wine strains during wine fermentation. *Microb Cell Fact* **13**: 109.

Crépin, L., Truong, N.M., Bloem, A., Sanchez, I., Dequin, S., and Camarasa, C. (2017) Management of multiple nitrogen sources during wine fermentation by *Saccharomyces cerevisiae*. *Appl Environ Microbiol* **83**:.

Dikicioglu, D., Kırdar, B., and Oliver, S.G. (2015) Biomass composition: the “elephant in the room” of metabolic modelling. *Metabolomics* **11**: 1690–1701.

Efron, B. and Tibshirani, R.J. (1993) An introduction to the bootstrap. *Monogr Stat Appl Probab* **57**: 1–436.

Egea, J.A., Vazquez, E., Banga, J.R., and Martí, R. (2009) Improved scatter search for the global optimization of computationally expensive dynamic models. *J Glob Optim* **43**: 175–190.

Gamero, A., Tronchoni, J., Querol, A., and Belloch, C. (2013) Production of aroma compounds by cryotolerant *Saccharomyces* species and hybrids at low and moderate fermentation temperatures. *J Appl Microbiol* **114**: 1405–1414.

Goffeau, A., Barrell, G., Bussey, H., Davis, R.W., Dujon, B., Feldmann, H., et al. (1996) Life with 6000 genes. *Science (80-)* **274**: 546–567.

Goold, H.D., Kroukamp, H., Williams, T.C., Paulsen, I.T., Varela, C., and Pretorius, I.S. (2017) Yeast’s balancing act between ethanol and glycerol production in low-alcohol wines. *Microb Biotechnol* **10**: 264–278.

Guo, W., Huang, Q., Feng, Y., Tan, T., Niu, S., Hou, S., et al. (2020)

Rewiring central carbon metabolism for tyrosol and salidroside production in *Saccharomyces cerevisiae*. *Biotechnol Bioeng* **117**: 2410–2419.

Hittinger, C.T., Rokas, A., Bai, F.Y., Boekhout, T., Gonçalves, P., Jeffries, T.W., et al. (2015) Genomics and the making of yeast biodiversity. *Curr Opin Genet Dev* **35**: 100–109.

Hjersted, J.L., Henson, M.A., and Mahadevan, R. (2007a) Genome-scale analysis of *Saccharomyces cerevisiae* metabolism and ethanol production in fed-batch culture. *Biotechnol Bioeng* **97**: 1190–1204.

Hjersted, J.L., Henson, M.A., and Mahadevan, R. (2007b) Genome-scale analysis of *Saccharomyces cerevisiae* metabolism and ethanol production in fed-batch culture. *Biotechnol Bioeng* **97**: 1190–1204.

Kelly, J.M., van Dyk, S.A., Dowling, L.K., Pickering, G.J., Kemp, B., and Inglis, D.L. (2020) *Saccharomyces uvarum* yeast isolate consumes acetic acid during fermentation of high sugar juice and juice with high starting volatile acidity. *Oeno One* **54**: 199–211.

Klein, M., Swinnen, S., Thevelein, J.M., and Nevoigt, E. (2017) Glycerol metabolism and transport in yeast and fungi: established knowledge and ambiguities. *Environ Microbiol* **19**: 878–893.

Lewis, N.E., Hixson, K.K., Conrad, T.M., Lerman, J.A., Charusanti, P., Polpitiya, A.D., et al. (2010) Omic data from evolved E. coli are consistent with computed optimal growth from genome-scale models. *Mol Syst Biol* **6**: 390.

Liu, H., Marsafari, M., Deng, L., and Xu, P. (2019) Understanding lipogenesis by dynamically profiling transcriptional activity of lipogenic promoters in *Yarrowia lipolytica*. *Appl Microbiol Biotechnol* **103**: 3167–3179.

Liu, Q., Liu, Y., Chen, Y., and Nielsen, J. (2020) Current state of aromatics production using yeast: achievements and challenges.

Curr Opin Biotechnol **65**: 65–74.

Liu, Q., Yu, T., Li, X., Chen, Y., Campbell, K., Nielsen, J., and Chen, Y. (2019) Rewiring carbon metabolism in yeast for high level production of aromatic chemicals. *Nat Commun* **10**: 1–13.

Lopes, H. and Rocha, I. (2017) Genome-scale modeling of yeast: chronology, applications and critical perspectives. *FEMS Yeast Res* **17**: 1–14.

López-Malo, M., Querol, A., and Guillamon, J.M. (2013) Metabolomic comparison of *Saccharomyces cerevisiae* and the cryotolerant species *S. bayanus* var. *uvarum* and *S. kudriavzevii* during Wine Fermentation at Low Temperature. *PLoS One* **8**:.

Lu, H., Li, F., Sánchez, B.J., Zhu, Z., Li, G., Domenzain, I., et al. (2019) A consensus *S. cerevisiae* metabolic model Yeast8 and its ecosystem for comprehensively probing cellular metabolism. *Nat Commun* **10**:.

Machado, D. and Herrgård, M. (2014) Systematic Evaluation of Methods for Integration of transcriptomic data into constraint-based models of metabolism. *PLoS Comput Biol* **10**: 1003580.

Mara, P., Fragiadakis, G.S., Gkountromichos, F., and Alexandraki, D. (2018) The pleiotropic effects of the glutamate dehydrogenase (GDH) pathway in *Saccharomyces cerevisiae*. *Microb Cell Fact* **17**: 170.

Martinez, M.J., Roy, S., Archuletta, A.B., Wentzell, P.D., Santa Anna-Arriola, S., Rodriguez, A.L., et al. (2004) Genomic analysis of stationary-phase and exit in *Saccharomyces cerevisiae*: Gene expression and identification of novel essential genes. *Mol Biol Cell* **15**: 5295–5305.

Mendes-Ferreira, A., Del Olmo, M., García-Martínez, J., Jiménez-Martí, E., Leão, C., Mendes-Faia, A., and Pérez-Ortín, J.E. (2007) *Saccharomyces cerevisiae* signature genes for predicting nitrogen deficiency during alcoholic fermentation. *Appl Environ Microbiol* **73**: 5363–5369.

Minebois, R., Pérez-Torrado, R., and Querol, A. (2020a) A time course metabolism comparison among *Saccharomyces cerevisiae*, *S. uvarum* and *S. kudriavzevii* species in wine fermentation. *Food Microbiol* **90**: 103484.

Minebois, R., Pérez-Torrado, R., and Querol, A. (2020b) Metabolome segregation of four strains of *Saccharomyces cerevisiae*, *S. uvarum* and *S. kudriavzevii* conducted under low temperature oenological conditions. *Environ Microbiol* 1462-2920.15135.

Morard, M., Macías, L.G., Adam, A.C., Lairón-Peris, M., Pérez-Torrado, R., Toft, C., and Barrio, E. (2019) Aneuploidy and Ethanol Tolerance in *Saccharomyces cerevisiae*. *Front Genet* **10**:.

Możejko-Ciesielska, J. and Kiewisz, R. (2016) Bacterial polyhydroxyalkanoates: Still fabulous? *Microbiol Res* **192**: 271–282.

Müller-Santos, M., Koskimäki, J.J., Alves, L.P.S., de Souza, E.M., Jendrossek, D., and Pirttilä, A.M. (2021) The protective role of PHB and its degradation products against stress situations in bacteria. *FEMS Microbiol Rev* **45**:.

Nielsen, J. and Keasling, J.D. (2016) Engineering Cellular Metabolism. *Cell* **164**: 1185–1197.

Oberhardt, M.A., Palsson, B., and Papin, J.A. (2009) Applications of genome-scale metabolic reconstructions. *Mol Syst Biol* **5**: 320.

Orth, J.D., Thiele, I., and Palsson, B.O. (2010) What is flux balance analysis? *Nat Biotechnol* **28**: 245–248.

Otto, T.D., Dillon, G.P., Degrave, W.S., and Berriman, M. (2011) RATT: Rapid Annotation Transfer Tool. *Nucleic Acids Res* **39**: e57–e57.

Perli, T., van der Vorm, D.N.A., Wassink, M., van den Broek, M., Pronk, J.T., and Daran, J.M. (2021) Engineering heterologous molybdenum-cofactor-biosynthesis and nitrate-assimilation pathways enables nitrate utilization by *Saccharomyces cerevisiae*. *Metab Eng* **65**: 11–29.

Pizarro, F., Varela, C., Martabit, C., Bruno, C., Pérez-Correa, J.R., and Agosin, E. (2007) Coupling kinetic expressions and metabolic networks for predicting wine fermentations. *Biotechnol Bioeng* **98**: 986–998.

Querol, A., Barrio, E., Huerta, T., and Ramon, D. (1992) Molecular monitoring of wine fermentations conducted by active dry yeast strains. *Appl Environ Microbiol* **58**: 2948–2953.

Raghunathan, A.U., Pérez-Correa, J.R., Agosin, E., and Biegler, L.T. (2006) Parameter estimation in metabolic flux balance models for batch fermentation-formulation & Solution using differential variational inequalities. *Ann Oper Res* **148**: 251–270.

Rossignol, T., Dulau, L., Julien, A., and Blondin, B. (2003) Genome-wide monitoring of wine yeast gene expression during alcoholic fermentation. *Yeast* **20**: 1369–1385.

Saitua, F., Torres, P., Pérez-Correa, J.R., and Agosin, E. (2017) Dynamic genome-scale metabolic modeling of the yeast *Pichia pastoris*. *BMC Syst Biol* **11**:.

Sánchez, B.J., Pérez-Correa, J.R., and Agosin, E. (2014) Construction of robust dynamic genome-scale metabolic model structures of *Saccharomyces cerevisiae* through iterative re-parameterization. *Metab Eng* **25**: 159–173.

Sánchez, B.J., Zhang, C., Nilsson, A., Lahtvee, P., Kerkhoven, E.J., and Nielsen, J. (2017) Improving the phenotype predictions of a yeast genome-scale metabolic model by incorporating enzymatic constraints. *Mol Syst Biol* **13**: 935.

Schellenberger, J., Que, R., Fleming, R.M.T., Thiele, I., Orth, J.D., Feist, A.M., et al. (2011) Quantitative prediction of cellular metabolism with constraint-based models: The COBRA Toolbox v2.0. *Nat Protoc* **6**: 1290–1307.

Schulze, U., Lidén, G., Nielsen, J., and Villadsen, J. (1996) Physiological effects of nitrogen starvation in an anaerobic batch culture of *Saccharomyces cerevisiae*. *Microbiology* **142**: 2299–2310.

Scott, W.T., Smid, E.J., Notebaart, R.A., and Block, D.E. (2020) Curation and analysis of a *Saccharomyces cerevisiae* genome-scale metabolic model for predicting production of sensory impact molecules under enological conditions. *Processes* **8**: 1195.

Shopska, V., Denkova, R., Lyubenova, V., and Kostov, G. (2019) Kinetic characteristics of alcohol fermentation in brewing: State of art and control of the fermentation process. In, *Fermented Beverages: Volume 5. The Science of Beverages*. Elsevier, pp. 529–575.

Steensels, J. and Verstrepen, K.J. (2014) Taming wild yeast: Potential of conventional and nonconventional yeasts in industrial fermentations. *Annu Rev Microbiol* **68**: 61–80.

Su, Y., Seguinot, P., Sanchez, I., Ortiz-Julien, A., Heras, J.M., Querol, A., et al. (2020) Nitrogen sources preferences of non-*Saccharomyces* yeasts to sustain growth and fermentation under winemaking conditions. *Food Microbiol* **85**:.

Tosi, E., Azzolini, M., Guzzo, F., and Zapparoli, G. (2009) Evidence of different fermentation behaviours of two indigenous strains of *Saccharomyces cerevisiae* and *Saccharomyces uvarum* isolated from Amarone wine. *J Appl Microbiol* **107**: 210–218.

Varela, C., Barker, A., Tran, T., Borneman, A., and Curtin, C. (2017) Sensory profile and volatile aroma composition of reduced alcohol Merlot wines fermented with *Metschnikowia pulcherrima* and *Saccharomyces uvarum*. *Int J Food Microbiol* **252**: 1–9.

Varela, C., Pizarro, F., and Agosin, E. (2004) Biomass content governs fermentation rate in nitrogen-deficient wine musts. *Appl Environ Microbiol* **70**: 3392–3400.

Vargas, F.A., Pizarro, F., Pérez-Correa, J.R., and Agosin, E. (2011) Expanding a dynamic flux balance model of yeast fermentation to genome-scale. *BMC Syst Biol* **5**: 17–19.

Varma, A. and Palsson, B.O. (1994) Stoichiometric flux balance models quantitatively predict growth and metabolic by-product secretion in wild-type *Escherichia coli* W3110. *Appl Environ Microbiol* **60**: 3724–3731.

Vázquez-Lima, F., Silva, P., Barreiro, A., Martínez-Moreno, R., Morales, P., Quirós, M., et al. (2014) Use of chemostat cultures mimicking different phases of wine fermentations as a tool for quantitative physiological analysis. *Microb Cell Fact* **13**:.

Walter, E. and Pronzato, L. (1997) Identification of Parametric Models: from Experimental Data. *Comput Sci*.

Wang, G., Huang, M., and Nielsen, J. (2017) Exploring the potential of *Saccharomyces cerevisiae* for biopharmaceutical protein production. *Curr Opin Biotechnol* **48**: 77–84.

Wang, Y., Zhang, H., Lu, X., Zong, H., and Zhuge, B. (2019) Advances in 2-phenylethanol production from engineered microorganisms. *Biotechnol Adv* **37**: 403–409.

van Wyk, N., Kroukamp, H., and Pretorius, I.S. (2018) The smell of synthetic biology: Engineering strategies for aroma compound production in yeast. *Fermentation* **4**: 54.

Yuan, J., Chen, X., Mishra, P., and Ching, C.B. (2017) Metabolically engineered *Saccharomyces cerevisiae* for enhanced isoamyl alcohol production. *Appl Microbiol Biotechnol* **101**: 465–474.

CHAPTER 4

Metabolic differences between a wild and a wine strain of *Saccharomyces cerevisiae* during fermentation unveiled by multi-omic analysis

Romain Minebois[a], María Lairón-Peris[a], Eladio Barrio[a,b]; Roberto Pérez-Torrado[a] and Amparo Querol[a]*

[a] Instituto de Agroquímica y Tecnología de los Alimentos, IATA-CSIC. E-46980 Paterna, Spain.

[b] Departament de Genètica, Universitat de València, C/ Doctor Moliner, 50, E-46100 Burjassot, Valencia, Spain

*Corresponding author: aquerol@iata.csic.es

Published in **Environmental Microbiology**

[DOI: 10.1111/1462-2920.15523]

Abstract

Saccharomyces cerevisiae, a widespread yeast present both in the wild and in fermentative processes, like winemaking. During the colonization of these human-associated fermentative environments, certain strains of *S. cerevisiae* acquired differential adaptive traits that enhanced their physiological properties to cope with the challenges imposed by these new ecological niches. The advent of omics technologies allowed unveiling some details of the molecular bases responsible for the peculiar traits of *S. cerevisiae* wine strains. However, the metabolic diversity within yeasts remained poorly explored, in particular that existing between wine and wild strains of *S. cerevisiae*. For this purpose, we performed a dual transcriptomic and metabolomic comparative analysis between a wild and a wine *S. cerevisiae* strains during wine fermentations performed at high and low temperatures. By using this approach, we could correlate the differential expression of genes involved in metabolic pathways, such as sulfur, arginine, and thiamine metabolisms, with differences in the amounts of key metabolites that can explain some important differences in the fermentation performance between the wine and wild strains.

Chapter 4

1. Introduction

Saccharomyces cerevisiae is a widespread yeast species found both in the wild (Wang *et al.*, 2012) and in fermentative processes, including winemaking (Legras *et al.*, 2018). Natural isolates of *S. cerevisiae* have been isolated from highly diverse living environments, such as fruits, tree bark, rotten wood, cacti, soil, and exudates of oak trees. Over the last few decades, the increasing availability of *S. cerevisiae* strains and their genomes has continuously consolidated the position of this species as a model organism in ecology and population genomics (Almeida *et al*., 2015; Gallone *et al* ., 2016; Legras *et al* ., 2018; Liti *et al*., 2009; Peter *et al*., 2018; Peter & Schacherer, 2016; Schacherer *et al*. 2009).

Among the available strains, increased attention has been paid to *S. cerevisiae* wine strains. Indeed, the repeated exposure of wine *S. cerevisiae* strains to the variety of stresses occurring during alcoholic fermentation (e.g. osmotic stress, ethanol content, nitrogen starvation, addition of sulfites), has led to their passive domestication and the emergence of differential adaptive traits of biotechnological interest (Querol *et al.*, 2003; Barrio *et al*., 2006). In this aspect, different genomic changes of adaptive value, often referred to as “footprints” of the domestication process have been reported in wine strains (Marsit and Dequin, 2015; Gallone *et al.*, 2016, 2019; Gorter de Vries *et al.*, 2017). Nucleotide variation (Schacherer *et al*.,

2009; Eldarov *et al.*, 2018), chromosomal rearrangements (Guijo *et al.*, 1997; Pérez-Ortín *et al.*, 2002; García-Ríos *et al.*, 2019), gene copy number variation (Ibáñez *et al.*, 2014; Peter *et al.*, 2018), introgressions (Almeida *et al.*, 2014), hybridization (Dunn *et al.*, 2013; Morard *et al.*, 2020), aneuploidy (Hose *et al.*, 2015; Mangado *et al.*, 2018; Morard *et al.*, 2019) and horizontal gene transfer (HGT) (Marsit *et al.*, 2015, 2016) are the highlighted genetic mechanisms described in the adaptation of *S. cerevisiae* wine strains to winemaking. For instance, the reciprocal translocation between chromosomes VII and XVI is a well-documented case of gross chromosomal rearrangement with the adaptive advantage of sulfite resistance, only present in wine strains of *S. cerevisiae* (Pérez-Ortín *et al.*, 2002; Yuasa *et al.*, 2004; García-Ríos *et al.*, 2019). More recently, the genes of region C (Novo *et al.*, 2009), which results from a recent HGT event from *Torulaspora microellipsoides* to *S. cerevisiae* wine yeasts (Marsit *et al.*, 2015), were characterized in depth. It was shown that the tandem duplicated genes *FOT1–2*, encoding oligopeptide transporter, and the gene *FSY1*, encoding a high-affinity fructose/H+ symporter, provide a strong competitive advantage to wine strains during fermentation (Galeote *et al.*, 2010; Marsit *et al.*, 2015).

On the other hand, the advent of omic technologies has enabled to unveil some details of the transcriptomic, metabolomic, proteomic, or even metabolic flux differences responsible for the peculiar fermentative traits of *S. cerevisiae* strains isolated from diverse

environments. For instance, by using a transcriptomic approach, García-Ríos *et al.*, (2014) proposed that the up-regulation of the genes of the sulfur assimilation pathway and glutathione biosynthesis in *S. cerevisiae* wine strains may play a crucial role in their better performance at low temperature. A constraint-based model approach has also been employed to address the contribution of strain origin to the intra-species flux distribution in central carbon metabolism in *S. cerevisiae*, pointing out a significant effect of strain origin on flux distribution through the pentose phosphate pathway and glycerol synthesis (Nidelet *et al.*, 2016). Likewise, different metabolomic studies using phenotypic criteria with industrial interest other than growth, have detailed the extent of the metabolic diversity within *S. cerevisiae* (Spor *et al.*, 2009; Albertin *et al.*, 2011; Camarasa *et al.*, 2011; Deed and Pilkington, 2020). A common outcome of these experiments was that wine strains of *S. cerevisiae* display higher fermentative capacities and low acetate yield; however, natural isolates from ‘‘poor-sugar’’ environments, such as oak tree exudates, do not exhibit such efficient fermentation features and according to Will et al., (2010) strains collected from oaks exhibit a common phenotype, namely freeze-thaw resistance, which is crucial for survival in wintry environments.

Despite these massive progresses in genome sequencing and high-throughput phenotyping, metabolic diversity in yeast is still relatively unexplored, including metabolic differences between wine and wild

strains of *S. cerevisiae*. In this context, using a dual omics approach, we searched for differential transcriptomic and metabolic traits between a wild type strain (oak isolate) and a wine *S. cerevisiae* strain under winemaking conditions at high (25ºC) and low (12ºC) fermentation temperatures. To do so, we simultaneously collected samples for RNAseq and metabolome analysis across the fermentation process. We first used the RNAseq samples to seek for major differential expression between the two strains, revealing that several relevant secondary metabolic pathways were up-regulated in the wine strain accordingly or regardless of temperature. On the other hand, by combining these results with metabolomic data, we pointed out that transcriptomic results match with significant differences of key metabolites involved in the distinct up-regulated pathways in the wine strain including the sulfur, the arginine, and the thiamine metabolic pathways. Because of the number of strains used, it is important to emphasize that this study neither attempts nor allows to extend the results obtained from these two representative strains to the rest of the individuals of the same lineage. For this, the set of strains used should be increased. However, this study has confirmed some hypotheses put forward by other authors in other works, and also provides interesting new lines of research regarding the metabolic diversity between wild and wine strains of *S. cerevisiae*.

Chapter 4

2. Material and methods

2.1 Yeast strains

Two strains isolated from wine and wild lineages according to the established groupings by Liti et al., (2009) were selected for the transcriptomic and metabolomic analysis. The commercial *S. cerevisiae* strain T73 (Lallemand, Montreal) isolated from wine in Spain (Querol *et al.*, 1992) was used as our wine lineage representative. Regarding the wild lineage, we selected strain YPS128, isolated from Pennsylvania woodlands (Sniegowski *et al.*, 2002).

2.2 Microvinification experiments

Micro vinification experiments were performed in triplicates at 25ºC and 12ºC following the same procedure as Minebois *et al.* (2020b). Minibio reactors (Applikon, The Netherlands) were filled with 470 ml of natural white must of Merseguera previously clarified overnight and adjusted with 47 g/l of sucrose, 0.2 g/l of ammonium sulfate, and 0.1 mg/l of thiamine. Reactors were inoculated at OD_{600} 0.1 (approximately 1 x 10^6 cells/ml) from starter cultures which were prepared by growing cells in an Erlenmeyer flask containing 25 ml of GPY liquid medium (2% glucose, 0.5% peptone, 0.5% yeast extract) at 25ºC overnight for micro vinification performed at 25ºC, and at 12ºC for 48h for micro vinification carried out at this temperature.

Fermentations were followed by measuring residual sugar concentration by liquid chromatography and stopped when no residual sugar variation was detected. Across the fermentation process, extracellular metabolites (see details below) were quantified using approximately 3 ml of supernatant collected in ten points distributed from the beginning to the end of the fermentation. Additionally, a diluted volume of these samples was used for the determination of colonies-forming units (CFUs) after plating on GPY solid medium (2% glucose, 2% agar, 0.5% peptone, 0.5% yeast extract).

2.3 RNAseq analysis

The RNAseq analysis was performed using the cell samples collected from the fermentation in three time points: during the growth phase (GP: 20h and 65h at 25ºc and 12ºC, respectively), at the end of the growth phase (EGP: 27h and 115h at 25ºc and 12ºC, respectively) and early stationary phase (ESP: 43h and 162h at 25ºC and 12ºC, respectively). All RNAseq analyses were performed using at least biological duplicates. A broth volume was rapidly harvested from the reactor, transferred to a polypropylene tube, and centrifuged (4.000 rpm, 5 min, 4ºC) to pellet cells. Then the supernatant was removed, the tube was flash-frozen in liquid nitrogen and stored at −80ºC until total RNA extraction. Total RNA was extracted using the High Pure RNA Isolation Kit (Roche,

Mannheim, Germany) following the manufacturer's protocol. These samples were sequenced using the Illumina Hiseq 2000, paired-end reads 75 bases long, and were deposited under the BioProject ID: PRJNA635244. Sequence reads were trimmed and quality filtered using Sickle (Joshi and Fass, 2011) (minimum read length of 50, minimum quality per base of 23) and aligned to S288c genome reference using bowtie2 version 2.3.2 (Langmead and Salzberg, 2012). Gene counts were obtained using HTSeq-count version 0.9.0 (Anders *et al.*, 2015), with the S288c gff annotation file (release number R64-1-1; SGD) and the mapping files ordered by names. The mapping reads with a quality score lower than 2 or those that aligned in more than one genome position were discarded. The data were first analyzed by using a Principal Component Analysis (PCA) among samples included in the DESeq2 package (Anders and Huber, 2010), which clustered the samples. Gene counts for each one of the 33 files were extracted and used for differential expression analyses with the EdgeR package (Robinson *et al.*, 2009). Normalization factors were calculated among reads to scale the raw library sizes, the negative binomial conditional common likelihoods were maximized to estimate a common dispersion value across all genes, and finally, the tagwise dispersion values were estimated by an empirical Bayes method based on weighted conditional maximum likelihood.

2.4 Extracellular metabolites quantification

Sugars (glucose, fructose), fermentative by-products (glycerol, ethanol, 2,3 butanediol, and erythritol), and organic acids (succinate, lactate, and acetate) were respectively determined by HPLC (Thermo Fisher Scientific, Waltham, MA) using a refraction index detector and UV/VIS (210 nm) detector equipped with a HyperREZ^{TM} XP Carbohydrate H+ 8 mm column (Thermo Fisher Scientific, Waltham, MA) and HyperREZ^{TM} XP Carbohydrate Guard (Thermo Fisher Scientific, Waltham, MA). The analysis conditions were: eluent, 1.5 mM of H_2SO_4; 0.6 ml.min^{-1} flux and oven temperature of 50°C. For sucrose determination, the same HPLC was equipped with a Hi-Plex Pb, 300 x 7.7 mm column (Agilent Technologies, CA, USA) and peaks quantified by the RI detector. The analysis conditions were: eluent, Milli-Q water; 0.6 ml.min-1 flux and oven temperature of 50°C. The retention times of the eluted peaks were compared to those of commercial analytical standards (Sigma-Aldrich, Madrid, Spain). The concentrations of the target compounds, in g/l, were quantified by the calibration graphs (R2 value > 0.99) of the standards that were previously obtained from a linear curve fit of the peak areas using standards mixtures.

Determination of yeast assimilable nitrogen (YAN) in the form of amino-acids and ammonia was carried out using the same protocol as Su *et al.*, (2020). For derivatization, 400 µl of the sample was mixed with 430 µl borate buffer (1 M, pH 10.2), 300 µl absolute methanol, and 12 µl of diethyl ethoxymethylenemalonate (DEEMM),

and ultra-sonicated for 30 min at 20ºC. After ultra-sonicating, the sample was warmed up at 80ºC for 2 hours to allow the complete degradation of excess DEEMM, and once derivatization finished the sample was filtered with a 0.22 µm filter. The chromatographic instrument consisted of a UPLC Dionex Ultimate 3000 (Thermo Fisher Scientific, Waltham, MA) equipped with an Accucore C18 LC column and Accucore C18 10 x 4.6 mm 2.6 um Defender guards (Thermo Scientific, MA, USA). Amino-acids and ammonia in the samples were identified and quantified according to the retention times, UV-vis spectral characteristics, and calibration curves (R2 value > 0.99) of the derivatives of the corresponding standards. Amino acid standard (ref AAS18), asparagine, and glutamine purchased from Sigma-Aldrich were used for calibration.

2.5 Intracellular metabolite quantification

An additional volume of broth corresponding to approximately 30 OD_{600} of cells was rapidly harvested and quenched using cold methanol (-40ºC) for intracellular metabolites measurement in four (12ºC) and five (25ºC) points coinciding with RNAseq samplings. For fermentations performed at 12ºC, these samples were collected at times 65h (GP), 115h (EGP), 162h (ESP), and 232h. For fermentations carried out at 25ºC, intracellular samples were collected at times 20h (GP), 27h (EGP), 44h (ESP), 69h, and 93h. Intracellular samples collected at 25ºC were extracted and

analyzed at the metabolomic platform of the Instituto de Biología Molecular y Celular de Plantas (UPV–CSIC, Valencia, Spain) following the same protocol as Minebois *et al.*, (2020a). For fermentations carried out at 12ºC, the extraction and quantification of intracellular metabolites were performed at the Metabolon HD4 platform (Durham, NC, USA) as described elsewhere (Minebois *et al.*, 2020b). Data were normalized for internal consistency by processing a constant amount of sample per volume of extraction solvent. Data were scaled to the median value for each compound. Statistical calculations and figures were performed and obtained using natural log-transformed scaled imputed data.

2.6 Statistics analysis

To perform differential expression (DE) analysis among groups of RNAseq samples, gene-wise exact tests were computed among the groups of negative-binomially distributed counts. Only genes with a number of counts in all of the samples greater than 1 were taken into account. False discovery rate (FDR; $\alpha = 0.05$) adjustment (Benjamini and Hochberg, 1995) was further applied for multiple test correction. Standard GO term analysis and pathway analysis were performed on differentially expressed genes using SGD, with an FDR corrected α threshold of 0.05 (Benjamini and Hochberg, 1995). From the lists of the differentially expressed genes in wine and natural lineages, Venn diagrams were constructed to show which genes were overexpressed

in the three stages http://genevenn.sourceforge.net/. t-tests to determine whether a significant difference existed between one control and one test condition were carried out using the GraphPad Prism 8.0 Software package (La Jolla, CA).

3. Results

The scheme of the experimental design used to seek transcriptomic and metabolic differences between T73, belonging to the wine *S. cerevisiae* lineage, and YPS128, a representative of the wild lineage, is shown in **Figure 1A.** We first investigated the phenotypic diversity between the two *S. cerevisiae* strains by characterizing their fermentative kinetics and performances under the conditions of this study (**Figure 1B**). Afterward, we compared the totality of the RNAseq samples of the two strains to look for differences in gene expression considering only the strain factor. Then, these samples were subdivided into several files to distinguish between differences in gene expression due to different factors: the fermentation stage, temperature, strain, and a combination of these variables. Besides, the metabolic pathways involving many differentially expressed genes were schematically reconstructed with the available intracellular levels of their metabolic intermediates to give a comprehensive picture of the transcriptomic and metabolomic variations existing between the two strains (**Figure 1C**).

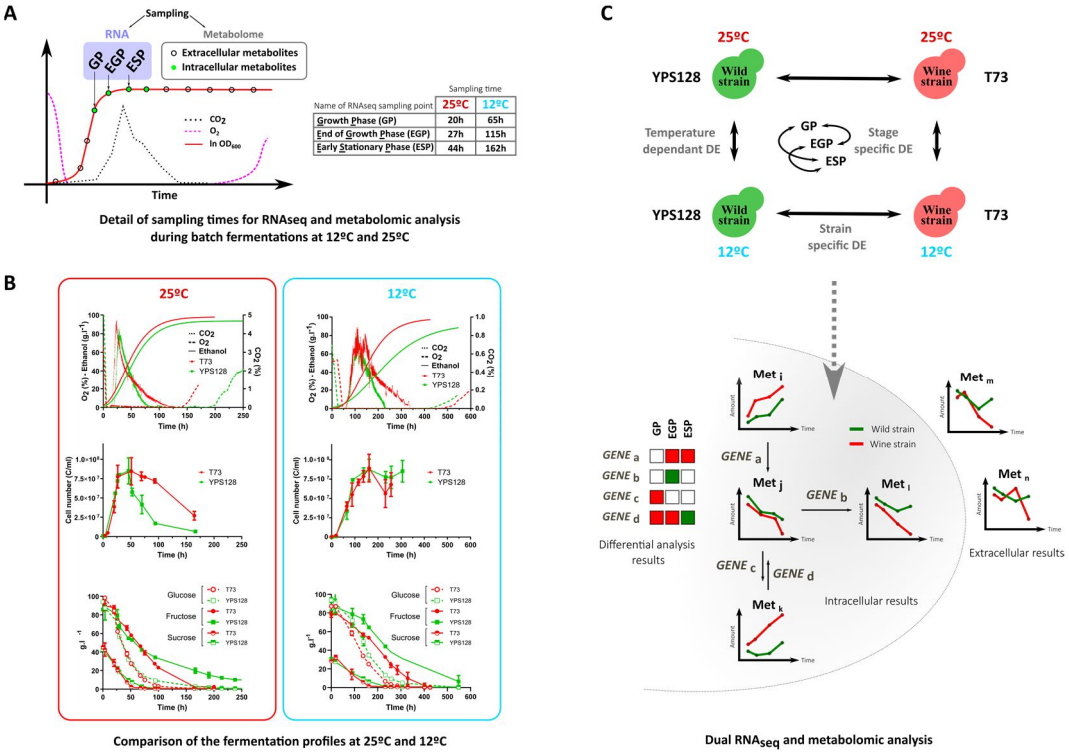

Figure 1. A) Scheme of the experimental design used for yeast cultivation including details of RNAseq as well as intra- and extracellular metabolome samplings. B) Comparison of the fermentation profiles of T73 and YPS128 at 25ºC and 12ºC, including the amount of CO_2 in the outgoing gas of the fermenter (in %), dissolved O_2 inside the fermenter (in %), ethanol concentration (in g/l), cell number (in C/ml) and extracellular concentrations of glucose, fructose and sucrose (in g/l). C) Scheme of the RNAseq and metabolomic data interpretation. The three defined variables in the transcriptomic analysis were the fermentation stage, the temperature, and the lineage. We first performed global differential expression analysis on the data set including all the RNAseq samples (DS). The RNAseq samples were then pooled specifically into different data sets

to identify genes differentially expressed according to temperature, strain, stage, or a combination of these variables (Supporting information Datasets_details). We combined the results of the differential expression analysis performed with the results of intra- and extracellular metabolites to correlate up-regulated processes or genes with phenotypic traits.

3.1 Phenotypic variations between the wine and wild strain of *S. cerevisiae*

The fermentation profile of the wine strain differed substantially from that of the wild strain at 25ºC, reflecting their diverse origin and fermentative performances (**Figure 1B**). Significant variations in the CO_2 kinetics were observed between both strains, with CO_2 dropping to 0 quicker in the wild strain. Interestingly, this timing was concordant with the early decrease of cell viability observed in the wild strain just after the entry into the stationary phase at 25ºC. Moreover, significant differences were found in the sugar consumption profiles and yields of some relevant fermentative by-products depending on the strain (**Figure 1B**, **Table 1**). Regarding sugar consumption profiles, both strains had comparable glucose and fructose consumption kinetics at the two temperatures studied. Besides, at both 12ºC and 25ºC, the wild strain was not able to consume all the fructose, which suggests that T73 is more fructophilic than the wild strain, and/or that YPS128 has a lower fermentative capacity probably due to a higher sensitivity to ethanol. Interestingly, the wine strain yielded lower acetate levels than the wild strain at

25ºC, while this trend was inverted at 12ºC (**Table 1**).

Table 1: Comparison of the sugar consumption and the yields of the main fermentative by-products during fermentations at 25ºC and 12ºC in natural white must of Merseguera with T73 and YPS128 strains.

	25ºC		12ºC	
	T73	**YPS128**	**T73**	**YPS128**
Sugar consumption (%)	98.24 ± 0.09	95.41 ± 0.45*	99.72 ± 0.02†	94.9 ± 2.17≈
Ethanol (g/g)	0.443 ± 0.032	0.477 ± 0.031	0.503 ± 0.014†	0.461 ± 0.014≈
Acetate (mg/g)	0.65 ± 0.11	1.73 ± 0.02*	1.79 ± 0.16†	0.66 ± 0.42º≈
Lactate (mg/g)	0.51 ± 0.06	0.78 ± 0.07*	0.36 ± 0.03†	0.38 ± 0.16º
Glycerol (mg/g)	22.6 ± 1.9	29.2 ± 1.5*	22.5 ± 1	23.1 ± 0.3º
Succinate (mg/g)	2.34 ± 0.28	3.2 ± 0.27*	1.76 ± 0.7	0.79 ± 0.59º
2,3 butanediol (mg/g)	0.4 ± 0.07	2.15 ± 0.19*	1.61 ± 0.11†	0.96 ± 0.47º
Erythritol (mg/g)	0.97 ± 0.14	0.85 ± 0.02	0.72 ± 0.03†	0.87 ± 0.21

* Significant differences compared to the control condition T73 25ºC (t-test, p-value <0.05): T73 25ºC vs YPS128 25ºC.

† Significant differences compared to the control condition T73 25ºC (t-test, p-value <0.05): T73 25ºC vs T73 12ºC.

º Significant differences compared to the control condition YPS128 25ºC (t-test, p-value <0.05): YPS128 25ºC vs YPS128 1

≈ Significant differences compared to the control condition T73 12ºC (t-test, p-value <0.05): T73 12ºC vs YPS128 12ºC.

3.2 Global transcriptome analysis

The principal component analysis (PCA) based on expression of 6320 genes in T73 and YPS128 during fermentation showed that 57% of the variance corresponded to component 1, which clustered samples according to the variable stage, meaning that the phase of fermentation was the main factor for sample variance (**Figure 2A**). However, according to component 1, we observed that EGP samples for T73 strain at 25ºC clustered with the rest of ESP samples at this temperature. Since gene expression is largely modulated during entry into the stationary phase, a slightly delayed sampling time for T73-EGP-25°C might have resulted in a different physiological state compared with the other EGP samples, explaining their outlier behavior. On the other hand, 19% of variance corresponded to PCA component 2 which unequivocally separated samples according to the variable strain, with wine T73 and wild YPS128 *S. cerevisiae* strains samples distributed horizontally on the top and the bottom of the plot, respectively. Moreover, in this defined space, samples from the same strain taken at the same stage tended to cluster regardless of the temperature, which suggested at first glimpse that most transcriptomic responses were shared between 12ºC and 25ºC.

Accordingly, we first performed a global differential expression (DE) analysis between strains on the data set (DS) including all the RNAseq samples. This initial DS was later split into different data sets to group

samples depending on the variables strain, temperature, or stage (Supporting information **Dataset_details**). This first differential expression analysis performed between the 15 RNAseq samples belonging to YPS128 wild yeast and the 18 samples belonging to T73 wine yeast showed that, of a total number of 6594 genes, 365 were up-regulated in the wine yeast and 337 in the wild yeast (BH p_{value} < 0.05). The gene ontology (GO) term enrichment analysis of the genes overexpressed in the wine yeast (YeastMine, p_{value} < 0.05) showed several significant biological process terms (**Table S1**). Thus, the arginine and glutamine family biosynthetic processes with 8 genes (*ARG1*, *ARG3*, *ARG4*, *ARG8, ORT1*, *CPA1*, *PUT1,* and *PUT2*) and several biological processes related to transmembrane transport, including genes *TAT1*, *VBA2*, *VBA3*, *SUL1*, and *SSU1* were overexpressed in the wine strain T73 (**Table S1**). On the other hand, the GO term enrichment analysis of the genes overexpressed in the wild yeast showed a variety of hexose transmembrane transport and cell wall organization processes, including genes belonging to the hexose transporter family (*HXT7*, *HXT13*, *HXT4*, *HXT8*, *HXT9,* and *HXT11*) and the seripauperin family (*PAU3*, *PAU8*, *PAU7*, *PAU13*, *PAU15*, *PAU19,* and *PAU24*) respectively (**Table S1**).

3.3 Identification of stage-specific differential expression in the wine and the wild strain

As explained above, we noticed that the variable stage

accounted for most of the variance observed in the global DE analysis, and hence, we could intuitively expect that several transcriptomic responses might be similar at 12ºC and 25ºC for each strain (**Figure 2A**). For this reason, we checked for the existence of strain-specific common DE genes at both temperatures, that could be related to the stage of the fermentation. Therefore, the data set containing the RNAseq samples from the wine and the wild strains at both temperatures were divided into two groups of files according to the fermentation stage (GP and ESP). We omitted the EGP samples for this specific analysis as triplicate samples of T73 at 25ºC were outliers that grouped with the ESP stage samples (**Figure 2A**). We called this data set DS_stage and its subsets DS_GP and DS_ESP (Supporting information **Dataset_details**).

When we performed the DE analysis with GP samples, we found that a total of 346 and 304 genes were up-regulated in the wine and wild yeast, respectively (**Figure 2B**). The arginine biosynthetic process was again among the overrepresented GO terms for the wine strain (**Figure 2B, Supplementary file 1**). We also found GO terms related to sulfur metabolism, with genes *SUL1*, *STR2*, *CIS2*, *HOM2*, *HOM3*, *YCT1,* and *MMP1,* and vitamin metabolism, notably several genes belonging to the thiamine metabolic process (*THI2*, *THI4*, *THI13,* and *THI22*). The isoleucine, valine, and glutamine amino acid family of biosynthetic processes were also in the list of enriched GO terms (Supporting

information **Supplementary file 1**), evidencing that the wine strain was more active in many amino-acid biosynthetic processes. In the wild strain, we found again the cell wall organization process, but also many GO terms related to ATP metabolism and aerobic respiration with distinct genes codifying for proteins and protein subunits involved in the mitochondrial respiratory chain (*ATP5*, *ATP20*, *ATP17*, *COX4*, *COX8*, *COX6*, *CYC1*, *CYT1*, etc.) (**Figure 2B, Supplementary file 2**).

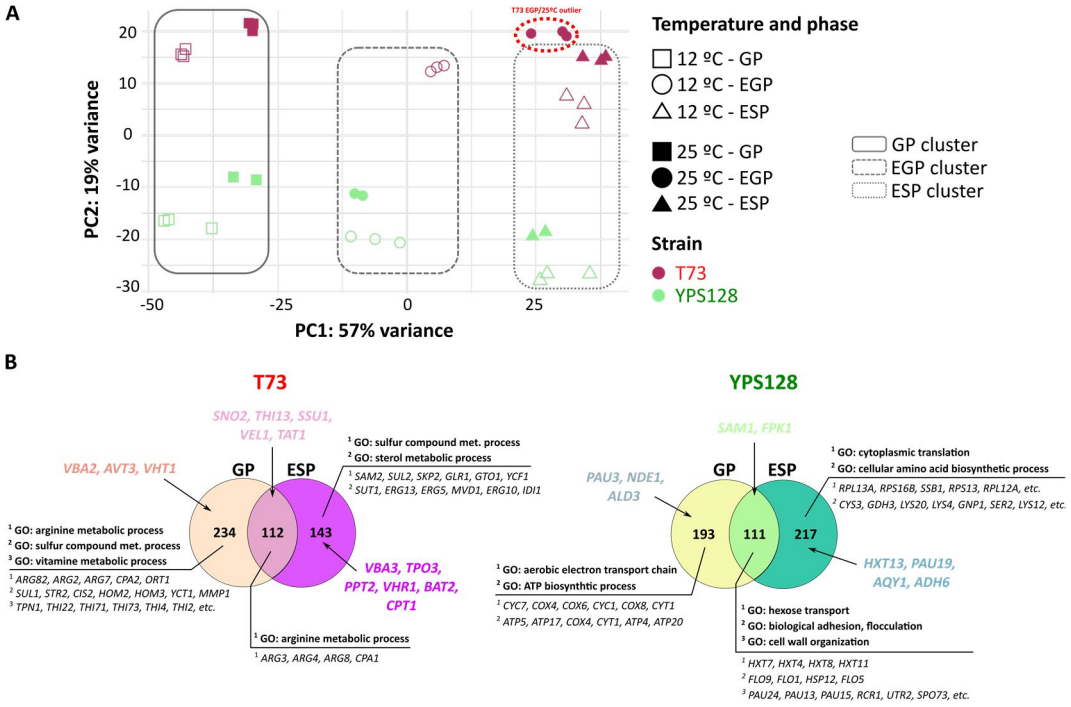

Figure 2. A) Principal component analysis plot of the total RNAseq replicates. The clustering of samples according to the variable stage is

indicated by rectangles. B) Differentially expressed genes in the wine (T73) and wild (YPS128) strains according to stage GP and ESP. Significantly altered gene numbers (BH $p_{value} < 0.05$) are represented in Venn diagrams with the remarkable genes and significant GO terms ($p_{value} < 0.05$) indicated for each stage. Stage EGP was not analyzed because samples of T73 at 25ºC did not group with the rest of the samples at stage EGP. Supporting information in Supplementary file 1 and Supplementary file 2.

When we performed the DE analysis with the ESP samples, we found that 255 and 328 genes were differentially expressed in the wine and the wild strains, respectively. When we sought GO enrichment in the wine strain, we found the sulfur compound metabolic process and many terms related to sterol metabolism, including genes as *ERG10*, *ERG5*, *ERG13*, *MVD1*, *SUT1,* and *IDI1* (**Figure 2**, **Supplementary file 1**). In the wild strain, we found numerous GO terms related to cytoplasmic translation, hexose transport, and cell to cell adhesion, among others (**Figure 2B**, **Supplementary file 2**).

3.4 Overexpression of the sulfur compounds pathway at low temperature is a wine-specific trait associated with phospholipids synthesis.

In the comparative stage-specific DE analysis, we found that the sulfur metabolism is among the most overexpressed GO terms at stage GP and ESP in the wine strain (**Figure 2B**). In this analysis, we

did not found any significant difference between 12ºC and 25ºC samples, so the "temperature" variable was not relevant. Therefore, we performed another DE analysis between wild and wine samples using DS_stage_12 (data set containing the RNAseq samples of T73 wine and YPS128 wild strain at 12ºC) and sought if we could find significant differences at the intracellular level of key metabolites of this pathway between both strains at 12ºC (**Figure 3A**). In this analysis, we found that numerous genes of the sulfur and glutathione pathways were overexpressed in the wine strain at 12ºC. Among them, 10 genes (*SUL1*, *SUL2*, *SSU1*, *MET10*, *STR3*, *CYS4*, *SAM2*, *GSH1, GTT1,* and *GTO1*) were up-regulated in more than one stage, and other 6 genes (*MET3, MET5*, *MET17*, *MET6*, *STR2,* and *GPX1*) were up-regulated at least in one stage (**Figure 3A**). When we incorporated intracellular metabolic data into this analysis, we observed that multiple key intermediates of this pathway, including methionine, S-adenosylmethionine (SAM), cysteine, γ-glutamyl-cysteine, and the reduced form of glutathione (GSH), were almost systematically found in significantly higher amounts in the wine strain at stage EGP (**Figure 3A**).

As a consequence of the higher requirement of sulfur precursors in the wine T73 strain due to its higher sulfur metabolic activity, the intracellular level of sulfate increased during the EGP stage and was found in significantly higher amounts after 232 h of fermentation.

A

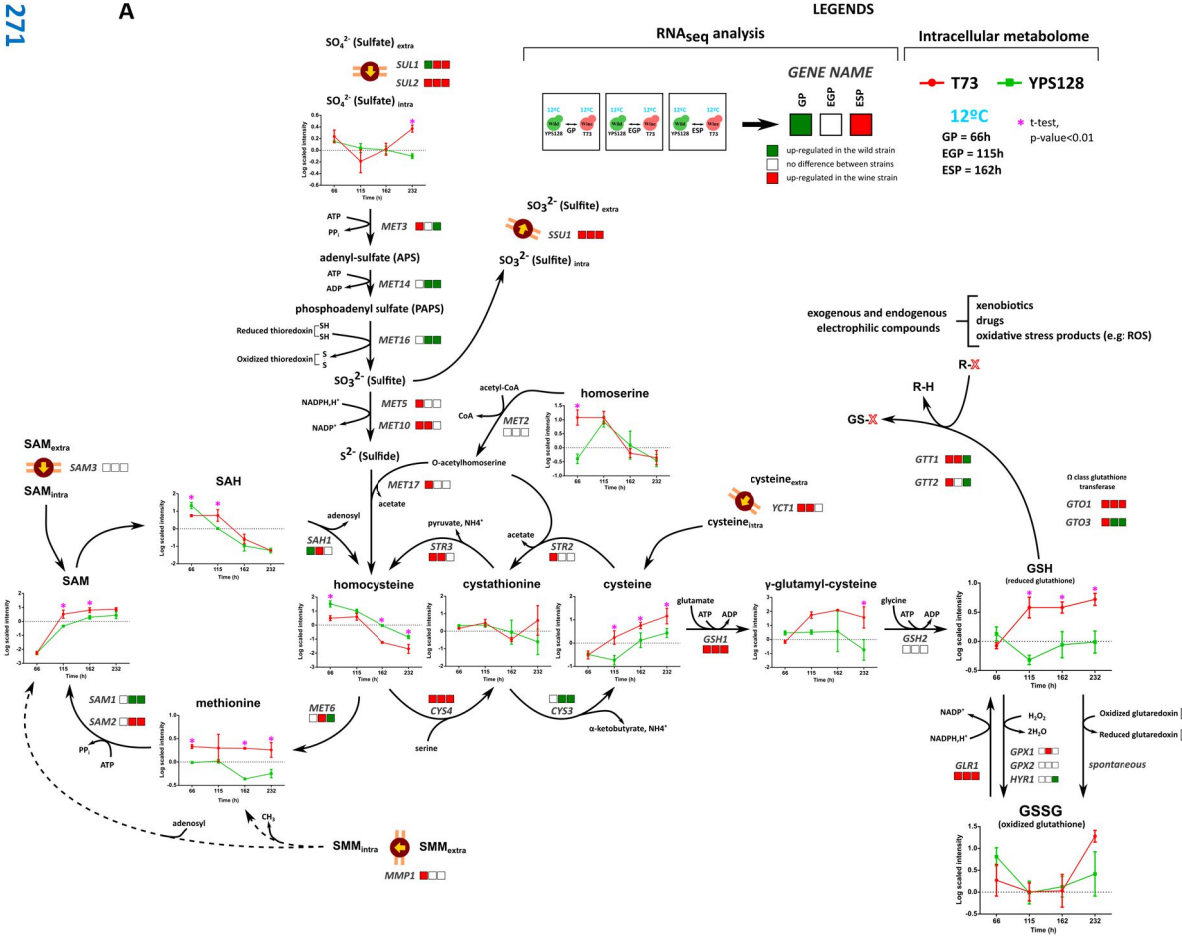

B

RNAseq analysis

	GP	ESP
Genes involved in the sulfur biosynthetic pathway	SUL1	SUL1
	SUL2	SUL2
	SSU1	SSU1
	SAM3	SAM3
	MMP1	MMP1
	YCT1	YCT1
	MET3	MET3
	MET14	MET14
	MET16	MET16
	MET5	MET5
	MET10	MET10
	MET2	MET2
	MET17	MET17
	MET6	MET6
	SAM1	SAM1
	SAM2	SAM2
	SAH1	SAH1
	CYS4	CYS4
	CYS3	CYS3
	STR2	STR2
	STR3	STR3
	GSH1	GSH1
	GSH2	GSH2
	GTT1	GTT1
	GTT2	GTT2
	GTO1	GTO1
	GTO3	GTO3
	GLR1	GLR1
	GPX1	GPX1
	GPX2	GPX2
	HYR1	HYR1
Regulators	MET4	MET4
	MET28	MET28
	MET31	MET31
	MET32	MET32
	CFD1	CFD1
	OPI1	OPI1

RNAseq analysis

	GP	ESP
Genes involved in the sulfur biosynthetic pathway	SUL1	SUL1
	SUL2	SUL2
	SSU1	SSU1
	SAM3	SAM3
	MMP1	MMP1
	YCT1	YCT1
	MET3	MET3
	MET14	MET14
	MET16	MET16
	MET5	MET5
	MET10	MET10
	MET2	MET2
	MET17	MET17
	MET6	MET6
	SAM1	SAM1
	SAM2	SAM2
	SAH1	SAH1
	CYS4	CYS4
	CYS3	CYS3
	STR2	STR2
	STR3	STR3
	GSH1	GSH1
	GSH2	GSH2
	GTT1	GTT1
	GTT2	GTT2
	GTO1	GTO1
	GTO3	GTO3
	GLR1	GLR1
	GPX1	GPX1
	GPX2	GPX2
	HYR1	HYR1
Regulators	MET4	MET4
	MET28	MET28
	MET31	MET31
	MET32	MET32
	CFD1	CFD1
	OPI1	OPI1

Up-regulated at 25ºC

Up-regulated at 12ºC

Figure 3. **(See previous page)** A) Scheme of the sulfur assimilation pathway. The transcriptomic data shown in the figure correspond to the results of the differential expression analysis performed at each stage with the RNAseq samples of T73 and YPS128 at 12ºC (data set DS_stage_12). Supporting information in Supplementary file 5. Results of the DE analysis are indicated next to the gene's name and are presented in the form of a 1*3 matrix in which each column corresponds to one stage. A red square indicates that the gene was found up-regulated in the wine strain T73, a green square that was found up-regulated in the wild strain YPS128, while a white square indicates that no significant difference was found (FDR corrected α threshold of 0.05). Intracellular levels of some metabolites of this pathway at 12ºC are also presented. Paired t-tests between T73 and YPS128 were performed at each sampling time to evaluate the statistical difference in the intracellular level of each metabolite. Statistical significance was determined using the Holm-Sidak method, with alpha = 0.01, and is represented by a pink star if it exists. Abbreviations: SAH (S-adenosylhomocysteine), SAM (S-adenosylmethionine), SMM (S-methylmethionine). B) Results of the differential expression analysis of genes of the sulfur assimilation pathway performed with data sets DS_stage_wine and DS_stage_wild for two stages (GP and ESP) to identify temperature-dependent genes. Stage EGP was not analyzed because samples of T73 at 25ºC did not group with the rest of the samples at stage EGP. Supporting information in Supplementary file 3 and Supplementary file 4.

Contrastingly, the intracellular amount of sulfate in YPS128 decreased

along the process. As shown in **Figure 3A**, homocysteine is a pivotal intermediate between the methyl cycle leading to SAM and methionine formation, and the cysteine forming transsulfuration reactions. The fact that it was almost always found at significantly lower amounts in T73 than in YPS128 suggests a higher homocysteine utilization through both methyl cycle and transsulfuration reactions. This correlates with the significantly higher intracellular contents of methionine, cysteine, γ-glutamyl-cysteine, GSH, and SAM and the up-regulation of genes *CYS4*, *GSH1*, *MET6,* and *SAM2* observed in the T73 strain.

Finally, we sought all the genes of this pathway that could be differentially expressed according to temperature. For this purpose, we compared samples taken at different stages from fermentations performed at 12ºC and 25ºC with the same strain (**Figure 3B, Dataset_details**). We observed that 19 and 15 genes of the sulfur metabolic pathway were up-regulated at 12ºC in the wine strain at stages GP and ESP, respectively (**Figure 3B**). On the contrary, most of the genes of this pathway affected by the low temperature in T73, such as *SAM3*, *YCT1*, *MET3*, *MET14*, *MET16, MET5*, *MET17*, *CYS4,* and *CYS3*, were not altered in the wild strain indicating that the up-regulation of the sulfur pathway is a specific regulatory mechanism of the wine strain at low temperature.

The activity of the sulfur pathway has a large influence on other metabolic pathways, some of which are relevant in the adaptation at low temperatures. This is the case of the phospholipid biosynthetic pathway, which is coregulated with the sulfur pathway by the transcriptional factors Opi1p and Met4p (Hickman *et al.*, 2011) (**Figure 4**). Remarkably, among the Opi1p targets, the genes *CDS1*, *PSD1*, *CHO2*, *OPI3* appeared up-regulated at the EGP stage in the T73 strain, while the genes *INO1* and *CKI1* were up-regulated at the EGP and ESP stages. We also found that gene *PAH1*, responsible for DAG synthesis from PA, was up-regulated in T73 at the three stages. Regarding intermediary metabolites of this pathway, a striking observation was that choline was present in significantly higher levels in the wine strain at the four intracellular sampling points. Besides, we observed that the levels of several phospholipids with long mono-unsaturated aliphatic tails, mainly 16:1 and 18:1, increased from stage EGP in wine strain T73, while decreased in the wild strain YPS128 (**Figure 4**).

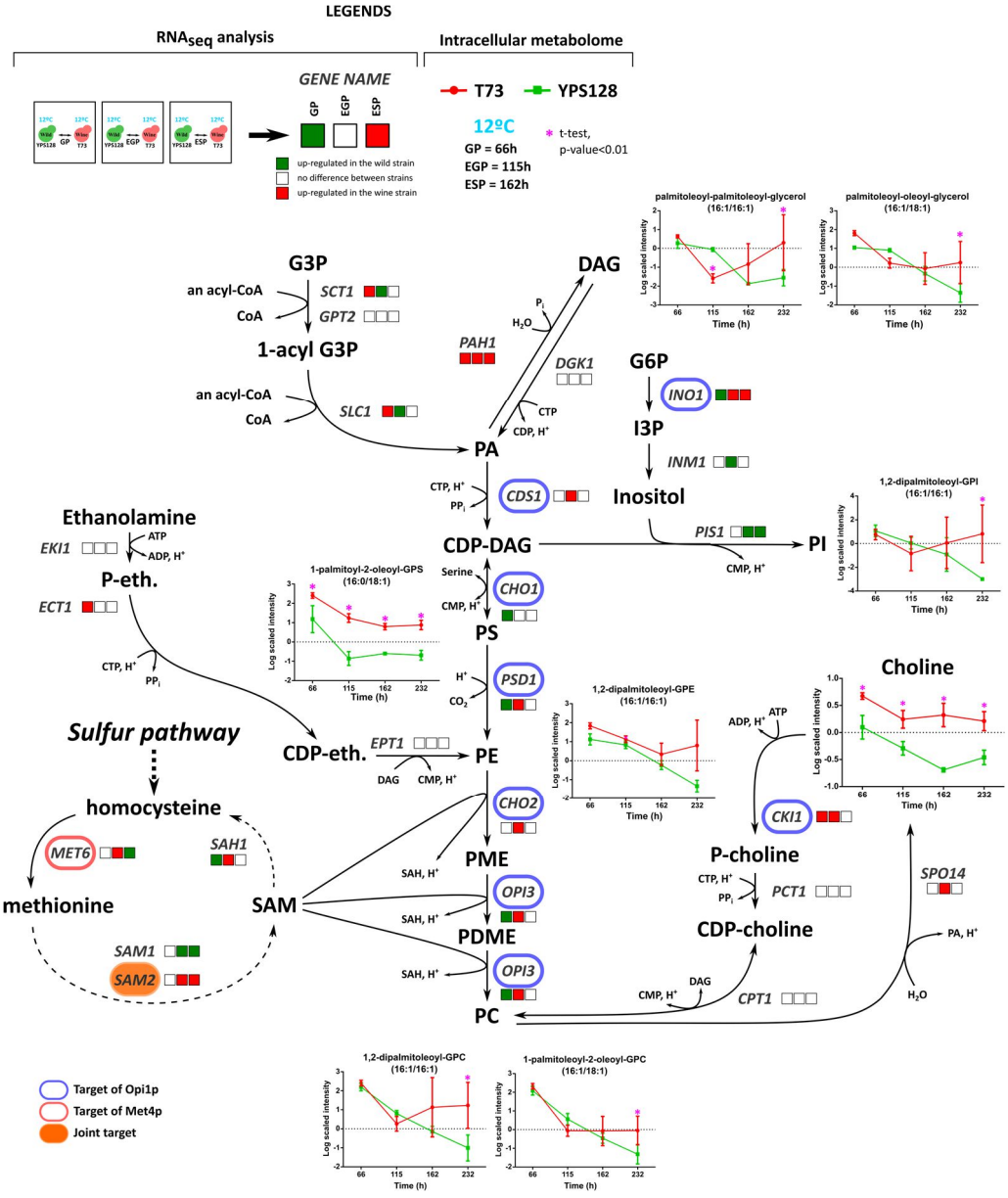

Figure 4. Scheme of the phospholipids biosynthetic pathway with the intracellular levels of metabolites and transcriptomic results obtained with

T73 and YPS128 strains at 12ºC. Results of the DE analysis are indicated next to the gene's name and are presented in the form of a 1*3 matrix in which each column corresponds to one stage. A red square indicates that the gene was found up-regulated in the wine strain T73, a green square that was found up-regulated in the wild strain YPS128, while a white square indicates that no significant difference was found (FDR corrected α threshold of 0.05). Paired t-tests between T73 and YPS128 were performed at each sampling time to evaluate the statistical difference in the intracellular level of each metabolite. Statistical significance was determined using the Holm-Sidak method, with alpha = 0.01, and is represented by a pink star if it exists. Abbreviations: CDP (cytidine-diphosphate), (G3P (glycerol 3-phosphate), 1-acyl G3P (1-acyl-sn-glycerol 3-phosphate), G6P (D-glucose-6-phosphate), I3P (1D-myo-inositol 3-phosphate), PI (phosphatidylinositol), DAG (diacylglycerol), CDP-DAG (CDP-diacylglycerol), PA (phosphatidic acid), PS (phosphatidylserine), PE (phosphatidylethanolamine), PME (phosphatidyl-N-methylethanolamine), PDME (phosphatidyl-N-dimethylethanolamine), PC (phosphatidylcholine), SAM (S-adenosylmethionine), P-choline (phosphocholine), P-eth (phosphoethanolamine), CDP-eth (CDP-ethanolamine).

3.5 Simultaneous expression of the arginine biosynthesis pathway and vacuolar amino acid transporters as a mechanism of nitrogen storage and redistribution at the end of the growth phase in the wine strain.

In the previous GO term analysis of the genes overexpressed

in T73 at both temperatures, amino acid biosynthesis processes, such as arginine, glutamine, and branched-chain amino acids, were identified (**Figure 2B**, **Supplementary file 1**). In yeast, the vacuole functions as a storage compartment for ions and nutrients, including most amino acids (Kawano-Kawada *et al.*, 2018), but also is the place where degradation of proteins occurs (Hecht *et al.*, 2014). During the exponential growth phase, yeasts generally accumulate non-preferential sources of nitrogen in the vacuole, before incorporating them directly into proteins or using them for *de novo* synthesis of other amino acids to meet the demands associated with the entry into the stationary phase. The passage of amino acids through the vacuolar membrane depends on specific symport type vacuolar transporters and ATPase activity required to maintain proton homeostasis (Kawano-Kawada *et al.*, 2018). In this aspect, we observed that several genes codifying for vacuolar transporters of amino acids (*VBA2*, *VBA3,* or *AVT3*), were found up-regulated at both temperatures in T73 (**Figure 2B**). It is interesting to recall that glutamate and glutamine, in addition to being the two main direct precursors of arginine biosynthesis, are essential actors of central nitrogen metabolism involved in transamination reactions.

As a result of these observations, we wondered whether the up-regulation of the arginine biosynthetic pathway in the wine strain could be related to faster extracellular incorporation of the most

abundant nitrogen sources by the wine yeast, including the arginine. For this purpose, we looked at the consumption profile at both temperatures of extracellular arginine, ammonia, and glutamine, the three major nitrogenous sources found in the grape must. As shown in **Figure 5**, we also looked at the intracellular level of these metabolites, while placing them in the context of the arginine biosynthesis pathway, with the differences observed in gene expression at each temperature and stage of fermentation between the two strains. Interestingly, strain T73 unequivocally consumed extracellular arginine faster than YPS128, with noticeable differences found in the extracellular concentration values at the GP and EGP stages at both temperatures (**Figure 5**). Regarding glutamine and ammonium, no clear differences between strains were observable at 25ºC, while at 12ºC strain T73 consumed more rapidly these compounds than wild strain YPS128. Consistent with the above results (**Figure 2B**), when using the data sets comparing samples of T73 and YPS128 at 12ºC and 25ºC separately, we observed that almost all genes of the arginine biosynthetic pathway were over-expressed in the wine strain at both 12ºC and 25ºC, and at almost all stages of fermentation (**Figure 5**).

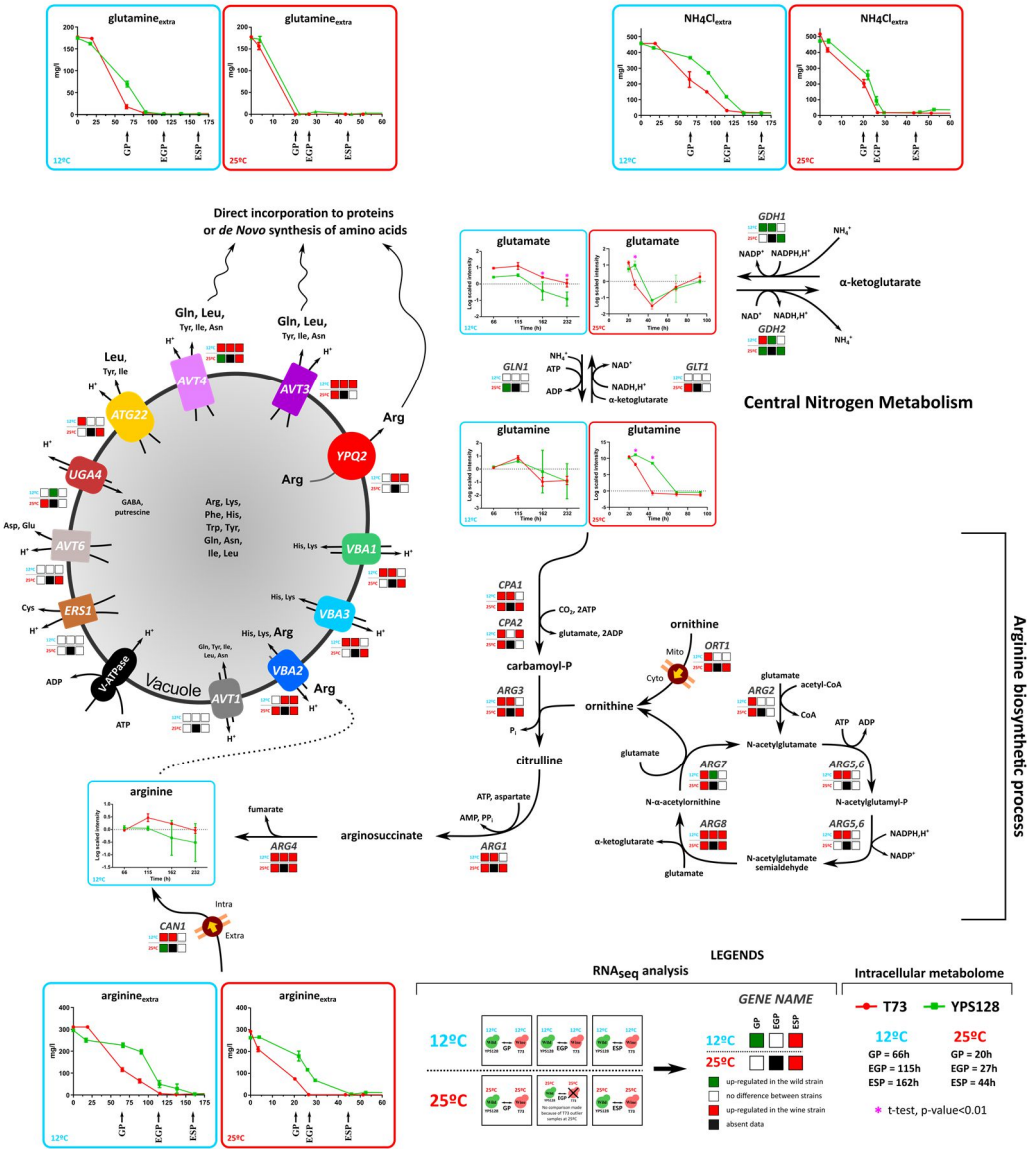

Figure 5. Dynamics of the extracellular concentrations (mg/l) of ammonium, arginine, and glutamine at 25ºC and 12ºC and scheme of the arginine biosynthetic pathway together with the vacuolar import and export system of amino acids in yeast. The transcriptomic data correspond to the results

of the differential expression analysis performed at each stage with the RNAseq samples of T73 and YPS128 at 12ºC (data set DS_stage_12) and with RNAseq samples of T73 and YPS128 at 25ºC (data set DS_stage_25). Results of the DE analysis are indicated next to the gene's name and are presented in the form of a 1*3 matrix in which each column corresponds to one stage. A red square indicates that the gene was found up-regulated in the wine strain T73, a green square that was found up-regulated in the wild strain YPS128, while a white square indicates that no significant difference was found (FDR corrected α threshold of 0.05). Intracellular levels of some metabolites of this pathway are also presented. Paired t-tests between T73 and YPS128 were performed at each sampling time to evaluate the statistical difference in the intracellular level of each metabolite. Statistical significance was determined using the Holm-Sidak method, with alpha = 0.01, and is represented by a pink star if it exists. Abbreviations: N-acetylglutamyl-P (N-acetylglutamyl-phosphate), carbamoyl-P (carbamoyl phosphate), P-5-C (pyrroline 5-carboxylate).

Interestingly, several genes codifying for vacuolar membrane proteins mediating amino acid import, including arginine, lysine, and histidine, and known as *VBA1*, *VBA2,* and *VBA3* were up-regulated during the growth phase in the wine strain at both temperatures. On the other hand, we observed that several genes codifying vacuolar membrane proteins mediating amino acid export (*AVT3*, *AVT4*, *ATG22,* and *YPQ2*) were also overexpressed in the wine strains. At the intracellular level, a remarkable result was that we did not observe significant differences in the arginine level between strains, at least at 12ºC (no

data available at 25ºC), which was rather surprising considering the over-expression of the entire arginine biosynthetic pathway observed in T73 at 12ºC and 25ºC. In contrast, glutamate was present in significantly higher amounts from stage EGP in T73 at 12ºC, but glutamine was not. At 25ºC, the data suggested an earlier decline in T73 than YPS128 in intracellular levels of these two key metabolites of central nitrogen metabolism.

3.6 Activation of the thiamine metabolic pathway in the wine strain

We found that several genes related to the vitamin metabolic processes were up-regulated during stage GP and at the two temperatures in the wine strain (**Figure 2B**). Interestingly, we found several genes among them, belonging to the thiamine metabolic pathway, that was overexpressed in more than one stage, e.g. *SNO2* and *THI13* (**Figure 2B**). Due to the relevance of thiamine in the cell metabolism as a cofactor of several central carbon metabolism enzymes, we decided to compare more in-depth the expression differences of the thiamine metabolism genes between our two strains and their relationships with differences in the intracellular levels of the pathway intermediates (**Figure 6**). However, due to challenges regarding the analytical determination of intracellular thiamine and its precursors, we were only able to compare the intracellular amounts of the metabolites of this pathway from samples at 12ºC sent to the Metabolon metabolomic platform. One

striking difference was observed in the amount of the active form of thiamine (vitamin B1), namely thiamine diphosphate (TDP). TDP was present in higher amounts in T73 than in YPS128 from the GP to the ESP stage. This was concordant with the broadly higher levels detected for the up-stream precursors pyridoxine, pyridoxal-5'-phosphate, pyridoxamine, pyridoxamine-5'-phosphate, and HET (**Figure 6**). These results are concordant with the overexpression in T73 of the gene *TPN1*, codifying for the plasma membrane pyridoxine (vitamin B6) transporter, at stage GP. Similarly, the gene *THI7*, encoding the thiamine membrane transporter, was over-expressed in T73 at the GP and EGP stages. This result together with the observation that genes *SNO2* and *SNZ3*, codifying for two upstream enzymes involved in the first steps of *de novo* synthesis of pyridoxine, were later up-regulated in T73, indicate that the wine strain promotes the incorporation of extracellular thiamine diphosphate precursors before its *de novo* synthesis. Remarkably, HMP was constitutively found at higher amounts in the wild strain YPS128 whilst its concentration decreased in T73. This was probably due to a higher conversion of HMP to HMP-P and the subsequent intermediaries, contributing to the higher intracellular TDP content observed in the wine strain (**Figure 6**). These reactions are catalyzed by enzymes encoded by genes *THI20*, *THI21, THI22,* and *THI6*, which were up-regulated in the wine strain earlier in the fermentation process, at stage GP.

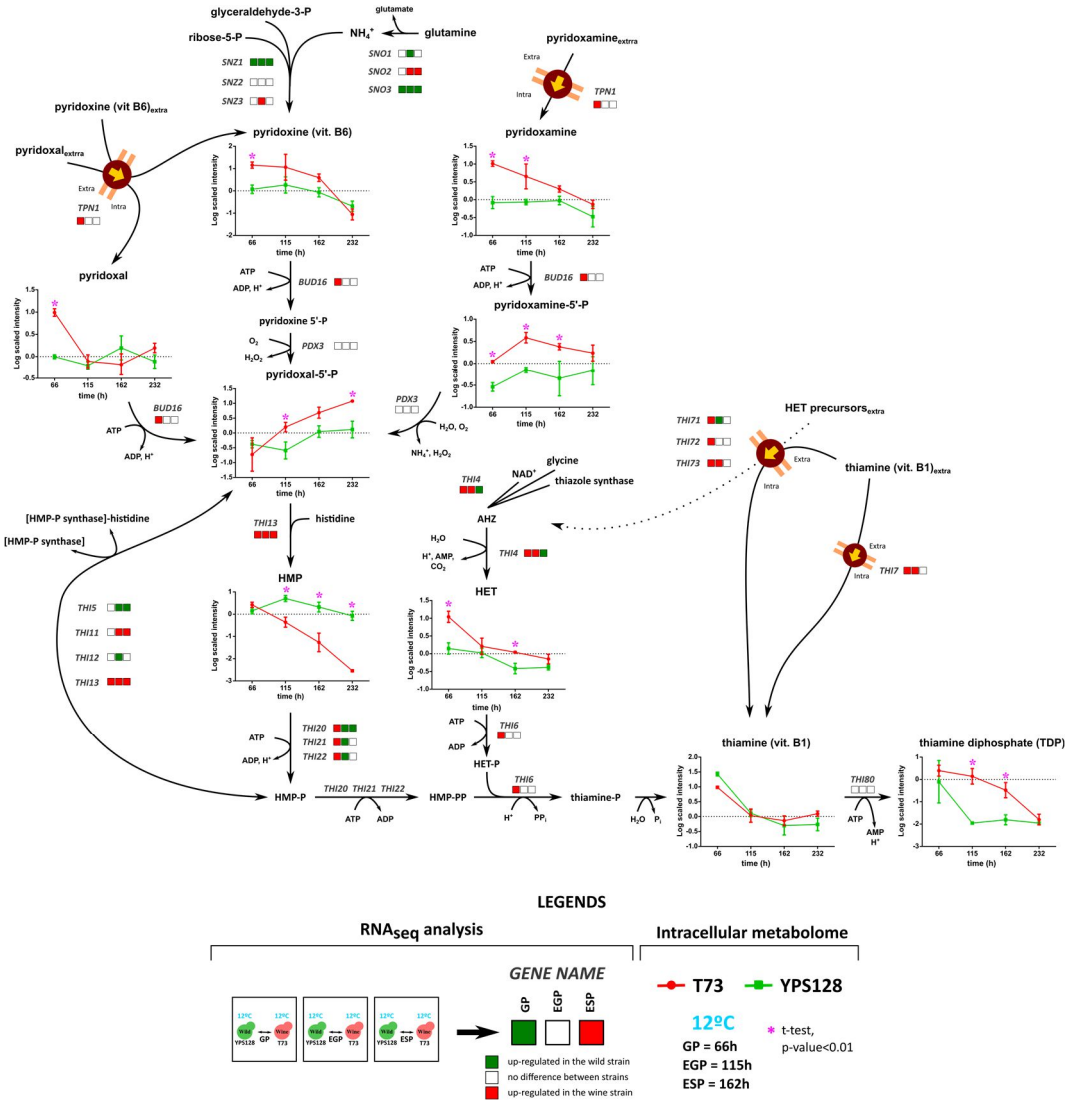

Figure 6. Scheme of the thiamine pathway with the intracellular levels of metabolites and transcriptomic results obtained with T73 and YPS128 strains at 12ºC. The transcriptomic data shown on the figure correspond to the results of the differential expression analysis performed at each stage with the RNAseq samples of T73 and YPS128 at 12ºC (data set

DS_stage_12). Results of the DE analysis are indicated next to the gene's name and are presented in the form of a 1*3 matrix in which each column corresponds to one stage (continued on next page). A red square indicates that the gene was found up-regulated in wine strain T73, a green square that was found up-regulated in wild strain YPS128, while a white square indicates that no significant difference was found (FDR corrected α threshold of 0.05). Paired t-tests between T73 and YPS128 were performed at each sampling time to evaluate the statistical difference in the intracellular level of each metabolite. Statistical significance was determined using the Holm-Sidak method, with alpha = 0.01, and is represented by a pink star if it exists. Abbreviations: AHZ (ADP-5-ethyl-4-methylthiazole-2-carboxylate), HET-P (4-methyl-5-(2-phosphoethyl)-thiazole), HMP (hydroxymethylpyrimidine), HMP-P (4-amino-5-hydroxymethyl-2-methylpyrimidine-phosphate), HMP-PP (4-amino-5-hydroxymethyl-2-methylpyrimidine-diphosphate), thiamine-P (thiamine phosphate).

4. Discussion

We observed that a wine strain of *S. cerevisiae* strain undergoes a transcriptional and metabolic program that differs in several aspects from that of a wild *S. cerevisiae* strain. The first significant difference we have found is the up-regulation of the sulfur assimilation pathway at low temperatures in the wine strain. Relevant sulfur-containing compounds such as cysteine, methionine, homocysteine, S-adenosylmethionine (SAM), and glutathione (GSH)

are produced from the incorporation of sulfate through this pathway (Penninckx, 2002; Ljungdahl and Daignan-Fornier, 2012). The biosynthetic genes of the sulfur assimilation pathway are controlled by a regulatory system whose main transcriptional activator is Met4p (Ljungdahl and Daignan-Fornier, 2012). Its activity is also coordinately regulated with that of the phospholipid biosynthesis pathway through the transcriptional repressor Opi1p (Hickman *et al.*, 2011). While Met4p activates, Opi1p represses *SAM2* encoding a SAM synthetase involved in the methyl cycle of the sulfur pathway, therefore balancing the level of the substrate used in most of the methyltransferase reactions. Likewise, it is well reported that *S. cerevisiae* modulates its membrane lipid composition in a temperature-dependent manner. In yeast fermenting at low temperature, the level of phosphatidylethanolamine (PE) and phosphatidylcholine (PC) with shorter-chain unsaturated fatty acids increase, while there is a general decrease in the chain length of fatty acids and the concentration of phosphatidic acid (PA) (Redón *et al.*, 2011; Tronchoni *et al.*, 2012; Henderson *et al.*, 2013). In that sense, it was proposed that the higher demand for PC at low temperature may increase the requirements of SAM for the methyltransferase reactions of the phospholipid biosynthesis, requiring the activation of the entire sulfur metabolism pathway in *S. cerevisiae* wine strains (García-Ríos *et al.*, 2014). However, until now this hypothesis remained unproven at the metabolomic level. Our results confirm the

assumptions made by the aforementioned authors. In the wine strain T73, we reported a greater amount of choline, a precursor of PC, as well as an increase in the level of several diacylglycerols (DAG) with medium-chain unsaturated fatty acids (e.g., 1,2-dipalmitoleoyl-GPC, 1-palmitoleoyl-2-oleoyl-GPC, dipalmitoleoyl-glycerol, palmitoleoyl-oleoyl-glycerol). At the transcriptomic level, this was consistent with the up-regulation of *SAM2* and most of the genes involved in PC synthesis, including *CHO2*, *OPI3,* and *CKI1* in the T73 strain. Also, *PAH1* which encodes the enzyme responsible for the dephosphorylation of PA to yield diacylglycerol (DAG) was induced at the three stages in T73. The DAG obtained in the latter reaction could then be used in the PC forming reactions from choline which involves Cki1p, Ptc1p, and Cpt1p. Once more, this was concordant with the simultaneous increase in the levels of DAG and PC of the same unsaturated fatty acid chain length, and with the up-regulation of the gene *CKI1* in the strain T73 reported above. On the contrary, the gene *OPI1* was up-regulated transiently at the GP stage in the YPS128 fermentation, indicating a down-regulation of phospholipids synthesis before the entry into the stationary phase in the wild strain.

In a sugar-rich medium such as grape must lacking lipid nutrients, *S. cerevisiae* suffers oxidative stress and oxidative damage to cell membranes and proteins due to the presence of reactive oxygen species (ROS) (Landolfo *et al.*, 2008, 2010). In this regard, the glutathione/glutaredoxin (GSH/GSSG) and thioredoxin systems play a

key role in ROS scavenging, and Gtt1p and Gtt2p are the main enzymes that conjugate GSH to a variety of exogenous and endogenous electrophilic compounds in *S. cerevisiae* (Grant, 2001), thereby delaying the cellular aging process, enhancing chronological life span, and extending the fermentative capacity of yeast (Aranda *et al.*, 2019). Besides increasing cell life span, oxidative stress resistance has been strongly correlated with low-temperature fitness in *S. cerevisiae* (García-Ríos *et al.*, 2016). We found a noticeable difference in the level of GSH in the wine strain at low temperatures. This is supported by the induction of genes *GSH1* and *GLR1* involved in GSH formation from cysteine and GSSG respectively, and also with the up-regulation of genes *GTT1* and *GTT2*, indicating a greater oxidative stress response of the wine strain to cope with the products of oxidative stress or environmental xenobiotics. In contrast to the wine strain, CO_2 production dropped in the wild strain representative shortly after the onset of the stationary phase, at both low and high fermentation temperatures, which is consistent with the lower fermentative capacities of the wild strains (Camarasa *et al.*, 2011). Altogether these transcriptomic and metabolomic results regarding the sulfur and glutathione pathway are in agreement with an adaptation mechanism to a low temperature specific to wine *S. cerevisiae* strains (García-Ríos *et al.*, 2014, 2016).

The second important difference we observed concerns the up-regulation of the arginine biosynthetic pathway and several vacuolar

membrane transporters in the wine strain during the transition from growth to stationary phase. Along with ammonium and glutamine, arginine is one of the most abundant nitrogen source found in grape juice, constituting around 25% of YAN (Bell and Henschke, 2005). However, arginine is not such a valuable source of nitrogen as ammonium or glutamine for *S. cerevisiae,* which is why it is late incorporated by this species during growth as a consequence of both NCR and SPS control (Magasanik and Kaiser, 2002; Ljungdahl and Daignan-Fornier, 2012). Moreover, yeast vacuole plays a determinant role in the differential formation of cytosolic and vacuolar amino acid pool during growth according to their acidic or basic character, and a large amount of arginine can accumulate in this compartment in yeast (Kitamoto *et al.*, 1988). Several works have notably described in more detail the intracellular fate of incorporated arginine during cell growth in *S. cerevisiae*. Among them, using ^{15}N-arginine as an isotopic tracer in wine strain EC1118, Crépin *et al.*, (2017) showed that proteinogenic arginine originated almost exclusively (>97%) from the uptake of exogenous arginine, i.e. there is little *de novo* synthesis of arginine. They also revealed a stage-dependent contribution of the consumed arginine not incorporated to proteins to anabolic processes: a significant portion of the remaining exogenous arginine is transiently stored during early growth and is then remobilized to provide NH3 for *de novo* synthesis of other amino acids upon entry into the stationary phase. The timing of gene expression observed for

vacuolar importer and exporter of arginine in our wine strain T73, namely *VBA2* and *YPQ2*, are in line with an efficient storage and redistribution mechanism across vacuole of arginine during the transition from growth phase to nitrogen limited conditions (Cools *et al.*, 2020), which is determinant to explain the fermentative capacity of wine yeasts (Crépin *et al.*, 2014). What is surprising in this context, however, is the over expression of genes of the arginine biosynthetic process (e.g., *ARG2*, *ARG3*, *ARG4*, *ARG5,6*, *ARG7*, *ARG8*, *CPA1*, *CPA2,* and *ORT1*) that we observed in T73. Indeed, in the absence of *de novo* synthesis of arginine, the genes involved in its biosynthesis should not be overexpressed, and in the presence of cytoplasmic arginine they should even be repressed (Godard *et al.*, 2007). One plausible explanation would be that, during the exponential growth phase, the fast assimilation of ammonia and glutamine mediated by transamination reactions may lead to the increase of cytosolic glutamate levels in the wine yeast. However, acidic amino acids, like glutamate, are excluded from the vacuole (Kitamoto *et al.*, 1988; Kawano-Kawada *et al.*, 2018), whereas arginine is easily stored and mobilized from this compartment. Thus, to control this hypothetical surplus of cytosolic glutamate not incorporated into proteins or not used for *de novo* synthesis of amino, it is plausible that the wine strain uses coordinately the arginine biosynthetic pathway and the related vacuolar transporter to store glutamate in the form of arginine inside the vacuole until an advanced stage of growth. Then,

once entering into stationary phase this stored arginine could act as a nitrogen donor for nitrogen transfer during the last stages of exponential growth.

Besides amino acids, vitamins are micronutrients with a crucial role in the fermentative performance of yeasts (Perli *et al.*, 2020). The active form of thiamine (vitamin B1) called thiamine diphosphate (TDP) is a determinant co-factor for many enzymes (e.g. decarboxylases, dehydrogenases, and transketolases) (Jurgenson *et al.*, 2009). Like plants and many other microorganisms, *S. cerevisiae* can produce TDP *de novo* (Hohmann and Meacock, 1998), but at a large energy cost (Perli *et al.*, 2020). This is the reason why yeast cells generally assimilate all exogenous thiamine and upstream precursors before initiating *de novo* biosynthesis. Extracellular thiamin as a precursor for TDP synthesis can be internalized through the high (THI7p) and low (THI71p, THI72p, THI73p) affinity plasma membrane transporters. Otherwise, diverse forms of vitamin B6 internalized via the Tpn1p transporter, including pyridoxal, pyridoxine, and pyridoxamine, can be used as more upstream precursors of TDP (Hohmann and Meacock, 1998; Stolz and Vielreicher, 2003; Mojzita and Hohmann, 2006; Paxhia and Downs, 2019). We observed that a great number of genes of this pathway were overexpressed in a transient and coordinated manner at the GP stage in the wine strain, at low and high fermentation temperatures. This is consistent with the higher levels of TDP and its precursors of the vitamin B6 family (e.g., pyridoxine,

pyridoxal-5'-phosphate, pyridoxamine, and pyridoxamine-5'-phosphate) found at 12ºC in the wine strain T73 in comparison to the wild strain YPS128. Rossignol *et al.* (2003) also reported such activation of this pathway during the growth phase and under similar winemaking conditions at 24ºC. Most sugar fermentation takes place after cells enter into the stationary phase, which means that TDP availability is a crucial factor when yeast cells are starved from nitrogen. Once again, the success of vinification depends on the viability and vitality of *S. cerevisiae* in the stationary phase. Recently, a correlation was observed between growth parameters and Vmax for an ORF (A9), located in the subtelomeric region A horizontally transferred from *Torulaspora microellipsoides* to the wine yeast lineage (Marsit *et al.*, 2015), which encodes an orthologue to a thiamine transporter whose deletion decreased the growth rate, growth efficiency, and CO_2 production (Devia *et al.*, 2020). In this sense, we can assume that the up-regulation of the thiamine biosynthetic pathway may allow the wine strain to sustain the TDP requirements of the cell during alcoholic fermentation.

5. Conclusion

Overall, this dual-omic study pointed out interesting gene expression variations that could contribute to the differential metabolomic and fermentation performance observed between our wild and wine *S. cerevisiae* strains. Of course, these differences in

both the transcriptome and metabolome may be specific to these two strains, and these results cannot be extended in any way to the rest of the wine or wild strains of *S. cerevisiae*. Nevertheless, this study confirmed or gave new evidence to some of the hypotheses proposed by other authors in other works, and also provides interesting new lines of research regarding the metabolic and transcriptomic diversity between wild and wine strains of *S. cerevisiae*.

Acknowledgments

RM was supported by an FPI grant from the Ministerio de Economía y Competitividad (ref. BES-2016-078202). ML-P was supported by an FPU contract from Ministerio de Ciencia, Innovación y Universidades (ref. FPU15/01775). This work was supported by the Spanish government and FEDER projects RTI2018-093744-B-C31 awarded to AQ, and RTI2018-093744-B-C32 to EB.

Supplementary files

Supplementary files can be downloaded from https://doi:10.1111/1462-2920.15523 or found at **page 382** of this manuscript.

Data accessibility

RNAseq results are available at BioProject ID: PRJNA635244

References

Albertin, W., Marullo, P., Aigle, M., Dillmann, C., de Vienne, D., Bely, M., and Sicard, D. (2011) Population size drives industrial *Saccharomyces cerevisiae* alcoholic fermentation and is under genetic control. *Appl Environ Microbiol* **77**: 2772–2784.

Almeida, P., Barbosa, R., Zalar, P., Imanishi, Y., Shimizu, K., Turchetti, B., et al. (2015) A population genomics insight into the Mediterranean origins of wine yeast domestication. *Mol Ecol* **24**: 5412–5427.

Almeida, P., Gonçalves, C., Teixeira, S., Libkind, D., Bontrager, M., Masneuf-Pomarède, I., et al. (2014) A Gondwanan imprint on global diversity and domestication of wine and cider yeast *Saccharomyces uvarum*. *Nat Commun* **5**: 1–12.

Anders, S. and Huber, W. (2010) Differential expression analysis for sequence count data. *Genome Biol* **11**: R106.

Anders, S., Pyl, P.T., and Huber, W. (2015) HTSeq-A Python framework to work with high-throughput sequencing data. *Bioinformatics* **31**: 166–169.

Aranda, A., Orozco, H., Picazo, C., and Matallana, E. (2019) Yeast life span and its impact on food fermentations. *Fermentation* **5**: 37.

Bell, S.J. and Henschke, P.A. (2005) Implications of nitrogen nutrition for grapes, fermentation and wine. *Aust J Grape Wine Res* **11**: 242–295.

Benjamini, Y. and Hochberg, Y. (1995) Controlling the False Discovery Rate: A Practical and Powerful Approach to Multiple Testing. *J R Stat Soc Ser B* **57**: 289–300.

Camarasa, C., Sanchez, I., Brial, P., Bigey, F., and Dequin, S. (2011) Phenotypic landscape of *Saccharomyces cerevisiae* during wine fermentation: Evidence for origin-dependent metabolic traits. *PLoS One* **6**: e25147.

Cools, M., Lissoir, S., Bodo, E., Ulloa-Calzonzin, J., DeLuna, A., Georis, I., and André, B. (2020) Nitrogen coordinated import and export of arginine across the yeast vacuolar membrane. *PLoS Genet* **16**:.

Crépin, L., Sanchez, I., Nidelet, T., Dequin, S., and Camarasa, C. (2014) Efficient ammonium uptake and mobilization of vacuolar arginine by *Saccharomyces cerevisiae* wine strains during wine fermentation. *Microb Cell Fact* **13**: 109.

Crépin, L., Truong, N.M., Bloem, A., Sanchez, I., Dequin, S., and Camarasa, C. (2017) Management of multiple nitrogen sources during wine fermentation by *Saccharomyces cerevisiae*. *Appl Environ Microbiol* **83**:.

Deed, R.C. and Pilkington, L.I. (2020) Lifestyle, lineage, and geographical origin influence temperature-dependent phenotypic variation across yeast strains during wine fermentation. *Microorganisms* **8**: 1–22.

Devia, J., Bastías, C., Kessi-Pérez, E.I., Villarroel, C.A., De Chiara, M., Cubillos, F.A., et al. (2020) Transcriptional Activity and Protein Levels of Horizontally Acquired Genes in Yeast Reveal Hallmarks of Adaptation to Fermentative Environments. *Front Genet* **11**:.

Dunn, B., Paulish, T., Stanbery, A., Piotrowski, J., Koniges, G., Kroll, E., et al. (2013) Recurrent Rearrangement during Adaptive Evolution in an Interspecific Yeast Hybrid Suggests a Model for Rapid Introgression. *PLoS Genet* **9**: 1003366.

Eldarov, M.A., Beletsky, A. V., Tanashchuk, T.N., Kishkovskaya, S.A., Ravin, N. V., and Mardanov, A. V. (2018) Whole-genome analysis of three yeast strains used for production of sherry-like wines revealed genetic traits specific to flor yeasts. *Front Microbiol* **9**:.

Galeote, V., Novo, M., Salema-Oom, M., Brion, C., Valério, E., Gonçalves, P., and Dequin, S. (2010) FSY1, a horizontally transferred gene in the *Saccharomyces cerevisiae* EC1118 wine yeast strain, encodes a high-affinity fructose/H+ symporter.

Microbiology **156**: 3754–3761.

Gallone, B., Steensels, J., Mertens, S., Dzialo, M.C., Gordon, J.L., Wauters, R., et al. (2019) Interspecific hybridization facilitates niche adaptation in beer yeast. *Nat Ecol Evol* **3**: 1562–1575.

Gallone, B., Steensels, J., Prahl, T., Soriaga, L., Saels, V., Herrera-Malaver, B., et al. (2016) Domestication and Divergence of *Saccharomyces cerevisiae* Beer Yeasts. *Cell* **166**: 1397-1410.e16.

García-Ríos, E., López-Malo, M., and Guillamón, M.M. (2014) Global phenotypic and genomic comparison of two *Saccharomyces cerevisiae* wine strains reveals a novel role of the sulfur assimilation pathway in adaptation at low temperature fermentations. *BMC Genomics* **15**: 1059.

García-Ríos, E., Nuévalos, M., Barrio, E., Puig, S., and Guillamón, J.M. (2019) A new chromosomal rearrangement improves the adaptation of wine yeasts to sulfite. *Environ Microbiol* **21**: 1771–1781.

García-Ríos, E., Ramos-Alonso, L., and Guillamón, J.M. (2016) Correlation between low temperature adaptation and oxidative stress in *Saccharomyces cerevisiae*. *Front Microbiol* **7**:.

Godard, P., Urrestarazu, A., Vissers, S., Kontos, K., Bontempi, G., van Helden, J., and Andre, B. (2007) Effect of 21 Different Nitrogen Sources on Global Gene Expression in the Yeast *Saccharomyces cerevisiae*. *Mol Cell Biol* **27**: 3065–3086.

Gorter de Vries, A.R., Pronk, J.T., and Daran, J.M.G. (2017) Industrial relevance of chromosomal copy number variation in *Saccharomyces* yeasts. *Appl Environ Microbiol* **83**:.

Grant, C.M. (2001) Role of the glutathione/glutaredoxin and thioredoxin systems in yeast growth and response to stress conditions. *Mol Microbiol* **39**: 533–541.

Guijo, S., Mauricio, J.C., Salmon, J.M., and Ortega, J.M. (1997)

Determination of the relative ploidy in different *Saccharomyces cerevisiae* strains used for fermentation and "flor" film ageing of dry sherry-type wines. *Yeast* **13**: 101–117.

Hecht, K.A., O'Donnell, A.F., and Brodsky, J.L. (2014) The proteolytic landscape of the yeast vacuole. *Cell Logist* **4**: e28023.

Henderson, C.M., Zeno, W.F., Lerno, L.A., Longo, M.L., and Block, D.E. (2013) Fermentation Temperature Modulates Phosphatidylethanolamine and Phosphatidylinositol Levels in the Cell Membrane of *Saccharomyces cerevisiae*. *Appl Environ Microbiol* **79**: 5345–5356.

Hickman, M.J., Petti, A.A., Ho-Shing, O., Silverman, S.J., McIsaac, R.S., Lee, T.A., and Botstein, D. (2011) Coordinated regulation of sulfur and phospholipid metabolism reflects the importance of methylation in the growth of yeast. *Mol Biol Cell* **22**: 4192–4204.

Hohmann, S. and Meacock, P.A. (1998) Thiamin metabolism and thiamin diphosphate-dependent enzymes in the yeast *Saccharomyces cerevisiae*: genetic regulation. *Biochim Biophys Acta - Protein Struct Mol Enzymol* **1385**: 201–219.

Hose, J., Yong, C.M., Sardi, M., Wang, Z., Newton, M.A., and Gasch, A.P. (2015) Dosage compensation can buffer copy-number variation in wild yeast. *Elife* **4**:.

Ibáñez, C., Pérez-Torrado, R., Chiva, R., Guillamón, J.M., Barrio, E., and Querol, A. (2014) Comparative genomic analysis of *Saccharomyces cerevisiae* yeasts isolated from fermentations of traditional beverages unveils different adaptive strategies. *Int J Food Microbiol* **171**: 129–135.

Joshi, N. and Fass, J. (2011) Sickle: A sliding-window, adaptive, quality-based trimming tool for FastQ files (Version 1.33) [Software]. *Available at https://github.com/najoshi/sickle* 2011.

Jurgenson, C.T., Begley, T.P., and Ealick, S.E. (2009) The structural and biochemical foundations of thiamin biosynthesis. *Annu Rev*

Biochem **78**: 569–603.

Kawano-Kawada, M., Kakinuma, Y., and Sekito, T. (2018) Transport of amino acids across the vacuolar membrane of yeast: Its mechanism and physiological role. *Biol Pharm Bull* **41**: 1496–1501.

Kitamoto, K., Yoshizawa, K., Ohsumi, Y., and Anraku, Y. (1988) Dynamic aspects of vacuolar and cytosolic amino acid pools of *Saccharomyces cerevisiae*. *J Bacteriol* **170**: 2683–2686.

Landolfo, S., Politi, H., Angelozzi, D., and Mannazzu, I. (2008) ROS accumulation and oxidative damage to cell structures in *Saccharomyces cerevisiae* wine strains during fermentation of high-sugar-containing medium. *Biochim Biophys Acta - Gen Subj* **1780**: 892–898.

Landolfo, S., Zara, G., Zara, S., Budroni, M., Ciani, M., and Mannazzu, I. (2010) Oleic acid and ergosterol supplementation mitigates oxidative stress in wine strains of *Saccharomyces cerevisiae*. *Int J Food Microbiol* **141**: 229–235.

Langmead, B. and Salzberg, S.L. (2012) Fast gapped-read alignment with Bowtie 2. *Nat Methods* **9**: 357–359.

Legras, J.L., Galeote, V., Bigey, F., Camarasa, C., Marsit, S., Nidelet, T., et al. (2018) Adaptation of *S. cerevisiae* to fermented food environments reveals remarkable genome plasticity and the footprints of domestication. *Mol Biol Evol* **35**: 1712–1727.

Liti, G., Carter, D.M., Moses, A.M., Warringer, J., Parts, L., James, S.A., et al. (2009) Population genomics of domestic and wild yeasts. *Nature* **458**: 337–341.

Ljungdahl, P.O. and Daignan-Fornier, B. (2012) Regulation of amino acid, nucleotide, and phosphate metabolism in *Saccharomyces cerevisiae*. *Genetics* **190**: 885–929.

Magasanik, B. and Kaiser, C.A. (2002) Nitrogen regulation in

Saccharomyces cerevisiae. *Gene* **290**: 1–18.

Mangado, A., Morales, P., Gonzalez, R., and Tronchoni, J. (2018) Evolution of a yeast with industrial background under winemaking conditions leads to diploidization and chromosomal copy number variation. *Front Microbiol* **9**:.

Marsit, S. and Dequin, S. (2015) Diversity and adaptive evolution of *Saccharomyces* wine yeast: a review. *FEMS Yeast Res* **15**:.

Marsit, S., Mena, A., Bigey, F., Sauvage, F.X., Couloux, A., Guy, J., et al. (2015) Evolutionary advantage conferred by an eukaryote-to-eukaryote gene transfer event in wine yeasts. *Mol Biol Evol* **32**: 1695–1707.

Marsit, S., Sanchez, I., Galeote, V., and Dequin, S. (2016) Horizontally acquired oligopeptide transporters favour adaptation of *Saccharomyces cerevisiae* wine yeast to oenological environment. *Environ Microbiol* **18**: 1148–1161.

Minebois, R., Pérez-Torrado, R., and Querol, A. (2020a) A time course metabolism comparison among *Saccharomyces cerevisiae*, *S. uvarum* and *S. kudriavzevii* species in wine fermentation. *Food Microbiol* **90**: 103484.

Minebois, R., Pérez-Torrado, R., and Querol, A. (2020b) Metabolome segregation of four strains of *Saccharomyces cerevisiae*, *S. uvarum* and *S. kudriavzevii* conducted under low temperature oenological conditions. *Environ Microbiol* 1462-2920.15135.

Mojzita, D. and Hohmann, S. (2006) Pdc2 coordinates expression of the THI regulon in the yeast *Saccharomyces cerevisiae*. *Mol Genet Genomics* **276**: 147–161.

Morard, M., Benavent-Gil, Y., Ortiz-Tovar, G., Pérez-Través, L., Querol, A., Toft, C., and Barrio, E. (2020) Genome structure reveals the diversity of mating mechanisms in *Saccharomyces cerevisiae* x *Saccharomyces kudriavzevii* hybrids, and the genomic instability that promotes phenotypic diversity. *Microb*

Genomics **6**:.

Morard, M., Macías, L.G., Adam, A.C., Lairón-Peris, M., Pérez-Torrado, R., Toft, C., and Barrio, E. (2019) Aneuploidy and Ethanol Tolerance in *Saccharomyces cerevisiae*. *Front Genet* **10**:.

Nidelet, T., Brial, P., Camarasa, C., and Dequin, S. (2016) Diversity of flux distribution in central carbon metabolism of *S. cerevisiae* strains from diverse environments. *Microb Cell Fact* **15**: 58.

Novo, M., Bigey, F., Beyne, E., Galeote, V., Gavory, F., Mallet, S., et al. (2009) Eukaryote-to-eukaryote gene transfer events revealed by the genome sequence of the wine yeast *Saccharomyces cerevisiae* EC1118. *Proc Natl Acad Sci U S A* **106**: 16333–8.

Paxhia, M.D. and Downs, D.M. (2019) SNZ3 encodes a PLP synthase involved in thiamine synthesis in *Saccharomyces cerevisiae*. *G3 Genes, Genomes, Genet* **9**: 335–344.

Penninckx, M.J. (2002) An overview on glutathione in *Saccharomyces* versus non-conventional yeasts. *FEMS Yeast Res* **2**: 295–305.

Pérez-Ortín, J.E., Querol, A., Puig, S., and Barrio, E. (2002) Molecular characterization of a chromosomal rearrangement involved in the adaptive evolution of yeast strains. *Genome Res* **12**: 1533–9.

Perli, T., Wronska, A.K., Ortiz-Merino, R.A., Pronk, J.T., and Daran, J.M. (2020) Vitamin requirements and biosynthesis in *Saccharomyces cerevisiae*. *Yeast* **37**: 283–304.

Peter, J., De Chiara, M., Friedrich, A., Yue, J.X., Pflieger, D., Bergström, A., et al. (2018) Genome evolution across 1,011 *Saccharomyces cerevisiae* isolates. *Nature* **556**: 339–344.

Peter, J. and Schacherer, J. (2016) Population genomics of yeasts: Towards a comprehensive view across a broad evolutionary scale. *Yeast* **33**: 73–81.

Querol, A., Fernández-Espinar, M.T., Del Olmo, M., and Barrio, E.

(2003) Adaptive evolution of wine yeast. *Int J Food Microbiol* **86**: 3–10.

Querol, A., Huerta, T., Barrio, E., and Ramon, D. (1992) Dry Yeast Strain For Use in Fermentation of Alicante Wines: Selection and DNA Patterns. *J Food Sci* **57**: 183–185.

Redón, M., Guillamón, J.M., Mas, A., and Rozès, N. (2011) Effect of growth temperature on yeast lipid composition and alcoholic fermentation at low temperature. *Eur Food Res Technol* **232**: 517–527.

Robinson, M.D., McCarthy, D.J., and Smyth, G.K. (2009) edgeR: A Bioconductor package for differential expression analysis of digital gene expression data. *Bioinformatics* **26**: 139–140.

Rossignol, T., Dulau, L., Julien, A., and Blondin, B. (2003) Genome-wide monitoring of wine yeast gene expression during alcoholic fermentation. *Yeast* **20**: 1369–1385.

Schacherer, J., Shapiro, J. a, Ruderfer, D.M., and Kruglyak, L. (2009) Comprehensive polymorphism survey elucidates population structure of *Saccharomyces cerevisiae*. *Nature* **458**: 342–345.

Schacherer, J., Shapiro, J.A., Ruderfer, D.M., and Kruglyak, L. (2009) Comprehensive polymorphism survey elucidates population structure of *Saccharomyces cerevisiae*. *Nature* **458**: 342–345.

Sniegowski, P.D., Dombrowski, P.G., and Fingerman, E. (2002) *Saccharomyces cerevisiae* and *Saccharomyces paradoxus* coexist in a natural woodland site in North America and display different levels of reproductive isolation from European conspecifics. *FEMS Yeast Res* **1**: 299–306.

Spor, A., Nidelet, T., Simon, J., Bourgais, A., De Vienne, D., and Sicard, D. (2009) Niche-driven evolution of metabolic and life-history strategies in natural and domesticated populations of *Saccharomyces cerevisiae*. *BMC Evol Biol* **9**: 296.

Stolz, J. and Vielreicher, M. (2003) Tpn1p, the plasma membrane vitamin B6 transporter of Saccharomyces cerevisiae. *J Biol Chem* **278**: 18990–18996.

Su, Y., Seguinot, P., Sanchez, I., Ortiz-Julien, A., Heras, J.M., Querol, A., et al. (2020) Nitrogen sources preferences of non-*Saccharomyces* yeasts to sustain growth and fermentation under winemaking conditions. *Food Microbiol* **85**:.

Tronchoni, J., Rozès, N., Querol, A., and Guillamón, J.M. (2012) Lipid composition of wine strains of *Saccharomyces kudriavzevii* and *Saccharomyces cerevisiae* grown at low temperature. *Int J Food Microbiol* **155**: 191–198.

Wang, Q.-M., Liu, W.-Q., Liti, G., Wang, S.-A., and Bai, F.-Y. (2012) Surprisingly diverged populations of *Saccharomyces cerevisiae* in natural environments remote from human activity. *Mol Ecol* **21**: 5404–17.

Will, J.L., Kim, H.S., Clarke, J., Painter, J.C., Fay, J.C., and Gasch, A.P. (2010) Incipient balancing selection through adaptive loss of aquaporins in natural *Saccharomyces cerevisiae* populations. *PLoS Genet* **6**:.

Yuasa, N., Nakagawa, Y., Hayakawa, M., and Iimura, Y. (2004) Distribution of the sulfite resistance gene SSU1-R and the variation in its promoter region in wine yeasts. *J Biosci Bioeng* **98**: 394–397.

General discussion

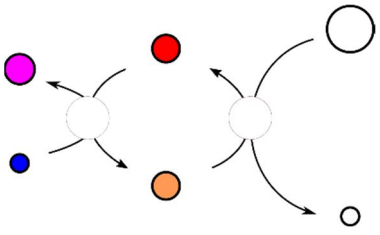

General discussion

S. cerevisiae, as a model organism in biology and the main species employed in winemaking, benefits from an extensive bibliography due to the many years of investigation that have been attributed to it. In this context, the metabolism of *S. cerevisiae* wine strains under fermentative conditions is well described since it has been and continues to be subject of intensive research. Besides *S. cerevisiae, S. uvarum* and *S. kudriavzevii* species have recently received the special attention of the wine research sector for their attractive oenological properties (Querol *et al.*, 2018). However, the existing data regarding the specificity of their metabolism in winemaking conditions are still scarce, while it is relevant to design new utilization strategies of these alternative yeast species. Similarly, while *S. cerevisiae* is also a widespread species in nature, most of the metabolic studies have focused the metabolism of *S. cerevisiae* wine strains. Therefore, getting a deeper knowledge of the fermentative metabolism of these alternative species, as well as that of non-wine strains of *S. cerevisiae*, was the focus of this thesis.

During wine fermentation, yeast cells continuously adapt their metabolism to cope with the environmental variations occurring at the different phases of the fermentation. Consequently, neither exogenous nutrients are consumed, nor fermentation by-products are produced continuously over time, but they are consumed and/or produced at varying rates over time according to their relevance in the

yeast metabolism (e.g. building blocks, precursor metabolites, cofactors, etc.), the environmental conditions, the anabolic requirement of the cell, the redox status, and the regulatory mechanisms. In view of this, a common objective of all the chapters of this thesis was to capture and understand specific variations over time in the fermentative metabolism of *S. cerevisiae*, *S. uvarum,* and *S. kudriavzevii* species, whether using a metabolic, transcriptomic, or *in silico* approach.

In **chapter 1** and **chapter 2** of this thesis, we used an experimental design based on the combined analysis of on-line recorded key environmental parameters in oenology (e.g. dissolved oxygen in grape must and carbon dioxide released), with that of the dynamic of intra- and extracellular metabolomes over time of yeasts, at 12 °C and 25 °C, in batch cultures. This enabled us to capture specific metabolic behaviors of representative strains of *S. cerevisiae*, *S. uvarum,* and *S. kudriavzevii* under conditions illustrative of industrial fermentation, while ultimately trying to discern intra-specific metabolomic strategies between low (12 °C) and high temperature (25 °C). Overall, among our set of *S. cerevisiae*, *S. uvarum,* and *S. kudriavzevii* strains, we observed important differences in the dynamic of their intra- and extracellular metabolomes at the beginning (when oxygen was still available) and during the fermentation process, once exogenous nitrogen sources were depleted. Additionally, the differences observed in the yields and the timing of the production of several by-products contributing to

redox homeostasis other than ethanol (e.g. glycerol, succinate, and 2.3 butanediol) among the strains of the three species, were indicative of differential redox balancing strategies. Finally, when comparing the global fermentation performances at low and high temperatures of the *S. uvarum* (BMV58) and *S. kudriavzevii* (CR85) strains used in **chapter 1** and **chapter 2**, we were not in measure to identify clear temperature dependent changes at the metabolic levels beyond variations in aroma profiles or in the yield of some other fermentative by-product, excluding ethanol. Without doubt, the transcriptomic study we are currently working on, using RNAseq samples of *S. uvarum* and *S. kudriavzevii* during the batch culture performed at 12 °C and 25 °C, will help us to determine some temperature dependent changes. On the contrary, regarding the wine *S. cerevisiae* strain T73, we have managed to identify some of them in **chapter 4**, as explained below.

A relevant metabolic and technological feature that we captured in **chapter 1** and **chapter 2** is, without doubt, the "production and consumption" profile of acetate in *S. uvarum* strains at 12 °C and 25 °C and in the *S. kudriavzevii* strain CR85 at 25 °C. Shortly after publishing this result, another group also reported this striking phenotype in another strain of *S. uvarum* (Kelly *et al.*, 2020), but they did not give any further details regarding the intracellular fate of this metabolite. In this regard, in **chapter 2** we provided intracellular evidence that acetate, once incorporated, could be used for acetyl CoA synthesis, used for lipid biosynthesis, probably for membrane remodeling in *S.*

uvarum strain BMV58. Moreover, this metabolic trait was correctly predicted in both *S. uvarum* strains BMV58 and CECT12600 at 25 °C and associated with mevalonate biosynthesis after implementing the genome-scale metabolic model that we developed in **chapter 3**. This characteristic of *S. uvarum* strains to produce and then consume acetate, regardless of temperature, is particularly interesting and could be deeper investigated in the context of reducing the volatile acidity of wines. In the case of *S. kudriavzevii* strain, as this phenomenon was only observed at 25 °C, and the final content of acetate in wine was still significantly higher than in must fermented with *S. cerevisiae* strain T73, this species represents a less promising alternative than *S. uvarum* for acetate reduction.

Likewise, we first evidenced the production of erythritol, a pentose phosphate pathway derivative, by three *Saccharomyces* species under wine fermentation. An interesting feature of erythritol synthesis is that the extracellular detection does not start until the exogenous nitrogen sources had been exhausted by our *S. cerevisiae*, *S. kudriavzevii,* and *S. uvarum* strains. This common timing of production underlines the tight connection existing between central carbon and nitrogen metabolisms among *S. cerevisiae*, *S. uvarum,* and *S. kudriavzevii* species. A plausible explanation is that, in the absence of exogenous amino acids to be catabolized and still in the presence of a great quantity of exogenous sugars to be fermented, the fraction of glycolytic flux that is required to provide alpha ketoglutarate as amine

group receiver becomes less necessary. Consequently, in order to not accumulate alpha ketoglutarate and to alleviate downstream glycolysis, part of this glycolytic flux could be temporarily shuttled towards the pentose phosphate pathway, ultimately leading to erythritol formation from eryhtrose-4-phosphate. This hypothetical scenario could be even more pronounced in *S. uvarum* strains. Indeed, in this species, a major carbon flux through the pentose phosphate pathway is in accordance with its greater erythritol synthesis but also with its nature to produce high levels of 2-phenylethanol and 2-phenylethyl acetate *de novo* from its precursors erythrose-4-phosphate and PEP. This is in line with the results obtained Cadière *et al.* (2011) with the evolutionary engineered *S. cerevisiae* ECA5 strain, with increased *in vivo* flux through the pentose phosphate pathway. Because of its interest in the food industry as a low-calorie sweetener, some aspects of erythritol biosynthesis have already been explored and optimized (by transgenesis) in yeasts, but only in other genera different to *Saccharomyces* (Moon *et al.*, 2010). In this aspect, by using a genomic and mutagenesis approach, we are currently trying to identify which gene(s) are involved in the biosynthesis of erythritol from erythrose-4-phosphate in *Saccharomyces* species and to determine which are the mechanisms responsible for its production.

In **chapter 3** we developed a genome-scale model able to describe carbon and nitrogen metabolisms of yeast in batch cultures, in combination with a refined multi-phase multi-objective flux balance

analysis to successfully predict metabolism and biomass dynamics. For instance, beyond ATP we incorporated the production of protein as a cellular objective, and also introduced protein turnover to model amino acids homeostasis during the stationary phase. So far, we have used this model with data from *S. cerevisiae* (T73) and *S. uvarum* (BMV58 and CECT12600) fermentations at 25 °C, but we are presently working with the values obtained from batch cultures with *S. kudriavzevii* strain (CR85), and also at 12 °C, which would help us to increase our understanding of their metabolism at a cooler temperature and to discriminate temperature dependent differential flux distribution. When implementing the model with the values of *S. cerevisiae* (T73) and *S. uvarum* (BMV58 and CECT12600), the distribution of intracellular fluxes predicted by the model were consistent with most of the intra- and extracellular phenotypes observed in *S. uvarum* strains in **chapter 1**, and **chapter 2**, whether it was at the level of primary carbon and nitrogen metabolism, or that of secondary metabolism, like fermentative aromas. We confirmed that strains of *S. uvarum* differ from *S. cerevisiae* in the way that they redistribute carbon flux towards the production of fermentative by-products involved in redox homeostasis (e.g. succinate, 2.3 butanediol and glycerol). We also reaffirmed that acetate consumed by *S. uvarum* strains could serve for lipids biosynthesis through its incorporation into mevalonate. An important result of this chapter was that, besides the reductive branch of the TCA cycle, the GABA shunt highly

contributes to the synthesis of succinate and NADPH equivalents in *S. uvarum* strains during alcoholic fermentation, especially during the stationary phase. From the entry into the stationary phase, the model also predicted a higher flux through the non-oxidative branch of the pentose phosphate pathway in *S. uvarum* species. In line with the results of **chapter 1** and **chapter 2**, although erythritol was not contemplated in this version of the model (it will be in a future version), this prediction made by the model is concordant with the hypothesis presented above regarding the contribution of the pentose phosphate pathway in the higher erythritol yield found in *S. uvarum* and clarifies which of the two branches (oxidative or non-oxidative) could be the largest contributor for this phenotype in the cryotolerant species.

In the last chapter of this thesis (**chapter 4**), we used the same approach employed in **chapter 1** and **chapter 2** in combination with a transcriptomic analysis to deeply investigate the metabolomic and transcriptomic response at 12 °C and 25 °C of two *S. cerevisiae* strains: one from winemaking environment (T73) and the other isolated from oak tree (YPS128). We identified several gene expression and metabolite variations in the *S. cerevisiae* wine industrial strain that could contribute to its differential fermentative behavior compared to a genetically differentiated strain adapted to the wild environment. First, the up-regulation of most of the genes of the sulfur assimilation pathway as well as those of the phospholipids' biosynthetic pathway

at 12 °C in the wine strain correlate well with the higher levels of several key metabolites, including S-adenosylmethionine, reduced glutathione, and various phospholipids. Altogether, these transcriptomic and metabolomic results confirmed the previously proposed hypothesis (García-Ríos *et al.*, 2014) that this combined up-regulation is an adaptation mechanism to low temperatures, specific of *S. cerevisiae* wine strains.

A second striking observation that we made in **chapter 4** was that most of the genes of the arginine biosynthetic pathway were up-regulated in the *S. cerevisiae* wine strain regardless of the temperature at the end of the growth phase, indicating the existence of *de novo* synthesis of arginine at this stage of the process. This is quite surprising given that other authors have clearly shown that arginine is transiently stored inside the vacuole before being used as nitrogen donor at the end of the growth phase, and that more than 96% of proteinogenic arginine comes from the direct incorporation of exogenous arginine in *S. cerevisiae* wine strain (Crépin *et al.*, 2017). Therefore, considering that the anabolic requirements of arginine at this stage of the process are low, that several genes encoding arginine-specific vacuolar transporters were overexpressed synchronously with those of its biosynthetic pathway, and that glutamate and glutamine are two main precursors of arginine biosynthesis, we hypothesized that it could be a regulation mechanism for storage and redistribution of nitrogen from central nitrogen metabolism in the form of arginine in the *S.*

cerevisiae wine strain during the transition from the exponential growth to stationary phase. This is in line with a recent work (Cools *et al.*, 2020) describing the regulation of arginine vacuolar transporters when yeast cells are starved of nitrogen.

Finally, the dual omics analysis used in **chapter 4** also shows that the higher intracellular levels of thiamine diphosphate found in the *S. cerevisiae* wine strain corroborate with the up-regulation of the genes involved in its biosynthetic pathway, and also with the longer viability and fermentative ability of the wine strain. Given the essential role of thiamine diphosphate as a cofactor of key glycolytic and pentose phosphate pathway enzymes (Perli *et al.*, 2020), we assumed that the up-regulation of the thiamine biosynthetic pathway may allow the wine strain to sustain the TDP requirements of the cell during alcoholic fermentation, in particular after nitrogen starvation.

To recapitulate, in this work we applied different omics technologies and a mathematical modeling approach to better understand how some representative strains of *S. cerevisiae*, *S. uvarum,* and *S. kudriavzevii* species metabolically behaved during wine fermentation. We explored the dynamic of their central carbon but also nitrogen metabolisms in conditions representative of winemaking fermentation, i.e. in batch culture mode. We found a variety of metabolic traits of industrial interest in the cryotolerant species *S. uvarum* and *S. kudriavzevii,* and also gained new insights into the

metabolic and transcriptomic response of wine and non-wine strain of *S. cerevisiae* that could explain their differential fermentative behavior. Besides, we developed a genome scale metabolic model applicable to yeast batch culture, which represents an important computational tool for the wine research sector that can be used whether to prospect phenotypic traits or metabolically engineer novel yeast cell factories. Because of their biotechnological relevance, several of the metabolic features identified in this thesis (e.g. erythritol synthesis, acetate production and consumption by *S. uvarum* y *S. kudriavzevii* species, contribution of the GABA shunt to succinate and stress response in *S. uvarum* species, arginine management by *Saccharomyces* species) are currently further explored in our laboratory or in collaboration with other groups, by using transcriptomic, genetical modifications, isotopic tracer approaches or our genome scale metabolic model.

Cadière, A., Ortiz-Julien, A., Camarasa, C., and Dequin, S. (2011) Evolutionary engineered *Saccharomyces cerevisiae* wine yeast strains with increased in vivo flux through the pentose phosphate pathway. *Metab Eng* **13**: 263–271.

Cools, M., Lissoir, S., Bodo, E., Ulloa-Calzonzin, J., DeLuna, A., Georis, I., and André, B. (2020) Nitrogen coordinated import and export of arginine across the yeast vacuolar membrane. *PLoS Genet* **16**:.

Crépin, L., Truong, N.M., Bloem, A., Sanchez, I., Dequin, S., and Camarasa, C. (2017) Management of multiple nitrogen sources during wine fermentation by Saccharomyces cerevisiae. *Appl*

Environ Microbiol **83**:.

García-Ríos, E., López-Malo, M., and Guillamón, M.M. (2014) Global phenotypic and genomic comparison of two Saccharomyces cerevisiae wine strains reveals a novel role of the sulfur assimilation pathway in adaptation at low temperature fermentations. *BMC Genomics* **15**: 1059.

Kelly, J.M., van Dyk, S.A., Dowling, L.K., Pickering, G.J., Kemp, B., and Inglis, D.L. (2020) Saccharomyces uvarum yeast isolate consumes acetic acid during fermentation of high sugar juice and juice with high starting volatile acidity. *Oeno One* **54**: 199–211.

Moon, H.J., Jeya, M., Kim, I.W., and Lee, J.K. (2010) Biotechnological production of erythritol and its applications. *Appl Microbiol Biotechnol* **86**: 1017–1025.

Perli, T., Wronska, A.K., Ortiz-Merino, R.A., Pronk, J.T., and Daran, J.M. (2020) Vitamin requirements and biosynthesis in Saccharomyces cerevisiae. *Yeast* **37**: 283–304.

Querol, A., Pérez-Torrado, R., Alonso-del-Real, J., Minebois, R., Stribny, J., Oliveira, B.M., and Barrio, E. (2018) New Trends in the Uses of Yeasts in Oenology. In *Advances in Food and Nutrition Research*. pp. 177–210.

Conclusions

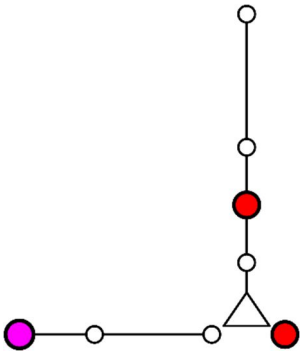

1. The variations existing between our representative strains of *S. cerevisiae*, *S. uvarum* and *S. kudriavzevii* in the yields of fermentative by-products affecting NADH/NAD+ ratios other than ethanol, suggest that these three species use different metabolic strategies to maintain redox homeostasis across alcoholic fermentation.

2. The presence of dissolved oxygen during the first hours of an alcoholic fermentation differentially influenced the carbon and nitrogen metabolisms of our set of *S. cerevisiae, S. uvarum* and *S. kudriavzevii* strains, indicating that they could have a transient respiro-fermentative metabolism at this stage of the process.

3. Beyond variations in their aroma profile and in the yield of some fermentative by-products, excluding ethanol, no clear intra-specific metabolic differences were found between low and high fermentation temperatures in the *S. uvarum* and *S. kudriavzevii* strains that we characterized. Application of the genome-scale metabolic model that we developed with the metabolome values of *S. kudriavzevii* at 12 °C and 25 °C, and that of *S. uvarum* at 12 °C will undoubtedly help us to discern them.

4. We reported for the first time the synthesis of erythritol, a pentose phosphate pathway polyol derivative, by *Saccharomyces* species under winemaking conditions.

5. Regardless of the species, extracellular detection of erythritol starts after the onset of nitrogen starvation, suggesting that its synthesis might be the result of a common mechanism of

carbon flux readjustment from glycolysis to the pentose phosphate pathway to alleviate downstream glycolysis once exogenous amino acids are not any more catabolized in *S. cerevisiae*, *S. uvarum* and *S. kudriavzevii*.

6. The higher synthesis of erythritol and chorismate derivatives (e.g. 2-phenyl ethanol) by *S. uvarum* strains is concordant with a higher carbon flux through the non-oxidative branch of the pentose phosphate pathway in this species after the onset of nitrogen starvation.

7. The exhaustion of exogenous nitrogen sources triggered the consumption of exogenous acetate by *S. uvarum* strains at 12 °C and 25 °C, and in *S. kudriavzevii* strain at 25 °C.

8. Even though a complementary survey is required to identify the specific molecular and environmental drivers responsible for these phenotypes in both cryotolerant species, intracellular data at 12 °C and genome-scale model prediction converge towards the utilization of consumed acetate by *S. uvarum* strain for lipid biosynthesis.

9. The developed genome scale model is useful to explore the dynamics of batch processes for different yeast species and media. It offers a systematic and rational approach to prospect the metabolism of non-conventional yeast species and engineer novel cell factories.

10. The GABA shunt has an important contribution in the formation of succinate and in the maintenance of

NADPH/$NADP^+$ ratio during the stationary phase in *S. uvarum* strains at 25 °C.

11. Most fusel alcohols are produced *de novo* from sugars by *S. cerevisiae* and *S. uvarum* strains and not from the catabolism of their exogenous amino acids' precursors.

12. The up-regulation of the sulfur assimilation and phospholipids biosynthetic pathways in the wine *S. cerevisiae* strain at 12 °C correlate with higher levels of key metabolites involved in low temperature response, thus confirming it is a specific adaptation mechanism of *S. cerevisiae* wine strains to low temperatures.

13. The coordinated overexpression, regardless of the temperature, of the genes involved in the biosynthesis and vacuolar transport of arginine in the wine strain of *S. cerevisiae* could be related to a storage and redistribution mechanism of nitrogen from the central nitrogen metabolism during the transition from the exponential growth phase to the stationary phase.

14. The greater intracellular availability of thiamine diphosphate, an essential cofactor for many glycolytic and pentose phosphate enzymes, in the *S. cerevisiae* wine strain is likely the result of the over expression of the thiamine biosynthetic genes, ultimately explaining the higher and longer fermentative ability of the wine *S. cerevisiae* strain.

Annex I

Supplementary material

SUPPLEMENTARY MATERIAL - Chapter 1

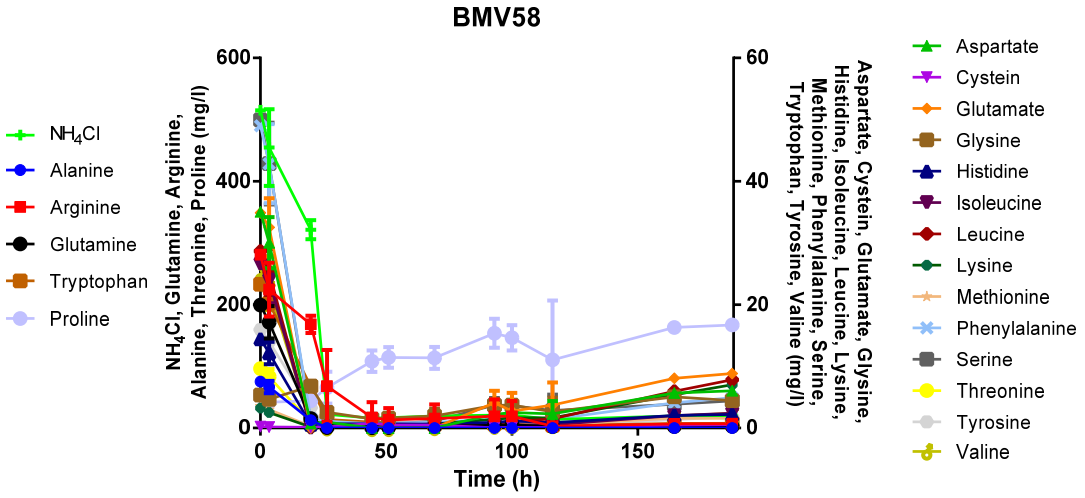

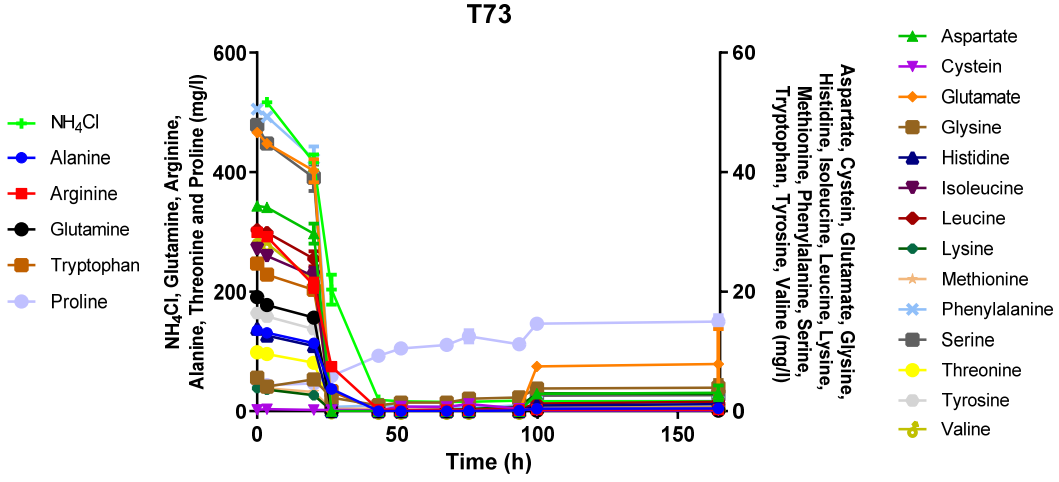

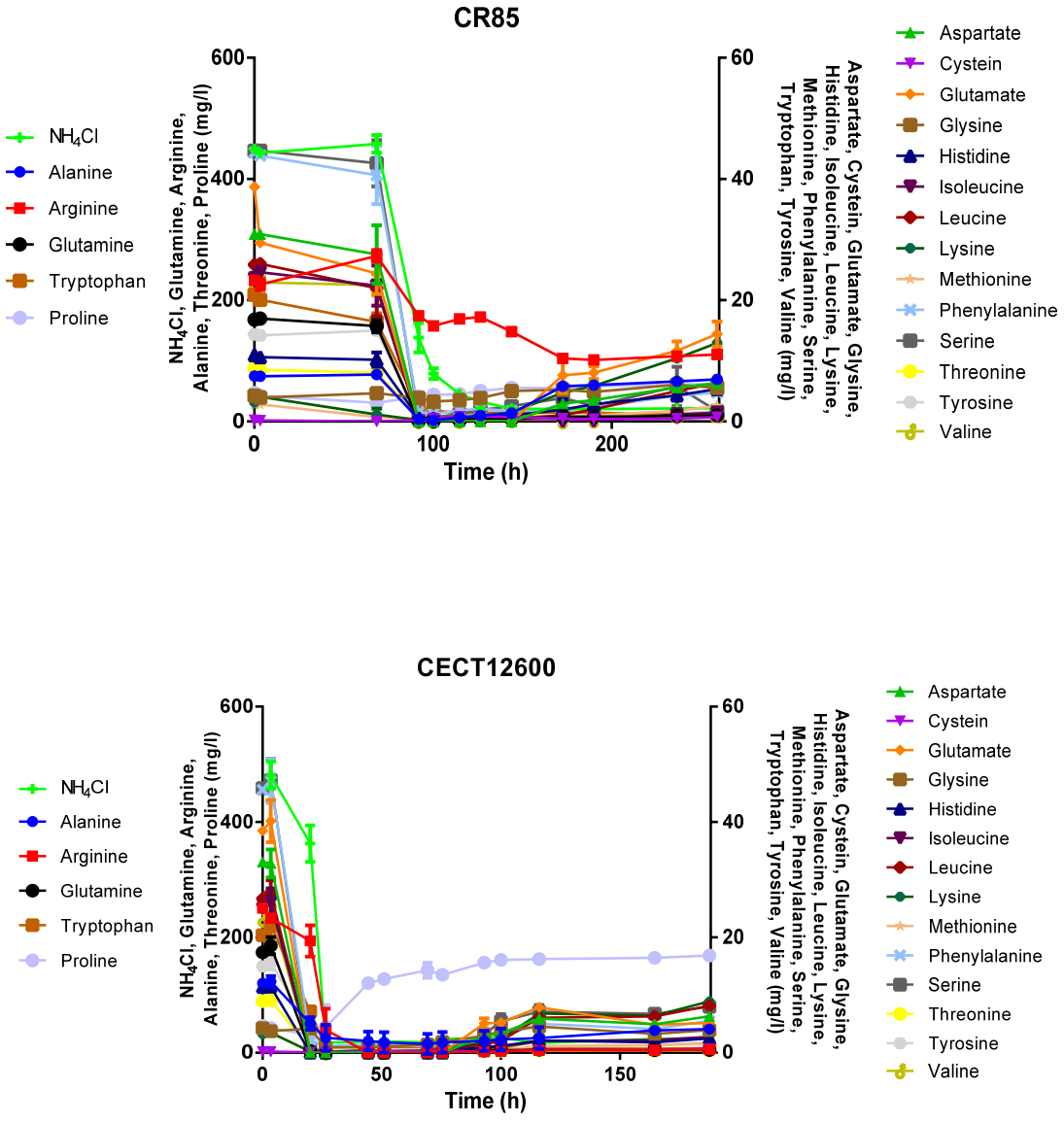

Figure S1. Extracellular amino-acids and ammonium concentration expressed in mg/l along the fermentation process. The values are displayed as mean from triplicate experiments.

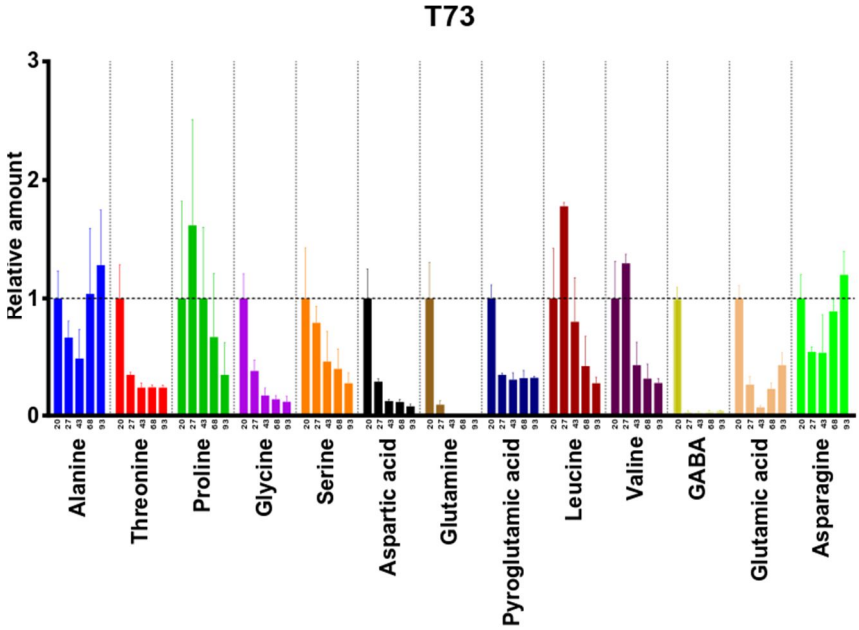
T73
Relative amount
0
1
2
3
Alanine
Threonine
Proline
Glycine
Serine
Aspartic acid
Glutamine
Pyroglutamic acid
Leucine
Valine
GABA
Glutamic acid
Asparagine

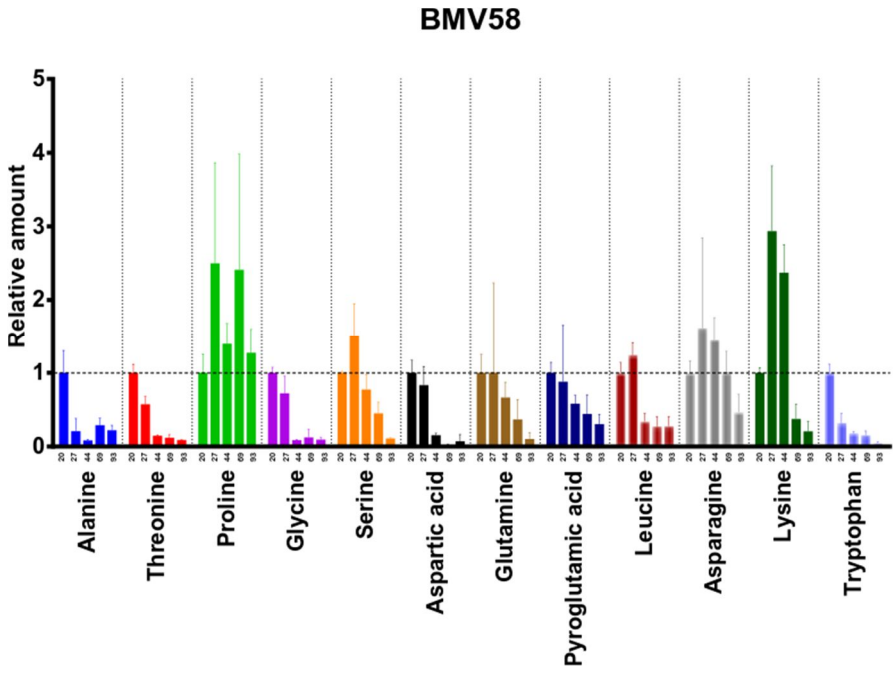
BMV58
Relative amount
0
1
2
3
4
5
Alanine
Threonine
Proline
Glycine
Serine
Aspartic acid
Glutamine
Pyroglutamic acid
Leucine
Asparagine
Lysine
Tryptophan

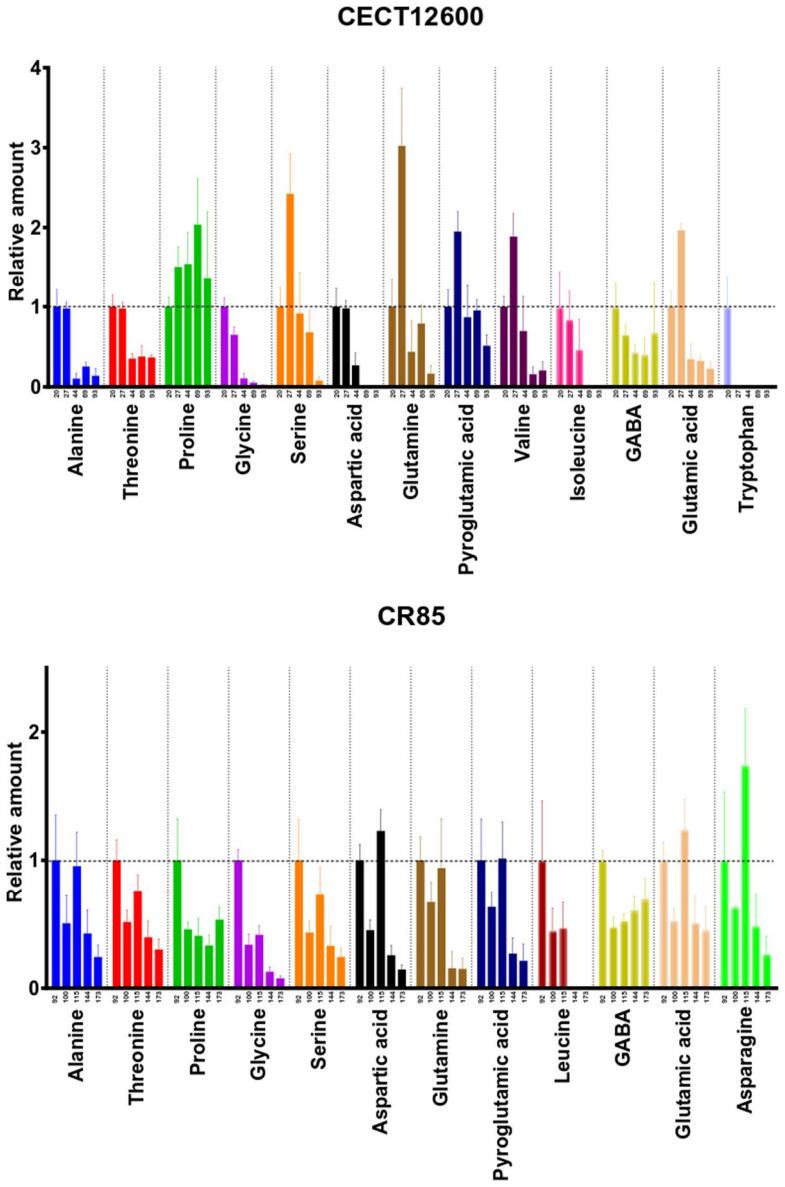

Figure S2. Intracellular level of amino-acids along the fermentation process relative to the first sampling time point. The timing (in hours) of the sampling points is indicated below the x-axis of the graph. The values are displayed as mean from triplicate experiments.

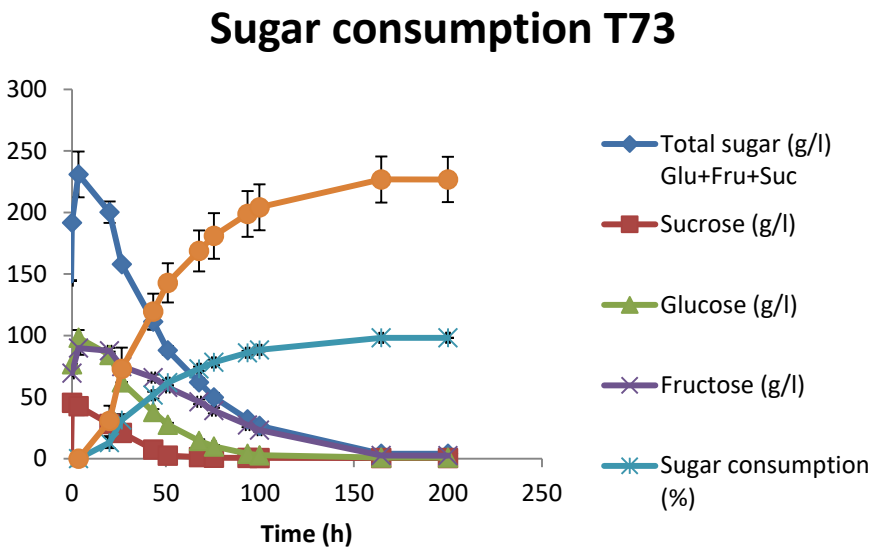
Sugar consumption T73
300
250
200
150
100
50
0
0
50
100
150
200
250
Time (h)
Total sugar (g/l) Glu+Fru+Suc
Sucrose (g/l)
Glucose (g/l)
Fructose (g/l)
Sugar consumption (%)

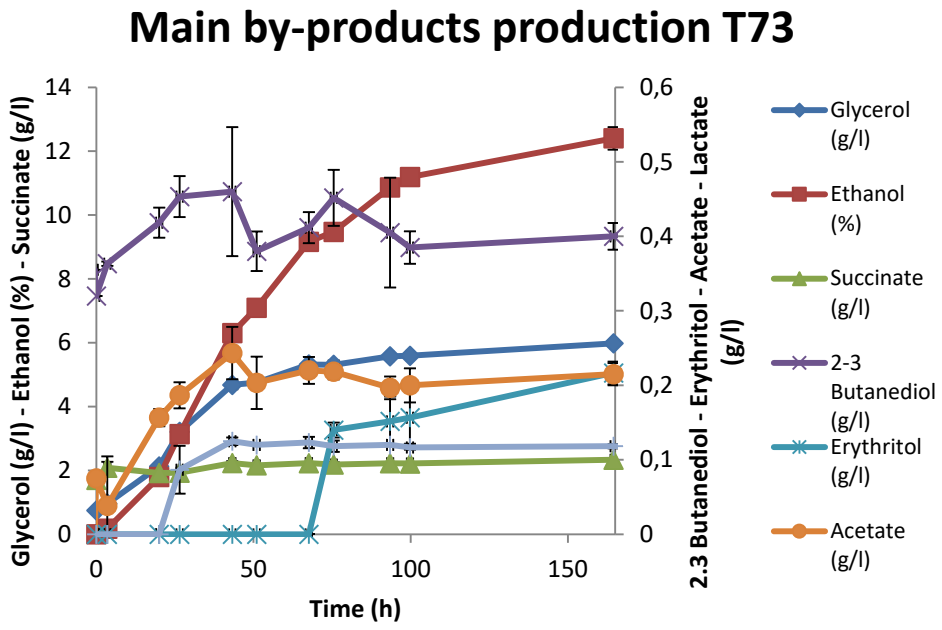
Main by-products production T73
Glycerol (g/l) - Ethanol (%) - Succinate (g/l)
2.3 Butanediol - Erythritol - Acetate - Lactate (g/l)
14
12
10
8
6
4
2
0
0,6
0,5
0,4
0,3
0,2
0,1
0
0
50
100
150
Time (h)
Glycerol (g/l)
Ethanol (%)
Succinate (g/l)
2-3 Butanediol (g/l)
Erythritol (g/l)
Acetate (g/l)

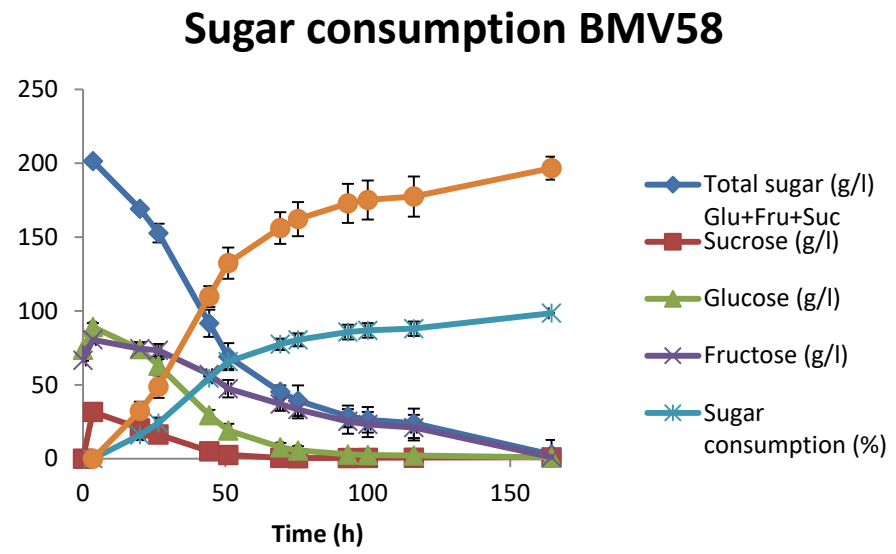
Sugar consumption BMV58
250
200
150
100
50
0
0
50
100
150
Time (h)
Total sugar (g/l) Glu+Fru+Suc
Sucrose (g/l)
Glucose (g/l)
Fructose (g/l)
Sugar consumption (%)

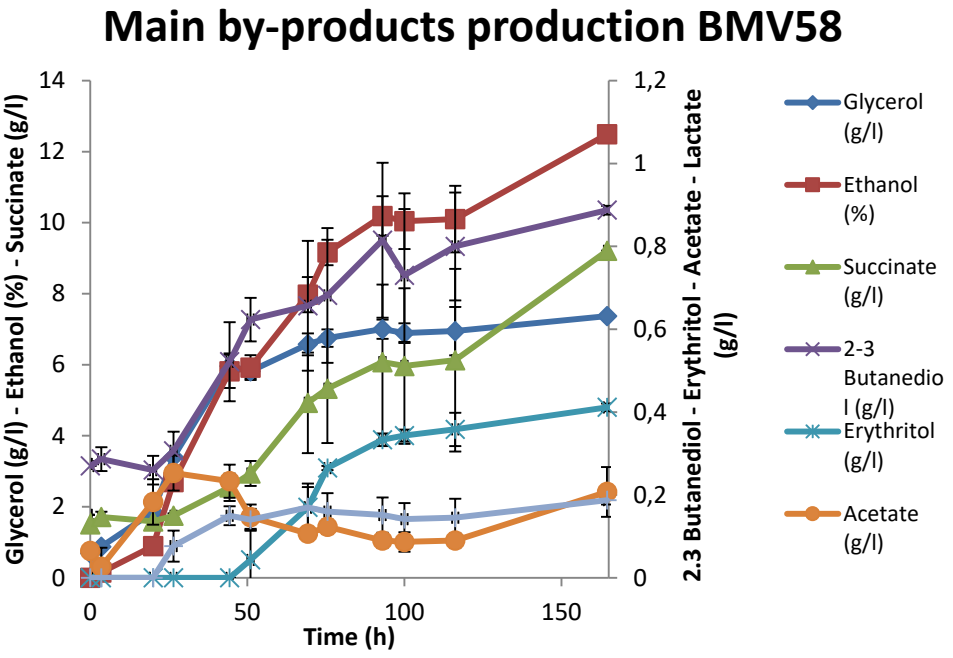
Main by-products production BMV58
Glycerol (g/l) - Ethanol (%) - Succinate (g/l)
2.3 Butanediol - Erythritol - Acetate - Lactate (g/l)
14
12
10
8
6
4
2
0
1,2
1
0,8
0,6
0,4
0,2
0
0
50
100
150
Time (h)
Glycerol (g/l)
Ethanol (%)
Succinate (g/l)
2-3 Butanediol (g/l)
Erythritol (g/l)
Acetate (g/l)

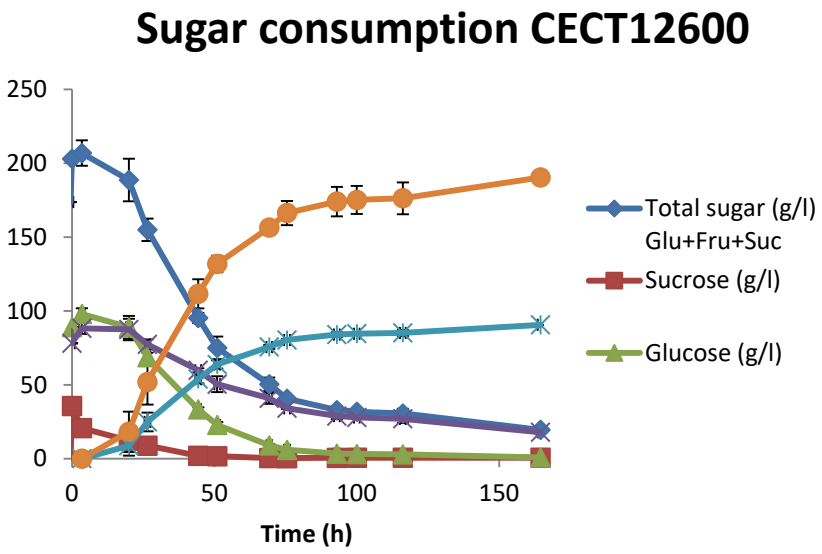
Sugar consumption CECT12600
250
200
150
100
50
0
0
50
100
150
Time (h)
Total sugar (g/l) Glu+Fru+Suc
Sucrose (g/l)
Glucose (g/l)

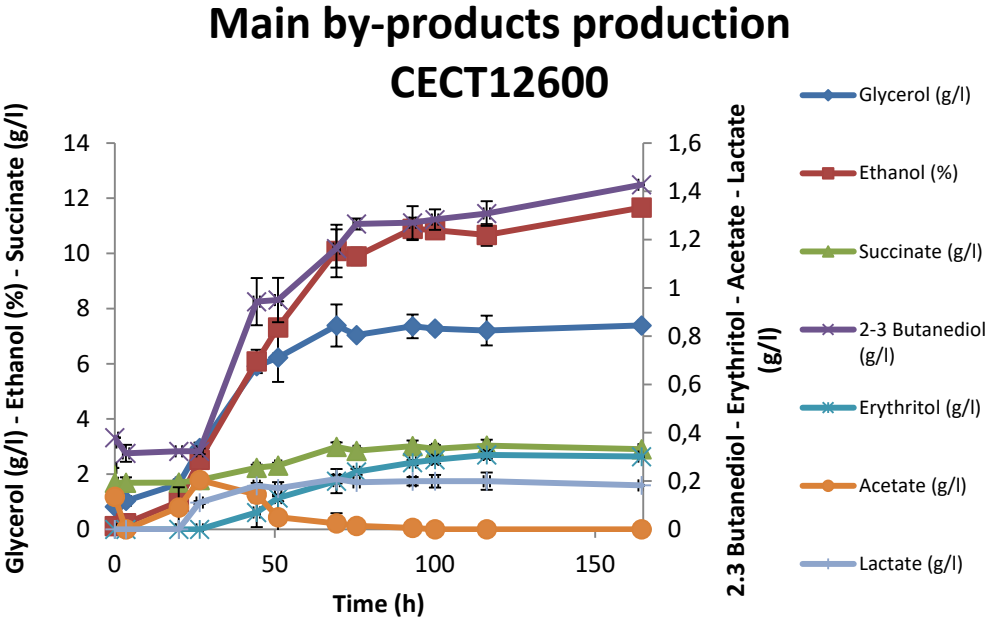
Main by-products production CECT12600
Glycerol (g/l) - Ethanol (%) - Succinate (g/l)
2.3 Butanediol - Erythritol - Acetate - Lactate (g/l)
14
12
10
8
6
4
2
0
1,6
1,4
1,2
1
0,8
0,6
0,4
0,2
0
0
50
100
150
Time (h)
Glycerol (g/l)
Ethanol (%)
Succinate (g/l)
2-3 Butanediol (g/l)
Erythritol (g/l)
Acetate (g/l)
Lactate (g/l)

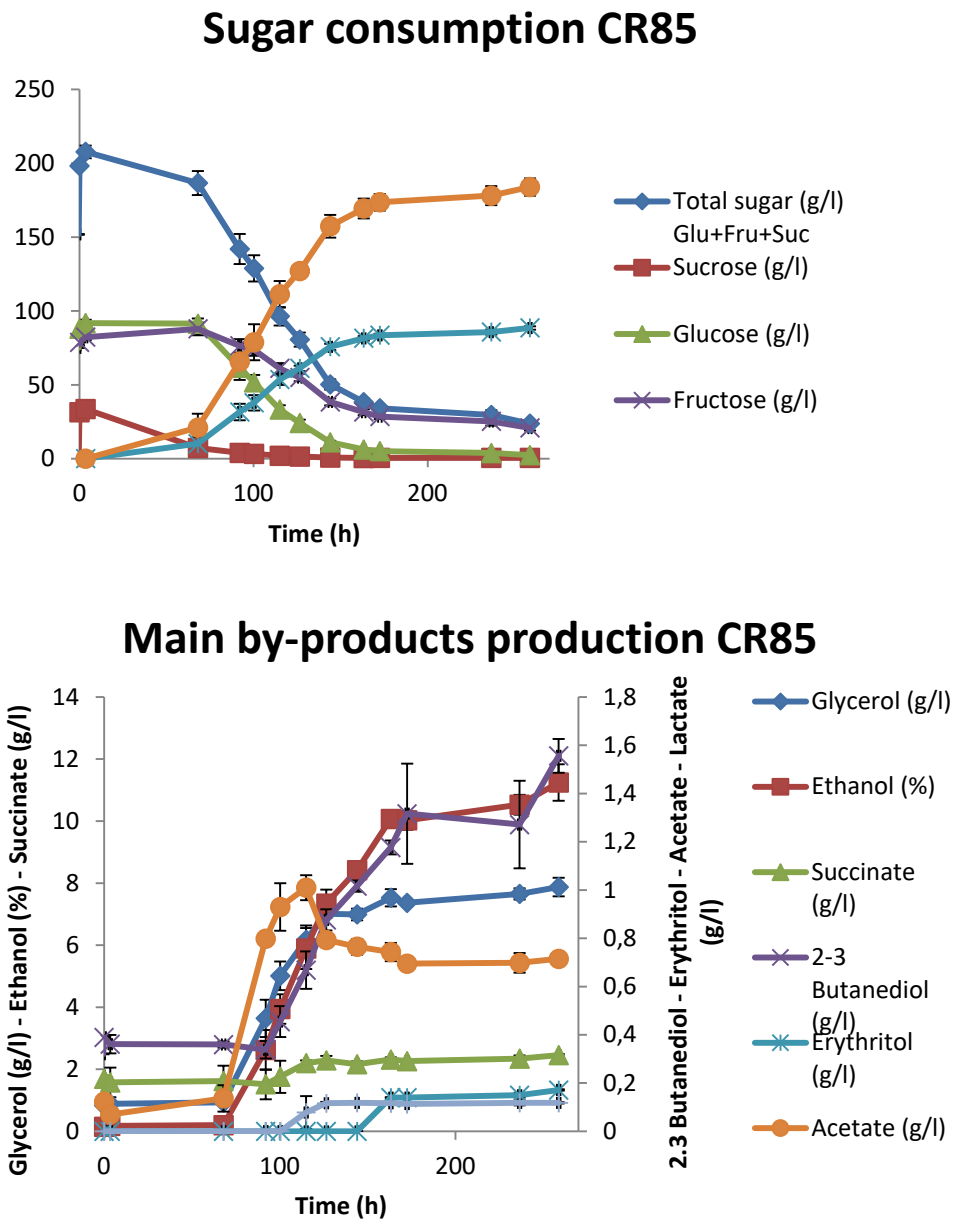

Figure S3. Sugars and main fermentative by-products concentration (g/l) along the fermentation process. The values are displayed as mean and standard deviations from triplicate experiments.

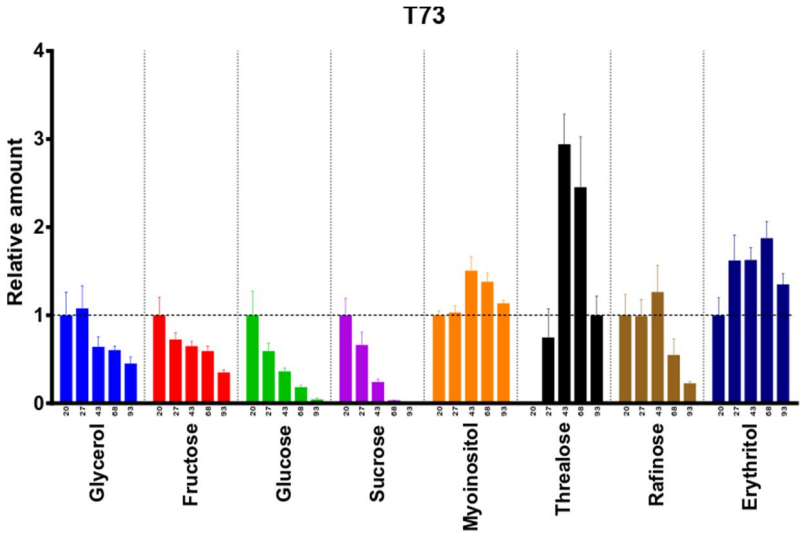
T73
Relative amount
0
1
2
3
4
Glycerol
Fructose
Glucose
Sucrose
Myoinositol
Threalose
Rafinose
Erythritol

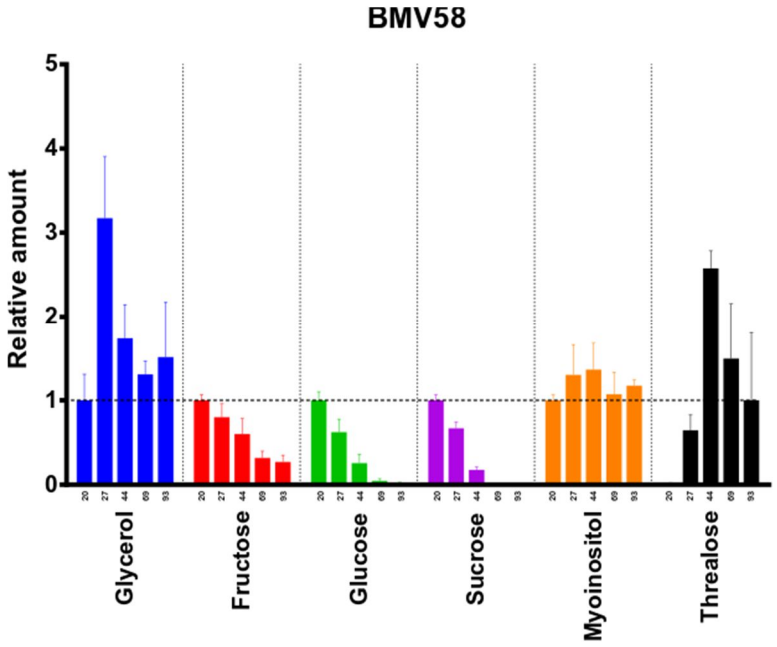
BMV58
Relative amount
0
1
2
3
4
5
Glycerol
Fructose
Glucose
Sucrose
Myoinositol
Threalose

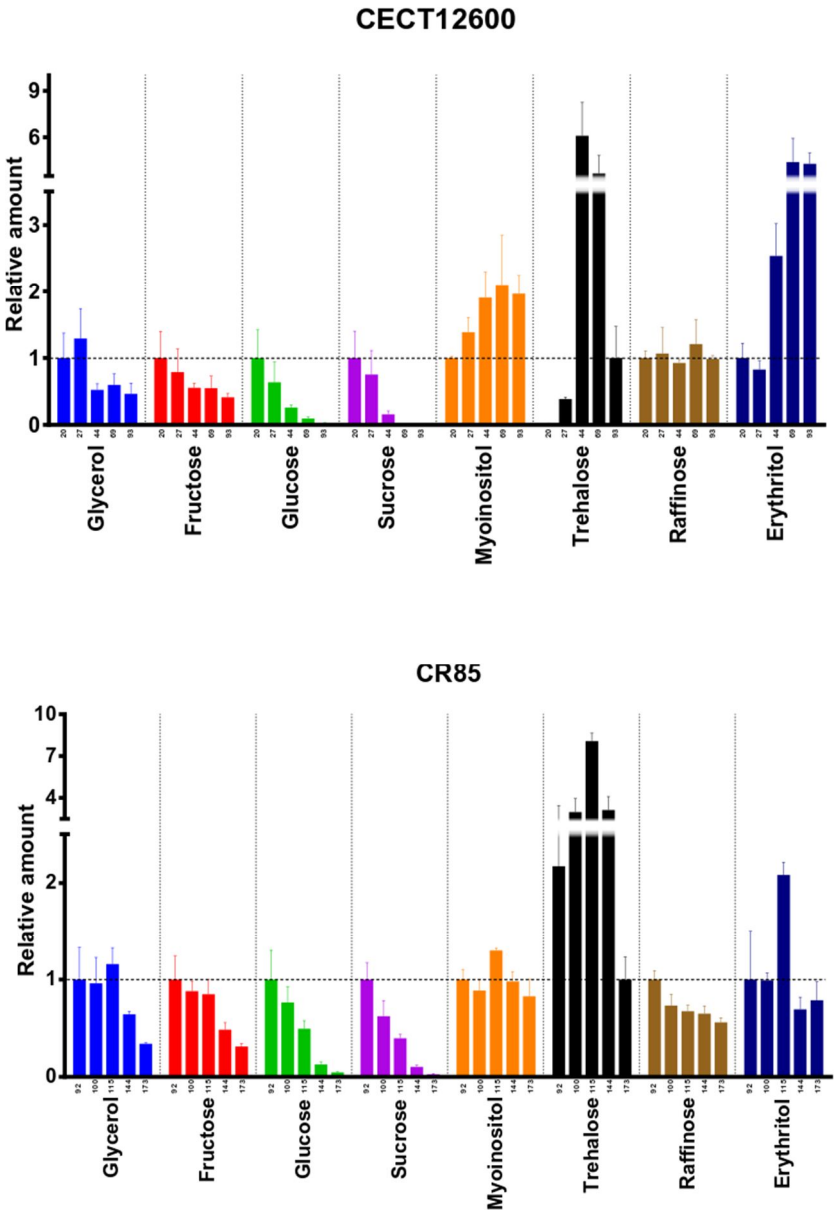

Figure S4. Intracellular level of carbohydrates along the fermentation process relative to the first sampling point. For trehalose, the last sampling point was used as reference. The timing (in hours) of the sampling points is indicated below the x-axis of the graph. The values are displayed as mean from triplicate experiments.

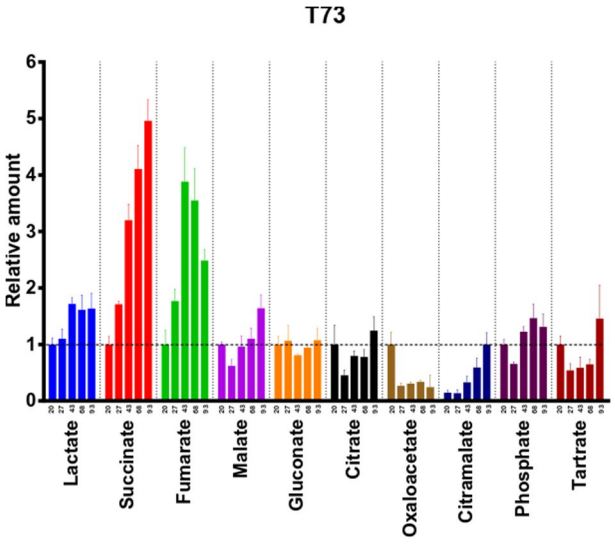
T73
Relative amount
0
1
2
3
4
5
6
Lactate
Succinate
Fumarate
Malate
Gluconate
Citrate
Oxaloacetate
Citramalate
Phosphate
Tartrate

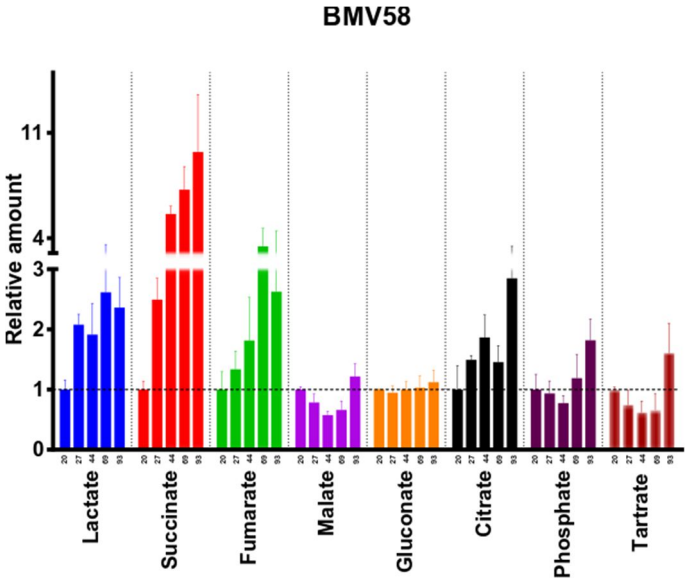
BMV58
Relative amount
0
1
2
3
4
11
Lactate
Succinate
Fumarate
Malate
Gluconate
Citrate
Phosphate
Tartrate

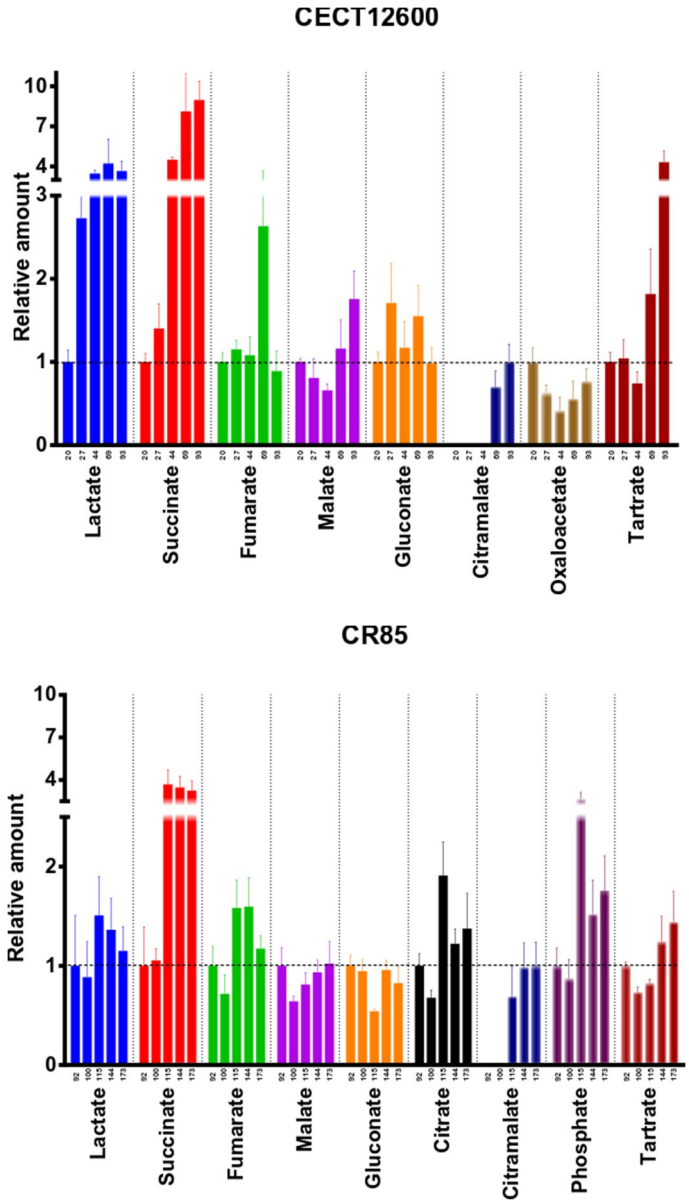

Figure S5. Intracellular level of organic acids along the fermentation process relative to the first sampling point. For citramalate, the last sampling point was used as reference. The timing (in hours) of the sampling points is indicated below the x-axis of the graph. The values are displayed as mean from triplicate experiments.

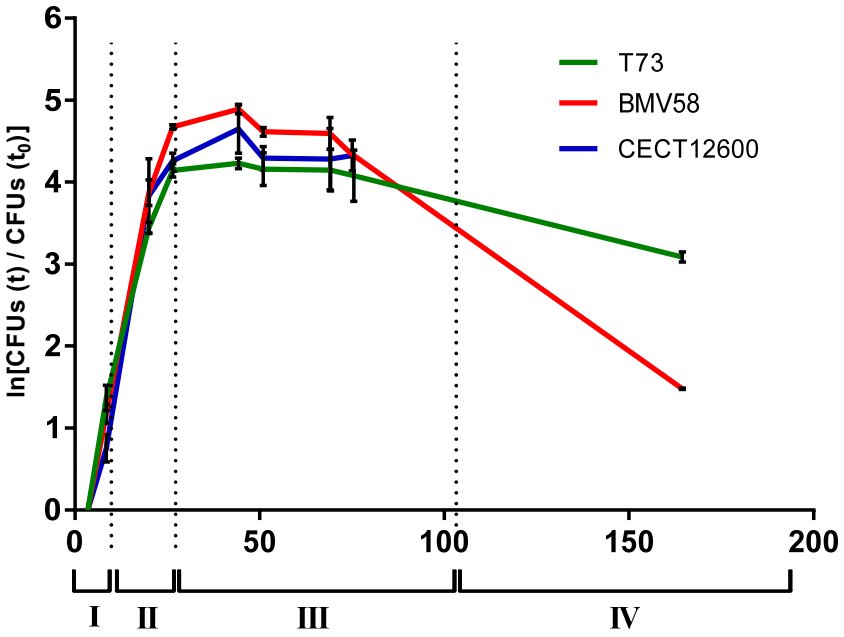

Figure S6. Cell viability along the fermentation process, expressed as natural logarithm of the ratio of the colony forming units at time t (CFUs(t)) by the colony forming units at the time of inoculation (CFUs(t0)). The values are displayed as mean and standard deviations from triplicate experiments. Metabolic phase (I, II, III and IV) are indicated below the x-axis of time expressed in hours.

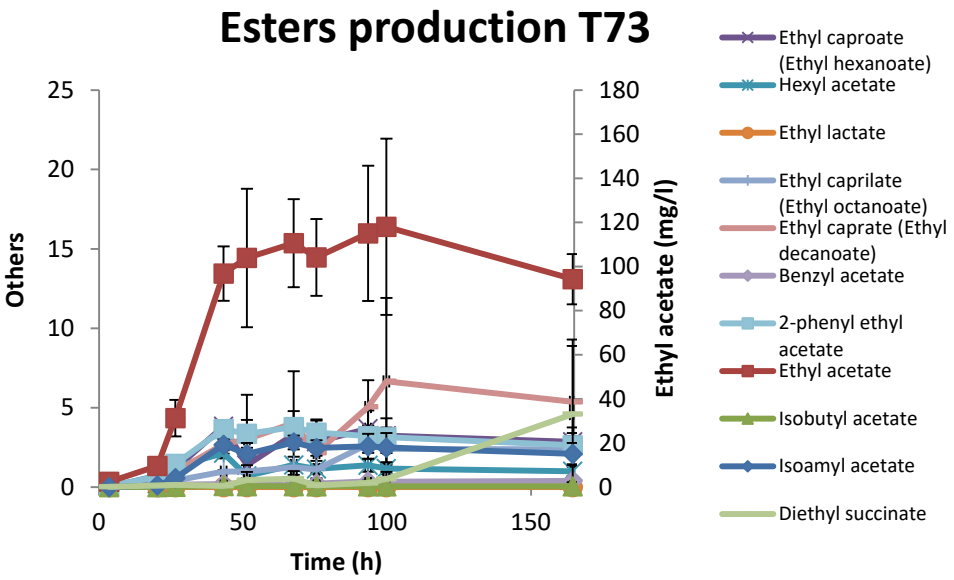
Esters production T73
Others
Ethyl acetate (mg/l)
Time (h)
0
5
10
15
20
25
0
20
40
60
80
100
120
140
160
180
0
50
100
150
Ethyl caproate (Ethyl hexanoate)
Hexyl acetate
Ethyl lactate
Ethyl caprilate (Ethyl octanoate)
Ethyl caprate (Ethyl decanoate)
Benzyl acetate
2-phenyl ethyl acetate
Ethyl acetate
Isobutyl acetate
Isoamyl acetate
Diethyl succinate

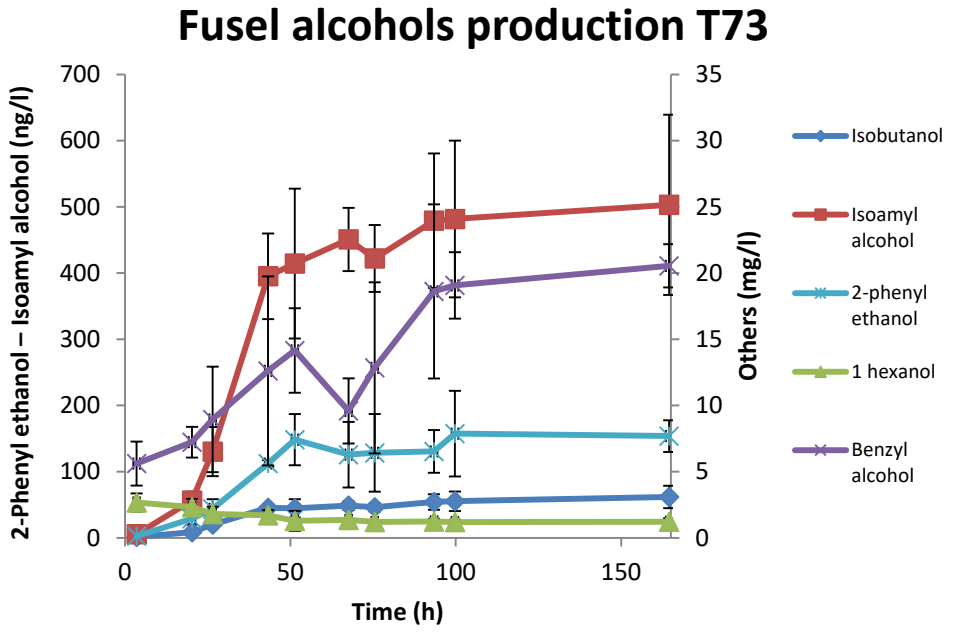
Fusel alcohols production T73
2-Phenyl ethanol – Isoamyl alcohol (ng/l)
Others (mg/l)
Time (h)
0
100
200
300
400
500
600
700
0
5
10
15
20
25
30
35
0
50
100
150
Isobutanol
Isoamyl alcohol
2-phenyl ethanol
1 hexanol
Benzyl alcohol

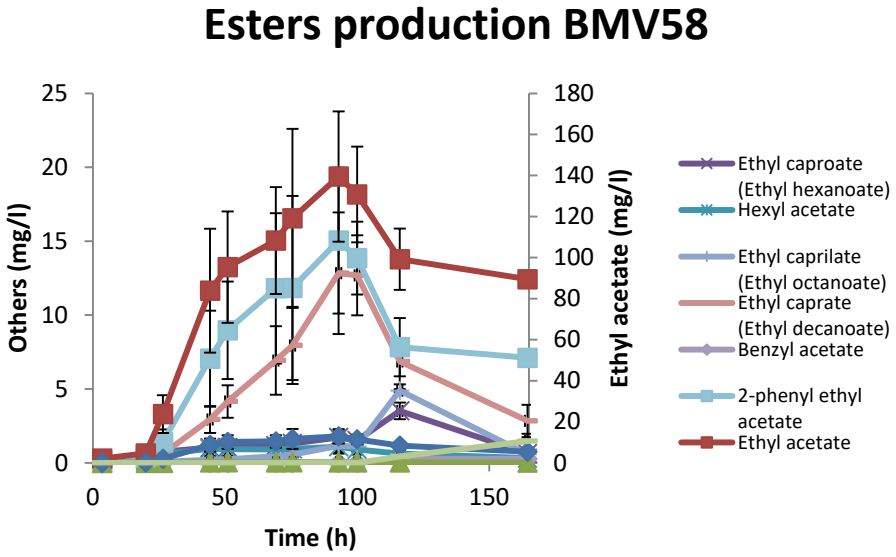
Esters production BMV58
Others (mg/l)
Ethyl acetate (mg/l)
Time (h)
Ethyl caproate (Ethyl hexanoate)
Hexyl acetate
Ethyl caprilate (Ethyl octanoate)
Ethyl caprate (Ethyl decanoate)
Benzyl acetate
2-phenyl ethyl acetate
Ethyl acetate

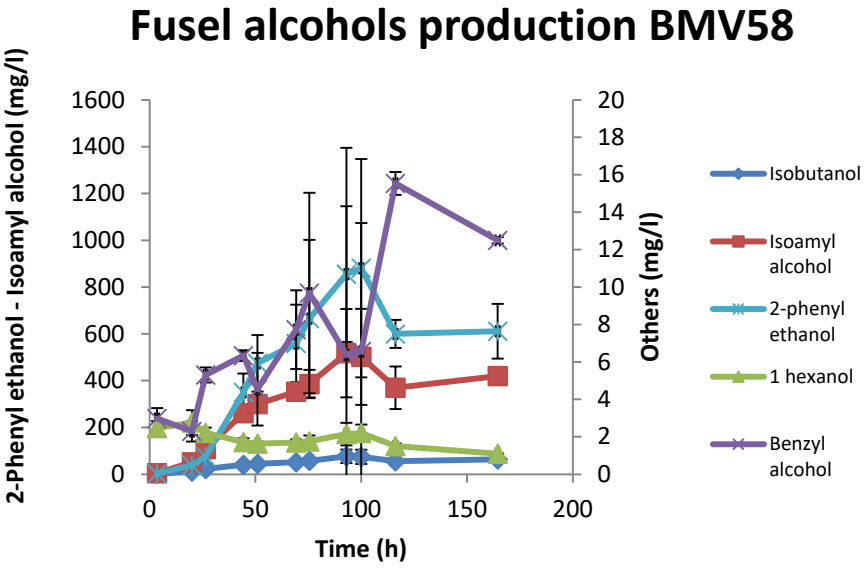
Fusel alcohols production BMV58
2-Phenyl ethanol - Isoamyl alcohol (mg/l)
Others (mg/l)
Time (h)
Isobutanol
Isoamyl alcohol
2-phenyl ethanol
1 hexanol
Benzyl alcohol

Esters production CECT12600

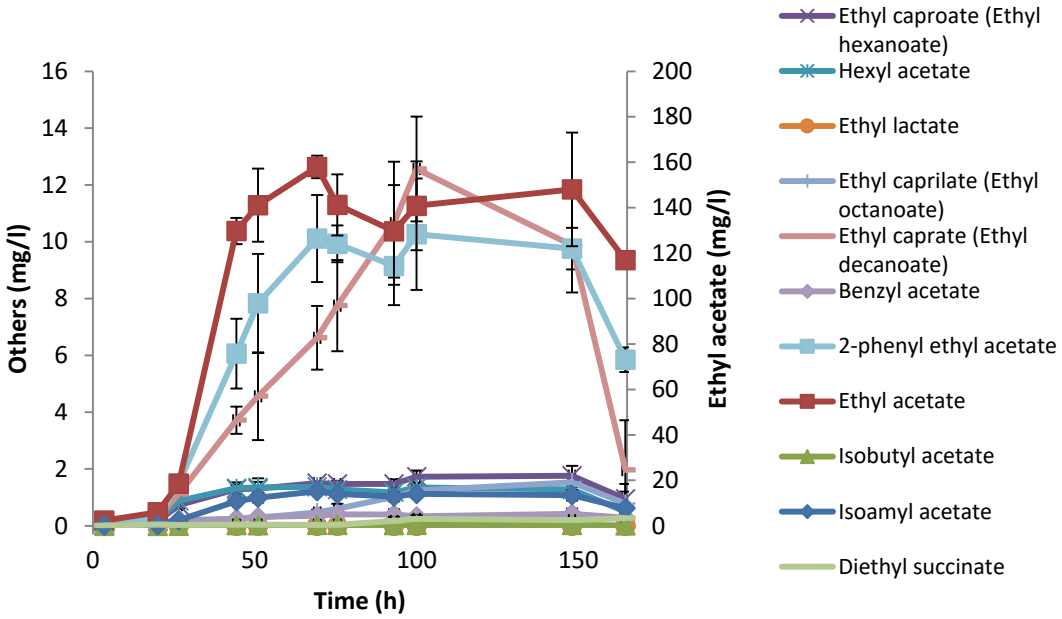

Fusel alcohols production CECT12600

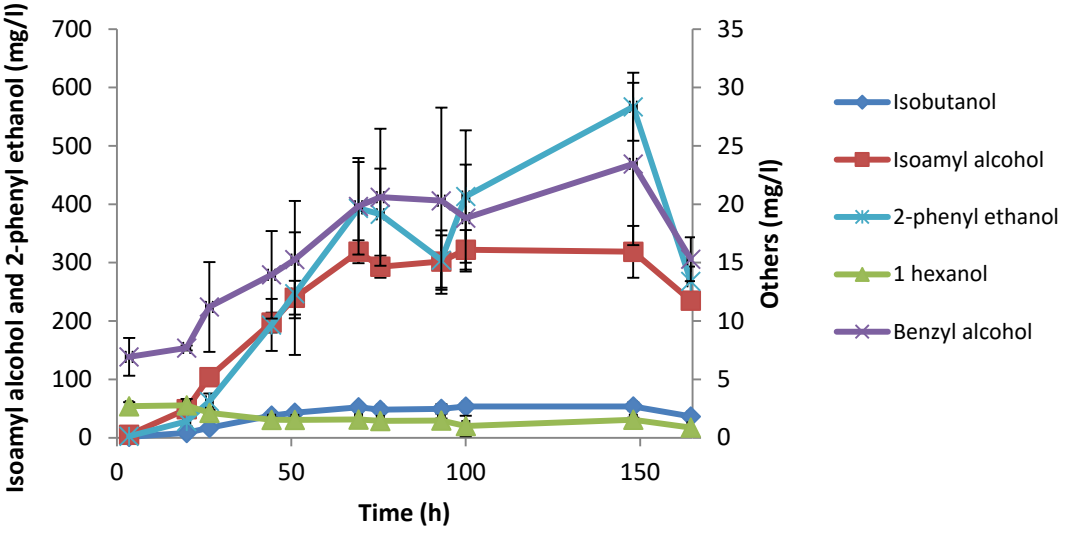

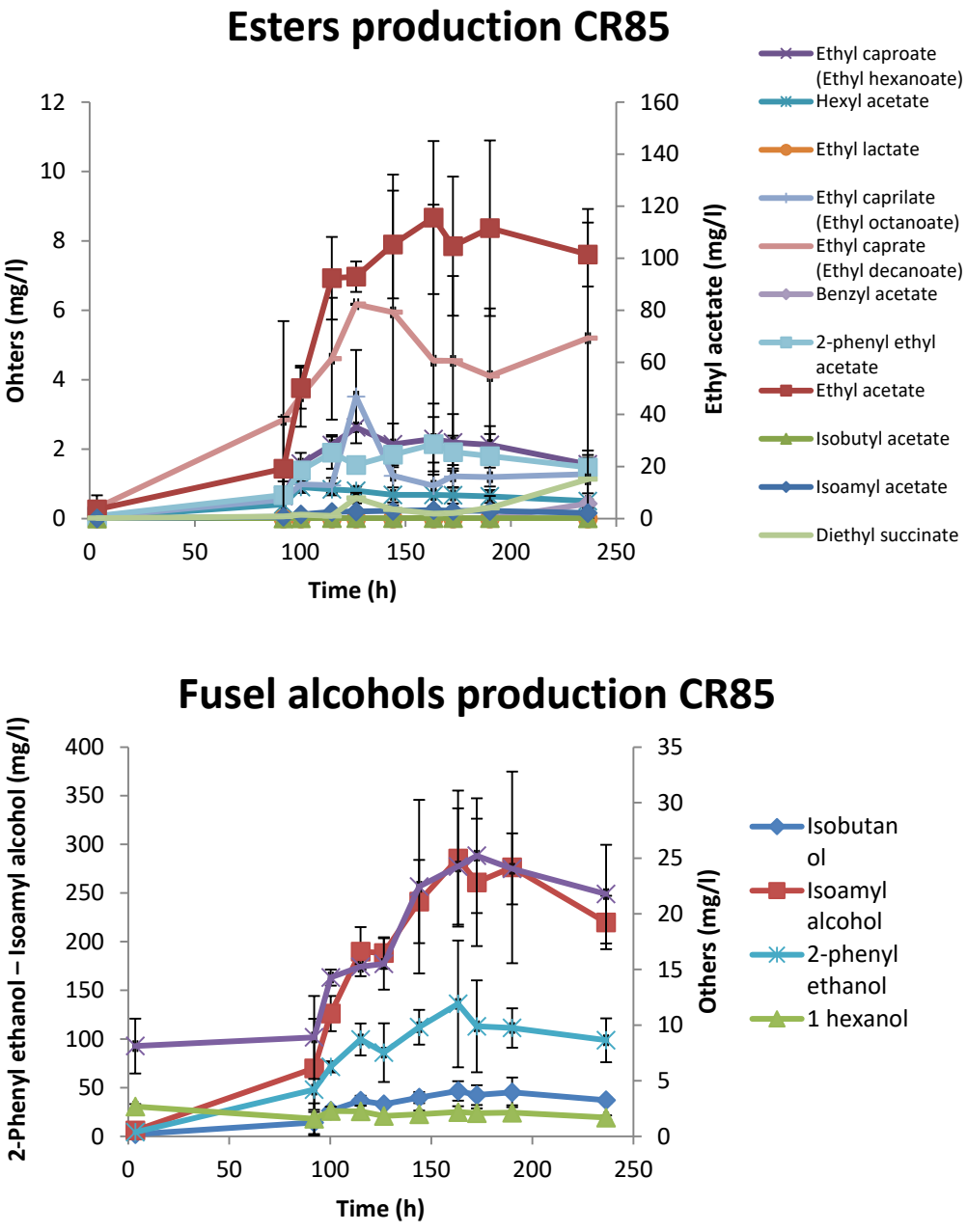

Figure S7. Extracellular aromas compounds concentration (mg/l) along the fermentation process. The values are displayed as mean from triplicate experiments.

Table S1

Mean concentration of nitrogen sources in the merseguera grape juice at the time of inoculation

Nitrogen source	Concentration (mg/l)
Alanine	130,75 ± 5,04
Arginine	281,85 ± 19,13
Aspartate	33,89 ± 0,52
Cystein	0,23 ± 0,02
Glutamate	43,79 ± 3,11
Glutamine	190,82 ± 0,14
Glysine	5,46 ± 0,16
Histidine	13,09 ± 0,8
Isoleucine	26,64 ± 0,59
Leucine	29,1 ± 1,33
Lysine	3,54 ± 0,36
Methionine	4,08 ± 0,16
Phenylalanine	49,19 ± 1,49
Proline	52,79 ± 1,65
Serine	48,21 ± 0,37
Threonine	96,08 ± 2,66
Tryptophan	23,96 ± 0,8
Tyrosine	16,01 ± 0,45
Valine	26,51 ± 2,4
NH4Cl	491,74 ± 27,54

Table S2

Mean concentration of by-products and major volatile compounds in fermented musts at 25ºC

Compounds		Strain			
		T73	BMV58	CECT12600	CR85
Sugars and main extracellular fermentative by-products ($g.l^{-1}$)	Glucose	0,88±0,02^{a}	0,92±0,04^{a}	0,94±0,02^{a}	2,42±0,24^{b}
	Fructose	2,6±0,21^{a}	1,06±0,05^{a}	17,96±0,26^{b}	20,82±1,73^{c}
	Erythritol	0,22±0,02^{b}	0,41±0,01^{d}	0,30±0,01^{c}	0,17±0,01^{a}
	Glycerol	5,96±0,07^{a}	7,37±0,03^{b}	7,39±0,09^{b}	7,88±0,3^{c}
	2,3 Butanediol	0,45±0,01^{a}	0,88±0,06^{b}	1,41±0,05^{c}	1,56±0,07^{d}
	Ethanol (%)	12,6±0,12^{b}	12,5±0,04^{b}	11,67±0,13^{a}	11,25±0,59^{a}
	Succinic acid	2,32±0,04^{a}	9,22±0^{d}	2,91±0,01^{c}	2,46±0,04^{b}
	D-Lactic acid	0,12±0,01^{a}	0,19±0,01^{b}	0,19±0,01^{b}	0,12±0,03^{a}
	Acetic acid	0,23±0,03^{b}	0,19±0,01^{b}	0,00±0,01^{a}	0,72±0,02^{c}
Aroma compounds ($mg.l^{-1}$)	***Higher alcohols***				
	Isobutanol	54,3±6,78^{b}	59,6±6,7^{b}	36,5±0,98^{a}	37,1±3,37^{a}
	Isoamyl alcohol	441,1±63^{b}	396,9±39,3^{b}	234,9±3,9^{a}	219,8±27,5^{a}
	1-Hexanol	1,052±0,182^{a}	1,047±0,092^{a}	0,876±0,013^{a}	1,686±0,205^{b}
	Benzyl alcohol	17,9±5,5^{a}	14,1±2,8^{a}	15,3±1,9^{a}	21,8±4,4^{a}
	2-Phenylethanol	133,9±22,6^{a}	608,9±83^{c}	268,2±25^{b}	98,8±22,5^{a}
	ΣTotal Higher alcohols	648,2±82^{b}	1080,5±94,2^{c}	555,8±24,5^{a,b}	379,1±57,7^{a}
	Esters				
	Ethyl acetate	96,4±9,3^{a,b}	90,1±1,8^{a}	116,9±2,9^{b}	101,5±12,3^{a,b}
	Isobutyl acetate	0,259±0,067^{b}	0,136±0,017^{a}	0,195±0,029^{a,b}	0,143±0,016^{a}
	Isoamyl acetate	11,5±2,55^{c}	5,3±0,3^{a,b}	7,69±1,25^{b}	2,15±0,32^{a}
	Ethyl caproate	2,09±0,53^{b}	0,84±0,36^{a}	0,95±0,25^{a}	1,56±0,19^{a,b}
	Hexyl acetate	0,726±0,27^{b}	0,33±0,03^{a}	0,49±0,11^{a,b}	0,504±0,05^{a,b}
	Ethyl caprylate	1,889±1,02^{a}	1,345±1,32^{a}	0,781±0,7^{a}	1,281±0,55^{a}
	Ethyl caprate	4,218±4,31^{a}	3,502±1,38^{a}	1,966±1,75^{a}	5,198±3,73^{a}
	Benzyl acetate	0,345±0,15^{a}	0,303±0,06^{a}	0,284±0,04^{a}	0,432±0,08^{a}
	2-Phenylethyl acetate	2,324±0,37^{a}	6,59±0,9^{b}	5,848±0,43^{b}	1,475±0,08^{a}
	ΣTotal esters	119,7±10,8^{a,b}	108,4±3,8^{a}	135,1±2,4^{b}	114,2±9,5^{a}

Results are the mean value of three replicates with their standard deviation. Statistically significant differences regarding the concentration of compounds between strains are indicated by super-indexes. Statistically different groups were established with 95% confidence.

SUPPLEMENTARY MATERIAL - Chapter 2

Results

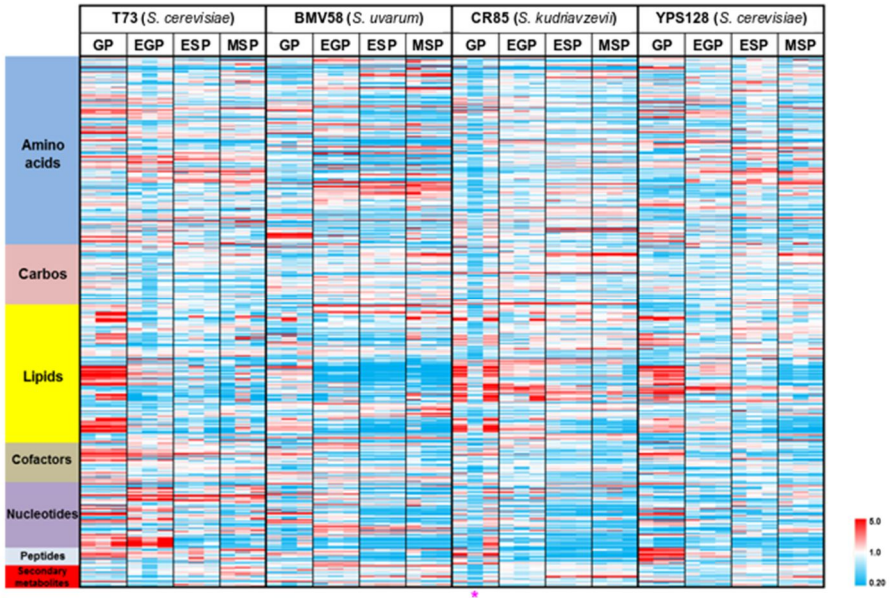

Figure S1. Heat map of the intracellular samples grouped by treatment block (X-axis) and compounds grouped by major biochemical pathway class (Y-Axis). On the X-axis, the four sampling time points are indicated as GP (mid-exponential growth phase), EGP (end of exponential growth phase), ESP (early stationary phase) and MSP (mid stationary phase). Pink star indicates the outlier sample within the triplicate GP group of the CR85 strain.

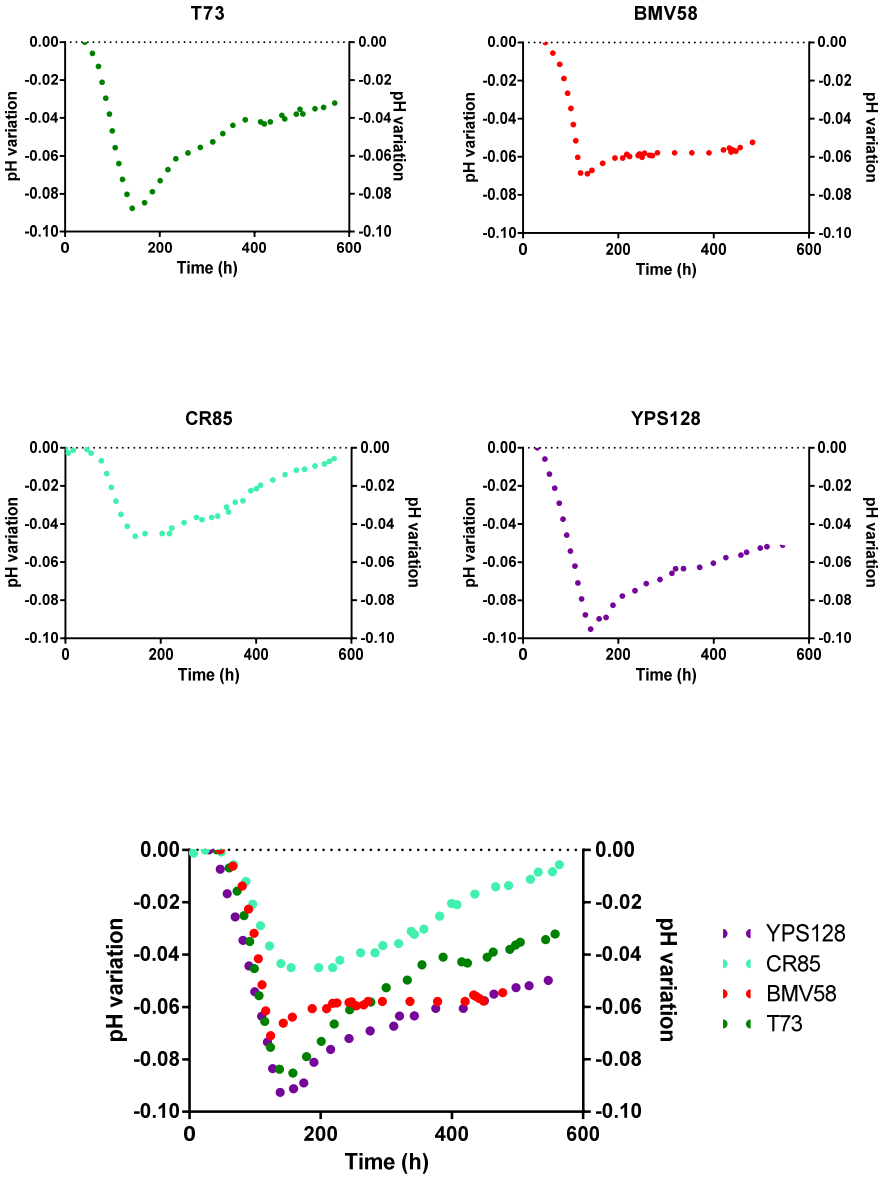

Figure S2. pH variation during alcoholic fermentation

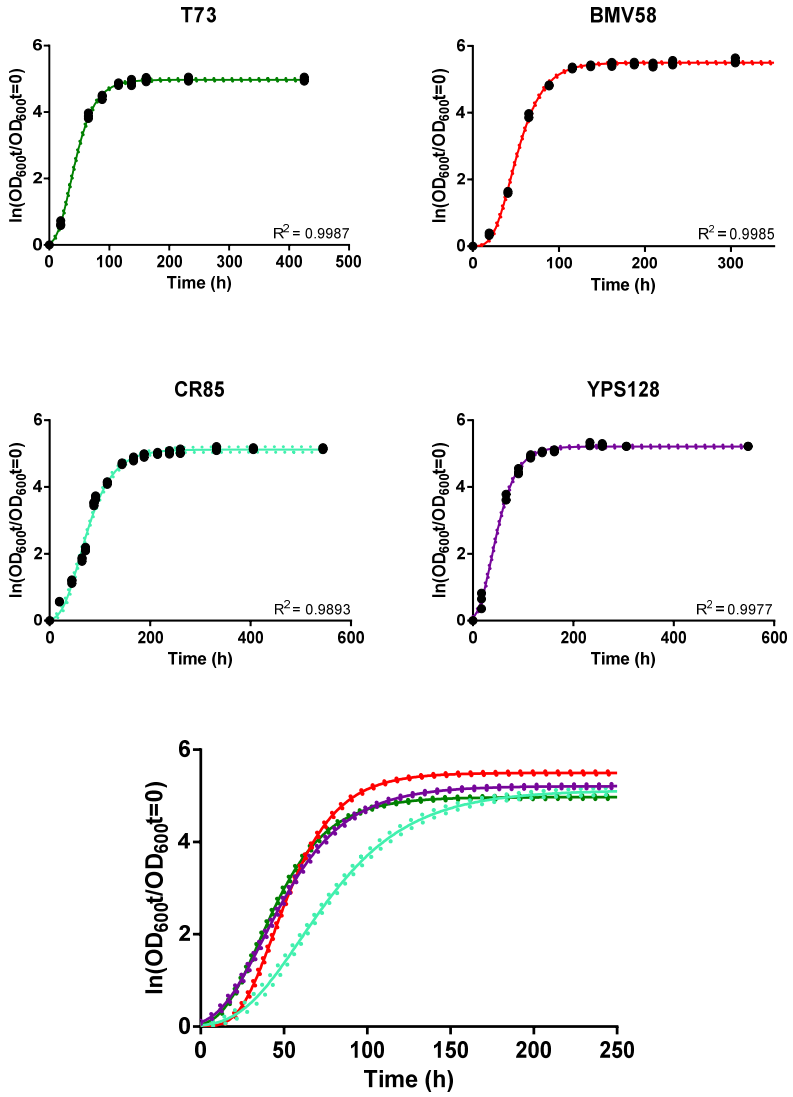

Figure S3. Fitted curves of cell population during alcoholic fermentation expressed as of ln(OD600(t)/OD600(t=0)). Green solid line represents T73 strain, red solid line the BMV58 strain, light blue solid line the CR85 strain and purple solid line the YPS128 strain. For each strain, the 95% confidence band of the best-fit curve is represented by dashed line of the same color as the solid line.

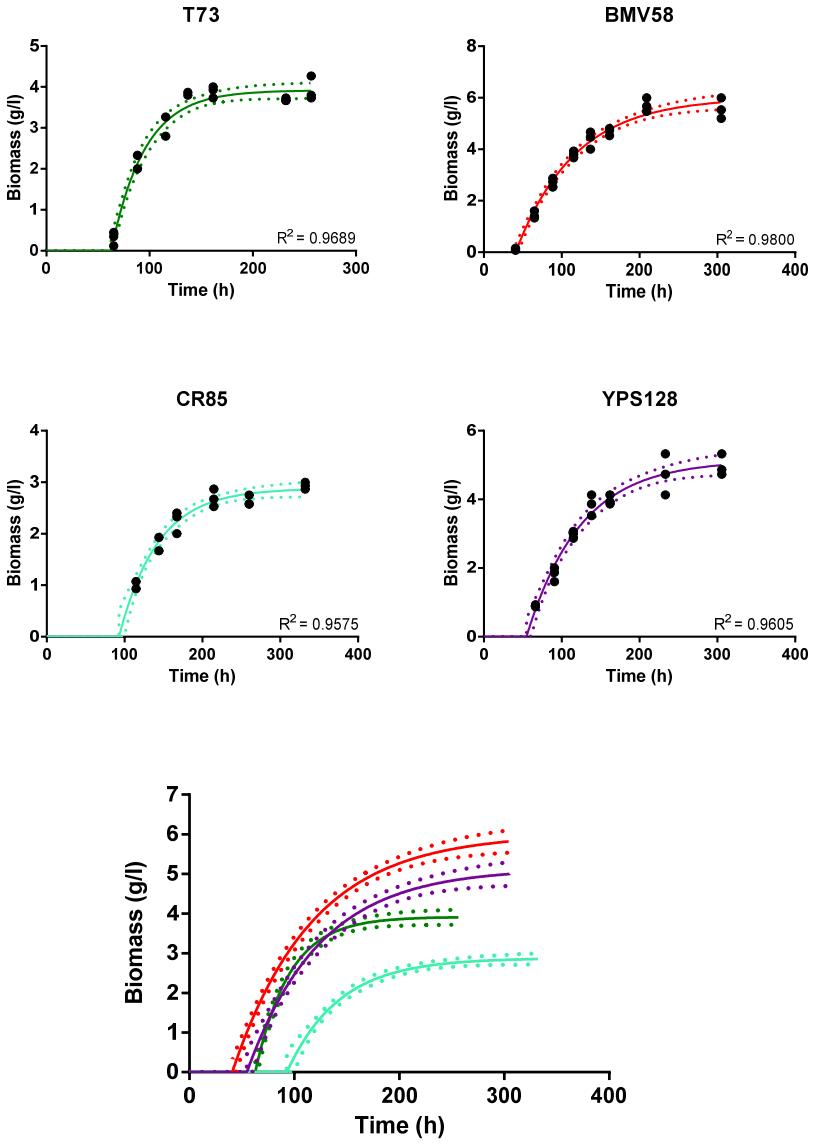

Figure S3. Fitted curves of biomass during alcoholic fermentation expressed in g/l. Green solid line represents T73 strain, red solid line the BMV58 strain, light blue solid line the CR85 strain and purple solid line the YPS128 strain. For each strain, the 95% confidence band of the best-fit curve is represented by dashed line of the same color as the solid line.

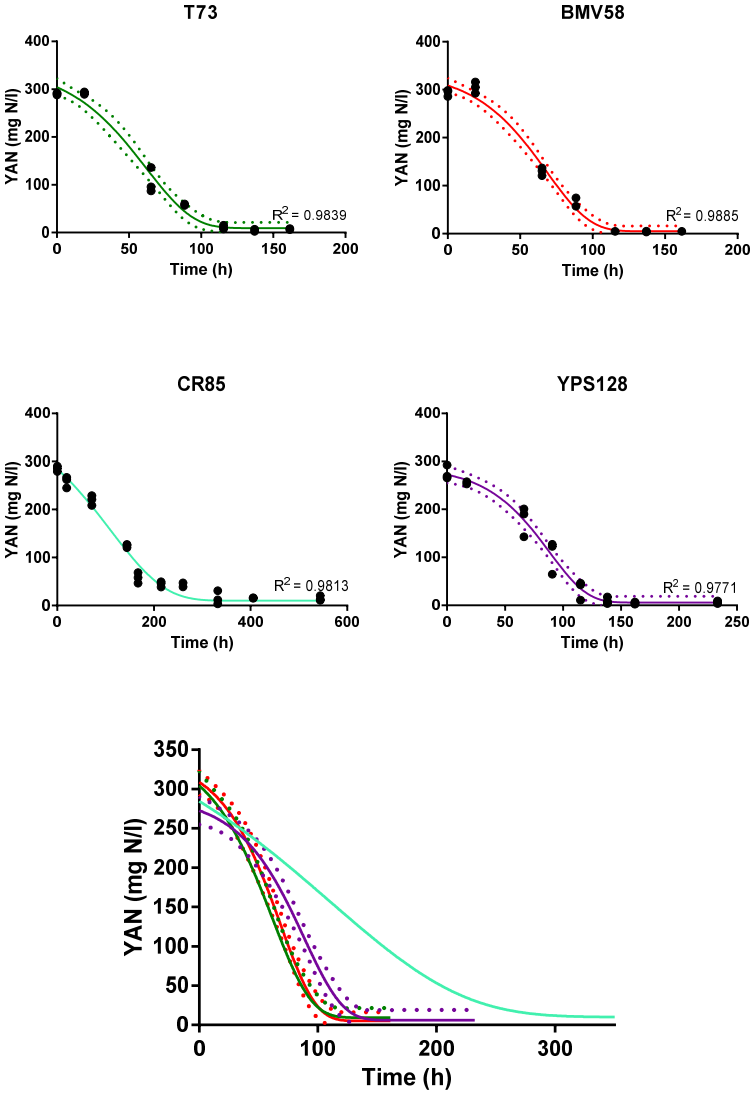

Figure S4. Fitted curves of yeast assimilable nitrogen (YAN) expressed as mg N/l during alcoholic fermentation. Green solid line represents T73 strain, red solid line the BMV58 strain, light blue solid line the CR85 strain and purple solid line the YPS128 strain. For each strain, the 95% confidence band of the best-fit curve is represented by dashed line of the same color as the solid line.

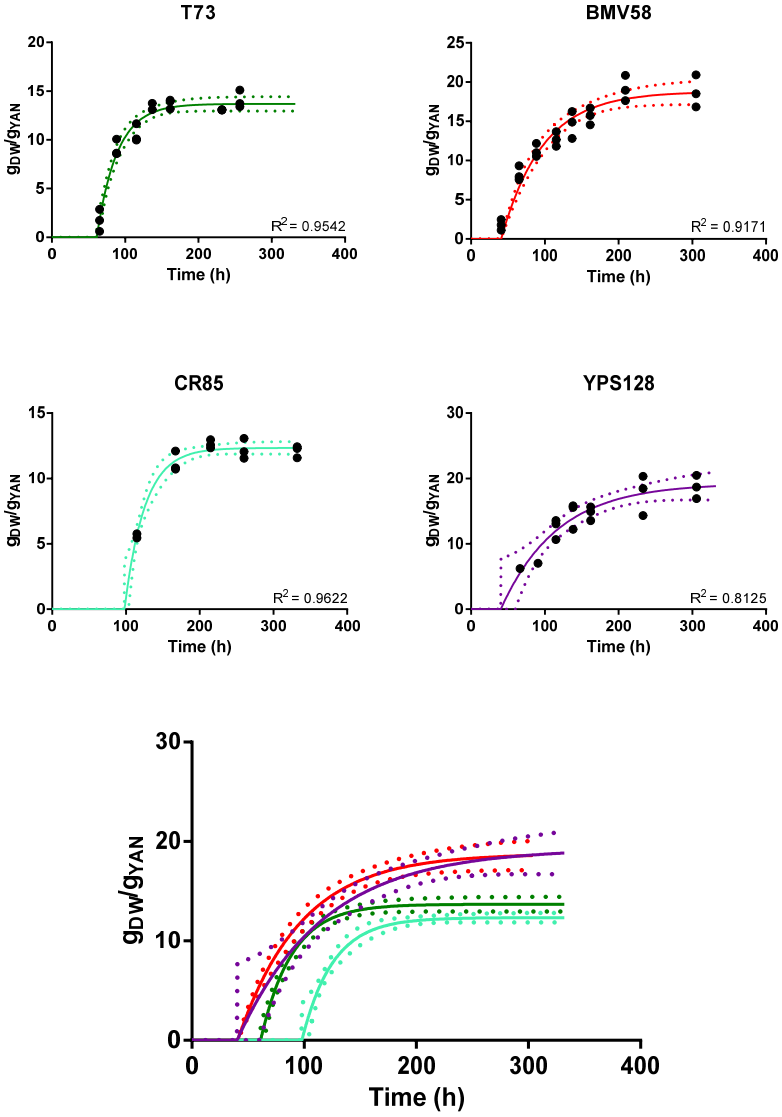

Figure S5. Fitted curves of biomass yield expressed as gDW/gYAN during alcoholic fermentation. Green solid line represents T73 strain, red solid line the BMV58 strain, light blue solid line the CR85 strain and purple solid line the YPS128 strain. For each strain, the 95% confidence band of the best-fit curve is represented by dashed line of the same color as the solid line.

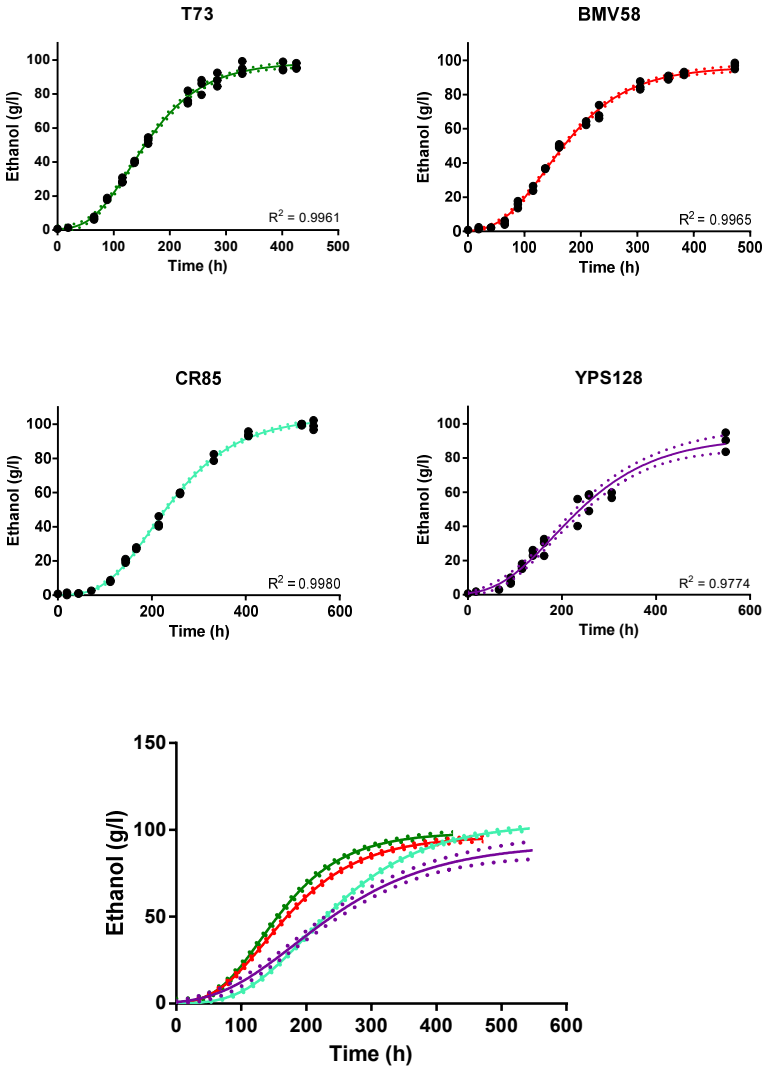

Figure S6. Fitted curves of extracellular concentration of ethanol expressed in g/l during alcoholic fermentation. Green solid line represents T73 strain, red solid line the BMV58 strain, light blue solid line the CR85 strain and purple solid line the YPS128 strain. For each strain, the 95% confidence band of the best-fit curve is represented by dashed line of the same color as the solid line.

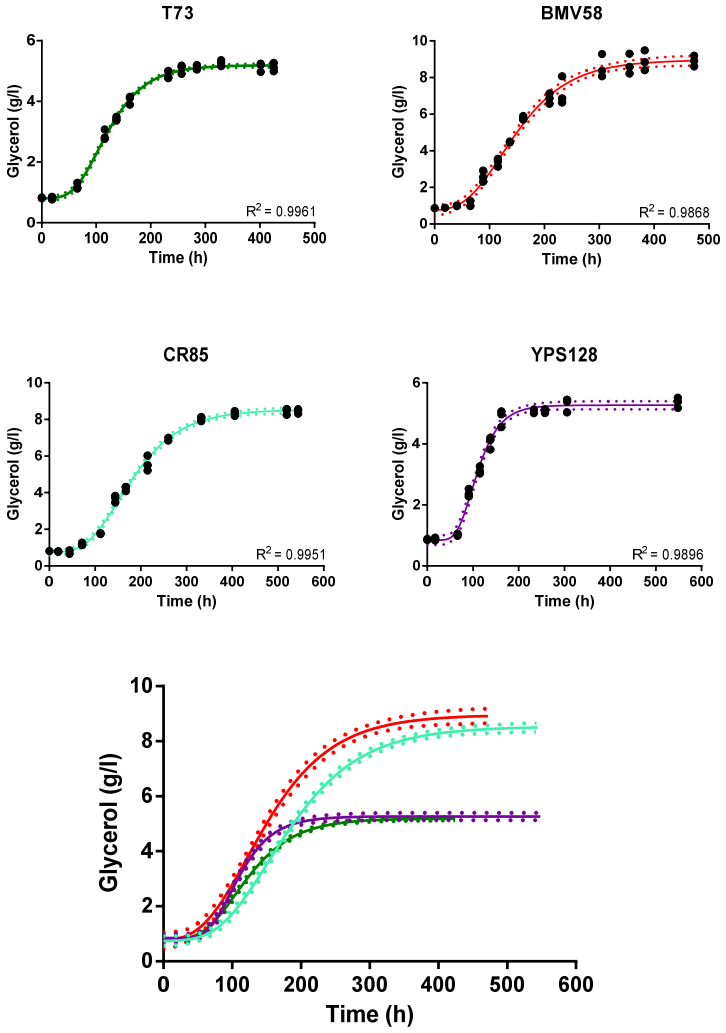

Figure S7. Fitted curves of extracellular concentration of glycerol expressed in g/l during alcoholic fermentation. Green solid line represents T73 strain, red solid line the BMV58 strain, light blue solid line the CR85 strain and purple solid line the YPS128 strain. For each strain, the 95% confidence band of the best-fit curve is represented by dashed line of the same color as the solid line.

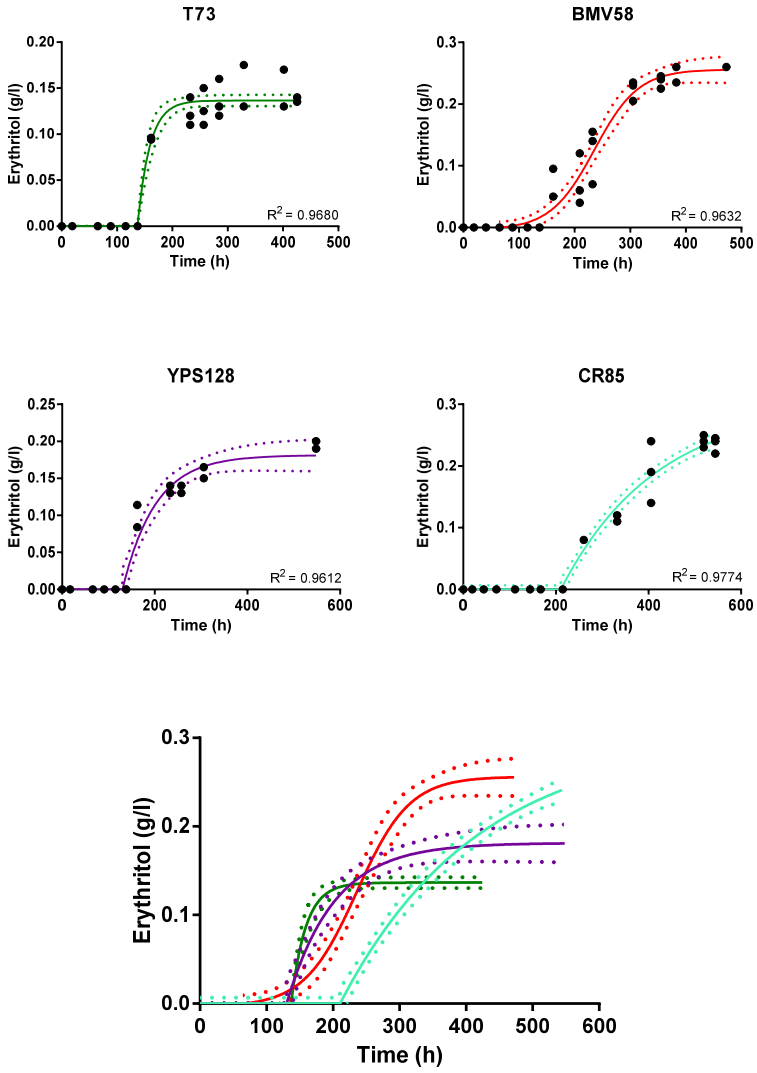

Figure S8. Fitted curves of extracellular concentration of erythritol expressed in g/l during alcoholic fermentation. Green solid line represents T73 strain, red solid line the BMV58 strain, light blue solid line the CR85 strain and purple solid line the YPS128 strain. For each strain, the 95% confidence band of the best-fit curve is represented by dashed line of the same color as the solid line.

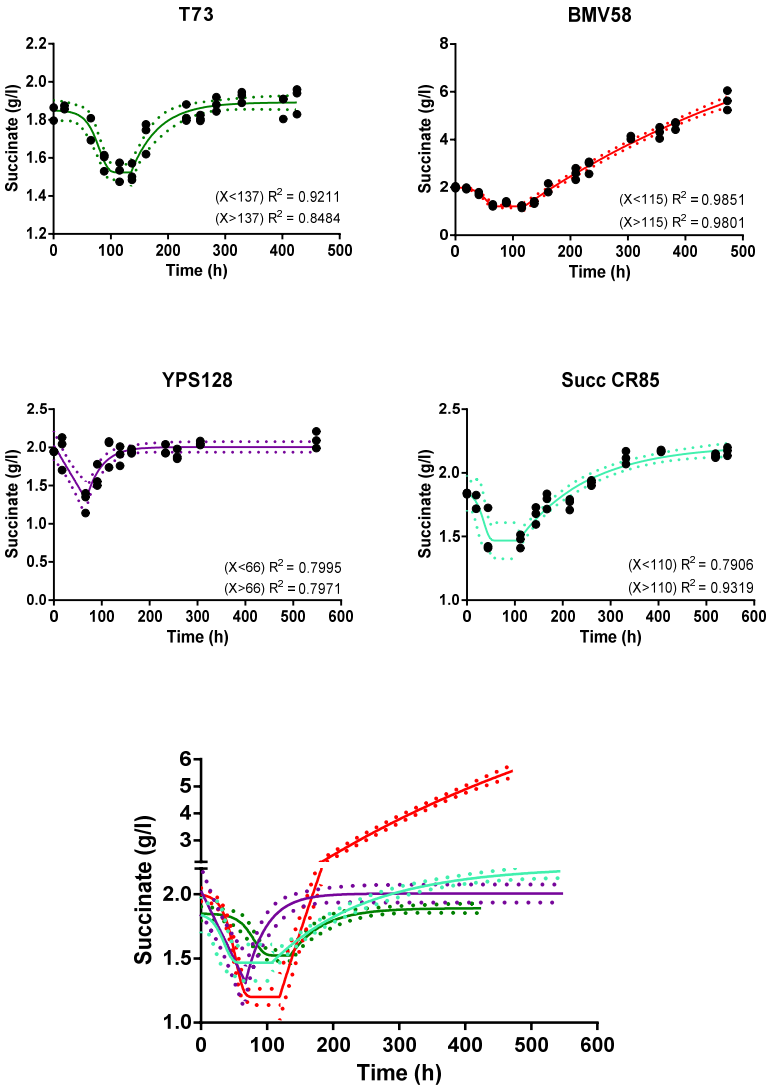

Figure S9. Fitted curves of extracellular concentration of succinate expressed in g/l during alcoholic fermentation. Green solid line represents T73 strain, red solid line the BMV58 strain, light blue solid line the CR85 strain and purple solid line the YPS128 strain. For each strain, the 95% confidence band of the best-fit curve is represented by dashed line of the same color as the solid line.

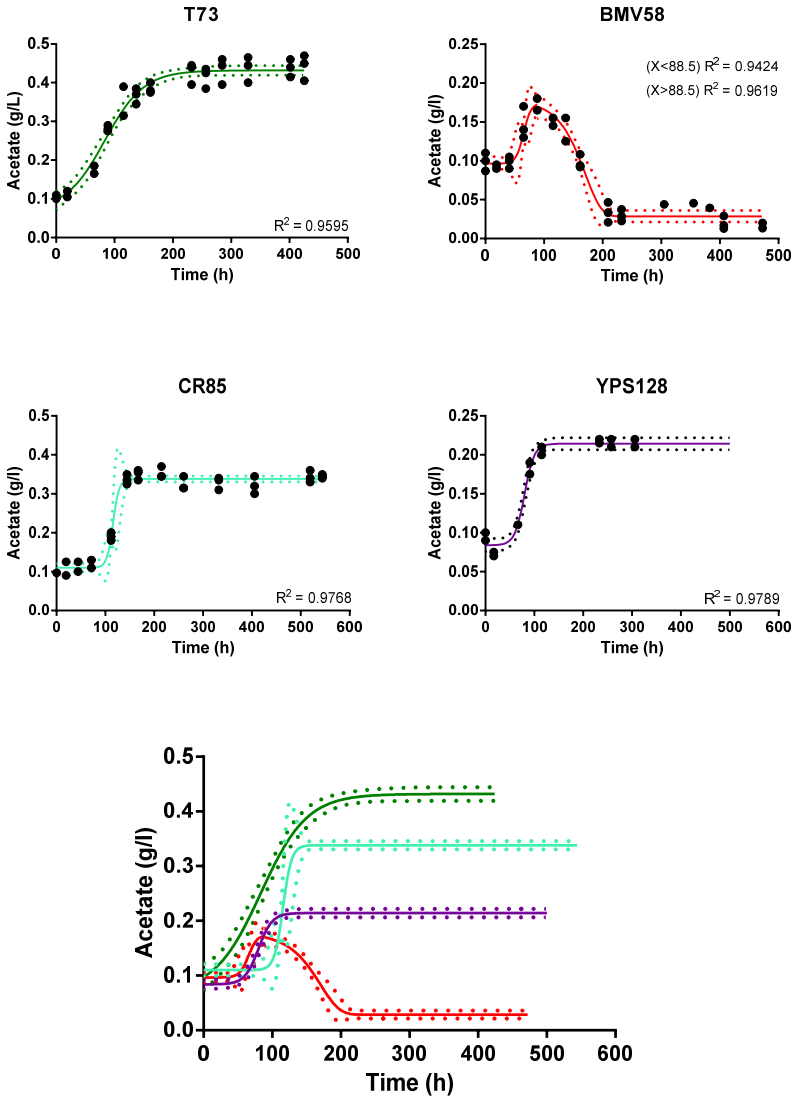

Figure S10. Fitted curves of extracellular concentration of acetate expressed in g/l during alcoholic fermentation. Green solid line represents T73 strain, red solid line the BMV58 strain, light blue solid line the CR85 strain and purple solid line the YPS128 strain. For each strain, the 95% confidence band of the best-fit curve is represented by dashed line of the same color as the solid line.

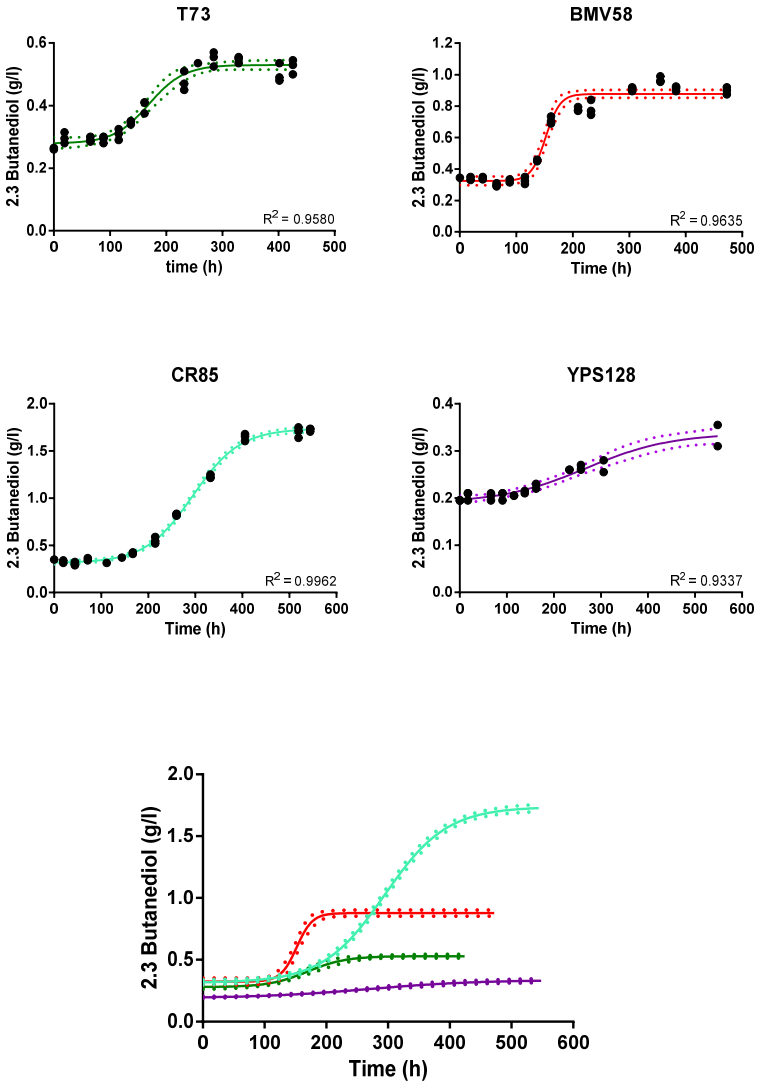

Figure S11. Fitted curves of extracellular concentration of 2.3 butanediol expressed in g/l during alcoholic fermentation. Green solid line represents T73 strain, red solid line the BMV58 strain, light blue solid line the CR85 strain and purple solid line the YPS128 strain. For each strain, the 95% confidence band of the best-fit curve is represented by dashed line of the same color as the solid line.

Table S1: Mean concentration (mg/l) of major volatile compounds in fermented musts at 12ºC

Results are the mean value of three replicates with their standard deviation.

	T73	YPS128	BMV58	CR85
Ethyl acetate	41 ± 7.2^{a}	66.3 ± 10^{a}	142 ± 17.7^{b}	150.5 ± 8^{b}
Isobutyl acetate	0 ± 0^{a}	0.1 ± 0^{a}	0.3 ± 0^{b}	0.4 ± 0.1^{b}
Isobutanol	25.1 ± 3.1^{a}	29.7 ± 1.6^{a}	146.9 ± 71.7^{b}	134.3 ± 12.2^{b}
Isoamyl acetate	4.5 ± 0.8^{a}	2.9 ± 0.5^{a}	13.1 ± 2.4^{b}	3.3 ± 0.3^{a}
Isoamyl alcohol	214.7 ± 5.1^{a}	350.8 ± 20.4^{b}	921.7 ± 96.3^{c}	421.7 ± 26.3^{b}
2-phenylethyl acetate	1.2 ± 0.2^{a}	0.6 ± 0.1^{a}	12.3 ± 0.5^{b}	1.3 ± 0.3^{a}
2-phenyl ethanol	67.9 ± 0^{a}	127.1 ± 58.9^{a}	1023.4 ± 67^{b}	141.7 ± 18.9^{a}
Ethyl hexanoate	4.6 ± 0.2^{d}	2 ± 0.1^{a}	2.8 ± 0.4^{b}	3.6 ± 0.1^{c}
Ethyl octanoate	10.7 ± 0.8^{c}	3.7 ± 0.5^{a}	2.8 ± 1.1^{a}	7.5 ± 0.4^{b}
Ethyl decanoate	5.7 ± 2.4^{a}	4.3 ± 0.4^{a}	2.4 ± 2.1^{a}	4.1 ± 0.8^{a}

Statistically significant differences regarding the concentration of compounds between strains are indicated by super-indexes. Statistically different groups were established by one-way ANOVA analysis (Tukey HSD test, n = 3, p-value<0.05).

Supplementary material – Chapter 2

Material and methods

Ultrahigh Performance Liquid Chromatography-Tandem Mass Spectroscopy (UPLC-MS/MS) procedure details for intracellular metabolites

All methods utilized a Waters ACQUITY ultra-performance liquid chromatography (UPLC) and a Thermo Scientific Q-Exactive high resolution/accurate mass spectrometer interfaced with a heated electrospray ionization (HESI-II) source and Orbitrap mass analyzer operated at 35,000 mass resolution. The sample extracted was dried then reconstituted in solvents compatible to each of the four methods. Each reconstitution solvent contained a series of standards at fixed concentrations to ensure injection and chromatographic consistency. One aliquot was analyzed using acidic positive ion conditions, chromatographically optimized for more hydrophilic compounds. In this method, the extract was gradient-eluted from a C18 column (Waters UPLC BEH C18-2.1x100 mm, 1.7 µm) using water and methanol, containing 0.05% perfluoropentanoic acid (PFPA) and 0.1% formic acid (FA). A second aliquot was also analyzed using acidic positive ion conditions, but was chromatographically optimized for more hydrophobic compounds. In this method, the extract was gradient eluted from the aforementioned C18 column using methanol, acetonitrile, water, 0.05% PFPA and 0.01% FA, and was operated at an overall higher organic content. A third aliquot was analyzed using basic negative ion optimized conditions using a separate dedicated

C18 column. The basic extracts were gradient-eluted from the column using methanol and water, however with 6.5mM Ammonium Bicarbonate at pH 8. The fourth aliquot was analyzed via negative ionization following elution from a HILIC column (Waters UPLC BEH Amide 2.1x150 mm, 1.7 µm) using a gradient consisting of water and acetonitrile with 10mM Ammonium Formate, pH 10.8. The MS analysis alternates between MS and data-dependent MS^n scans using dynamic exclusion. The scan range varies slightly between methods, but covers approximately 70-1000 m/z.

SUPPLEMENTARY MATERIAL - Chapter 3

SUPPLEMENTAL TEXT 1: Orthology analysis and genome-scale metabolic reconstruction

Genomes of ScT73, SuBMV58 and SuCECT12600 were sequenced and assembled in previous works (Goffeau *et al.*, 1996; Morard *et al.*, 2019). Genome assemblies were annotated by homology and gene synteny using RATT (Otto *et al.*, 2011). This approach let us transfer the systematic gene names of *S. cerevisiae* S288c annotation (Goffeau *et al.*, 1996) to our assemblies and therefore, to select only those syntenic orthologous genes in T73, CECT12600 and BMV58 genomes for subsequent analyses.

We added to the consensus genome-scale reconstruction of *Saccharomyces cerevisiae* S288C (v.8.3.1) metabolites and reactions related to amino acid degradation and higher-alcohols and esters formation. This refined model was then used as a template for reconstructing strain-specific genome-scale models for SuBMV58, SuCECT12600 and ScT73. First, AuReMe was used to generate draft genome-scale metabolic models for each strain using the refined model as a template. As a result, we obtained draft networks that included both gene-associated reactions (supported by genomic evidence and orthology) and non-gene associated reactions, such as transport reactions based on diffusion and exchange reactions, which were assumed to also occur in the strain-specific models. In addition,

Metadraft was also used to generate draft networks for each strain using the refined yeast8 as a template. Reactions from MetaDraft were added to the drafts generated with AuReMe. Finally, the models were gap-filled using the refined template of yeast8 as the universe dataset from which reactions are taken to gap-fill the draft models. **Figure S1** presents the differences between model reconstructions as compared to the consensus Yeast8.Sc T73 Su BMV58 Su CECT12600 Yeast8

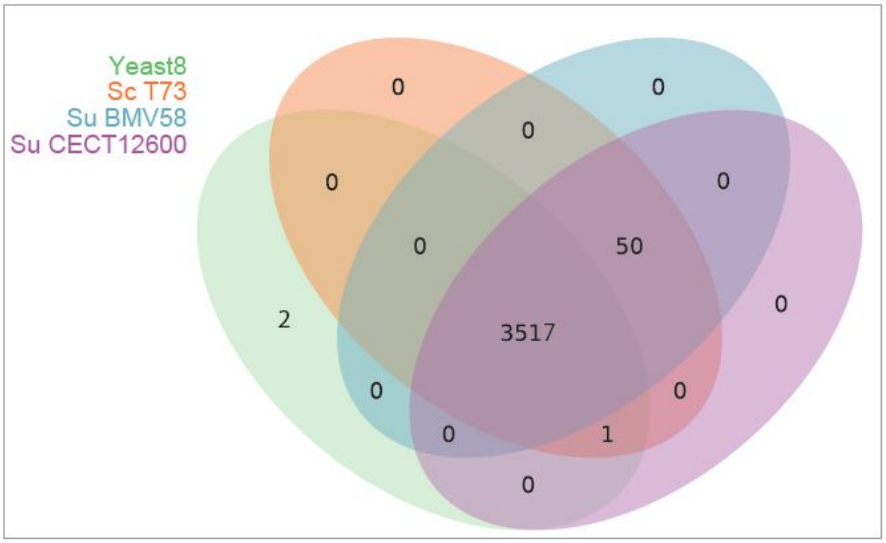

Figure S1. Differences between model reconstructions as compared to Yeast8.

SUPPLEMENTAL TEXT 2: Bootstrap parameter estimation and goodness-of-fit of the model

The model depends on 66 unknown parameters, estimated from the experimental data using a bootstrap approach. The **Figure S1**

presents the parameter estimation convergence curves for the different strains and bootstrap realizations. Convergence to the optimal solution is in general achieved after 6000 evaluations of the model. The highest distribution of optimal values is observed in SuBMV58 which is induced by the higher experimental error also found for the experimental data. **Figure S2** presents the bootstrap parameter distributions showing that uncertainty on the parameter estimates was reasonably low. Its value varied between parameters and species. The mean standard deviation corresponds to a 9.5% for the parameter values estimated for ScT73 (excluding the parameter NGAM, whose optimal value was zero). A slightly higher mean standard deviation (12.6%) was obtained for the parameter values estimated for SuBMV58 (excluding the kinetic constant describing benzyl alcohol production whose optimal value was zero), and a significantly lower mean uncertainty (2.5%) was obtained for those parameters corresponding to SuCECT12600. Some parameter values vary significantly between strains (**Supplemental Table 3**). The comparison between the wine strains ScT73 and SuBMV58, reveals substantial differences – above 100% relative difference, in the growth-associated ATP maintenance: the rate of transport of specific amino acids and hexoses and the production of certain alcohols and acids. GAMfitted for SuBMV58 is around twice the value for ScT73. The rate of transport of phenylalanine, leucine, alanine, and cysteine is between 106% and 778% larger for SuBMV58 than for ScT73. Similarly,

hexoses uptake rate is around two times higher at the beginning of fermentation for SuBMV58 than for ScT73. Regarding products, the most noticeable difference appears in the production rate of succinate and, to a lesser extent, in the production of 2-phenylethanol, 2-phenylethyl acetate, and 2,3-butanediol. The comparison between the wine strains and the natural strain showed that the lag phase is more than three times longer for the natural strain; besides, the non-growth associated maintenance is practically zero for wine strains while it is around 0.8 for the SuCECT12600 strain. The rates of hexoses uptake are pretty similar between *S. uvarum* strains; on the contrary, we found substantial differences in the uptake of various amino acids. In particular, the uptake rate for threonine is 740% higher for SuCECT12600 than for SuBMV58. The **Figure S3** shows the best fit to the data. We determined the R-squared measure of goodness of fit (R^2) for each measured variable and each strain-based fermentation. The **Supplemental Table 3** presents the corresponding values. The vast majority of the coefficients were positive with few exceptions (10 out 141), typically associated with low signal-to-noise ratio and high data dispersion observed in the measured variable, e.g., cysteine. The mean R^2 (excluding negative values) was of 0.88 for *S. cerevisiae* T73, 0.92 for *S. uvarum* BMV58 and 0.91 for *S. uvarum* CECT12600; the median R^2 values are above 0.94 for all strains.

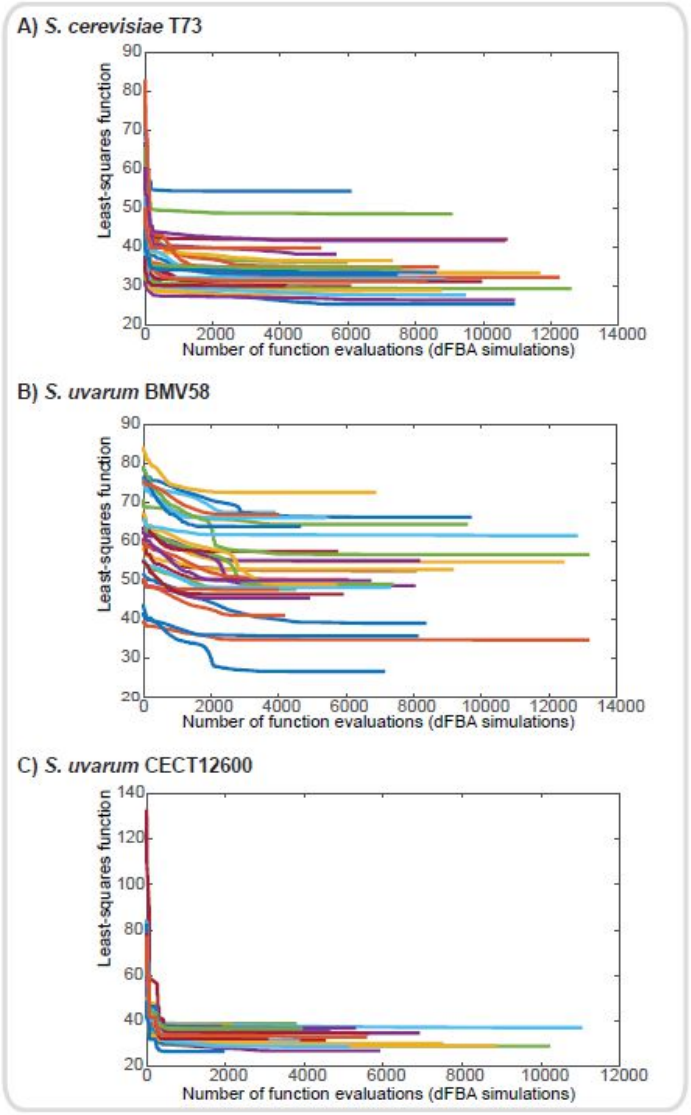

Figure S1. Convergence of the bootstrap approach for the strain-specific parameter estimation.

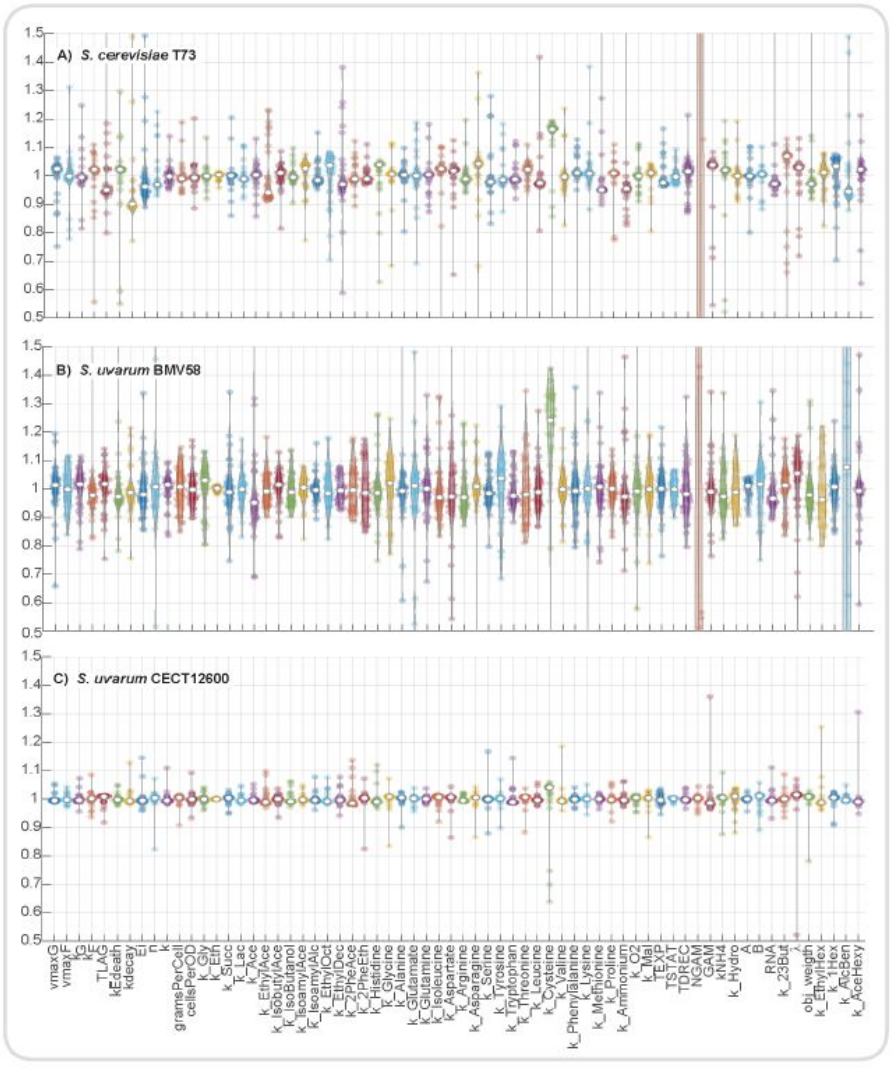

Figure S2. Distribution of parameter values as obtained by the bootstrap approach. The normalized values are computed by dividing each best solution by the mean of all solutions.

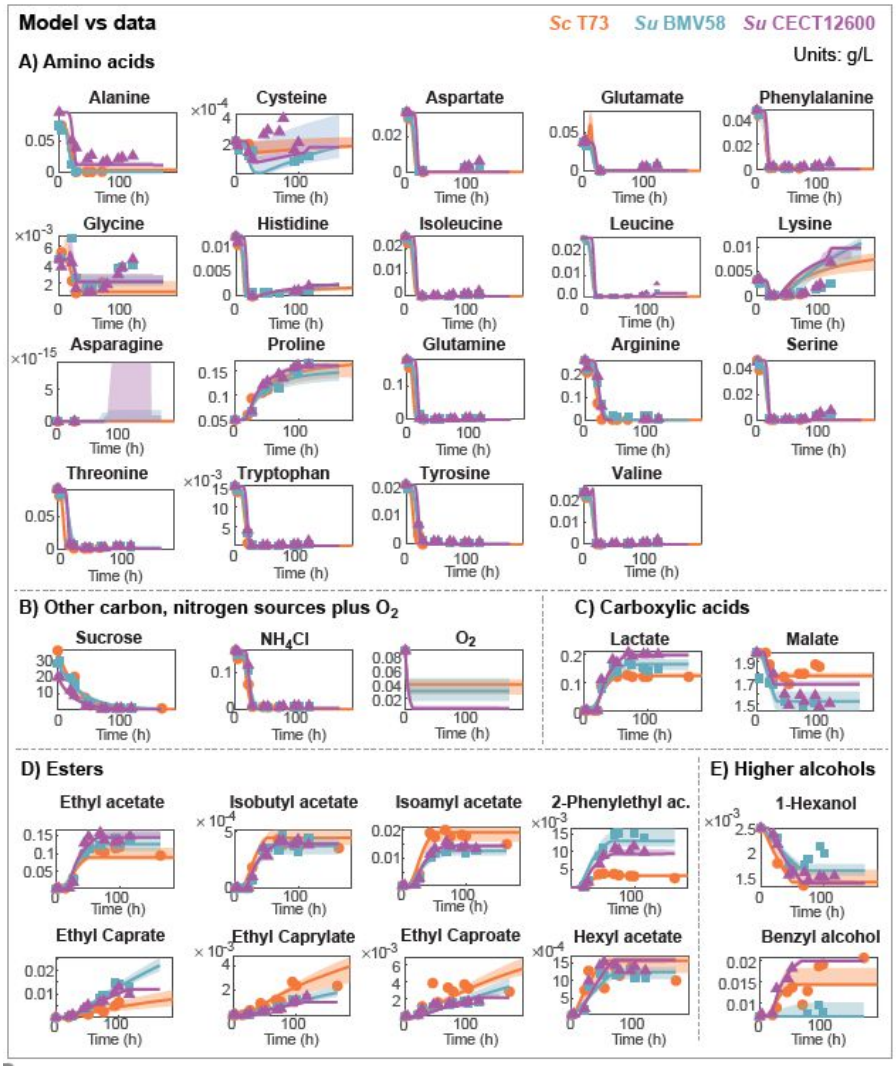

Figure S3. Best fit to the data and model associated uncertainty. Figures show the data (symbols) and the model (continuous lines) for several measured variables: nutrients and products. Shading areas correspond to model uncertainty as predicted by the bootstrap approach. The quality of model is visually good. Besides goodness of fit as measured by R2 was obtained for each measured quantity. The vast majority of the R2 values

were positive with few exceptions (10 out 141), typically associated with low signal-to-noise ratio and high data dispersion observed in the measured variable, e.g., cysteine. The mean R2 (excluding negative values) was of 0.88 for *S. cerevisiae* T73, 0.92 for *S. uvarum* BMV58 and 0.91 for S. uvarum CECT12600.

SUPPLEMENTAL TEXT 3: Detailed description of the redox balance mechanisms used by the different strains.

The comparative analysis of dynamic flux ratios showed that most significant differences between strains occur in the stationary phase. **Figure S1** presents the relative differences between the fluxes obtained for *S. uvarum* species and those obtained for *S. cerevisiae.* Only those fluxes resulting in a relative difference above 100% are shown. Remarkably, the figure illustrates that not only a significantly higher number of fluxes differ in the stationary phase but also, the relative difference is also higher.

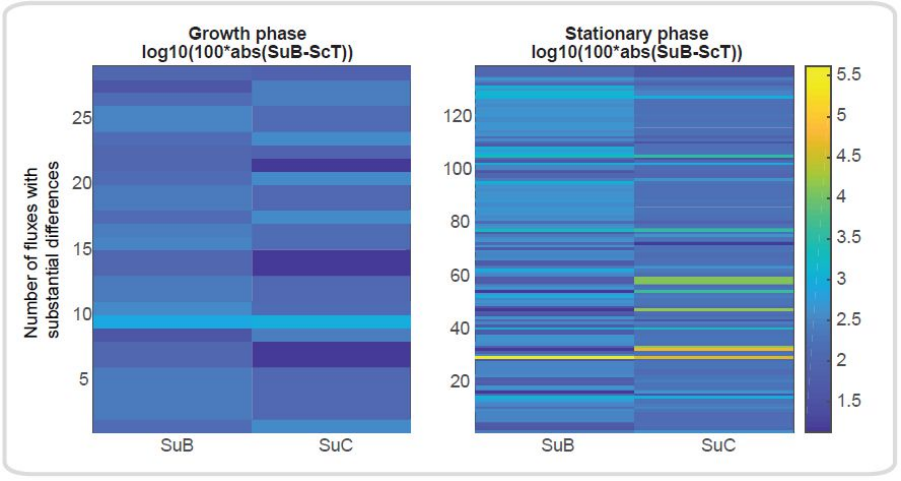

Supplementary material – Chapter 3

Figure S1. Comparison of fluxes between growth and stationary phases. Figure shows relative differences of S. uvarum species with respect to *S. cerevisiae*. Only those relative differences above 100% are shown. Note that while for the growth phase only 29 fluxes are between 100−150% relative difference; for the stationary phase more than 140 fluxes differ between the 100− 550%.

Our results show that *S. uvarum* and *S. cerevisiae* strains use different redox balance strategies markedly visible during the fermentation stationary phase. Here we present a detailed view of the differences found in the central carbon metabolism and the production of higher alcohols.

Central carbon metabolism

Production of ethanol. Taking the entire course of the fermentation in consideration, *S. uvarum* strains had a lower ethanol production rate than *S. cerevisiae* strain (187.40, 179.14, 182.40 mmol/mmolH in ScT73, SuBMV58 and SuCECT12600, respectively; **Table S4**, r_2115). Also, the model predicted slightly lower ethanol rates during growth phase for the three strains (173.10, 177.24, 183.34 mmol/mmolH), while they were quite similar during stationary phase (186.86, 177.24, 183.34 mmol/mmolH) (**Figure S2**). Part of the 'missing' carbon was to be found in the yield of glycerol and other downstream pathways using pyruvate as substrate.

Production of glycerol. During the growth phase, the two *S. uvarum* strains had higher glycerol production rates, with SuBMV58 and SuCECT12600 strains producing 8.37 and 8.34 mmol/mmolH respectively, while the ScT73 strain only produced 7.25 mmol/mmolH (**Table S4**, r_0489). Afterward, the model predicted a smaller but still significant difference in glycerol production during the stationary phase (7.09, 7.84 and 7.81 mmol/mmolH for ScT73, SuBMV58 and SuCECT12600 respectively; **Figure S2**). Consistent with this, the overall score for the production of glycerol was lower for ScT73 (4.21 mmol/mmolH) than for both *S. uvarum* (> 6mmol/mmolH) (**Table S4**, r_0489). As an NADH-consuming process, biosynthesis of glycerol plays an essential role in maintaining cytosolic redox balance during anaerobic conditions by oxidizing excess NADH to NAD+. Glycerol is also the only compatible solute to counterbalance the osmotic pressure in *S. cerevisiae* with glucose as a carbon source (Babazadeh *et al.*, 2017). Directed evolution experiments exposing *S. cerevisiae* to osmotic stress led strains to produce a higher amount of glycerol, 2,3-butanediol, and succinate (Tilloy *et al.*, 2014). In winemaking conditions, cells suffer hyperosmotic stress due to the elevated amount of sugars. The fact that *S. uvarum* strains present a higher amount of extracellular glycerol may indicate that *S. cerevisiae* tends to accumulate intracellular glycerol at early times during fermentation as previously reported by Pérez-Torrado *et al.* (2016).

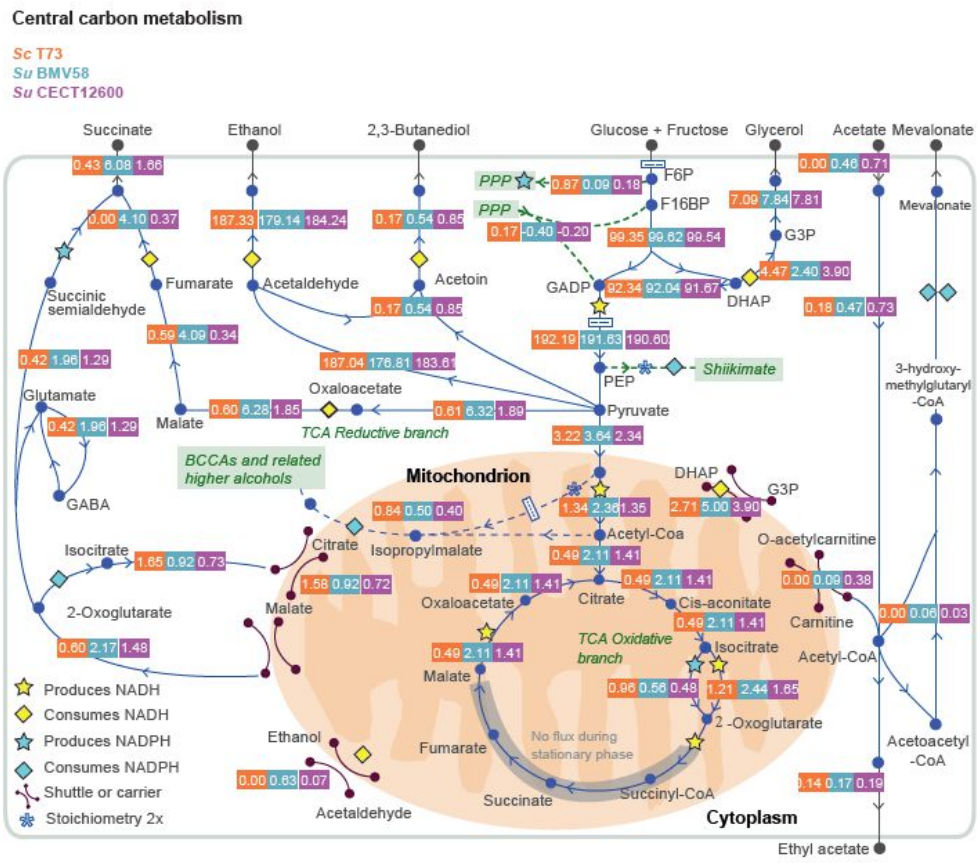

Figure S2. Redox balance in Central Carbon Metabolism. Figure shows the predicted intracellular dynamic flux ratios associated with the central carbon metabolism during the stationary phase.

Production of succinate. The model predicted that the fraction of pyruvate incorporated into the mitochondria during the stationary phase accounted for 3.22, 3.64, 2.34 mmol/mmolH in ScT73, SuBMV58 and SuCECT12600 respectively (r_2034). Once inside mitochondria, pyruvate was either used for acetyl-CoA formation (1.37, 2.49, 1.43

mmol/mmolH for ScT73, SuBMV58 and SuCECT12600 respectively, r_0961) or directed towards the *de novo* production of valine and isobutanol (0.95, 0.59, 0.50, mmol/mmolH **Figure S3**). Consistent with succinate raw data, the model estimated a significantly higher production rate of this by-product on the overall fermentative process in SuBMV58 (3.59 mmol/mmolH) and SuCET12600 (1.10 mmol/mmolH) than ScT73 (0.35 mmol/mmolH) (Table S4, r_2057). Remarkably, the difference in production between *S. uvarum* strains was noteworthy. We also reported interesting variations in the rate and the origin of succinate according to the fermentation phase between strains. In anaerobic conditions during growth and stationary phases, there are three possible routes of producing succinate: the oxidative and reductive branch of the tricarboxylic acid cycle (TCA) and the GABA shunt. In anaerobic conditions, the TCA is truncated at the succinate level: TCA does not work cyclically but follows either a mitochondrial oxidative branch or a cytoplasmic reductive branch (**Figure S2**). In the former case, succinate is produced from pyruvate via four cytoplasmic reactions, yielding two NAD^+ per pyruvate. In the other case, pyruvate is internalized into mitochondria and oxidized until succinate, producing three NADH per pyruvate. As for the GABA shunt, it is the pathway that circumvents the formation of succinyl-CoA in the oxidative branch of the TCA cycle. Instead, it converts 2-oxoglutarate into succinate with the intermediaries glutamate, GABA, and succinate semi-aldehyde, yielding two NADH and one NADPH per

pyruvate (**Figure S2**). In this regard, our model predicted that during the growth phase, a carbon flux existed through the oxidative branch of TCA, but only until 2-oxoglutarate in the three strains and that there was no flux through the GABA shunt (**Table S4**). Therefore, the succinate formed during growth was yielded only by the reductive branch of TCA in ScT73, SuBMV58 and SuCECT12600. However, the most significant fraction of succinate was produced during the stationary phase, and with a significant higher rate by SuBMV58 (6.08 mmol/mmolH) and SuCECT1600 (1.66 mmol/mmolH) than ScT73 (0.43 mmol/mmolH). Interestingly, the model predicted that during the stationary phase, the GABA pathway (0.42, 1.96 and 1.29 mmol/mmolH for ScT73, SuBMV58 and SuCECT12600 respectively; **Figure S2**) summed to the reductive branch of TCA (0.00, 4.10 and 0.37 mmol/mmolH for ScT73, SuBMV58 and SuCECT12600 respectively; **Figure S2**). Once again, the model suggested that during the stationary phase, the TCA oxidative branch was active until 2-oxoglutarate, and the GABA shunt was responsible for completing the conversion of pyruvate-derived acetyl-CoA into succinate. Remarkably, the contribution of the TCA reductive branch succinate formation was almost twice that of the GABA shunt in SuBMV58, while it was almost equal in ScT73 and SuCECT12600 strains. Also, as shown in **Figure S2**, the model suggested that the NADH produced in the oxidative branch of the TCA cycle could be re-oxidized at the level of the mitochondrial shuttles responsible for: i) the reduction of cytoplasmic DHAP to G3P

(2.71, 5.00 and 3.90 mmol/mmolH), ii) the reduction of cytoplasmic acetaldehyde to ethanol (0, 0.63 and 0.07 mmol/mmolH).

The finding that the GABA shunt would contribute to succinate formation in the case of *S. uvarum* strains was somewhat unexpected given previous results on *S. cerevisiae*. Bach *et al.*, (2009) concluded that for *S. cerevisiae* the GABA shunt was of little relevance on redox metabolism and that glutamate decarboxylase (*GAD1*) was poorly expressed when wine succinate is produced. Nevertheless, López-Malo *et al.* (2013) observed substantial differences regarding intracellular levels of GABA in cryotolerant species. This fact and our results indicate that the production of succinate among *Saccharomyces* species requires further investigation.

Production of 2,3-butanediol. *S. uvarum* strains were also more active in the production of 2,3 butanediol -a fermentative by-product involved in NADH oxidation from acetoin- than *S. cerevisiae*. The model correctly fitted extracellular raw data and consistently predicted higher flux toward 2,3-butanediol production in *S. uvarum* strains during growth (0.22, 0.55, 0.98 mmol/mmolH in ScT73, SuBMV58 and SuCECT12600, respectively, r_1097) and stationary phases (0.17, 0.54 and 0.85 mmol/mmolH in ScT73, SuBMV58 and SuCECT12600, respectively). Again, but inversely to succinate, the flux difference towards 2,3-butanediol production between *S. uvarum* strains was noteworthy **(Figure S2)**. Because both succinate and 2,3-

butanediol generate from pyruvate, our results indicate that the two *S. uvarum* strains might use two different carbon redirection strategies around the pyruvate node: SuCECT12600 directing a larger fraction of pyruvate to the synthesis of 2,3-butanediol, and SuBMV58 to the synthesis of succinate.

Production and consumption of acetate. Finally, we observed another striking difference between the three strains in the dynamics of acetate. As shown in **Figure 3** in the main text, the three strains produced acetate during the growth phase and until the entry into the stationary phase. Afterward, while extracellular acetate concentration remained constant in ScT73, it decreased in both *S. uvarum* strains indicating an acetate consumption. Our model successfully described these phenotypes. On the first hand, we reported quite similar flux towards acetate production during the growth phase in the three strains (1.08, 1.14 and 1.42 mmol/mmolH in ScT73, SuBMV58 and SuCECT12600, respectively; **Table S4**, r_1106). On the other hand, during the stationary phase, we obtained that SuBMV58 and SuCECT12600 strains consumed acetate with a rate of −0.46 and −0.71 mmol/mmolH respectively; on the contrary, ScT73 displayed an acetate rate equal to 0 mmol/mmolH (**Table S4**, r_1106). Considering the entire fermentation process, we determined an overall acetate consumption of −0.12 mmol/mmolH for SuCECT12600, while a limited production of 0.036 mmol/mmolH was computed for SuBMV58. In the case of the ScT73 strain, this production was five times higher (0.17

mmol/mmolH; **Table S4**, r_106). In our first simulations, the model determined that *S. uvarum* strains used a significant part of this consumed acetate to produce succinate through the glyoxylate pathway. This result made sense from a pFBA point of view because this path resulted in the smallest overall flux throughout the metabolic network. However, we could not find literature supporting the production of glyoxylate in the presence of a large glucose concentration. Therefore, we decided to constrain the isocitrate lyase flux to zero. The revised model then suggested that during stationary phase SuBMV58 and SuCECT12600 strains incorporated the acetate derivative, acetyl-CoA, into ethyl acetate in the cytoplasm (0.17 and 0.19 mmol/mmolH); shifted most of the remaining fraction (0.09 and 0.38 mmol/mmolH) into the mitochondria through the carnitine shuttle system and the last part (0.06 and 0.03) was directed towards mevalonate (**Figure S2**). The fact that an amount of the acetate carbon was directed towards mevalonate is in line with recent experimental work by Minebois *et al.*, (2020). Inside the mitochondria, acetyl-CoA was used to form isopropylmalate (IPM, precursor of isoamyl alcohol, (**Figure S3**) or further used in the TCA towards the synthesis of 2-oxoglutarate (**Figure S2**).

Contributions to redox balance. All the aforementioned fermentative by-products (ethanol, glycerol, succinate, 2,3-butanediol and acetate) impact NADH/NAD^+ and/or NADPH/$NADP^+$ balance (**Figure S2**). However, their relative contribution to maintaining co-factors

equilibrium varies according to the stoichiometry of the reaction, the function of the cell compartment in which they are produced (cytoplasm or mitochondria) and the activity of redox shuttles between compartments. Most of the glycolytic pyruvate was directed towards ethanol production for the three strains, known to be redox neutral. However, we noticed that both glycerol synthesis and reductive succinate production were more pronounced in *S. uvarum* strains during the stationary phase. Thus, according to the stoichiometry and localization of these pathways, it may result in a cytoplasmic surplus of NAD^+ that should be compensated elsewhere in the metabolism of *S. uvarum* strains.

Production of higher alcohols. Higher alcohol production started during the growth phase and ceased at the end of the stationary phase. Our results reflect substantial differences in the accumulation of some higher alcohols between strains. In particular, the model predicted that the carbon skeletons of isoamyl alcohol, isobutanol and 2-phenyl ethanol were in a significant part synthesized *de novo* from glycolytic and pentose phosphate pathway intermediates, rather than coming from the catabolism of precursor exogenous amino acids (leucine, valine, and phenylalanine respectively). Furthermore, the model shows that isoamyl alcohol and 2-phenyl ethanol contribute to glycerol formation in wine fermentation.

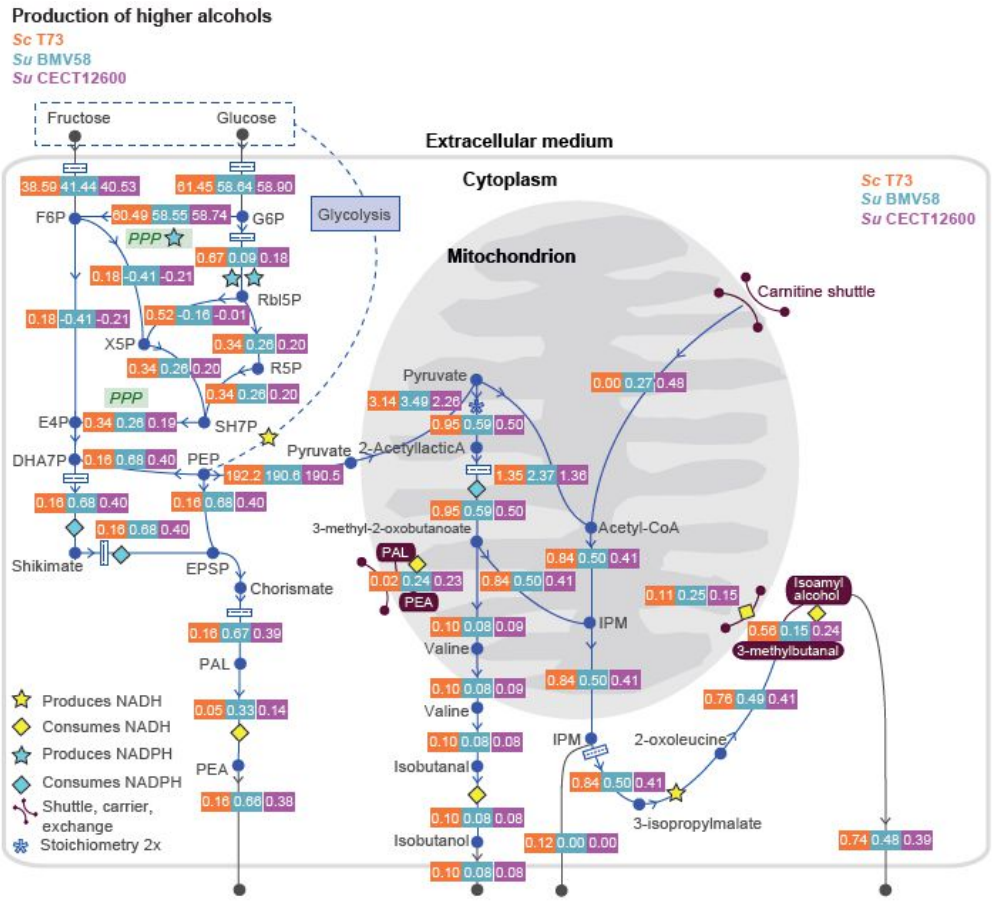

Figure S3. Redox balance in production of higher alcohols. Figure shows the predicted intracellular fluxes related to higher alcohols during the stationary phase and its corresponding impact on the redox co-factors balance NADPH/NADP+ and NADH/NAD+.

Figure S3 shows the predicted intracellular fluxes related to higher alcohols during the stationary phase and its corresponding impact on the redox co-factors balance NADPH/$NADP^+$ and NADH/NAD^+. Readers

can find the dynamic flux ratios in **Table S4**. During the stationary phase, *S. uvarum* strains produced more 2-phenylethanol than ScT73 strain per unit of consumed hexoses (0.16, 0.66 and 0.38 mmol/mmolH for ScT73, SuBMV58 and SuCECT12600 respectively, r_1590) while the opposite pattern was observed for isoamyl alcohol (0.74, 0.48 and 0.39 mmol/mmolH for ScT73, SuBMV58 and SuCECT12600 respectively, r_1863). In contrast, the model prediction was quite similar for the three strains for isobutanol (0.09 mmol/mmolH), as well as for other higher alcohols such as methionol and tyrosol which seemed to accumulate in minimal quantities (0.001 mmol/mmolH) in response to perturbations in the amino acid pool.

Production of 2-phenylethanol. De novo synthesis of 2-phenylethanol (PEA, **Figures S3.A, S3.B**) from carbohydrates contributed to redox homeostasis. Erythrose-4-phosphate (E4P, **Figure S3**) and phosphoenolpyruvate (PEP) are two sugar-phosphate intermediates of the pentose phosphate pathway (PPP) and glycolysis. They are the starting substrates of the chorismate pathway that lead to phenylalanine, which can subsequently be catabolized to 2-phenylethanol (Ehrlich pathway). From the beginning of the chorismate pathway to 2-phenylethanol, one NADPH (3-dihydroshikimate → shikimate) and one NADH (phenylacetaldehyde (PAL) → PEA) are consumed **(Figure S3)**. However, to fully understand the impact of de novo production of 2-phenylethanol on redox homeostasis, it is also important to remember that the PPP consists of

two branches: i) an oxidative and irreversible branch from glucose-6-phosphate (G6P) to ribulose-5-phosphate (Rbl5P) resulting in the net formation of two reduced NADPH co-factors per molecule of glucose-6-phosphate (**Figure S3**), and ii) a non-oxidative branch consisting of reversible carbon shuffling reactions between sugar-phosphate molecules leading to important precursor metabolites (e.g., ribose-5-phosphate (R5P) and erythrose-4-phosphate (E4P)) and glycolytic intermediates (e.g., fructose-6-phosphate (F6P) and glyceraldehyde-3-phosphate (G3P)). Thus, the transketolase and transaldolase enzymes of this branch of the PPP provide a reversible link between the PPP and glycolysis. In this context, if E4P required for *de novo* synthesis of PEA was generated through the oxidative branch of PPP, PEA production would result in NADPH accumulation. However, if E4P was generated by the non-oxidative branch of PPP from sugar phosphate intermediates of the glycolysis, we would expect an $NADP^+$ accumulation. As shown in **Figure S3**, our model predicted that during stationary phase ScT73 had a greater flux through the oxidative branch of the PPP than *S. uvarum* strains (0.67, 0.09 and 0.18 mmol/mmolH for ScT73, SuBMV58 and SuCECT12600, respectively). On the contrary, dynamic flux ratios through several non-oxidative reactions of the PPP were higher in both *S. uvarum* strains (F6P → E4P: 0.18, −0.41 and −0.21 mmol/mmolH; F6P → X5P :0.18, −0.41 and −0.21 mmol/mmolH; **Figure S3**). Consistent with a higher 2-phenylethanol synthesis by SuBMV58 and SuCECT12600, the model predicted an increase in flux

towards chorismate synthesis in both *S. uvarum* strains (0.17, 0.68 and 0.40 mmol/mmolH for ScT73, SuBMV58 and SuCECT12600, respectively). The higher flux through the PPP oxidative branch in ScT73 can be partially explained by NADPH requirement (at the level of 3-methyl-2-oxobutanoate formation) in *de novo* synthesis of isoamyl alcohol. On the other hand, the alternative non-oxidative PPP strategy used by *S. uvarum* strains may contribute to provide $NADP^+$ co-factors required in the $NADP^+$-dependent glutamate degradation to succinate in the GABA shunt (0.42, 1.96 and 1.29 mmol/mmolH for ScT73, SuBMV58 and SuCECT12600, respectively; **Figure S2**).

Production of isoamyl alcohol. During the stationary phase, the model predicted a substantial flux from pyruvate to 2-acetyllactic acid inside the mitochondria (0.95, 0.59 and 0.50 mmol/mmolH for ScT73, SuBMV58 and SuCECT12600 respectively; **Figure S3**; r_0097). In this reaction, two pyruvates are required per 2-acetyllactic molecule formed. The model also suggested that 2-acetyllactic acid was mainly directed to forming 3-isopropylmalate (IPM, 0.84, 0.50 and 0.41 mmol/mmolH for ScT73, SuBMV58 and SuCECT12600 respectively; **Figure S3**; r_0025), consuming one NADPH and one Acetyl-CoA. 3-isopropylmalate was mainly converted in isoamyl alcohol (0.76, 0.49 and 0.41 mmol/mmolH for ScT73, SuBMV58 and SuCECT12600, respectively) rather than for de novo leucine synthesis. The conversion of 3-isopropylmalate into 2-oxoleucine releases one NADH (r_0061), consumed during the reduction of 3-methylbutanal to isoamyl alcohol

(**Figure S3**, r_0179). Following these reactions, the formation of each isoamyl alcohol molecule consumes two pyruvate molecules, one acetyl-CoA and one NADPH (**Figure S3**). Besides, the formation of two pyruvates from one glucose release two NADH, and two NADH are produced per acetyl-CoA formed. Summing up, de novo synthesis of one isoamyl alcohol should result in excess of four NADH and one $NADP^+$. Accordingly, this *de novo* synthesis of isoamyl alcohol from pyruvate has a relevant impact on redox balance. The citrate/2-oxoglutarate could provide the $NADP^+$ required to synthesize 3-methyl-2-oxobutanoate inside the mitochondrion NADPH shuttle. Remarkably, the production of higher alcohols contributed substantially to redox metabolism related to glycerol accumulation. During the stationary phase, approximately 43% of the glycerol produced by the ScT73 strain was attributable to NADH derived from isoamyl-alcohol and 2-phenyl ethanol production. In the cases of SuBMV58 and SuCECT12600 strains, these values dropped to 36% and 27%, respectively.

References

Babazadeh, R., Lahtvee, P.J., Adiels, C.B., Goksör, M., Nielsen, J.B., and Hohmann, S. (2017) The yeast osmostress response is carbon source dependent. *Sci Rep* **7**: 1–11.

Bach, B., Sauvage, F.-X., Dequin, S., and Camarasa, C. (2009) Role of γ-Aminobutyric Acid as a Source of Nitrogen and Succinate in Wine. *Am J Enol Vitic* **60**: 508 LP – 516.

Goffeau, A., Barrell, G., Bussey, H., Davis, R.W., Dujon, B., Feldmann, H., et al. (1996) Life with 6000 genes. *Science (80-)* **274**: 546–567.

López-Malo, M., Querol, A., and Guillamon, J.M. (2013) Metabolomic Comparison of *Saccharomyces cerevisiae* and the Cryotolerant Species *S. bayanus* var. *uvarum* and *S. kudriavzevii* during Wine Fermentation at Low Temperature. *PLoS One* **8**:.

Minebois, R., Pérez-Torrado, R., and Querol, A. (2020) Metabolome segregation of four strains of *Saccharomyces cerevisiae*, *S. uvarum* and *S. kudriavzevii* conducted under low temperature oenological conditions. *Environ Microbiol* 1462-2920.15135.

Morard, M., Macías, L.G., Adam, A.C., Lairón-Peris, M., Pérez-Torrado, R., Toft, C., and Barrio, E. (2019) Aneuploidy and Ethanol Tolerance in *Saccharomyces cerevisiae*. *Front Genet* **10**:.

Otto, T.D., Dillon, G.P., Degrave, W.S., and Berriman, M. (2011) RATT: Rapid Annotation Transfer Tool. *Nucleic Acids Res* **39**: e57–e57.

Pérez-Torrado, R., Oliveira, B.M., Zemancíková, J., Sychrová, H., and Querol, A. (2016) Alternative glycerol balance strategies among *Saccharomyces* species in response to winemaking stress. *Front Microbiol* **7**: 435.

Tilloy, V., Ortiz-Julien, A., and Dequin, S. (2014) Reduction of ethanol yield and improvement of glycerol formation by adaptive evolution of the wine yeast *Saccharomyces cerevisiae* under hyperosmotic conditions. *Appl Environ Microbiol* **80**: 2623–2632.

SUPPLEMENTARY MATERIAL - Chapter 4

Table S1: Top 5 significant GO terms retrieved (p_{value}<0.05) from the differentially expressed genes from the 18 RNA_{seq} samples of wine strain T73 and the 15 RNA_{seq} samples from wild strain YPS128.

	GO	GO description	p_{value}	Matches
Wine (T73)	GO:0055085	transmembrane transport	2.24E-6	*SSU1, SEO1, ATP3, TAT1, VBA2, VBA3, HXT15, ENA5, YCF1, YPQ2, ORT1, etc.*
	GO:0006526	arginine biosynthetic process	3.54E-6	*ARG1, ARG3, ARG4, ARG8, ORT1, CPA1*
	GO:0009084	glutamine family amino acid biosynthetic process	1.44E-5	*ARG1, ARG3, ARG4, ARG8, ORT1, CPA1, PUT1, PUT2*
	GO:0003333	amino acid transmembrane transport	1.51E-5	*TAT1, VBA2, VBA3, YPQ2, AVT3, YCT1, LYP1, ORT1, PUT4, YMC1*
	GO:0098656	anion transmembrane transport	2.78E-5	*TAT1, VBA2,SUL1, HXT15,RDI1, YPQ2, MPH3,HOT13, MRX21, YMC1, ATO3, etc.*
Wild (YPS128)	GO:0015761	mannose transmembrane transport	2.42E-5	*HXT7, HXT13, HXT4, HXT8, HXT9, HXT11*
	GO:0015755	fructose transmembrane transport	5.24E-5	
	GO:0015711	organic anion transport	5.63E-5	*FLC2, YBR220C, GEX1, GIT1, GNP1, MUP1, MPC3, TNA1, VBA5, GEX2, etc.*
	GO:0071852	fungal-type cell wall organization or biogenesis	7.10E-5	*PAU3, PAU8, PAU7, PAU13, PAU15, PAU19, PAU24, LDS1, FLC2, SPO73, CRH1, SLT2, CHS7, CWP1, CWP2, NCW2, PUN1, CMP2, ROT1, CHS1, HPF1,SSP2, OSW1*
	GO:0045229	external encapsulating structure organization	7.61E-5	

Annex II

Publications

Chapter 1

Food Microbiology 90 (2020) 103484

Contents lists available at ScienceDirect

Food Microbiology

journal homepage: www.elsevier.com/locate/fm

A time course metabolism comparison among *Saccharomyces cerevisiae*, *S. uvarum* and *S. kudriavzevii* species in wine fermentation

Romain Minebois, Roberto Pérez-Torrado, Amparo Querol*

Instituto de Agroquímica y Tecnología de Los Alimentos, IATA-CSIC, E-46980, Paterna, Spain

ARTICLE INFO

Keywords:
S. uvarum
S. kudriavzevii
Central carbon metabolism
Nitrogen metabolism
Redox balance
Wine fermentation

ABSTRACT

In this study, we presented the first metabolome time course analysis performed among a set of *S. uvarum*, *S. kudriavzevii* and *S. cerevisiae* strains under winemaking conditions. Extracellular and intracellular metabolites, as well as physiological parameters of yeast cells, were monitored along the process to find evidence of different metabolic strategies among species to perform alcoholic fermentation. A thorough inspection of time trends revealed several differences in utilization or accumulation of fermentation by-products. We confirmed the ability of *S. uvarum* and *S. kudriavzevii* strains to produce higher amounts of glycerol, succinate or some fusel alcohols and their corresponding esters. We also reported differences in the yields of less common fermentative by-products involved in redox homeostasis, namely 2,3 butanediol and erythritol. 2,3 butanediol yield was higher in must ferment with cryophilic strains and erythritol, a pentose phosphate pathway derivative, was particularly overproduced by *S. uvarum* strains. Contrary to *S. cerevisiae*, a singular production-consumption rate of acetate was also observed in *S. uvarum* and *S. kudriavzevii* fermentations. Since acetate is a precursor for acetyl-CoA production which is involved in the biosynthesis of membrane lipids, cryophilic strains might take advantage of extracellular acetate to remodel cell membrane as ethanol content increased during fermentation.

1. Introduction

During wine fermentation, the majority of sugar content is metabolized by yeasts to produce ethanol and carbon dioxide. The remaining fraction of sugars is used for the synthesis of biomass and hundreds of additional metabolites, including organic acids (acetic acid, succinate), flavor-active secondary metabolites (esters, fusel alcohols, aldehydes, ketones, volatile sulfur compounds) or sugar alcohols such as glycerol, the most important by-product after carbon dioxide and ethanol. Therefore, there is a high diversity in the fermentative compounds originated from central carbon metabolism of yeasts, which determine the organoleptic properties (flavor and aroma) of wine. For this reason, the knowledge of their individual contribution to the global profile of the wine is a principal concern for oenologists who look for the most equilibrated beverages in terms of aromas, astringency, acidity and alcohol perception (Lambrechts and Pretorius, 2000). Today, with the increase of temperature during the growing season of grapes - as a result of climate change - the sugar level of grape musts tends to be higher at the cost of phenolic ripeness and acidity in most of the wine-producing regions (Cohen et al., 2008; Mira de Orduña, 2010). This high sugar content – subsequently converted to ethanol by yeasts – lead wines to be more alcoholic, increasing the perception of heat, altering the perception of wine aromas complexity and decreasing the color intensity and stability (Goldner et al., 2009; Pickering and Vanhanen, 1998). Thus, the production of wines with reduced ethanol concentration and enhanced aroma content without weakening product value has been the focus of extensive research over the past decades.

Viticulture techniques and dealcoholization treatments are some of the techniques currently employed to reduce alcohol concentration (Aguera et al., 2010; Catarino and Mendes, 2011; Kontoudakis et al., 2011; Pickering, 2000; Schmidtke et al., 2012). However, these approaches are difficult and expensive to implement. Alternative *Saccharomyces* species have attracted attention as a poor exploited resource of yeast biodiversity with interesting attributes not present in *S. cerevisiae*, the dominant species in alcoholic fermentation. Notably, the cryophilic species *S. uvarum* and *S. kudriavzevii* and their interspecific hybrids, have recently demonstrated interesting properties, especially at low fermentation temperatures. In particular, *S. uvarum* and *S. kudriavzevii* fermentation profiles differ from that of *S. cerevisiae* in terms of fermentative by-products yields and biomass production. Both cryophilic species generate higher levels of volatile fermentative compounds, particularly 2-phenylethanol and 2-phenylethyl acetate in *S. uvarum* (Gamero et al., 2013; Masneuf-Pomarède et al., 2010). These differences in aroma production have been correlated with differential

* Corresponding author.
E-mail address: aquerol@iata.csic.es (A. Querol).

https://doi.org/10.1016/j.fm.2020.103484
Received 1 August 2019; Received in revised form 2 March 2020; Accepted 9 March 2020
Available online 12 March 2020

Chapter 2

environmental microbiology

Environmental Microbiology (2020) **00**(00), 00–00 doi:10.1111/1462-2920.15135

Metabolome segregation of four strains of *Saccharomyces cerevisiae*, *Saccharomyces uvarum* and *Saccharomyces kudriavzevii* conducted under low temperature oenological conditions

Romain Minebois, Roberto Pérez-Torrado and Amparo Querol*

Instituto de Agroquímica y Tecnología de los Alimentos, IATA-CSIC, Paterna, E-46980, Spain.

Summary

The monitoring of fermentation at low temperatures (12–15°C) is a current practice in the winery for retention and enhancement of the flavour volatile content of wines. Among *Saccharomyces* species, *Saccharomyces uvarum* and *Saccharomyces kudriavzevii* have revealed interesting industrial properties, including better adaptation at low temperatures. To gather deeper knowledge of the fermentative metabolism at a low temperature of these species together with *S. cerevisiae*, we performed a comparative metabolomic analysis using four representative strains. We used batch cultures to obtain an exhaustive and dynamic image of the metabolome of strains passing through the sequential stresses related to the winemaking environment. A great variety of intra- and extracellular metabolites (>500 compounds) were quantified across fermentation using distinct chromatographic methods. Besides a global decrease in the lipid composition of the four strains when they entered into the stationary phase, we reported some strain-specific high magnitude changes. Examples of these differences included divergent patterns of production of short-chain fatty acids and erythritol in the *S. uvarum* strain. Strains also differed in expression for aromatic amino acid biosynthesis and sulphur metabolism, including the glutathione pathway. These data will allow us to refine and obtain the most value of fermentations with this alternative *Saccharomyces* species.

Received 4 March, 2020; revised 7 June, 2020; accepted 16 June, 2020. *For correspondence. E-mail aquerol@iata.csic.es; Tel. +34 963900022, Fax +34 963636301

Introduction

In wine making, fermentation temperature and yeast strains are two critical parameters that govern the final organoleptic qualities of wine. The use of low temperatures (12–15°C) during fermentation is a current practice in the winery. It enables not only retention but also enhancement of the flavour volatile content of wines (Molina *et al*., 2007). Nowadays, *S. cerevisiae* is the most important yeast involved in wine fermentation. However, *S. cerevisiae* has an optimal growth temperature around 32°C, which supposes some disadvantages for the winemakers when fermenting at low temperatures (12–15°C). For instance, the lag phase of *S. cerevisiae* increases, and its growth rate decreases, which can lead to prolong the duration of the process with a greater risk of halted or sluggish fermentation (Blateyron and Sablayrolles, 2001).

Consequently, the finding of new *Saccharomyces* and non-*Saccharomyces* yeasts able to correctly ferment in low temperature environments has been in the spotlight of worldwide wine yeast research over the past few years (Pérez-Torrado *et al*., 2018). Within the *Saccharomyces* genus, this is the case of the cryotolerant yeasts *S. uvarum* and *Saccharomyces kudriavzevii*. *Saccharomyces kudriavzevii* has been isolated only from natural environments (Sampaio and Gonçalves, 2008; Lopes *et al*., 2010), most likely because of its poor ethanol resistance (Belloch *et al*., 2008). On the contrary, *S. uvarum* has been mainly isolated from fermentation at cold temperatures (Naumov *et al*., 2000; Demuyter *et al*., 2004; Tosi *et al*., 2009; Masneuf-Pomarède *et al*., 2010). Previous physiological and oenological characterisations of *S. uvarum* and *S. kudriavzevii* strains have demonstrated their potential for fermenting wine musts at low temperatures. For instance, Masneuf-Pomarède *et al*. (2010) demonstrated that several strains of *S. uvarum* were able to complete alcoholic fermentation at 13°C faster than commercial *S. cerevisiae* strains. Regarding *S. kudriavzevii*, because even at low temperature, *S. cerevisiae* is the most fermentative competitive

Chapter 4

environmental microbiology

Environmental Microbiology (2021) **00**(00), 00–00 doi:10.1111/1462-2920.15523

Metabolic differences between a wild and a wine strain of *Saccharomyces cerevisiae* during fermentation unveiled by multi-omic analysis

Romain Minebois,[1] María Lairón-Peris,[1] Eladio Barrio,[1,2] Roberto Pérez-Torrado[1] and Amparo Querol[1]*

[1]*Instituto de Agroquímica y Tecnología de los Alimentos, IATA-CSIC, Paterna, E-46980, Spain.*

[2]*Departament de Genètica, Universitat de València, C/ Doctor Moliner, 50, Burjassot, Valencia, E-46100, Spain.*

Summary

***Saccharomyces cerevisiae*, a widespread yeast present both in the wild and in fermentative processes, like winemaking. During the colonization of these human-associated fermentative environments, certain strains of *S. cerevisiae* acquired differential adaptive traits that enhanced their physiological properties to cope with the challenges imposed by these new ecological niches. The advent of omics technologies allowed unveiling some details of the molecular bases responsible for the peculiar traits of *S. cerevisiae* wine strains. However, the metabolic diversity within yeasts remained poorly explored, in particular that existing between wine and wild strains of *S. cerevisiae*. For this purpose, we performed a dual transcriptomic and metabolomic comparative analysis between a wild and a wine *S. cerevisiae* strains during wine fermentations performed at high and low temperatures. By using this approach, we could correlate the differential expression of genes involved in metabolic pathways, such as sulfur, arginine and thiamine metabolisms, with differences in the amounts of key metabolites that can explain some important differences in the fermentation performance between the wine and wild strains.**

Introduction

Saccharomyces cerevisiae is a widespread yeast species found both in the wild (Wang *et al*., 2012) and in fermentative processes, including winemaking (Legras *et al*., 2018). Natural isolates of *S. cerevisiae* have been isolated from highly diverse living environments, such as fruits, tree bark, rotten wood, cacti, soil and exudates of oak trees. Over the last few decades, the increasing availability of *S. cerevisiae* strains and their genomes has continuously consolidated the position of this species as a model organism in ecology and population genomics (Almeida *et al*., 2015; Gallone *et al*., 2016; Legras *et al*., 2018; Liti *et al*., 2009; Peter *et al*., 2018; Peter & Schacherer, 2016; Schacherer *et al*., 2009).

Among the available strains, increased attention has been paid to *S. cerevisiae* wine strains. Indeed, the repeated exposure of wine *S. cerevisiae* strains to the variety of stresses occurring during alcoholic fermentation (e.g. osmotic stress, ethanol content, nitrogen starvation, addition of sulfites), has led to their passive domestication and the emergence of differential adaptive traits of biotechnological interest (Querol *et al*., 2003; Barrio *et al*., 2006). In this aspect, different genomic changes of adaptive value, often referred to as 'footprints' of the domestication process have been reported in wine strains (Marsit and Dequin, 2015; Gallone *et al*., 2016, 2019; Gorter de Vries *et al*., 2017). Nucleotide variation (Schacherer *et al*., 2009; Eldarov *et al*., 2018), chromosomal rearrangements (Guijo *et al*., 1997; Pérez-Ortín *et al*., 2002; García-Ríos *et al*., 2019), gene copy number variation (Ibáñez *et al*., 2014; Peter *et al*., 2018), introgressions (Almeida *et al*., 2014), hybridization (Dunn *et al*., 2013; Morard *et al*., 2020), aneuploidy (Hose *et al*., 2015; Mangado *et al*., 2018; Morard *et al*., 2019) and horizontal gene transfer (HGT) (Marsit *et al*., 2015, 2016) are the highlighted genetic mechanisms described in the adaptation of *S. cerevisiae* wine strains to winemaking. For instance, the reciprocal translocation between chromosomes VII and XVI is a well-documented case of gross chromosomal rearrangement with the adaptive advantage of sulfite resistance, only present in wine strains of *S. cerevisiae* (Pérez-Ortín *et al*., 2002; Yuasa *et al*., 2004; García-Ríos *et al*., 2019). More recently, the genes of region C (Novo *et al*., 2009), which results from

Received 19 February, 2021; revised 30 March, 2021; accepted 8 April, 2021. *For correspondence. E-mail aquerol@iata.csic.es. Tel. +34 963900022, Fax +34 963636301


UNIVERSITAT
POLITÈCNICA
DE VALÈNCIA


iata
Instituto de Agroquímica
y Tecnología de Alimentos


CSIC
Consejo Superior de Investigaciones Científicas